

CHARACTERIZATION OF HYDROXYPROPYLCELLULOSE
CHOLESTERIC LYOMESOPHASES

by



Rita Stephania Werbowyj
B.Sc. (Hons.) McGill University

A thesis submitted to the Faculty of Graduate
Studies and Research in partial fulfilment of
the requirements for the degree of
Doctor of Philosophy

Department of Chemistry
McGill University
Montréal, Quebec
Canada

April 1982

CHARACTERIZATION OF HPC CHOLESTERIC LYOMESOPHASES

To my parents and sister

"I am at a loss to give a distinct idea of the nature of this liquid, and cannot do so without many words. Although it flowed with rapidity in all declivities where common water would do so, yet never, except when falling in a cascade, had it the customary appearance of limpidity. It was, nevertheless, in point of fact, as perfectly limpid as any limestone water in existence, the difference being only in appearance. At first sight, and especially in cases where little declivity was found, it bore resemblance, as regards consistency, to a thick infusion of gum-arabic in common water. But this was only the least of its extraordinary qualities. It was not colorless, nor was it of any one uniform color — presenting to the eye, as it flowed, every possible shade of purple, like the hues of a changeable silk. This variation in shade was produced in a manner which excited as profound astonishment in the minds of our party as the mirror had done in the case of Too-wit. Upon collecting a basinful, and allowing it to settle thoroughly, we perceived that the whole mass of liquid was made up of a number of distinct veins, each of a distinct hue; that these veins did not commingle; and that their cohesion was perfect in regard to their own particles among themselves, and imperfect in regard to neighboring veins. Upon passing the blade of a knife athwart the veins, the water closed over it immediately, as with us, and also, in withdrawing it, all traces of the passage of the knife were instantly obliterated. If, however, the blade was passed down accurately between the two veins, a perfect separation was effected, which the power of cohesion did not immediately rectify. The phenomena of this water formed the first definite link in that vast chain of apparent miracles with which I was destined to be at length encircled."

(From chapter XVIII of the "Narrative of Arthur Gordon Pym" by Edgar Allan Poe; Charles Scribner's Sons, 1914)

ABSTRACT

Concentrated solutions of hydroxypropylcellulose in aqueous and in polar organic solvents form lyotropic liquid crystalline phases. The critical concentration of hydroxypropylcellulose needed for anisotropic phase separation is dependent upon the solvent and is much greater than that expected for rod-like species in solution. The flexibility of the cellulosic chains in a particular solvent is believed to be the main factor governing the critical hydroxypropylcellulose volume fraction at phase separation. The anisotropic phase exhibits birefringence, iridescence, and very high optical activity, properties characteristic of cholesteric liquid crystals. The helicoidal pitch for most of these cholesteric samples in water and organic solvents varies from 280 to 700 nm, but in certain organic solvents the helicoidal pitch ranges up to 6000 nm. The latter samples exhibit fingerprint-like periodicity lines in the light microscope and distinctive "shimmering" colors. For both types of samples the helicoidal pitch is found to vary inversely with the third power of the hydroxypropylcellulose volume fraction. A model is proposed for the cholesteric structure in which the average separation, d , between the chain molecules varies with $\phi_2^{-1/2}$, where ϕ_2 is the polymer volume fraction. The experimental x-ray diffraction data are in accord with this relationship. The angular twist between the molecules in adjacent cholesteric layers is calculated to vary from 0.30 to 1.8° over the mesophase

concentration range investigated.

Light scattering measurements give twice the weight average molar mass for hydroxypropylcellulose as do sedimentation equilibrium measurements. Viscosity measurements in organic solvents show that the hydroxypropylcellulose conformation in dilute solution is neither that of a random coil nor that of a rigid rod. All aqueous hydroxypropylcellulose solutions show a lower consolute temperature that varies more with the sample molar substitution than with its molar mass. A qualitative "phase" diagram for aqueous hydroxypropylcellulose solutions is also included.

RESUME

Des solutions concentrées d'hydroxypropylcellulose dans des solvants aqueux et organiques polaires forment des phases lyotropiques de cristaux liquides. La concentration critique d'hydroxypropylcellulose nécessaire pour une séparation de phase anisotrope dépend du solvant et se trouve beaucoup plus grande que celle attendue pour des macromolécules en forme de bâtonnet. La flexibilité des chaînes cellulosiques dans un solvant donné semble être le principal facteur gouvernant la fraction volumique critique d'hydroxypropylcellulose produisant la séparation de phase. La phase anisotrope produit les propriétés caractéristiques des cristaux liquides cholestériques telles que la biréfringence, l'iridescence, et une activité optique très importante. Le pas de l'hélice pour la plupart de ces échantillons cholestériques varie de 280 à 700 nm, mais peut aller jusqu'à 6000 nm dans certains solvants organiques. Dans ce dernier cas, les échantillons vus au microscope optique présentent des lignes périodiques similaires à des empreintes digitales et des couleurs "réfléchissantes" (shimmering) distinctes. Pour les deux types d'échantillons les résultats montrent que le pas de l'hélice varie de façon inversement proportionnelle au cube de la fraction volumique d'hydroxypropylcellulose. Un modèle est proposé pour la structure cholestérique dans lequel la distance moyenne, d , entre deux chaînes moléculaires varie en fonction de $\phi_2^{-1/2}$, où ϕ_2 est la fraction volumique

de polymère. Les résultats de diffraction des rayons X confirment cette hypothèse. L'angle entre les molécules se trouvant dans deux couches cholestériques adjacentes varie entre 0.30 et 1.8° selon les concentrations de mésophase employées.

La masse molaire moyenne en poids d'hydroxypropylcellulose obtenue par diffusion de la lumière est deux fois plus grande que celle obtenue par équilibre de sédimentation. La viscosité de l'hydroxypropylcellulose en solution diluée dans les solvants organiques montre que sa conformation n'est ni celle d'une pelotte statistique ni celle d'un bâtonnet rigide. Toutes les solutions aqueuses d'hydroxypropylcellulose ont une température de démixtion inférieure qui varie plus en fonction de la substitution molaire de l'échantillon qu'en fonction de sa masse molaire. Un diagramme de "phase" qualitatif pour les solutions aqueuses d'hydroxypropylcellulose est également donné.

PREFACE

The commercialization of high strength fibers spun from anisotropic polymer solutions has renewed scientific interest in the structure and properties of these macromolecular mesophases. This thesis describes the detection and subsequent investigation of the first cellulosic to form a lyotropic liquid crystal.

The first chapter of this thesis is a general introduction to the topic of liquid crystals from a historical perspective. This chapter ends with a brief description of hydroxypropylcellulose, the polymer found to form a lyomesophase. Chapter II begins with a succinct review of the published literature on hydroxypropylcellulose. The remainder of this chapter is devoted to the characterization of this polymer by light scattering, sedimentation equilibrium, and viscosity measurements. Chapter III outlines the theories currently in vogue that try to account for anisotropic phase separation and mesophase formation. The applicability of these theories to the hydroxypropylcellulose system is then evaluated by comparison with the experimentally determined phase separation data. Chapter IV is a detailed investigation of the optical properties of hydroxypropylcellulose solutions which leads to the conclusion that hydroxypropylcellulose is a cholesteric lyomesophase in water and in polar organic solvents. Chapter V details the results and consequences of an

x-ray diffraction study on the hydroxypropylcellulose mesophase. This chapter is followed by a short section consisting of concluding remarks and suggestions for future work. The thesis ends with a brief summary of claims to original research.

ACKNOWLEDGEMENTS

The author wishes to express her gratitude and sincere thanks to:

Dr. D.G. Gray, for his tireless guidance, assistance, and suggestions throughout this work and thesis preparation, for his enthusiasm and thoughtful advice, and for giving generously of his time. His consideration and efforts on my behalf are greatly appreciated.

Dr. D.A.I. Goring, for his kind interest and helpful advice on conventional light scattering.

Dr. A.A. Robertson, for allowing the use of the differential interference refractometer.

Dr. R.St.J. Manley, for his interest and timely comments on hydroxyethylcellulose aggregation in solution.

Mr. W.Q. Yean, for his expert operation of the analytical ultracentrifuge and for his being available for consultation.

Dr. S.L. Tseng, for various useful advice and stimulating discussions about this work.

Miss J. Svedman, for running preliminary Raman and FTIR spectra, for the liberal use of her automobile, and for various technical supplies.

Mr. G. Suranyi, for his help in locating equipment in the laboratory.

Dr. J.F. Revol and Mr. F.St. Germain, for kindly translating the abstract into French.

Drs. G.M. Dorris, L. Larrondo, J.M. Yang, P. Whiting, J. Abbot, J. Aspler, B. Kalb, P. Smith, S. Chang, B. Favis, R. Mbachu, Mr. G.V. Laivins, R. Leung, and Miss S. Katz, for helping the time pass more pleasantly and for sharing equipment.

McGill University, Chemistry Department, for Demonstratorships during 1976-77, 1977-78, 1978-79, and 1979-80.

The Quebec Government, for a Postgraduate Scholarship during 1977-78.

The National Science and Engineering Research Council of Canada, for Postgraduate Scholarships during 1978-79 and 1979-80.

The Pulp and Paper Research Institute of Canada, for a Studentship during 1976-77, for the S.G. Mason Fellowship during 1980-81, for a Special Scholarship during 1981-82, and for Merit Awards during 1977, 1978, and 1979.

The Pulp and Paper Research Institute of Canada and McGill University, for laboratory accommodation and for liberal use of their supplies and technical services.

TABLE OF CONTENTS

CHAPTER I

INTRODUCTION

I.1	Low Molar Mass Mesophases	2
I.2	Polymeric Mesophases	9
I.3	Cellulosic Mesophases	31
	References	33

CHAPTER II

CHARACTERIZATION OF HYDROXYPROPYLCELLULOSE

II.1	Preparation	43
II.2	Structure	43
II.3	Properties	46
II.4	Characterization	49
II.4.1	LIGHT SCATTERING	
	Introduction	50
	Experimental	
	A. Solution Preparation	53
	B. Differential Index of Refraction	56
	C. Light Scattering	59
	Results and Discussion	64

II.4	Characterization	
II.4.2	SEDIMENTATION EQUILIBRIUM	
	Introduction	86
	Experimental	88
	Results and Discussion	90
II.4.3	COMPARISON OF MOLAR MASS TECHNIQUES	94
II.4.4	VISCOSITY	
	Introduction	98
	Experimental	102
	Results and Discussion	102
II.4.5	MOLAR SUBSTITUTION	
	Introduction	112
	Experimental	112
	Results and Discussion	113
II.5	Conclusion	115
	References	116

CHAPTER III

PHASE SEPARATION OF HYDROXYPROPYLCELLULOSE SOLUTIONS

III.1	Introduction	122
III.2	Experimental	
III.2.1	CLOUD POINT MEASUREMENTS	129
III.2.2	LYOMESOPHASE PREPARATION	130

III.3	Results and Discussion	
III.3.1	PHASE SEPARATION IN AQUEOUS SOLUTION ON HEATING	133
III.3.2	CONCENTRATED AQUEOUS MESOPHASE FORMATION	140
III.3.3	MESOPHASE FORMATION IN ORGANIC SOLVENTS	152
III.3.4	FLORY'S THEORY AND HYDROXYPROPYLCELLULOSE	158
III.4	Conclusion	162
	References	164

CHAPTER IV

OPTICAL PROPERTIES OF HYDROXYPROPYLCELLULOSE
LYOMESOPHASES

IV.1	Introduction	169
IV.2	Experimental	
IV.2.1	LYOMESOPHASE PREPARATION	179
IV.2.2	OPTICAL ACTIVITY AND REFLECTION	180
IV.2.3	LASER LIGHT DIFFRACTION	182
IV.2.4	REFRACTIVE INDEX AND BIREFRINGENCE	184
IV.3	Results and Discussion	
IV.3.1	OPTICAL ROTATORY DISPERSION	186
IV.3.2	BIREFRINGENCE	197
IV.3.3	CHOLESTERIC COLORS AND SHORT PITCH SAMPLES	208
IV.3.4	SHIMMERING COLORS AND LONG PITCH SAMPLES	225
IV.3.5	SHORT AND LONG PITCH SAMPLES IN METHANOL	235

IV.4	Conclusion	236
	References	240

CHAPTER V

X-RAY DIFFRACTION OF CELLULOSIC LYOMESOPHASES

V.1	Introduction	244
V.2	Experimental	245
V.3	Results	247
V.4	Discussion	254
V.5	Conclusion	270
	References	272

APPENDIX

CONCLUDING REMARKS AND SUGGESTIONS FOR FUTURE WORK . . .	275
CLAIMS TO ORIGINAL RESEARCH	281

LIST OF FIGURES

Figure		Page
Chapter I		
I.1	Schematic view of a nematic liquid crystal with orientational order	4
I.2	Schematic view of the spiral molecular arrangement found in a cholesteric liquid crystal	6
I.3	Illustration of the stratified layers to be found in a smectic liquid crystal	8
Chapter II		
II.1	Idealized structure for hydroxypropylcellulose with a degree of substitution of 2 and a molar substitution of 4	44
II.2	Schematic view of the components of a Chromatix LALLS photometer	61
II.3	The change in refractive index difference with concentration for aqueous HPC-E solutions	65
II.4	The variation in refractive index difference with concentration for aqueous HPC-L solutions	66
II.5	The change in refractive index difference with concentration for aqueous HPC-J solutions	67
II.6	The variation in refractive index difference with concentration for aqueous HPC-G solutions	68
II.7	Typical Zimm plot of light scattering data for HPC-G in aqueous solution	72

Figure		Page
II.8	LALLS data for aqueous dextran solutions	74
II.9	Chromatix LALLS results for several aqueous HPC-G solutions	76
II.10	LALLS data for aqueous HPC-L solutions	79
II.11	LALLS data for HPC-L solutions in THF	81
II.12	LALLS results for HPC-L solutions in ethanol	82
II.13	LALLS results for aqueous HPC-E solutions	84
II.14	LALLS results for aqueous HPC-J solutions	85
II.15	Typical sedimentation equilibrium schlieren pattern obtained for an aqueous HPC-E solution	92
II.16	Variation in apparent molar mass with concentration for several HPC samples in aqueous solution	93
II.17	Huggins and Kraemer equation plots of the viscosity data for HPC-E, L, and J in 1-pentanol	104
II.18	Huggins and Kraemer equation plots of the viscosity data for HPC-E, L, J, and G in acetic acid	105
II.19	Martin equation plot of the viscosity data for HPC-E, L, and J in 1-pentanol	106
II.20	Martin equation plot of the viscosity data for HPC-E, L, J, and G in acetic acid	107
II.21	A typical NMR spectrum for HPC-L in $CDCl_3$	114

Chapter III

III.1	Microscopic view of the particles formed on heating a dilute aqueous HPC solution above 40°C	134
-------	--	-----

Figure		Page
III.2	Typical fibrillar structure visible in the light microscope on examination of the precipitate found to form with time in dilute aqueous HPC solutions	138
III.3	The change in solution turbidity with temperature for two aqueous HPC-L solutions	139
III.4	Solutions depicting the three distinct phases which aqueous HPC solutions can exhibit	142
III.5	A schematic view of two aqueous HPC-J solutions which phase separated into the two distinct layers characterizing the coexistence region	143
III.6	Typical iridescent colors exhibited by different HPC concentrations in water	147
III.7	Characteristic texture exhibited by lyotropic aqueous HPC solutions between the crossed polars of a light microscope	149
III.8	Microscopic texture of an aqueous HPC solution under crossed polars	150
III.9	Sketch illustrating the various "phases" which aqueous HPC solutions can exhibit	151
III.10	Polarizing micrograph of a HPC acetic acid solution exhibiting distinct coexisting isotropic and anisotropic regions	155
III.11	Unusual cell structure found in a HPC acetic acid sample	156
III.12	Polarizing micrograph of a HPC methanol solution	157

Chapter IV

IV.1	Idealized molecular arrangement found in a cholesteric lyomesophase	170
------	---	-----

Figure		Page
IV.2	Idealized helicoidal arrangements possible when a cholesteric structure is constrained between two flat surfaces	174
IV.3	Cholesteric iridescent color of a typical concentrated aqueous HPC-L sample	176
IV.4	Shimmering iridescent color of a typical concentrated HPC-L acetic acid sample	177
IV.5	The schematic view of an anisotropic aqueous HPC solution through an Abbé refractometer telescope.	185
IV.6	Typical plain negative ORD spectra for HPC in water, methanol, acetic acid, and cellosolve	188
IV.7	Dependence of the solution optical activity on wavelength for a typical dilute aqueous HPC solution	190
IV.8	Typical anomalous negative ORD curves for HPC-L in methanol and in water	191
IV.9	Refractive index data for aqueous HPC-L solutions as a function of the HPC volume fraction	193
IV.10	The variation in refractive index with HPC-J volume fraction in aqueous solution	194
IV.11	Refractive index data for HPC-L methanol solutions as a function of the HPC volume fraction	195
IV.12	The variation in refractive index with HPC-L weight fraction in acetic acid solution	196
IV.13	The variation in rotatory power with wavelength for an aqueous solution of 0.57 volume fraction HPC-E	198
IV.14	The change in optical activity as a function of wavelength for an aqueous HPC-J solution	200
IV.15	The variation in birefringence with wavelength for an aqueous HPC-L solution	203
IV.16	Schematic view of the model invoked to account for the difference in birefringence measured with the Abbé refractometer and the layer birefringence as required by De Vries' rotatory power theory	206

Figure		Page
IV.17	Spectrophotometric data illustrating the change in reflection wavelength maxima with the HPC-E and L concentration in water	209
IV.18	Variation in reflection wavelength from ORD spectra with HPC-E and L concentration in aqueous solution	210
IV.19	Three typical examples of the lovely cholesteric iridescent color exhibited by short pitch aqueous HPC solutions	211
IV.20	Planar texture exhibited by a HPC-L aqueous solution when examined in the light microscope without crossed polars	213
IV.21	The variation in helicoidal pitch with HPC-E, L, and J weight fraction in aqueous solution	215
IV.22	Variation in the helicoidal pitch calculated from ORD data with the HPC-L volume fraction in aqueous solution	216
IV.23	Variation in the helicoidal pitch calculated from spectrophotometric data with the HPC-L volume fraction in aqueous solution	217
IV.24	Variation in the helicoidal pitch calculated from ORD data with the HPC-E volume fraction in aqueous solution	218
IV.25	Variation in the helicoidal pitch calculated from spectrophotometric data with the HPC-E volume fraction in aqueous solution	219
IV.26	The variation in helicoidal pitch with HPC-E volume fraction in aqueous solution	222
IV.27	The variation in reflection wavelength with incident light angle for a 0.58 HPC-L weight fraction aqueous solution	223
IV.28	The variation in reflection wavelength with incident light angle for a 0.64 weight fraction HPC-L solution in water	224
IV.29	Typical periodicity or fingerprint lines visible in the light microscope on examination of an organic HPC solution with large pitch	226

Figure		Page
IV.30	A schematic view of the probable helicoidal orientation of HPC in a dished and a flat microscope slide	227
IV.31	Variation in helicoidal pitch with HPC-L volume fraction in acetic acid solutions	229
IV.32	Print illustrating the light diffraction pattern for a HPC-L acetic acid solution using a He-Ne laser as the light source	230
IV.33	Illustration of the rainbow-like diffraction pattern for a HPC-L acetic acid solution which is illuminated by white light	231
IV.34	Shimmering iridescent colors of a HPC-L acetic acid solution viewed at three slightly different incident light angles	233
IV.35	Variation in helicoidal pitch with HPC-L volume fraction in methanol solution	237

Chapter V

V.1	X-ray diffraction pattern for a HPC-L aqueous solution	248
V.2	X-ray diffraction pattern for a HPC methanol solution and for an APC acetone solution	250
V.3	The variation in x-ray d spacing with HPC volume fraction in methanol solutions	252
V.4	The variation in x-ray d spacing with APC volume fraction in acetone solutions	253
V.5	A schematic view of the model proposed to represent the arrangement of rod-like molecules within a small cross-sectional area A	256
V.6	The variation in x-ray d spacing with the inverse square root of the HPC volume fraction in methanol solutions	258

Figure		Page
V.7	The change in the x-ray d spacing with the inverse square root of the APC volume fraction in acetone solutions	259
V.8	The variation in the x-ray d spacing with the cellulose volume fraction of HPC in methanol and APC in acetone solutions	263
V.9	An expanded view of two successive layers in the model proposed to represent a cholesteric lyomesophase	265
V.10	The variation in the angular twist of the cholesteric structure with the APC volume fraction in acetone solutions	269

LIST OF TABLES

Table		Page
Chapter I		
I.1	Representative Listing of Polymeric Thermotropic Liquid Crystals	13
I.2	Typical Polymeric Compounds Reported to Form Lyotropic Liquid Crystals	18
Chapter II		
II.1	Manufacturer's Data for Nominal Molar Mass (\bar{M}_w) and Molar Substitution (MS) of Several HPC Samples	54
II.2	Concentration Range of HPC Solutions Prepared for Differential Index of Refraction Measurements	57
II.3	Differential Index of Refraction (dn/dc) Values at 25°C and $\lambda \approx 560$ nm for Several HPC Types in Order of Increasing Molar Mass	70
II.4	Molar Mass Results for Aqueous HPC-G Solutions from LALLS Data Collected Over a Three Day Time Period	77
II.5	Calculated Molar Masses (\bar{M}_w) and Second Virial Coefficients (A_2) for HPC Samples from Low Angle Laser Light Scattering (LALLS) and Sedimentation Equilibrium (SE) Measurements	96
II.6	Summary of Limiting Viscosity Number ($[\eta]$) and k , k' , k'' Constants from the Huggins, Kraemer, and Martin Equations Respectively for HPC Samples at 25°C	108
II.7	Data Used to Evaluate the Mark - Houwink K and a Parameters for HPC in 1-Perflanol and Acetic Acid	110

Table

Page

II.8 Mark - Houwink Constants for HPC in Various Solvents 111

Chapter III

III.1 Variation of the Cloud Point with Molar Mass and Concentration for Aqueous HPC Solutions 135

III.2 Variation in Mesophase Iridescence with HPC Volume Fraction in Aqueous Solution 146

III.3 Weight and Volume Fraction of HPC Required to Form a Mesophase in Various Organic Solvents 153

Chapter IV

IV.1 Layer Birefringence Values Calculated by Fitting De Vries' Rotatory Power Equation to the Experimental ORD Results for Aqueous HPC Solutions 202

IV.2 Birefringence Values Measured for HPC Solutions with the Abbé Refractometer 204

IV.3 Hydroxypropylcellulose Weight Fraction in Water Needed to Produce a Particular Cholesteric Iridescence 212

IV.4 Slope and Intercept Values from Plots of Pitch Versus Volume Fraction for HPC in Several Solvents 238

Table

Page

Chapter V

V.1	Variation in X-ray d Spacing with HPC-L Concentration in Aqueous and Organic Solutions	249
V.2	Calculated Angular Twist (θ) Between Successive Layers of the Cholesteric Structure for HPC Methanol Lyomesophases	267
V.3	Calculated Angular Twist (θ) Between Successive Layers of the Cholesteric Structure for APC Lyomesophases in Acetone	268

GLOSSARY OF SYMBOLS

- A Area under low field NMR spectrum for HPC (Chapter II).
- A Volume element cross-sectional area in cholesteric model (Chapter V).
- A_2, A_3 Second and third virial coefficients respectively.
- α Exponent in the Mark - Houwink empirical relationship between intrinsic viscosity and molar mass.
- μ Molecular cross-sectional area in cholesteric model (Chapter V).
- B Area under high field NMR spectrum for HPC (Chapter II).
- B_e Non-ideality correction factor for apparent molar mass equation.
- c Solution concentration, usually in g/mL but sometimes (especially when used in relation to viscosity measurements) in g/100 mL.
- c_0 Initial solution concentration.
- D_0 Net transmittance of LALLS photometer attenuators.
- d Rod-like polymer molecule diameter (Chapter III).
- d Sample periodicity spacing giving rise to laser diffraction rings (Chapter IV).
- d Periodicity spacing calculated from x-ray diffraction rings (Chapter V).
- \bar{d} Center-to-center separation between polymer chains within the cholesteric structure.
- \underline{d} Interference refractometer fringe displacement.
- dn/dc Differential index of refraction (mL/g).
- G_0 LALLS photometer detector reading for transmitted light intensity.

G_{θ}	LALLS photometer detector reading for scattered light intensity at an angle θ .
I_0	Incident light intensity.
i_{θ}	Scattered light intensity per unit volume at an angle θ .
K	Optical constant relating the Rayleigh factor and molar mass.
K	Constant in the Mark - Houwink empirical relationship between intrinsic viscosity and molar mass.
K_s	Sedimentation equilibrium constant for a particular temperature, rotor speed, and phase plate angle.
k	Interference refractometer instrument constant (Chapter II).
k	Constant in Huggins' viscosity equation.
k'	Constant in Kraemer's viscosity equation.
k''	Constant in Martin's viscosity equation.
L	Rod-like polymer molecule length (Chapter III).
l	Effective length of scattering volume in LALLS photometer (Chapter II).
l	Length of equal links in a polymer chain (Chapter III).
l	Sample-to-film distance in x-ray diffraction experiments (Chapter V).
l'	Kuhn statistical segment length.
MS	Polymer molar substitution.
M_{cel}	Molar mass of repeat unit in cellulose.
M_{der}	Molar mass of repeat unit in cellulose derivative.
\bar{M}_w	Weight average molar mass of polymer.
$\bar{M}_{w,i}$	Apparent weight average molar mass of polymer.
m	Total mass of components in solution (Chapter II).
m	Reflection order (Chapter IV).

N_A	Avogadro's number.
n	Number of links, each of length l , in a polymer chain (Chapter III).
\bar{n}	Average refractive index of a solution or mesophase (Chapter IV).
n_a, n_r	Axial and radial refractive indices respectively.
n_x, n_y, n_z	Refractive indices in the x , y , and z axis directions respectively.
n_o	Refractive index of the pure solvent.
Δn	Refractive index difference between solution and solvent (Chapter II).
Δn	Layer birefringence (Chapter IV).
P	Cholesteric helicoidal pitch.
$P(\theta)$	Particle scattering function.
R_θ	Rayleigh factor at an angle θ .
\bar{R}_θ	Excess Rayleigh factor at an angle θ .
r	Distance of scattering volume from detector in LALLS photometer (Chapter II).
r	Laser or x-ray diffraction ring radius (Chapters IV and V).
$\langle r_o^2 \rangle$	Mean square unperturbed end-to-end distance of a polymer chain.
$\langle s^2 \rangle$	Mean square radius of gyration of a polymer chain.
V	Total volume of components in solution.
V_1	Volume of solvent in solution (Chapter II).
v	Specific volume of polymer.
v_{cel}	Volume of cellulose in derivative.
v_{der}, v_s	Volume of derivative and solvent respectively in solution (Chapter V).
w_1, w_2	Weight of solvent and solute respectively in solution (Chapter III).

w_{cel}	Weight of cellulose in derivative.
$w_{\text{der}}, w_{\text{s}}$	Weight of derivative and solvent respectively in solution (Chapter V).
x	Axial ratio of a polymer.
\underline{x}	Distance of the sample gradient midpoint from the rotor center in sedimentation equilibrium schlieren patterns.
y_e	Height of the sample gradient midpoint from a reference line on sedimentation equilibrium schlieren pattern films.
δ_x	Distance of the sample gradient midpoint from a fixed reference line on sedimentation equilibrium schlieren pattern films.
η_i	Logarithmic viscosity number or inherent viscosity.
η_r	Viscosity ratio or relative viscosity.
η_{red}	Viscosity number or reduced viscosity.
η_{sp}	Specific viscosity.
$[\eta]$	Limiting viscosity number or intrinsic viscosity (dL/g).
θ	Angle between transmitted and scattered beam in the LALLS photometer (Chapter II).
θ	Rotatory power or optical activity (rad/nm) (Chapter IV).
θ	Diffraction angle in laser light scattering patterns for HPC (Chapter IV).
θ	Diffraction angle in x-ray scattering experiments (Chapter V).
θ	Cholesteric twist angle or angular twist between adjacent cholesteric layers (Chapter V).
λ, λ	Incident light wavelength.
λ_o, λ_o	Cholesteric reflection wavelength at normal incidence.
$\lambda_{o,i}$	Cholesteric reflection wavelength at an arbitrary incident light angle of ϕ_i .
ρ	Solution density.
ρ_1, ρ_2	Solvent and solute densities respectively (Chapter III).

ρ_{cel}	Density of cellulose.
$\rho_{\text{der}}, \rho_{\text{s}}$	Density of cellulose derivative and solvent respectively (Chapter V).
σ	Solid angle over which detected radiation is viewed in the LALLS photometer.
$\phi_{\text{c}}^{\text{F}}$	Critical polymer volume fraction at anisotropic phase separation according to Flory's rigid rod theory.
$\phi_{\text{c}}^{\text{O}}$	Critical polymer volume fraction at anisotropic phase separation according to Onsager's theory.
ϕ_1, ϕ_2	Volume fraction of solvent and solute respectively in solution.
ϕ_{cel}	Volume fraction of cellulose in derivative.
ϕ_i, ϕ_r	Incidence and reflection angles in air.
$\chi_{1,2}$	Polymer-solvent interaction parameter.
ω_1, ω_2	Weight fraction of solvent and solute respectively in solution (Chapter III).
ω_{cel}	Weight fraction of cellulose in derivative.
ω_{der}	Weight fraction of derivative in solution (Chapter V).

CHAPTER I

INTRODUCTION

3

Liquid crystals or mesophases can be regarded as ordered fluids which exhibit some of the properties of both solids and liquids. The constituent molecules of a liquid crystal are very strongly elongated and are generally small organic molecules, long helical rods, or complex associated structures of molecules or ions. Liquid crystals can be classified as either thermotropic or lyotropic. Thermotropic liquid crystals or thermomesophases are formed when certain crystalline solids are heated. Lyotropic liquid crystals or lyomesophases are formed from isotropic solutions when a critical concentration of one of the components has been exceeded.

This introduction will be divided into three sections each of which will describe a particular group of liquid crystals. The first section will deal with low molar mass mesophases and the evolution of liquid crystal terminology. The next section will describe polymeric liquid crystals with emphasis on their structure, properties, and current commercial importance. The final section will detail the development of cellulosic mesophases and in particular hydroxypropylcellulose, the subject of this thesis.

I.1 Low Molar Mass Mesophases

Nearly a century has elapsed since the discovery of the first liquid crystalline compounds by Reinitzer (1-2) and Lehmann (3-5).

Reinitzer found that on heating solid cholesteryl benzoate it 'melted' to give a material which exhibited double refraction, a high optical activity, beautiful iridescent colors, yet was in a liquid state. Compounds possessing these four properties later came to be known as cholesteric liquid crystals. They were the first class of liquid crystals to be discovered, perhaps, because of their distinctive iridescent colors. The term liquid crystal was originally coined by Lehmann in 1890 (3). Lehmann and Reinitzer are regarded as the co-discoverers of liquid crystals.

Vorländer in 1908 (6) was the first to investigate the chemical nature of liquid crystalline systems. He concluded that the compounds most likely to exhibit liquid crystalline behavior on heating should be those that contained asymmetric molecules and a rigid linear structure. Friedel, in 1922 (7), developed a classification scheme for liquid crystals based on the microscopic appearance of the mesophase under crossed polars. Three distinct classes of liquid crystals were possible: nematic, cholesteric, and smectic.

Nematic ($\nu\eta\mu\alpha$ = thread) liquid crystals are substances that exhibit a thread-like appearance under the crossed polars of a light microscope. Subsequent work has shown that nematic mesophases possess an orientational order in that all the molecules are essentially parallel along their long axes, but the molecules themselves are positionally disordered as is illustrated schematically in Figure I.1. Cholesteric liquid crystals, so named because they are generally derivatives of

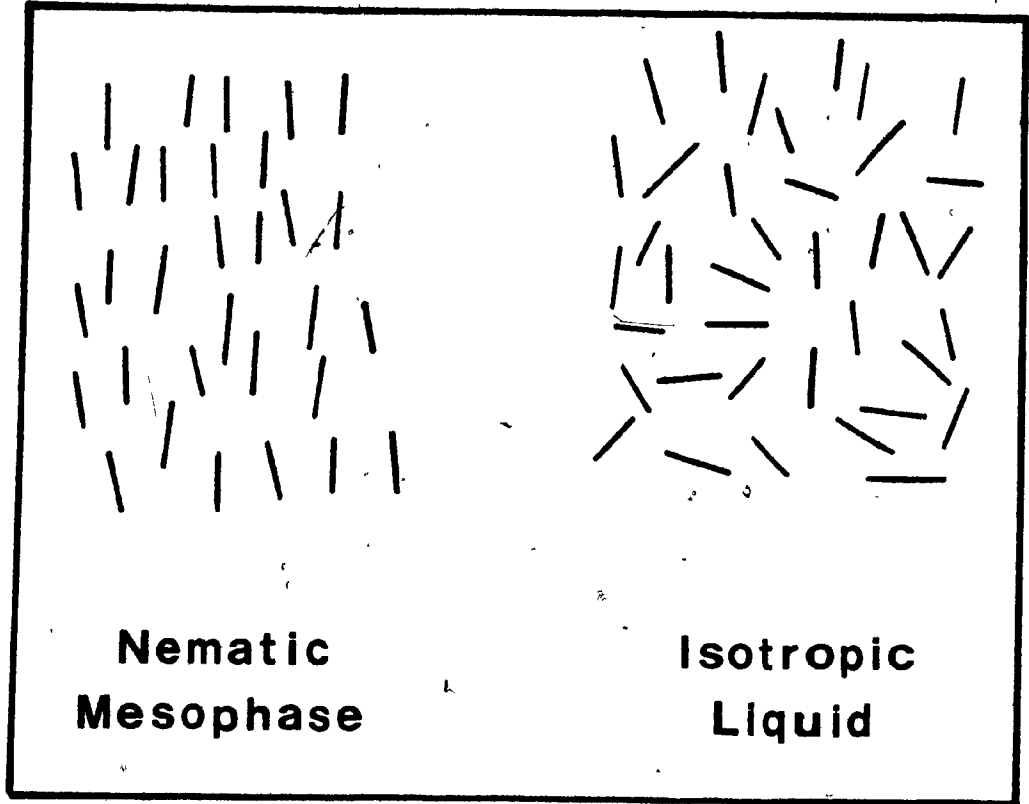


FIGURE I.1 Schematic view of a nematic liquid crystal with orientational order. Contrast this with an isotropic liquid in which the molecules are randomly oriented.

cholesterol (which itself does not form a mesophase), possess a parallel molecular alignment that is very reminiscent of that found in nematics and, for this reason, the cholesterics are sometimes regarded as a subgroup of the nematics rather than as a distinct class by themselves. Mauguin in 1911 (8-9) undertook a study of the unusual optical properties (high rotatory power and iridescence) of cholesterics. He found that the constituent chiral molecules of the cholesteric were distributed in a series of parallel layers that traced out a twisted or helicoidal structure. It was, in fact, the presence of this helicoidal structure — and not that of the chiral molecules themselves — that accounted for the very high optical activity of the cholesteric. The long axes of the chiral molecules were postulated to lie perpendicular to the helicoidal optical axis and this cholesteric arrangement is depicted schematically in Figure 1.2. The origin of the helicoidal twist was and today still is unknown, but it may, perhaps, be related to a combination of chiral and steric factors. When white light strikes the helicoidal structure it is split into its constituent components and is reflected in a unique manner. The polarizing ability of the helicoidal layers causes some wavelengths to be destructively scattered while others are constructively reflected. If the reflected wavelength is between 300 and 700 nm, then the cholesteric mesophase exhibits lovely iridescent colors. The iridescent color of the mesophase may be altered by changing the temperature (for thermomesophases) or the solution concentration (for lyomesophases). The iridescent color of the cholesteric also changes with the angle at which the mesophase is viewed. Cholesterics with their chiral molecules and helicoidal structure are the

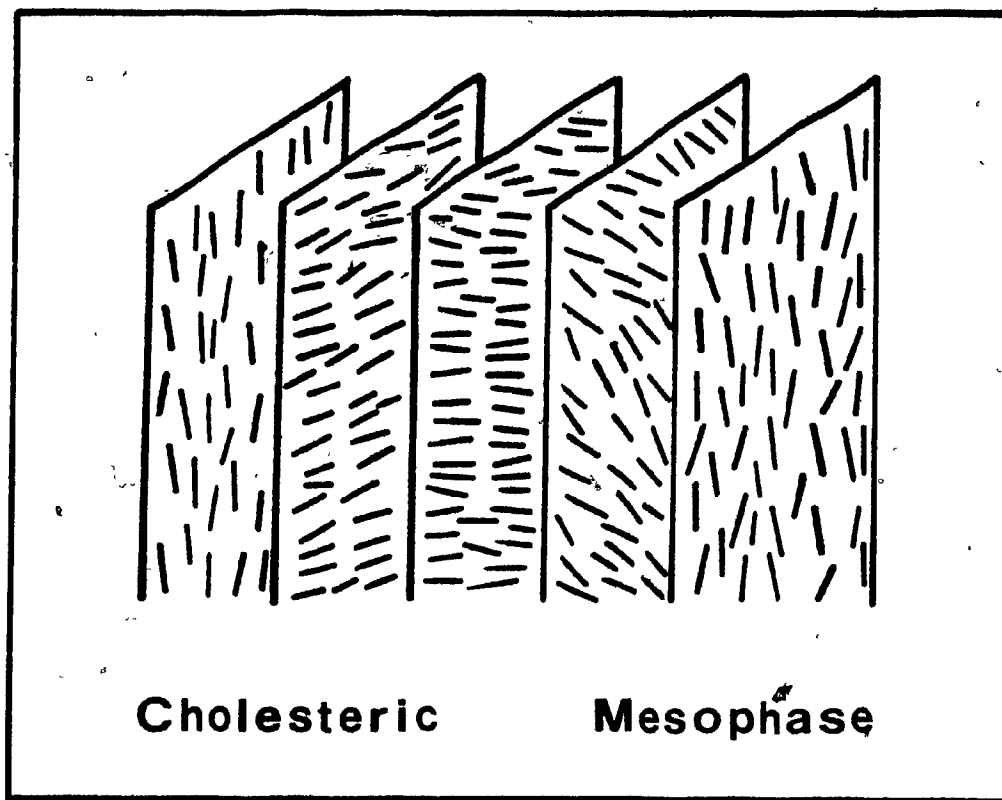


FIGURE I.2 Schematic view of the spiral molecular arrangement found in a cholesteric liquid crystal. Successive planes have been drawn for convenience rather than to represent any real physical condition. The diagram shows that the cholesteric is merely a twisted nematic.

only class of liquid crystals capable of exhibiting iridescent colors. Under crossed polars cholesterics may exhibit one of three possible textures (10), the focal conic being the most prevalent.

The third class of liquid crystals are the smectics. The molecules in this mesophase are arranged with their long axes essentially parallel. However, the molecules are further distributed in well defined and distinct layers that give the smectic a stratified structure. This particular molecular arrangement was first noted in soap (= σμπγμα) systems and, hence, the smectic name was derived. Within a layer the molecular alignment may be very regular or irregular and several smectic types ranging from A to H are recognized (10-11). Figure I.3 schematically depicts the molecular arrangement to be found in the smectic A and C mesophases. Smectics because of their stratified structure are the most ordered of the three liquid crystalline classes. Smectic liquid crystals exhibit focal conic textures when viewed in the light microscope. They are, for this reason, difficult to distinguish from cholesterics without further study.

Structural analysis by x-ray has shown that liquid crystals are neither crystals nor fluids; rather, the liquid crystal is intermediate in order between the three-dimensional molecular arrangement of a crystalline solid and the random molecular orientation found in a liquid. Optically, mesophases behave like crystalline solids in that they are birefringent; they do, however, retain the flow properties of liquids.

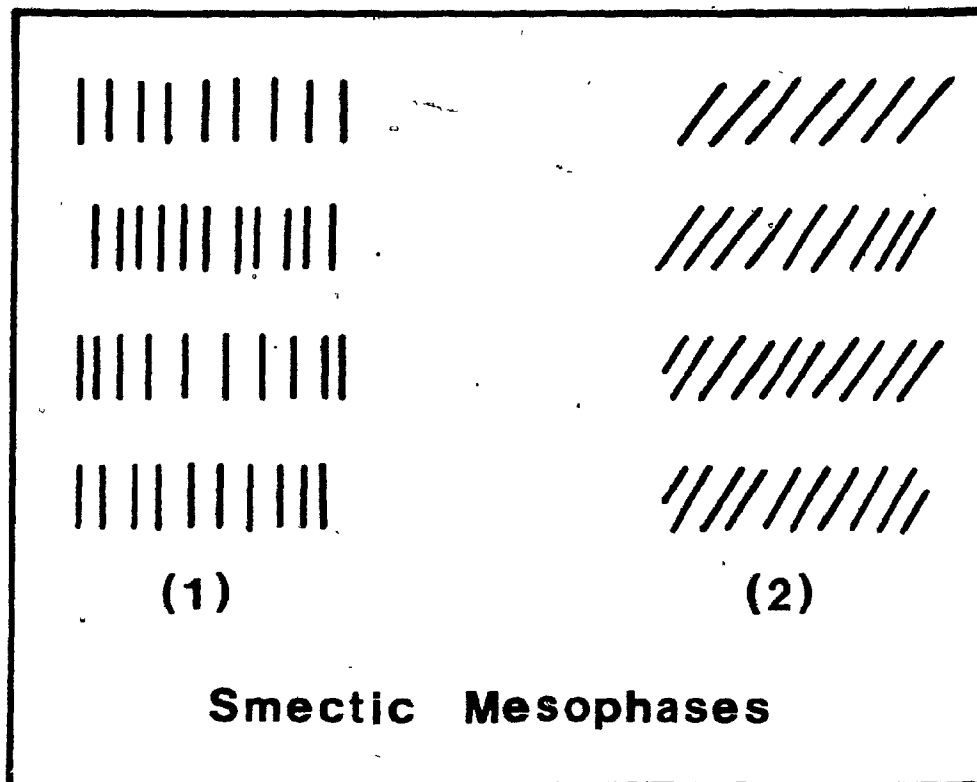


FIGURE I.3 Illustration of the stratified layers found in a smectic liquid crystal. The long axes of the molecules in each layer are parallel and they are also perpendicular to the plane of the layer: Smectic A structure (1) and Smectic C structure (2).

Electric (12-13) and magnetic (14-15) fields have been found to preferentially align the molecules in both nematic and smectic mesophases, thereby providing further evidence that liquid crystals behave very much like fluids. The most studied liquid crystals until 1940 had been the simple one-component thermotropics. The first lyotropic systems to be investigated were the sodium and ammonium soaps of fatty acids in aqueous (16) and organic (17-18) solvents. The phase diagrams for these systems (19-20) confirmed Vorländer's postulate that liquid crystals could exhibit polymorphism (21).

By 1960 the number of low molar mass compounds exhibiting mesomorphic behavior was very large as can be seen in the tabular listing of these materials by Kast (22). A more detailed history of low molar mass liquid crystals can be found in the excellent review by Kelker (23).

I.2 Polymeric Mesophases

Aqueous tobacco mosaic virus (TMV) solutions were found to undergo an anisotropic phase separation when a critical concentration of TMV (~ 5%) in solution had been exceeded (24). Since the TMV molecules were known to have a rod-like conformation in solution it appeared that, in addition to the lyotropic soap systems described above, there existed a second type of lyotropic liquid crystalline system formed from rod-like species in solution. In 1949 Onsager developed a theory (25) to account

for the anisotropic phase separation exhibited by aqueous TMV solutions. He proposed that the asymmetric shape of the stiff TMV molecules in solution was alone sufficient to bring about anisotropic phase separation when some critical solute concentration, which depended on the length and the diameter of the constituent rod-like molecules, had been exceeded.

In 1951 De Vries developed a theory (26) to account for the variation in optical rotatory power with wavelength for cholesteric mesophases. His cholesteric model consisted of a series of birefringent layers each of which was slightly twisted from the other in such a manner as to trace out a helicoidal structure which could be either left- or right-handed. De Vries did not offer an explanation for the origin of the twist between the layers beyond stating that if the twist angle were increased or decreased, the reflection wavelength of the cholesteric would be changed. De Vries' theory was found to qualitatively fit the experimental optical activity data for several cholesteric systems (27-28). Ferguson (29) and Chandrasekhar (30), in the late 1960's, each independently tried to refine and extend De Vries' theory.

The first group of conventional polymeric compounds found to form liquid crystals were the polypeptides. Elliott and Ambrose (31) found that poly- γ -benzyl-L-glutamate (PBLG) solutions, above some critical concentration, exhibited distinct birefringence and local regions of spontaneous orientation. In 1956 Robinson (32) found that PBLG solutions showed microscopic periodicity lines and very large optical activities

that were reminiscent of those characteristic of low molar mass cholesterics. This was the first indication that a polymer could form a type of liquid crystal analogous to those formed by low molar mass substances. Robinson found that, not only PBLG, but also other related polypeptides (33-36) could form the three classes of liquid crystals previously described by Friedel. Moffitt had studied the optical activity of PBLG in several solvents (37-38) and Robinson noted that only in those solvents in which PBLG was reported to be in a helical conformation would a lyotropic liquid crystal form. If the PBLG molecules in solution were in a random conformation, then no mesophase would form even at very high concentrations. Thus polymeric liquid crystals seem to require a stiff molecular structure for the formation of a stable mesophase.

Flory, at about this time, formulated a theory (39) to account for the anisotropic phase separation of polymeric systems. He postulated that as the number of stiff rod-like molecules in a solution was increased, the system could not tolerate a random distribution of these particles. Entropically at a high polymer density the most stable state was an ordered array of rods. Thus, as the polymer concentration in a solution was increased above some critical value, the system would undergo a phase separation into a dilute isotropic phase and an anisotropic ordered (liquid crystalline) phase. Flory developed a corresponding theory (40) for polymeric systems composed of semi-flexible molecules in which chain flexibility determined when anisotropic phase separation would occur.

The discovery that extended chain aromatic polyamides (41-43), notably KEVLAR or poly(p-phenylterephthalamide), exhibit liquid crystalline behavior in solution and that fibers extruded or spun from these solutions are highly oriented and very strong has spurred the growth, development, and commercialization of polymeric liquid crystals. The replacement of high cost and heavy metal fibers in materials by less expensive and lighter polymeric fibers of equal or superior tensile strength and modulus is very appealing commercially.

Both naturally occurring and synthetic polymers are found to form liquid crystals. Indeed, 2 to 5% of all organic compounds known are able to exist in a liquid crystalline phase. The exoskeleton of the scarabaeid beetle exhibits iridescent colors and is reported to be the optical analogue of a cholesteric liquid crystal (44). This discovery has prompted a number of biologists to suggest that naturally occurring liquid crystals with their unique left- and right-handedness might be important in biological processes that require stereospecific enantiomers.

There is some confusion in the literature arising from the assumption that all flowing materials exhibiting birefringence are liquid crystals. Care must be exercised before a polymeric melt or solution is classified as a liquid crystal because shear effects can induce a temporary birefringence which dissipates with time as the molecules in the polymer relax. Tables I.1 and I.2, albeit by no means complete, do provide an overview of the types of polymers which are reported to form thermotropic

TABLE I.1

Representative Listing of Polymeric Thermotropic Liquid Crystals

Polymer	Liquid Crystal Type (if reported)	Structure	References
Polyphosphazines		$\{N=P-R_1-R_2\}_n$	45
Poly(p-xylene)	Smectic	$\{ \text{C}_6\text{H}_4-\text{CH}_2-\text{CH}_2 \}_n$	45
Polydiethylsiloxane		$\{Si-(CH_3)_2-O\}_n$	45,46
Polymerized coal tars			45
Polymerized petroleum pitches			45,47
Poly(N-p-methoxybenzylilene-p-n-butylaniline)	Nematic	$\{ \text{C}_6\text{H}_4(R_1)-CH_2=N-C_6\text{H}_4(R_2)-O-(CH_2)_x-O \}_n$	45
Linear polyethylene melts	Smectic	$\{CH_2-CH_2\}_n$	48
Isotactic polypropylene	Smectic	$\{CH_2-CH-(CH_3)\}_n$	48
Poly[bis(chlorophenoxy)phosphazene]	Imperfect Smectic	$\{ \text{C}_6\text{H}_3(\text{Cl})-O \}_2 P=N \}_n$	49

TABLE I.1 (continued)

Representative Listing of Polymeric Thermotropic Liquid Crystals

Polymer	Liquid Crystal Type (if reported)	Structure	References
Poly(terephthalic hydrazide)			50
Copolyesters of poly(ethylterephthalate) and dicarboxylic acids or acetylated difunctional phenols		$\left[\text{CO}-\text{C}_6\text{H}_4-\text{COO}-(\text{CH}_2)_2-\text{O} \right]_n$ (PET)	51
Comblike methacrylic polymers with cholesteric mesogenic (R_3) side groups		$\left[\text{CH}_2-\overset{\text{CH}_3}{\underset{\text{CONH}(\text{CH}_2)_{2-11}-R_3}{\text{C}}} \right]_n$	52
Copolymers of poly(cholesteryl-methacrylate) and poly(cholesteryl acryloxybenzoate)	Smectic		53
Copolymer of cholesteryl methacrylate and <i>n</i> -alkyl methacrylates			54
Poly[N-(<i>p</i> -cyanobenzylidene)- <i>p</i> -aminostyrene]	Nematic		55

TABLE I.1 (continued)

Representative Listing of Polymeric Thermotropic Liquid Crystals

Polymer	Liquid Crystal Type (if reported)	Structure	References
Poly[p-phenylenebis(N-methylene-p-aminostyrene)]	Nematic		55
Poly(oxydodecanedioxy-1,4-phenylene-2-methylvinylene)-1,4-phenylene		$-\text{OOC}[(\text{CH}_2)_{10}-\text{COO}-\text{C}_6\text{H}_4-\text{C}(\text{CH}_3)=\text{CH}-\text{C}_6\text{H}_4]_n$	56
Polymers with rigid structures	Smectic or Nematic	$[\text{CH}=\text{C}(\text{CH}_3)-\text{COOR}-\text{C}_6\text{H}_4-\text{C}\equiv\text{N}-\text{C}_6\text{H}_4-\text{R}]_n$ or $[\text{CH}=\text{C}(\text{CH}_3)-\text{COO}-\text{C}_6\text{H}_4-\text{C}\equiv\text{N}-\text{C}_6\text{H}_4-\text{O}]_n$	57
Polyakanoates of dimethylbenzazine	Smectic or Nematic	$[\text{C}_6\text{H}_4-\text{C}(\text{CH}_3)=\text{N}-\text{N}=\text{C}(\text{CH}_3)-\text{C}_6\text{H}_4-\text{O}]_n$	45
Copolyester of PET and p-hydroxybenzoic acid melts			45
Copolyester of PET and p-acetoxybenzoic acid			58

TABLE I.1 (continued)

Representative Listing of Polymeric Thermotropic Liquid Crystals

Polymer	Liquid Crystal Type (if reported)	Structure	References
Copolymers of cholesteryl acrylate and cholesteryl methacrylate			59
Copolymers of alkyl or alkylmethacrylates and cholesteric esters of methacryloyl- ω -aminocarboxylic acids		$\left[\text{CH}_2 - \underset{\text{CONH}(\text{CH}_2)_n - \text{COOCH}}{\text{C}(\text{CH}_3)} \right]_n$	60,61
Poly(N-methacryloyl-N-acyl-)derivatives of L-lysine		$\left[\text{CH}_2 - \underset{\text{CONH}(\text{CH}_2)_4 \text{CH-NHCOR}'}{\text{C}(\text{CH}_3)} \right]_n$ COOH	61,62
Composite of poly(γ -butyl-L-glutamate) and butyl acrylate or poly(butyl acrylate)	Cholesteric	<p style="text-align: center;">OR</p> $\left[\text{CH}_2 - \underset{\text{COO}-\text{C}_6\text{H}_4-\text{C}(=\text{O})-\text{C}_6\text{H}_4-\text{O}-\text{C}_6\text{H}_{13}}{\text{C}(\text{CH}_3)} \right]_n$	63

TABLE I.1 (continued)

Representative Listing of Polymeric Thermotropic Liquid Crystals

Polymer	Liquid Crystal Type (if reported)	Structure	References
Polyesters of dihydroxy-diphenoxy-alkanes and terephthalic acid	Nematic	$\left[\text{O}-\text{C}_6\text{H}_4-\text{O}-(\text{CH}_2)_n-\text{O}-\text{C}_6\text{H}_4-\text{O}-\text{C}(=\text{O})-\text{C}_6\text{H}_4-\text{C}(=\text{O}) \right]_n$	64
Polyesters of (p-carboxyphenoxy)decane and hydroquinones	Nematic	$\left[\text{C}(=\text{O})-\text{C}_6\text{H}_4-\text{O}-(\text{CH}_2)_{10}-\text{O}-\text{C}_6\text{H}_4-\text{O}-\text{C}(=\text{O})-\text{C}_6\text{H}_3(\text{Cl})(\text{CH}_3) \right]_n$	64
Co[poly(ethylene terephthalate)-p-oxybenzoate]	Nematic		65
Propoxypropylcellulose	Cholesteric		66

* By convention, the symbol C_6H_4 is used throughout to represent the benzene ring, double bonds being omitted.

R_1, R_2 represent alkyl or alkyloxy groups

R_3 represents mesogenic cholesteric groups

R^t represents $\text{C}_x\text{H}_{2x+1}$ groups

R represents alkyloxy groups of variable length

Ch represents cholesteric groups

TABLE I.2

Typical Polymeric Compounds Reported to Form Lyotropic Liquid Crystals

Polymer	Structure	Solvent	Liquid Crystal Type (if reported)	References
Poly(1,4-benzamide)	$\text{[NH-}\langle\text{hexagon}\rangle\text{-CO]}_n$	DMAc-LiCl HF H_2SO_4 TMU-LiCl	Nematic " " "	42,67 42,68 42 42
Poly(1,4-phenyleneterephthalamide) or PPD-T	$\text{[NH-}\langle\text{hexagon}\rangle\text{-NHCO-}\langle\text{hexagon}\rangle\text{-CO]}_n$	H_2SO_4 HMPA-NMP-LiCl	Nematic "	43,69-71 43,68
Poly(chloro-PPD-T)		DMAc-LiCl H_2SO_4	Nematic "	43 69
Various extended chain aromatic polyamides	[NH-R-CO]_n	See reference	Nematic	41
Poly(γ -benzyl-L-glutamate) or PBLG	[NH-CH-CO]_n $(\text{CH}_2)_2\text{-COOCH}_2\text{-}\langle\text{hexagon}\rangle$	Dioxane m-Cresol DMF TFAA:m-cresol	Cholesteric " " "	69,72-76 70,75,77-80 73,75,81-82 83

TABLE I.2 (continued)

Typical Polymeric Compounds Reported to Form Lyotropic Liquid Crystals

Polymer	Structure	Solvent	Liquid Crystal Type (if reported)	References
Poly(γ -benzyl-L-glutamate) or PBLG	$\left[\begin{array}{c} \text{NH}-\text{CH}-\text{CO} \\ \\ (\text{CH}_2)_2-\text{COOCH}_2-\text{C}_6\text{H}_5 \end{array} \right]_n$	CHCl_3	Cholesteric	73-75
		CH_2Br_2	"	76
		CH_2Cl_2	"	73,75
		CH_2Cl_2 :dioxane	Nematic	36,75
		$\text{C}_2\text{H}_4\text{Cl}_2$	Cholesteric	80
		$\text{C}_2\text{H}_3\text{Cl}_3$	"	80
		$\text{C}_2\text{H}_2\text{Cl}_4$	"	73-74
		BA	"	78
		THF		84
		C_6H_6	Cholesteric	85
	C_6H_6	Smectic	75,86	
Poly(γ -methyl-D-glutamate)	$\left[\begin{array}{c} \text{NH}-\text{CH}-\text{CO} \\ \\ (\text{CH}_2)_2-\text{COOCH}_3 \end{array} \right]_n$	CH_2Cl_2	Cholesteric	87
Poly(γ -propyl-L-glutamate)		m-Cresol	Cholesteric	78

TABLE I.2 (continued)

Typical Polymeric Compounds Reported to Form Lyotropic Liquid Crystals

Polymer	Structure	Solvent	Liquid Crystal Type (if reported)	References
Poly(γ -ethyl-L-glutamate)	$\left[\text{NH}-\underset{\text{CH}_2\text{COOCH}_2\text{CH}_3}{\text{CH}}-\text{CO} \right]_n$	Dioxane	Cholesteric	76
		CH_2Cl_2	"	76
		CH_2Br_2	"	76
		$\text{CH}_3\text{COOC}_2\text{H}_5$	"	35
Poly(γ -butyl-L-glutamate) or PBuLG		BuA	Cholesteric	88
		TGDM	"	89
Poly(β -benzyl-L-aspartate) or PBLA	$\left[\text{NH}-\underset{\text{CH}_2\text{COOCH}_2\text{C}_6\text{H}_5}{\text{CH}}-\text{CO} \right]_n$	CHCl_3	Cholesteric	36
Composite of PBuLG and poly- merized butyl acrylate or PBuA		BuA	Cholesteric	88-89
Poly(L-glutamic acid) or PLGA	$\left[\text{NH}-\underset{\text{CH}_2\text{COOH}}{\text{CH}}-\text{CO} \right]_n$	DMAA		88-90

TABLE I.2 (continued)

Typical Polymeric Compounds Reported to Form Lyotropic Liquid Crystals

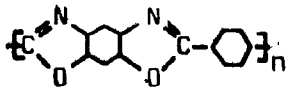
Polymer	Structure	Solvent	Liquid Crystal Type (if reported)	References
Composite of PLGA and poly-DMAA		DMAA	Cholesteric	90
Copolymer of PBLA and poly(γ -benzyl-D-glutamate)		CHCl_3	Cholesteric	35
Poly(bisbenzoxazole)		H_2SO_4 ClSO_3H $\text{CH}_3\text{SO}_3\text{H}$		91 91 91
Poly(phenylethyl)isocyanide			Cholesteric	92
Poly(terephthalic)hydrazide		$\text{C}_5\text{H}_5\text{N}$ $(\text{C}_2\text{H}_5)_2\text{NH}$		50 50

TABLE 1.2 (continued)

Typical Polymeric Compounds Reported to Form Lyotropic Liquid Crystals

Polymer	Structure	Solvent	Liquid Crystal Type (if reported)	References
Poly[bis(trifluoroethoxy)- phosphazene]		See reference		93
12-Hydroxyoctadecanoic acid		CCl_4	Smectic	94
Poly(ϵ -carbobenzoxyllysine)	$\left[\text{NH}-\underset{\text{CH}_2}{\text{CH}}-\text{CO} \right]_n$ $\text{(CH}_2\text{)}_4\text{NHCOOCH}_2\text{-}$ 	DMF	Cholesteric	82
Cellulose		NMNO TFAA: $\text{CH}_2\text{ClCH}_2\text{Cl}$	Nematic	95 96
Cellulose acetate		TFAA		97
Cellulose triacetate		See reference		93
Nitrocellulose		See reference		93

TABLE I.2 (continued)

Typical Polymeric Compounds Reported to Form Lyotropic Liquid Crystals

Polymer	Structure	Solvent	Liquid Crystal Type (if reported)	References
Hydroxypropylcellulose		H ₂ O	Cholesteric	69,98-101
		CH ₃ OH	"	102
		CH ₃ CH ₂ OH	"	103-104
		Dioxane	"	103,105
		THF	"	105
		C ₅ H ₅ N	"	103,105
		CH ₂ CH ₂ OCH ₃		103
		CH ₃ COOH	"	93,101
	See reference		"	105
Acetoxypopylcellulose		CH ₃ COCH ₃	Cholesteric	106
DNA		0.1M NaCl	Cholesteric	35
RNA			Cholesteric	58

TABLE I.2 (continued)

Typical Polymeric Compounds Reported to Form Lyotropic Liquid Crystals

Polymer	Structure	Solvent	Liquid Crystal Type (if reported)	References
Various biopolymers			Cholesteric	107-109
Poly(butylisocyanate)*				110
Poly trans-bis(tri-n-butylphosphine)platinum-1,4-butadiynediyl*	$\begin{array}{c} \text{P-n(C}_4\text{H}_9)_3 \\ \\ \text{[Pt-C}\equiv\text{C-C}\equiv\text{C}]_n \\ \\ \text{P-n(C}_4\text{H}_9)_3 \end{array}$			111
Polyquinolines*				66

* Polymeric systems likely to form lyotropic mesophases since they have rigid backbones

R represents aromatic ring groups

DMAc is N,N-dimethylacetamide	TFAA is trifluoroacetic acid	TGDM is triethylene glycol dimethacrylate
TMU is tetramethylurea	BA is benzyl alcohol	DMAA is N,N-dimethylacrylamide
HMPA is hexamethylphosphoramide	THF is tetrahydrofuran	DMF is dimethylformamide
NMP is N-methylpyrrolidone-2	BuA is butyl acrylate	NMNO is N-methylmorpholine-N-oxide

or lyotropic mesophases. The diversity of the polymers that form liquid crystals has led to a re-examination of the structural requirements, properties, and uses for these materials.

Polymeric liquid crystals by analogy with low molar mass mesophases can be classified as nematics, smectics, or cholesterics. Polymers can also be divided on the basis of whether the liquid crystal or mesogenic elements are incorporated into the main chain backbone or the side chains of the polymer. The mesogenic element of a polymeric liquid crystal must be asymmetric and relatively stiff. Internal hydrogen bonding (58), an extended series of alternating double or triple bonds (55), aromatic rings (55), and aromatic rings separated by flexible aliphatic groups (56) are the primary sources of main chain rigidity. In the last situation, as the length of the aliphatic groups is increased, the liquid crystalline character of the polymer is decreased until, finally, only an isotropic amorphous polymer remains. Thus although chain stiffness and molecular asymmetry are paramount requirements for the formation of ordered mesophases, the system can, nevertheless, tolerate a certain amount of main chain flexibility while still retaining its liquid crystalline character.

Polymers with rigid backbones can accommodate mesogenic side groups either by direct attachment or by separation with non-mesogenic spacers. If the mesogenic side groups are chemically linked directly to the main chain, steric factors arising from the interaction and subsequent packing of the side groups determine if a liquid crystal will form.

Semi-flexible main chains can be sufficiently distorted to permit a good packing of side groups and the resulting liquid crystals are smectic (52,57). Polymethylene spacers between the backbone and the mesogenic side groups provide sufficient flexibility for the side chains to pack well without distortion of the main chain and nematic liquid crystals are formed (57,61). Liquid crystals with methylene bridges or spacers are referred to as comb-like mesophases (52). Stereoregularity in the mesogenic side groups is not always required to form a mesophase (54); rather, it would seem that good mesogenic side group packing is the primary requirement for the formation of this type of polymeric mesophase (54). It is of note that in this type of polymeric liquid crystal the majority of the mesogenic side groups are cholesteric in character. Nematic and smectic side groups are found to produce amorphous or crystalline rather than mesomorphic polymers (61).

Polymerization of monomeric liquid crystals by irradiation or by use of initiators results in a mesomorphic polymer product in only one of every five attempts (61). The key requirement for mesomorphic polymerization seems to be extensive cross-linking amongst the liquid crystalline monomer units (55,88). The absence of cross-links or the addition of non-mesogenic comonomers (54) results in the formation of isotropic amorphous polymers. Bifunctional monomers (90) and cross-linking agents (63) seem to be able to freeze the mesomorphic character of the monomer into the polymer although the mesomorphic structure of the monomer is generally altered on polymerization (55).

It is impossible at present to predict if and what type of meso-phase will form when liquid crystal monomers are polymerized or when polymers are synthesized with mesogenic side groups. Geometric factors, main chain rigidity or flexibility, the presence of flexible spacers, side group packing, the distribution of the side groups on the main chain, and the polarizability of these groups acting either alone or in combination determine the type of liquid crystal which will ultimately form (55). Suffice it to say that, in general, molecules possessing strong lateral but weak longitudinal interactions will form ordered smectics, while those exhibiting strong longitudinal but weak lateral interactions will tend to form nematics (55,112). The balance that is achieved between molecular lateral and longitudinal forces also plays a role in determining the type of liquid crystal which will be formed (55).

Two novel polymeric liquid crystals must be mentioned. Optically active 12-hydroxyoctadecanoic acid gel is a unique smectic liquid crystal that is believed to have a super helicoidal structure (94). This helicoidal structure is thought to result from a series of helical fibers that are molecularly associated by hydrogen bonding in which the molecules appear to have a smectic C structure. This super helicoidal structure is quite different from that found in the cholesteric mesophase depicted in Figure I.2. Optically active N-acylamino acids form a liquid crystal suspension in benzene and chloroform (113). In these solvents the dispersed acid exhibits birefringence, optically negative spherulites, circular dichroism, and iridescence (113). The iridescence of these

solutions results from a refractive index difference that exists between the layers of solvent and suspended polymer (Christiansen effect) rather than from the presence of a series of equally spaced birefringent layers as is the case for most other liquid crystals. The iridescence of the acid changes reversibly with solvent composition, temperature, and increasing length of the acyl content of the acid.

Current research into the physical properties of polymeric liquid crystals is diversified and plentiful. Rheological (58,70) and rheo-optical (77) studies have shown that shear partially disrupts the cholesteric liquid crystalline structure, but that on relaxation the cholesteric structure readily re-forms (98,114). Diffusion and velocity flow studies (115) on model and liquid crystalline systems prove that motion parallel, rather than perpendicular, to the molecular axis is easier. Qualitative measurements have been made to evaluate the perfection of molecular order within the mesophase through the use of order parameters (72,116). Depolarized laser light scattering experiments (80) are reported to permit the quick and accurate evaluation of the helicoidal handedness of cholesteric mesophases. Extensive work has also been carried out on the conversion of cholesteric into nematic liquid crystals and vice versa. In the former case magnetic fields (68,85), electric fields (75), or equal mixtures of the left- and right-handed enantiomers of the cholesteric will produce a compensated or untwisted cholesteric (nematic). The conversion of nematics into cholesterics can be accomplished by the addition of optically active co-solvents (68) or

chiral solutes (117) to the nematic. The handedness of the resulting cholesteric is not always the same as that of the added solute; often a complex energy calculation is required to predict the handedness of the resulting cholesteric. Hajdo has found that the cholesteric helicoidal structure is sensitive to concentration and orientation gradients within the system (118-19). In addition, several theories have been developed to explain the origin of the cholesteric helicoidal twist. Samulski and Samulski (120) have invoked Van der Waals - Lifshitz forces and susceptibility theory to account for the helicoidal twist of cholesterics. Bouligand (107) has tried to relate the origin of the cholesteric helicoidal twist to the natural helical tendencies of many biological molecules. Goossens (121) has developed a statistical mathematical theory to explain the helicoidal twist and his theory is reported to work well for cholesterics formed by the addition of chiral solutes to nematics.

Liquid crystals in general, and cholesterics in particular, have been found to be very useful substances. They respond to very slight variations in temperature, electric and magnetic fields, and to ultrasonic waves. As a result liquid crystals have found use in radiology, surgery, and urology (122). They can be used as monitors, sensors, fever headbands, jewelry, reflection displays, digital displays in computers and watches, bandpass filters, circular polarizers, and a whole host of other optical devices (89,123). However, the most novel use of liquid crystals is as an art form (124-25). Since the mesophase can respond to temperature, humidity, and viewing angle changes, a liquid crystal painting can exhibit

many unusual visual effects. Cholesteric iridescence arises as a constructive interference effect making colors in this medium combine differently from those of conventional paints and pigments which absorb light (126). For example, the mixing of red and green paint will produce a gray-brown color; the same combination of red and green liquid crystals will result in a yellow color. This use of liquid crystals is still in its infancy.

Liquid crystals can be used as solvent media for chemical reactions. It has been reported (127-29) that reactions occurring in cholesteric mesophases exhibit enhanced rates and are more highly stereospecific than the same reactions carried out in non-mesomorphic solvents. Smectic and nematic liquid crystals, when used as solvents, appear to have little or no control over the stereospecificity of reactions. This property is unique to cholesteric mesophases. Racemic mixtures of sulfinates or sulfoxides exhibit a net optical activity when placed in a cholesteric solvent (130); however, the mixture does not necessarily have the same handedness as the cholesteric solvent. Untwisted or compensated cholesterics have been used as solvents to study solute molecular orientation in homogeneously oriented systems (131). The advantage in using compensated cholesterics rather than aromatic solvents is that the cholesterics do not absorb in the ultraviolet region of the spectrum. For more information about liquid crystals and polymeric mesophases in general, the reader is referred to any of the numerous papers (132-35) and books (136-48) which have appeared in the preceding

decade dealing with this topic.

1.3 Cellulosic Mesophases

Cellulose, which is found in the cell wall of virtually every plant (149), is the most abundant naturally occurring organic polymer. The importance of cellulose can be traced, not only to its abundance, but also to its use as a renewable source of fuel, paper, fiber, building and clothing materials. It is also the starting material for a number of important cellulose derivatives: mono-, di-, and triacetates, hydroxyethyl- and carboxymethylcellulose, cellulose nitrate, et cetera. Chemically cellulose is a polysaccharide consisting of several thousand glucose units joined together by 1,4 beta linkages (149). These bonds make the cellulose backbone relatively rigid and stiff. The inflexibility of the cellulosic chains was originally believed to play a dominant role in the crystallization of the cellulose and to preclude the formation of a stable cellulose based mesophase (40).

Hydroxypropylcellulose is the most recent cellulose ether to be commercially produced and its properties have not been as extensively investigated as those of the other cellulose derivatives (150). Hydroxypropylcellulose was the first cellulose derivative to form a lyotropic liquid crystal in both aqueous (98-100,104,114,151-52) and organic (101-05,153) solutions. Since the publication of this discovery

(99) it has been reported that cellulose itself (95-96,154-55) as well as several of its derivatives (97,106,156-62) also form liquid crystals.

The present investigation was undertaken, not only to amass more proof and information about the lyotropic behavior of hydroxypropylcellulose solutions, but also in the hope that by carefully examining the character and properties of hydroxypropylcellulose solutions, an explanation might be proposed as to why hydroxypropylcellulose and cellulose in general form lyomesophases.

References

1. F. Reinitzer, Monatsh. Chem., 9, 421 (1888).
2. F. Reinitzer, Ann. Physik., 27, 213-24 (1909).
3. O. Lehmann, Z. Phys. Chem., 5, 427 (1890).
4. O. Lehmann, Verhandl. d. Deutschen Phys. Ges. Sitzung V (16.3) 1900, p. 1.
5. O. Lehmann, "Flüssige Krystalle und die Theorien des Leben", Verlag, Leipzig, 1908.
6. D. Vorländer, "Krystallinisch-flüssige Substanzen", Enke, Stuttgart, 1908.
7. G. Friedel, Ann. Phys., 18, 273-474 (1922).
8. C. Mauguin, C. R. Acad. Sci., 151, 886-88 (1910).
9. C. Mauguin, Bull. Soc. Fr. Min., 34, 71-117 (1911).
10. G.W. Gray in "Liquid Crystals & Plastic Crystals", G.W. Gray and P.A. Winsor, Eds., Ellis Horwood Ltd., England, 1974, Vol. 1, pp. 106-15.
11. G.W. Gray in "The Molecular Physics of Liquid Crystals", G.A. Luckhurst and G.W. Gray, Eds., Academic Press, New York, 1979, Chapter 12.
12. V. Fréderiks and V. Tzvetkov, C. R. Acad. Sci. URSS, 2, 528-31 (1935).
13. V. Frédericksz and V. Zolina, Trans. Faraday Soc., 29, 919-30 (1933).
14. V.N. Tsvetkov, Acta Physicochim. URSS, 10, 555-78 (1939).
15. Y. Björnstaahl, Z. Phys. Chem. (Frankfurt am Main), 175, 17-37 (1935).
16. J.W. McBain, R.D. Vold, and M. Frick, J. Phys. Chem., 44, 1013-24 (1940).
17. A.S.C. Lawrence, Trans. Faraday Soc., 34, 660-77 (1938).
18. R.D. Vold, C.W. Leggett, and J.W. McBain, J. Phys. Chem., 44, 1058-71 (1940).
19. R.D. Vold, J. Phys. Chem., 43, 1213-31 (1939).

20. V. Luzzati, H. Mustacchi, A. Skoulios, and F. Hussen, Acta Cryst., 13, 660-67 (1960).
21. D. Vorländer, Trans. Faraday Soc., 29, 913-14 (1933).
22. W. Kast in "Landolt-Börnstein", K. Schafer and E. Lax, Eds., Springer, Berlin, 1960, Vol. II, Part 2a.
23. H. Kelker, Mol. Cryst. Liq. Cryst., 21, 1-48 (1973).
24. J.D. Bernal and I. Fankuchen, J. Gen. Physiol., 25, 111-46 (1941).
25. L. Onsager, Ann. N.Y. Acad. Sci., 51, 627-59 (1949).
26. Hl. De Vries, Acta Cryst., 4, 219-26 (1951).
27. R. Cano, Bull. Soc. Fr. Min., 90, 333-51 (1967).
28. R. Cano and P. Chatelain, C. R. Acad. Sci., 253, 1815-17 (1971).
29. J.L. Ferguson, Mol Cryst., 1, 293-307 (1966).
30. S. Chandrasekhar and K.N. Srinivasa Rao, Acta Crystallogr., Sect. A, 24, 445-51 (1968).
31. A. Elliott and E.J. Ambrose, Discuss. Faraday Soc., 9, 246-51 (1950).
32. C. Robinson, Trans. Faraday Soc., 52, 571-92 (1956).
33. C. Robinson and J.C. Ward, Nature, 180, 1183-84 (1957).
34. C. Robinson, J.C. Ward, and R.B. Beevers, Discuss. Faraday Soc., 25, 29-42 (1958).
35. C. Robinson, Tetrahedron, 13, 219-34 (1961).
36. C. Robinson, Mol. Cryst., 1, 467-94 (1966).
37. W. Moffitt and J.T. Yang, Proc. Natl. Acad. Sci. USA, 42, 596-603 (1956).
38. W. Moffitt, Proc. Natl. Acad. Sci. USA, 42, 736-46 (1956).
39. P.J. Flory, Proc. R. Soc. London, Ser. A, 234, 73-89 (1956).
40. P.J. Flory, Proc. R. Soc. London, Ser. A, 234, 60-73 (1956).
41. P.W. Morgan, Macromolecules, 10, 1381-90 (1977).

42. S.L. Kwolek, P.W. Morgan, J.R. Schaefgen, and L.W. Gulrich, Macromolecules, 10, 1390-96 (1977).
43. T.I. Bair, P.W. Morgan, and F.L. Killian, Macromolecules, 10, 1396-1400 (1977).
44. A.C. Neville and S. Caveney, Biol. Rev., 44, 531-62 (1969).
45. E.T. Samulski and D.B. DuPré in "Advances in Liquid Crystals", G.H. Brown, Ed., Academic Press, New York, 1979, Vol. 4, pp. 133, 135, 137, 138.
46. C.L. Beatty, J.M. Pochan, M.F. Froix, and D.D. Hinman, Macromolecules, 8, 547-51 (1975).
47. K. Roberts, R. Österlund, and C. Axberg, Tappi, 59, 156-59 (1976).
48. P.P.A. Smit, Colloid & Polymer Sci., 250, 27-37 (1972).
49. C. Desper and N. Schnieder, Macromolecules, 9, 424-28 (1976).
50. J.D. Hartzler and P.W. Morgan in "Contemporary Topics in Polymer Science", E.M. Pearce and J.R. Schaefgen, Eds., Plenum Press, New York, 1977, Vol. II, pp. 19-53.
51. F.E. McFarlane, V.A. Nicaly, and T.G. Davis in "Contemporary Topics in Polymer Science", E.M. Pearce and J.R. Schaefgen, Eds., Plenum Press, New York, 1977, Vol. II, pp. 109-41.
52. V.P. Shibaev, V.M. Moiseenko, Ya.S. Freidzon, and N.A. Platé, Eur. Polym. J., 16, 277-81 (1980).
53. E.C. Hsu, S.B. Clough, and A. Blumstein, J. Polym. Sci., Polym. Lett. Ed., 15, 545-50 (1977).
54. Y. Osada and A. Blumstein, J. Polym. Sci., Polym. Lett. Ed., 15, 761-67 (1977).
55. A. Blumstein, Macromolecules, 10, 872-74 (1977).
56. V. Petraccone, A. Roviello, A. Sirigu, A. Tuzi, E. Martuscelli, and M. Pracella, Eur. Polym. J., 16, 261-67 (1980).
57. J.H. Wendorff, H. Finkelmann, and M. Ringsdorf, J. Polym. Sci., Polym. Symp., 63, 245-61 (1978).
58. J.L. White and J.F. Fellers, J. Appl. Polym. Sci., Appl. Polym. Symp., 33, 137-73 (1978).

59. L. Strzalecki and L. Liebert, Bull. Soc. Chim. Fr., 597-605 (1973).
60. V.P. Shibaev, N.A. Platé, and Ya.S. Freidzon, J. Polym. Sci., Polym. Chem. Ed., 17, 1655-70 (1979).
61. N.A. Platé and V.P. Shibaev, J. Polym. Sci., Polym. Symp., 67, 1-16 (1980).
62. V.P. Shibaev, R.V. Tal'roze, F.I. Karakhanova, and N.A. Platé, J. Polym. Sci., Polym. Chem. Ed., 17, 1671-84 (1979).
63. T. Tsutsui and R. Tanaka, J. Polym. Sci., Polym. Lett. Ed., 18, 17-23 (1980).
64. S. Antoun, R.W. Lenz and J.I. Jin, J. Polym. Sci., Polym. Chem. Ed., 19, 1901-20 (1981).
65. W.R. Krigbaum and F. Salaris, J. Polym. Sci., Polym. Phys. Ed., 16, 883-94 (1978).
66. S.L. Tseng, G.V. Lavin, and D.G. Gray, presented in part at the 21st High Polymer Forum, Kingston, August 1981.
67. M. Panar and L.F. Beste, Macromolecules, 10, 1401-06 (1977).
68. W.G. Miller, Ann. Rev. Phys. Chem., 29, 519-35 (1978).
69. Y. Onogi, J.L. White, and J.F. Fellers, J. Polym. Sci., Polym. Phys. Ed., 18, 663-82 (1980).
70. H. Aoki, J.L. White, and J.F. Fellers, J. Appl. Polym. Sci., 23, 2293-314 (1979).
71. M.G. Dobb, D.J. Johnson, and B.P. Saville, J. Polym. Sci., Polym. Phys. Ed., 15, 2201-11 (1977).
72. N.S. Murthy, J.R. Knox, and E.T. Samulski, J. Chem. Phys., 65, 4835-39 (1976).
73. E.T. Samulski and A.V. Tobolsky, Biopolymers, 10, 1013-19 (1971).
74. D.L. Patal and D.B. DuPré, J. Polym. Sci., Polym. Lett. Ed., 17, 299-303 (1979).
75. D.B. DuPré and J.R. Hammersmith, Mol. Cryst. Liq. Cryst., 28, 365-82 (1974).
76. E. Iizuka, Adv. Polym. Sci., 20, 79-107 (1976).

77. T. Asada, H. Muramatsu, R. Watanabe, and S. Onogi, Macromolecules, **13**, 867-71 (1980).
78. H. Toriumi, Y. Kusumi, I. Uematsu, and Y. Uematsu, Polym. J., **11**, 863-69 (1979).
79. J. Hermans, J. Colloid Sci., **17**, 638-48 (1962).
80. T. Hashimoto, S. Ebisu, and H. Kawai, J. Polym. Sci., Polym. Lett. Ed., **18**, 569-76 (1980).
81. W.G. Miller, C.C. Wu, E.L. Wee, G.L. Santee, J.H. Rai, and K.G. Goebel, Pure Appl. Chem., **38**, 37-58 (1974).
82. E.L. Wee and W.G. Miller, J. Phys. Chem., **75**, 1446-52 (1971).
83. H. Toriumi, S. Minakuchi, Y. Uematsu, and I. Uematsu, Polym. J., **12**, 431-37 (1980).
84. D.L. Patel and D.B. DuPré, J. Polym. Sci., Polym. Phys. Ed., **18**, 1599-607 (1980).
85. D.L. Patel and D.B. DuPré, Mol. Cryst. Liq. Cryst., **53**, 323-34 (1979).
86. P. Doty, J.H. Bradbury, and A.M. Holtzer, J. Am. Chem. Soc., **78**, 947-54 (1956).
87. R.W. Filas and H. Stefanou, J. Phys. Chem., **79**, 941-43 (1975).
88. T. Tsutsui, R. Tanaka, and T. Tanaka, J. Polym. Sci., Polym. Lett. Ed., **17**, 511-20 (1979).
89. T. Tsutsui and R. Tanaka, Polymer, **21**, 1351-52 (1980).
90. T. Tsutsui and T. Tanaka, J. Polym. Sci., Polym. Lett. Ed., **15**, 475-79 (1977).
91. G.C. Berry in "Contemporary Topics in Polymer Science", E.M. Pearce and J.R. Schaefgen, Eds., Plenum Press, New York, 1977, Vol. II, pp. 55-96.
92. F. Millich, Adv. Polym. Sci., **19**, 117-41 (1975).
93. S.M. Aharoni, Polym. Prepr., Am. Chem. Soc., Div. Polym. Chem., **22** (1), 116-17 (1981).
94. T. Tachibana, T. Mori, and K. Hori, Bull. Chem. Soc. Jpn., **53**, 1714-19 (1980).

95. H. Chanzy, A. Péguy, S. Chaunis, and P. Monzie, J. Polym. Sci., Polym. Phys. Ed., 18, 1137-44 (1980).
96. D.L. Patel and R.D. Gilbert, J. Polym. Sci., Polym. Phys. Ed., 19, 1231-36 (1981).
97. P. Navard, J.M. Haudin, S. Dayan and P. Sixou, J. Polym. Sci., Polym. Lett. Ed., 19, 379-85 (1981).
98. T. Asada, Y. Yoshida, and S. Onogi, Polym. Prepr. Jpn., 27, 1366-69 (1978).
99. R.S. Werbowyj and D.G. Gray, Mol. Cryst. Liq. Cryst., 34, 97-103 (1976).
100. H. Toriumi, K. Miyasaka, and I. Uematsu, Rep. Prog. Polym. Phys. Jpn., 22, 31-34 (1979).
101. R.S. Werbowyj and D.G. Gray, presented in part at the 179th ACS National Meeting, Houston, March 1980.
102. R.S. Werbowyj and D.G. Gray, Macromolecules, 13, 69-73 (1980).
103. T. Tautsui and R. Tanaka, Polym. J., 12, 473-74 (1980).
104. J. Bheda, J.F. Fellers, J.L. White, Colloid & Polymer Sci., 258, 1335-42 (1980).
105. This Thesis, Chapter III.
106. S.L. Tseng, A. Valente, and D.G. Gray, Macromolecules, 14, 715-19 (1981).
107. Y. Bouligand in "Mesomorphic Order in Polymers and Polymerization in Liquid Crystalline Media", A. Blumstein, Ed., ACS Symposium Series #74, Washington, D.C., 1978, Chapter 15.
108. A.C. Neville and B.M. Luke, J. Cell Sci., 8, 93-109 (1971).
109. Y. Bouligand in "Liquid Crystalline Order in Polymers", A. Blumstein, Ed., Academic Press, New York, 1978, pp. 262-94.
110. J.B. Milstien and E. Charney, Macromolecules, 2, 678-81 (1969).
111. H. Fujita, M. Motowoka, T. Norisuye, and A. Teramoto, Polym. Prepr., Am. Chem. Soc., Div. Polym. Chem., 20 (1), 38-41 (1979).
112. W.O. Statton, Ann. N.Y. Acad. Sci., 83, 27-36 (1959).
113. K. Sakamoto, R. Yoshida, M. Hatano, and T. Tachibana, J. Am. Chem. Soc., 100, 6898-902 (1978).

114. T. Asada, K. Toda, and S. Onogi, Mol. Cryst. Liq. Cryst., 68, 231-46 (1981).
115. M. Bishop and E.A. Dimarzio, Mol. Cryst. Liq. Cryst., 28, 311-33 (1974).
116. H.S. Subramhanyam, C.S. Prabha, and D. Krishnamurti, Mol. Cryst. Liq. Cryst., 28, 201-15 (1974).
117. F.D. Saeva, Mol. Cryst. Liq. Cryst., 23, 171-77 (1973).
118. L.E. Hajdo and A.C. Eringen, J. Opt. Soc. Am., 69, 1017-23 (1979).
119. L.E. Hajdo and A.C. Eringen, J. Opt. Soc. Am., 69, 1509-13 (1979).
120. T.V. Samulski and E.T. Samulski, J. Chem. Phys., 67, 824-30 (1977).
121. W.J.A. Goossens, Mol. Cryst. Liq. Cryst., 12, 237-44 (1971).
122. H. Elser and R.D. Ennulat in "Advances in Liquid Crystals", G.H. Brown, Ed., Academic Press, New York, 1977, Vol. 2, pp. 63-163.
123. J.L. Ferguson, T.R. Taylor, and T.B. Harsch, Emerging Technology, 1970 (January).
124. M. Brochu, Science Dimension, 11, 4-7 (1979).
125. D.M. Makow, Color, 4, 25-32 (1979).
126. H. Simon, "The Splendor of Iridescence", Dodd Mead & Co., New York, 1971.
127. J.M. Nerbonne and R.G. Weiss, J. Am. Chem. Soc., 100, 2571-73 (1978).
128. J.M. Nerbonne and R.G. Weiss, J. Am. Chem. Soc., 100, 5953-54 (1978).
129. J.M. Nerbonne and R.G. Weiss, J. Am. Chem. Soc., 101, 402-07 (1979).
130. W.H. Pirkle and P.L. Rinaldi, J. Am. Chem. Soc., 99, 3510-11 (1977).
131. E. Sackmann, P. Krebs, H.U. Rega, J. Voss, and H. M \ddot{o} hwald, Mol. Cryst. Liq. Cryst., 24, 283-303 (1973).
132. G.H. Brown, Ed., Mol. Cryst. Liq. Cryst., 1966-82.
133. J.L. Ferguson, Scientific American, 211, 77-85 (August 1965).
134. G.H. Brown, Chemistry, 40, 10-18 (1967).
135. G.H. Brown, Anal. Chem., 41, 26A-39A (1969).

136. G.H. Brown, "Liquid Crystals", Gordon & Breach Sci. Publ., New York, 1969.
137. G.H. Brown, J.W. Doane, and V.D. Neff, "A Review of the Structure and Physical Properties of Liquid Crystals", Butterworths, London, 1971.
138. "Liquid Crystals", S. Chandrasekhar, Ed., Bangalore Book Printers, Bangalore, India, 1973.
139. "Liquid Crystals and Ordered Fluids", J.F. Johnson and R.S. Porter, Eds., Plenum Press, New York, 1970-78, Vols. 1-3.
140. "Liquid Crystals & Plastic Crystals", G.W. Gray and P.A. Winsor, Eds., Ellis Horwood Ltd., England, 1974, Vols. 1-2.
141. E.B. Priestley, P.J. Wojtowicz, and P. Sheng, "Introduction to Liquid Crystals", Plenum Press, New York, 1974.
142. P.G. de Gennes, "The Physics of Liquid Crystals", Clarendon Press, Oxford, 1974.
143. "Mesomorphic Order in Polymers and Polymerization in Liquid Crystalline Media", A. Blumstein, Ed., ACS Symposium Series #74, Washington, D.C., 1978.
144. "Advances in Liquid Crystals", G.H. Brown, Ed., Academic Press, New York, 1976-81, Vols. 1-6.
145. S. Chandrasekhar, "Liquid Crystals", Cambridge Univ. Press, London, 1977.
146. "Liquid Crystalline Order in Polymers", A. Blumstein, Ed., Academic Press, New York, 1978.
147. Septième Congrès International sur les Cristaux Liquides (Bordeaux, France), J. Phys., 40, Colloque C-3, Supplément 4 (1979).
148. "Liquid Crystals: The Fourth State of Matter", F.D. Saeva, Ed., Marcel Dekker Inc., New York, 1979.
149. J. Barsha and P. Van Wyck in "Encyclopedia of Chemical Technology", R.E. Kirk and D.F. Othmer, Eds., Interscience Publ., New York, 1949, Vol. 3, pp. 342-90.
150. G.D. Hiatt and W.J. Rebel in "High Polymers", N.M. Bikales and L. Segal, Eds., Wiley Interscience, New York, 1971, Vol. V, Part V, Chapter 17.
151. R.S. Werbowyj and D.G. Gray, presented in part at the Second Joint CIC-ACS Conference, Montreal, May-June 1977.

152. R.S. Werbowy and D.G. Gray, presented in part at the 177th ACS National Meeting, Hawaii, April 1979. Polym. Prepr., Am. Chem. Soc., Div. Polym. Chem., 20 (1), 102-05 (1979).
153. S.M. Aharoni, Polym. Prepr., Am. Chem. Soc., Div. Polym. Chem., 22 (1), 116-17 (1981).
154. H. Chanzy, A. Péguy, S. Chaunis, and P. Monzie, presented in part at the 179th ACS National Meeting, Houston, March 1980.
155. R.H. Marchessault and M. Dube, presented in part at the 179th ACS National Meeting, Houston, March 1980.
156. S.M. Aharoni, Mol. Cryst. Liq. Cryst., 56, 237-41 (1980).
157. J. Maeno, U.S. Patent 4 132 464, 1979.
158. M. Panar and O.B. Willcox, Belg. Patent 656 359, 1976.
159. M. Panar and O.B. Willcox, Fr. Patent 2 340 344, 1977.
160. M. Panar and O.B. Willcox, Fed. Rep. Ger. Patent 2 705 382, 1977.
161. S. Dayan, P. Maissa, M.J. Vellutini, and P. Sixou, J. Polym. Sci., Polym. Lett. Ed., 20, 33-43 (1982).
162. K. Shimamura, J.L. White, and J.F. Fellers, J. Appl. Polym. Sci., 26, 2165-80 (1981).

CHAPTER II

CHARACTERIZATION OF HYDROXYPROPYLCELLULOSE

II.1 Preparation

Hydroxypropylcellulose is a high molar mass polymer prepared commercially by a base catalyzed reaction at high temperature and pressure between cellulose and propylene oxide (1). The starting cellulose material may be of any type: cotton linters, chemical cotton, or even conventional wood pulp. The cellulose is combined with alkali (usually NaOH), water, and an inert water-miscible organic diluent such as tertiary butanol (2). This mixture is heated and alkaline cellulose is produced. The alkaline cellulose is then etherified under pressure using propylene oxide in the presence of a water-immiscible second diluent (hexane). The resulting product, hydroxypropylcellulose (HPC), precipitates out of solution as a flaky white powder and is easily recovered by filtration. Details concerning the exact reaction conditions, usable alkylating agents, and diluents can be found in the patents (2-4) and literature (5) on HPC preparation.

II.2 Structure

The HPC backbone consists of several thousand anhydroglucose units joined together by 1,4 beta linkages (6). An idealized structure for the HPC molecule is schematically depicted in Figure II.1. As illustrated in Figure II.1, propylene oxide is bonded to the cellulose backbone by ether linkages at two of the three available reactive hydroxyls. The extent of

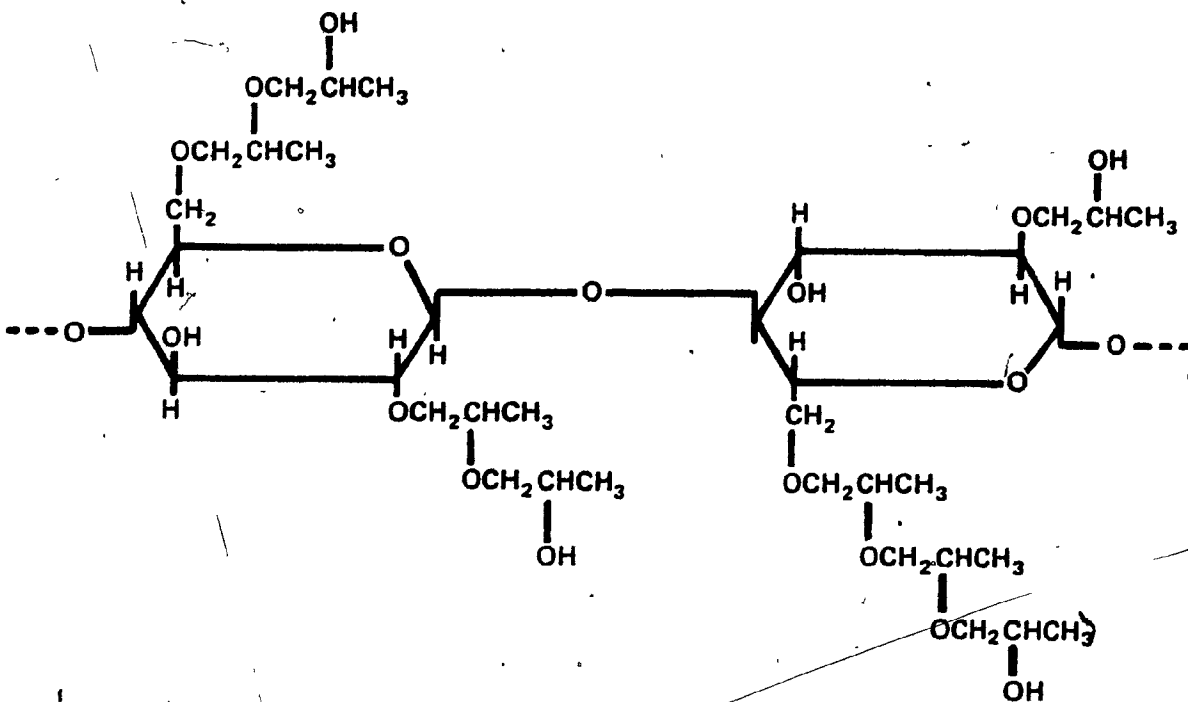


FIGURE II.1 Idealized structure for hydroxypropylcellulose with a degree of substitution of 2 and a molar substitution of 4.

reaction or molar substitution (MS) refers to the average number of propylene oxide molecules combined with an anhydroglucose unit in the HPC. The MS is distinct and different from the degree of substitution (DS) which has a maximum value of three and is defined as the average number of hydroxyls substituted per anhydroglucose unit in the cellulose (7). This distinction is necessary because propylene oxide can react with hydroxyl groups both on the cellulose and on previously attached hydroxypropyl substituents.

Published reports indicate that from 60 (8) to 99.7% (9) of the anhydroglucose units in HPC are substituted. No information is available on the distribution of substituents or their position on the cellulose. However, studies are currently underway on monomer and dimer model systems (10). The range of DS values reported for HPC varies from 2.1 (9) to 2.5 (11). Although these values seem somewhat high for a cellulose derivative they are, nevertheless, the best values currently available due to the absence of a standard analytical technique to measure the DS.

The MS, which has a marked effect on the properties of the polymer, is easily varied by the conditions used during etherification. The longer the hydroxypropylation reaction is allowed to continue, the higher is the MS of the final product since it is believed that essentially only the secondary hydroxyls of the side chains are available for reaction (1). The MS for HPC may be determined by the use of a slightly modified terminal methyl method (12). The MS value that is obtained in this way is

relatively precise but the accuracy of the technique has been questioned (4). A recently developed NMR technique (13) is claimed to give good results for the MS of HPC as well as an estimate of the DS.

II.3 Properties

Hydroxypropylcellulose behaves like a typical cellulose ether (14-15) but it also has some unique properties (16). Hydroxypropylcellulose is soluble in water below a critical temperature that depends on the MS of the polymer. Specifically, a HPC sample with a MS of 4 is soluble to 40°C but if the MS is only 2 then the solubility temperature is increased to 60°C. The lower the hydrocarbon content of the side chains, the greater the affinity of the polymer for water (4). At the point of insolubility solutions turn a cloudy white and the HPC precipitates out of solution as a highly swollen floc. On cooling, this floc easily redissolves to produce a clear solution. This reverse temperature solubility behavior is characteristic of all non-ionic water soluble cellulose derivatives (8,17).

In contrast to other cellulose ethers, HPC is found to be soluble in many common organic solvents including anhydrous ethanol. However, unlike aqueous solutions, the solubility of HPC in organic solvents increases as the temperature is raised. The higher the MS of the polymer, the more readily HPC dissolves in polar organic solvents (2). This dual solubility of HPC in aqueous and organic media is attributed to its

amphiphilic character. A delicate balance seems to exist between the hydrophilic (water soluble) and the lipophilic (hydrocarbon soluble) parts of the HPC molecule resulting not only in dual solubility but also in marked solubility in mixed solvents.

Hydroxypropylcellulose with a MS of at least 3 exhibits extremely good thermoplastic flow. It is readily injection molded or extruded to form materials of any size or shape (1,18). The high substitution ratio of HPC improves its resistance to both biological and chemical degradation — making it the most stable cellulose ether. Highly acidic or alkaline solutions do degrade HPC but only over a very long time period. The stability of HPC makes it an ideal starting material in the preparation of new compounds such as steroid esters (19), mixed cellulose ethers (20), and non-ionic derivatives of HPC (21-24). Hydroxypropylcellulose is odorless, tasteless, and non-toxic to both animals and humans. The polymer is surface active (1-2) and in aqueous solution has a steady state surface tension that is independent of solution concentration and molar mass (25). These properties make HPC usable as a foaming and thickening agent in foods, cosmetics, and laundry detergents (1). In combination with dextrin particles HPC bonds to paper without curling and is used extensively in binding glue to envelopes (4). In the printing process HPC acts as a suspending agent for inks. In pharmaceutical work HPC may be used as a coating for pills.

Elliott undertook a rheological study of HPC melts and he

concluded that HPC has a supermolecular structure consisting of a crystalline portion imbedded in an amorphous matrix (26). The highly non-Newtonian flow exhibited by the melt was attributed to the bulky hydroxypropyl side groups which cause HPC to have a fairly stiff structure. Roberts and Thomas (27) have examined the solubility of HPC in solvents of various polarizing and hydrogen bonding abilities. They postulate that the solubility of HPC may be directly attributed to the large number of hydroxyl groups on the HPC that are available for hydrogen bonding with polar solvents. The enzymic degradation of HPC has been investigated (9) and it was found that the substitution pattern for HPC is very different from that of hydroxyethylcellulose (HEC) (9,28-30). Ultrasonic degradation studies have also been performed on HPC solutions (31).

Wirick and Waldman (32) have successfully fractionated HPC and characterized each fraction by light scattering and gel permeation chromatography. They conclude that both the molar mass and the molar mass distribution in HPC depend very strongly on these properties in the original starting cellulose. The substitution pattern for HPC appears to be very uniform although shorter chains are more substituted than longer ones. Hydrodynamic and conformational parameters for both HPC and HEC seem to be very similar. A gas chromatographic study of the solute activity for dilute and concentrated HPC solutions was recently completed and in it the authors try to explain how the thermodynamic parameters of HPC solutions vary over a large concentration range in different solvents (33-36). Sedimentation velocity (37-38) and diffusion transport (39-40)

studies have been conducted on aqueous HPC solutions at various temperatures and concentrations.

To date, the most detailed study on solid state HPC has been conducted by Samuels (41). Using films cast from both water and ethanol solutions he has performed density measurements, X-ray and infrared studies, birefringence and refractive index measurements, electron microscopy, differential scanning calorimetry, and small angle laser scattering experiments. Based on his experimental results, Samuels proposed a molecular model for HPC in the solid state.

II.4 Characterization

The characterization of high molar mass polymers is not yet routine, although many advances have been made in this area (42). Synthetically produced cellulose derivatives, like HPC, are often polydisperse and hard to fractionate and so the characterization process is not easy. Water soluble cellulose are also notoriously difficult to dissolve completely (43). Solutions are found to contain not only the molecularly dispersed cellulose chains but also undissolved fibers, gel particles, and aggregates of colloidal size (44). The presence of these materials complicates the characterization process for cellulose derivatives and this is unfortunately true for HPC. In addition, since HPC is the product of a heterogeneous reaction (2-3), the substitution

pattern for the side groups is not expected to be uniform and this may also contribute to characterization difficulties.

II.4.1 LIGHT SCATTERING

Introduction

One of the most powerful and versatile techniques available for polymer characterization is light scattering (45-46). The principles of solution light scattering have their origin in Rayleigh's theory (47) for the scattering of light by a dilute gas. This theory was extended by Debye to include macromolecular solutions (48-49). In this case inhomogeneities existing in the solution are responsible for the scattering of light. The solution inhomogeneity is a result of density, thermal, or concentration fluctuations. The effects of density fluctuations are usually eliminated by subtracting the pure solvent scattering from that of the solution. The angular dependence of light scattering (50) may be conveniently expressed by the Rayleigh factor, R_{θ} , defined in Equation II.1.

$$R_{\theta} = \frac{i_{\theta} r^2}{I_0} \quad \text{II.1}$$

where I_0 = incident light beam intensity
 r = distance of scattering volume from detector
 i_{θ} = scattered light intensity per unit volume

θ = angle of measurement relative to the incident beam direction

The molar mass (\bar{M}_w) of the solute can be found by using Debye's equation which is shown below.

$$\frac{Kc(1 + \cos^2\theta)}{\bar{R}_\theta} = \frac{1}{\bar{M}_w} + 2A_2c + 3A_3c^2 + \dots \quad \text{II.2}$$

where

$$K = \frac{2r^2 n_o^2 (dn/dc)^2}{N_A \lambda^4}$$

and

K = an optical constant

c = solute concentration (g/mL)

n_o = solvent refractive index

dn/dc = differential index of refraction (mL/g)

N_A = Avogadro's number

λ = incident light wavelength

\bar{M}_w = solute weight average molar mass

A_2, A_3 = second and third virial coefficients, respectively

\bar{R}_θ = excess Rayleigh factor ($R_{\theta, \text{solution}} - R_{\theta, \text{solvent}}$)

Equation II.2 is only applicable to systems where the molecular dimensions

are smaller than one twentieth of the incident light wavelength. When the size of the scattering particles is no longer small, the scattering becomes more complex. Both particle geometry and their interactions begin to play an important role. Destructive interference of light scattered from different parts of the same molecule now greatly reduces the measured intensity of the scattered light. For such systems, Equation II.2 must be modified as follows

$$\frac{Kc}{R_{\theta}} = \frac{1}{M_w P(\theta)} + 2A_2c + 3A_3c^2 + \dots \quad \text{II.3}$$

where $P(\theta)$ is the particle scattering factor (52) which corrects for the effects of internal interference and the other variables are as defined for Equation II.2. The size and shape of the scattering particles determines the value of $P(\theta)$; however, in all instances, $P(\theta)$ tends to unity as θ approaches zero. In the limiting case of small scattering angles the following relationship is valid:

$$\lim_{\theta \rightarrow 0} \frac{1}{P(\theta)} = 1 + \frac{16\pi^2}{3\lambda^2} \langle s^2 \rangle \sin^2(\theta/2) \quad \text{II.4}$$

where $\langle s^2 \rangle$ is the mean square radius of gyration for the polymer.

Therefore, at low angles and neglecting the third and higher order virial coefficients, Equation II.3 takes the form

$$\frac{Kc}{R_{\theta}} = \left[1 + \frac{16\pi^2}{3\lambda^2} \langle s^2 \rangle \sin^2(\theta/2) \right] \frac{1}{M_w} + 2A_2c \quad \text{II.5}$$

The intensity of light scattered by solutions is a function of both the concentration and angle of observation (50-51). Three limiting cases of Equation II.5 should be noted:

- (1) In the limit of $\theta = 0$, $\frac{Kc}{R_\theta} = \frac{1}{\bar{M}_w} + 2A_2c$
- (2) As $c \rightarrow 0$, $\frac{Kc}{R_\theta}$ is proportional to $\sin^2(\theta/2)$
- (3) If both c and θ are zero, then $\frac{Kc}{R_\theta} = \frac{1}{\bar{M}_w}$

To summarize, the weight average molar mass of a polymer solution may be determined by using Equation II.5 and measuring the scattered light intensity as a function of angle and concentration. A double extrapolation, known as a Zimm plot (52), then allows \bar{M}_w to be found from the reciprocal value of Kc/R_θ at $\theta = 0$ and $c = 0$. The second virial coefficient is obtained from the slope of the $\theta = 0$ line whereas the slope of the $c = 0$ line gives a value for the $\langle s^2 \rangle$.

Experimental

A. Solution Preparation

Hydroxypropylcellulose samples, marketed under the trade name KLUCEL, were supplied by Hercules Incorporated and the Aldrich Chemical Company. The Hercules samples were designated KLUCEL E, L, J, G, M, and H in order of increasing molar mass. Table II.1 lists the reported molar

TABLE II.1

Manufacturer's Data for Nominal Molar Mass (\bar{M}_w) and Molar Substitution (MS) of Several HPC Samples (1,11)

HPC Type	\bar{M}_w^1 (g/mol)	MS ²
E	60 000	3.84
L	100 000	3.65
J	*	3.61
G	300 000	3.50
M	*	3.93
H	1 000 000	4.21

* No molar mass reported

¹ based on empirical method for estimating the degree of polymerization (DP) of the original cellulose and then using the MS value to calculate the molar mass of the HPC

² terminal methyl method; average of two results

masses and MS for the various KLUCEL samples investigated. The Aldrich HPC samples had nominal molar masses (53) of 100 000, 300 000, and 1 000 000 and appeared to be identical with the KLUCEL L, G, and H samples, respectively. Attempts to purify the HPC samples by fractional precipitation (54) using ethanol as a solvent and n-heptane as the non-solvent were unsuccessful. Prior to use, the HPC was dried to constant weight in a vacuum oven at 65° to 70°C. This process was found to remove from 2 to 3% water depending on the HPC sample being dried.

All aqueous solutions were prepared with water distilled twice in a closed non-boiling still. The heating source was an infrared heat lamp (Sylvania 125 watts). Dried HPC was transferred into 100-ml volumetric flasks and 50 mL of hot water (~ 60°C), a non-solvent, were added. (Like most water soluble polymers, HPC tends to lump together when the powder is first wetted with solvent (1). To minimize agglomeration and facilitate dissolution, the polymer is preslurried in hot water to ensure complete wetting of the powder.) Next 30 mL of cold water were added to the flask which was then placed on a mechanical shaker for two hours. At this time solution of all gel particles seemed to be complete. Since HPC solutions have a tendency to foam when shaken, the solutions were allowed to settle for a further two hours before the flasks were made up to their volumetric capacity. The solutions were gently agitated with a magnetic stirrer for thirty minutes more to ensure homogeneity. To minimize aggregation effects, all aqueous solutions were prepared not more than twenty-four hours prior to use. The solutions were relatively clear

or slightly hazy depending on the HPC sample being dissolved. On standing, a fuzzy white precipitate was seen to develop in almost all of the solutions.

Organic HPC solutions were prepared following the procedure outlined above for aqueous samples but without the prewetting step. Before being used as a solvent, tetrahydrofuran (THF) was dried over molecular sieves (Linde Air Products Co, Type 3A, 8 - 12 mesh) for at least one week and ethanol was distilled twice in the closed non-boiling still. Solutions of HPC in THF were clear and essentially free of fibers and gel material. Ethanol solutions contained distinct gel-like particles, indicating that only a portion of the HPC had dissolved. These solutions were filtered through a 0.45- μ m Fluoropore filter prior to use.

B. Differential Index of Refraction

The differential index of refraction (dn/dc) was measured for all the KLUCEL types (E, L, J, G, M, and H) in water. Sixty-five solutions, approximately a dozen per HPC type, were prepared using the procedure outlined in the previous section. Table II.2 lists the solution concentration range that was prepared for each HPC sample. The higher the molar mass of the HPC, the more viscous and difficult the solution was to handle. Differential index of refraction measurements were also obtained for HPC-L in THF and ethanol. The concentration range prepared for these solutions is also listed in Table II.2. The solutions were made

TABLE II.2

Concentration Range of HPC Solutions Prepared for Differential
Index of Refraction Measurements

HPC Type	Solvent	Concentration Range (g/L)
E	H ₂ O	0.60 - 5.9
L	H ₂ O	0.39 - 5.2
L	C ₂ H ₅ OH	0.29 - 3.5
L	THF	1.9 - 9.7
J	H ₂ O	0.49 - 5.2
G	H ₂ O	0.31 - 4.8
M	H ₂ O	0.62 - 5.0
H	H ₂ O	0.069 - 0.43

up by following the procedure already described.

Differential index of refraction measurements were obtained using a Hilger and Watts M154 Rayleigh Interference Refractometer (55-56). The temperature was maintained at a constant $25^{\circ} \pm 0.1^{\circ}\text{C}$ by using a water jacket provided with the instrument (57) and an externally circulating water bath. The interferometer cell, available in path lengths of 0.1-m or 0.01-m, consisted of a solid piece of fused silica divided into two compartments — one for solvent and one for solution. The light source was an ordinary microscope lamp mounted in a suitable housing.

The interference refractometer operates on the principle of matching two sets of interference fringes. One set of fringes is stationary and functions as a reference point for a second mobile set of fringes. The displacement, d , of the mobile fringes with respect to the reference fringes is measured and is directly related to the refractive index difference, Δn , existing between the solution and the pure solvent. The interferometer is calibrated by measuring d for several solution concentrations of known refractive index difference. A plot of Δn versus d yields a straight line of slope k , an instrument constant. The Δn for the HPC solutions was then calculated using the equation, $\Delta n = kd$ (58). Aqueous NaCl and KCl solutions with accurate literature values (59-62) for Δn were used to evaluate k for the interferometer. Solutions were equilibrated for between ten and twenty minutes in the interference refractometer at which time distorted fringes had straightened out

indicating that temperature equilibrium had been attained.

C. Light Scattering

Conventional light scattering was performed using a SOFICA 42 000 Photo-Gonio-Diffusometer equipped with a mercury lamp ($\lambda = 546 \text{ nm}$). An excellent detailed description of the basic operation of this instrument has been given by Margerison and East (63). To avoid erroneous results in light scattering, the solutions used must be dust free. Aqueous solutions prepared according to the procedure outlined above were subjected to a two-step cleaning process. Solutions were first centrifuged (Beckman Spinco Model L) for one hour at 25 000 rpm in polycarbonate centrifuge tubes (Canlab). Glass beads (Chromatographic Specialties, 80 - 100 mesh) had previously been placed in the tubes to trap any dust or gel particles settling during centrifugation. Next, solutions were filtered using 30-ml syringes equipped with 0.22- μm Millipore filters. The above process was repeated a second time and the solutions were filtered directly into the 25-ml light scattering cells (64). Measurements were then made in triplicate at several scattering angles from 30° to 180° on four aqueous HPC-G solutions with concentrations between 1.4 and 4.2 g/L. The scattering intensity for the solutions was normalized by using benzene as a reference scatterer.

Low angle laser light scattering (LALLS) (65-69) was performed on HPC solutions using a Chromatix KMX-6 LALLS photometer. Since the

design of this instrument differs considerably from that of a conventional light scatterer, a brief description of the photometer and its operation (70-71) is presented here. Figure II.2 depicts schematically the basic components in a LALLS photometer. The light source is a two milliwatt He-Ne laser emitting vertically polarized red light of wavelength 633 nm. The laser beam is folded back on itself by two prisms which direct the beam to where the attenuators, sample cell, and detector optics are located. Three measuring and one calibrating attenuator are located between the second folding prism and the condensing lens. They function to attenuate the incident beam to within a factor of 0.25 of the scattered radiation of the solution. The calibrating attenuator serves as an internal calibration verifier. The condensing lens focusses the laser beam down to a spot size of 0.08 mm at the sample.

The solution being investigated is confined in a small aperture in the teflon spacer sandwiched between two, two-inch long fused silica windows. The window faces are polished as well as the state of the art permits. The cell volume with a 15-mm thick spacer is approximately 0.05 mL. Solution is introduced into the cell using a hypodermic syringe inserted into the spacer. The cell is mounted on a fine motion stage which allows the operator to choose the area of minimum scatter on the cell interface for measurements.

The laser beam next passes through a rotating annulus wheel which offers a choice of five available scattering angles ranging from 2° to 7° .

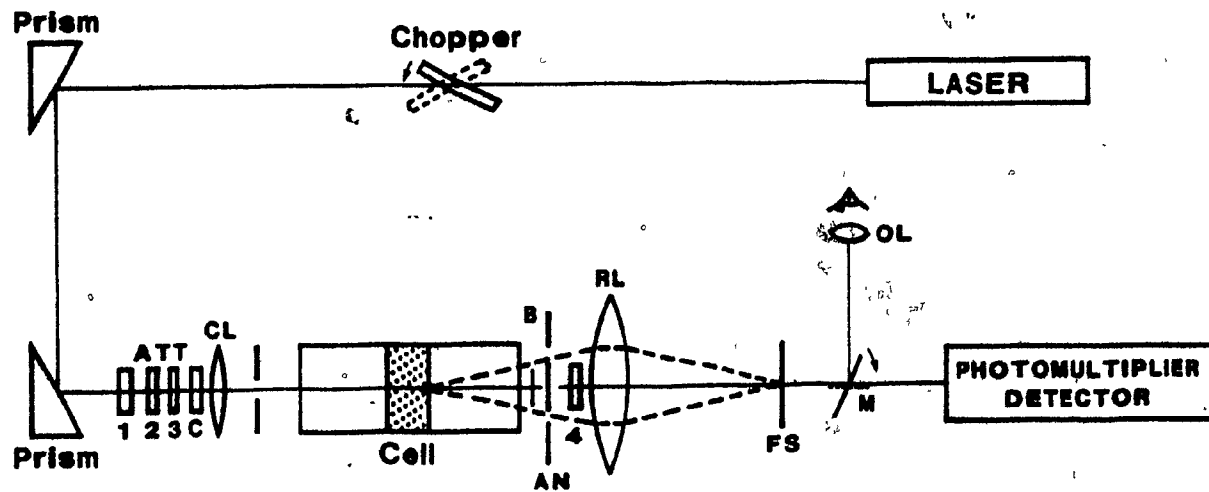


FIGURE II.2 Schematic view of the components of a Chromatix LALLS photometer:
 ATT = attenuators, CL = condensing lens, B = beam stop,
 AN = annulus, RL = relay lens, FS = field stop, M = mirror,
 OL = ocular lens. See text for details concerning the function
 of each component.

An aperture on the wheel allows the direct incident beam intensity to be measured. Beam stops centered in the annuli absorb most of the direct laser beam. Just behind the annuli is a fourth attenuator which serves as a safety shutter protecting the photomultiplier from excess light levels. Unless it is manually removed this attenuator is always in the beam path. Next along the optic path is the relay lens which serves to image the scattered light at a 1:1 magnification onto the field stop. There are twenty-four field stops ranging in size from 1.5 mm to 0.005 mm. Only light scattered from the center of the sample and passing through the annulus is focussed onto the field stop. The final destination of the light focussed through the field stop is the photomultiplier tube which records the intensity of the scattered laser beam. By inserting a mirror and ocular lens with a magnification of 50 just before the photomultiplier, it is possible to observe the scattered light from the solution and to align the optics of the system.

Unlike conventional light scattering instruments, the LALLS photometer requires no standard calibrating solutions. The instrument is absolutely calibrated (72-73) in that the Rayleigh factor, R_θ , is determined by geometric parameters and ratios of radiant power measurements. Specifically, the Rayleigh factor for a sample is given as

$$R_\theta = \frac{G_\theta D_0}{G_0 \sigma_1} \quad \text{II.6}$$

where G_θ = detector reading for scattered beam due to sample

- G_0 = detector reading for transmitted beam through sample
 D_0 = net transmittance of attenuators
 σ = solid angle over which detected radiation is viewed
 l = effective length of scattering volume

The product of σ and l is constant for a particular combination of solution refractive index, annulus, field stop, and cell spacer. The value of D_0 is constant for a given set of attenuators but its value must be checked periodically. The R_θ is therefore simply the ratio of G_θ/G_0 where both are measured under identical detector gain and optic element conditions except for the attenuator combination inserted in the beam path. Scattering measurements for polymer solutions give the Rayleigh factor as a function of polymer concentration. The small angles involved ($\sim 2^\circ - 7^\circ$) allow the weight average molar mass of the polymer to be evaluated without need of extrapolation to zero angle. No Zimm plot is required. As in conventional light scattering, LALLS measurements can also be made at high temperatures (74).

Low angle laser light scattering measurements were performed on all HPC types in water. In addition, measurements were made on HPC-L in ethanol and THF. Most solutions were prepared directly by using the dissolution procedure outlined above rather than by volumetric dilution of standard solutions. Experimentally, freshly prepared solutions gave more reproducible results than solutions prepared by volumetric dilution. Solutions were transferred to 10-ml Hamilton syringes equipped with Luer lock filter holders

containing pre^ofilters and 0.22- μ m Millipore (for aqueous solutions) or 0.45- μ m Fluoropore (for ethanol and THF solutions) filters. The syringe was placed on a syringe drive (Multispeed Transmission Harvard Apparatus Co., Model 600) which forced solution through the light scattering cell at a speed of 0.051 mL/min. The solution concentration range prepared for LALLS measurements in water was between 0.03 and 9.7 g/L, in ethanol between 0.5 and 4.9 g/L, and in THF between 0.2 and 1.4 g/L.

Results and Discussion

The differential index of refraction (dn/dc) of a solution is an important factor when the solute molar mass is evaluated from light scattering data. The optical constant, K , of Equation II.5 depends on the square of the dn/dc . In this work the difference in refractive index (Δn) between the solution and the pure solvent was measured by interference refractometry. Each measurement of Δn was made seven times and the results were averaged. This was repeated for several concentrations of HPC. The values of Δn obtained were plotted against solution concentration (c) and the slope of the resulting straight line gave a value for the dn/dc . Alternatively, the dn/dc may be evaluated as the intercept, at $c = 0$, of a plot of $\Delta n/c$ versus concentration. This latter method emphasizes any scatter in the experimental points and consequently exaggerates any non-linear variation in Δn with concentration. For this reason Huglin (61) states that it is the preferred method for evaluating the dn/dc . Figures II.3, II.4, II.5, and II.6 show typical plots of the variation in Δn with

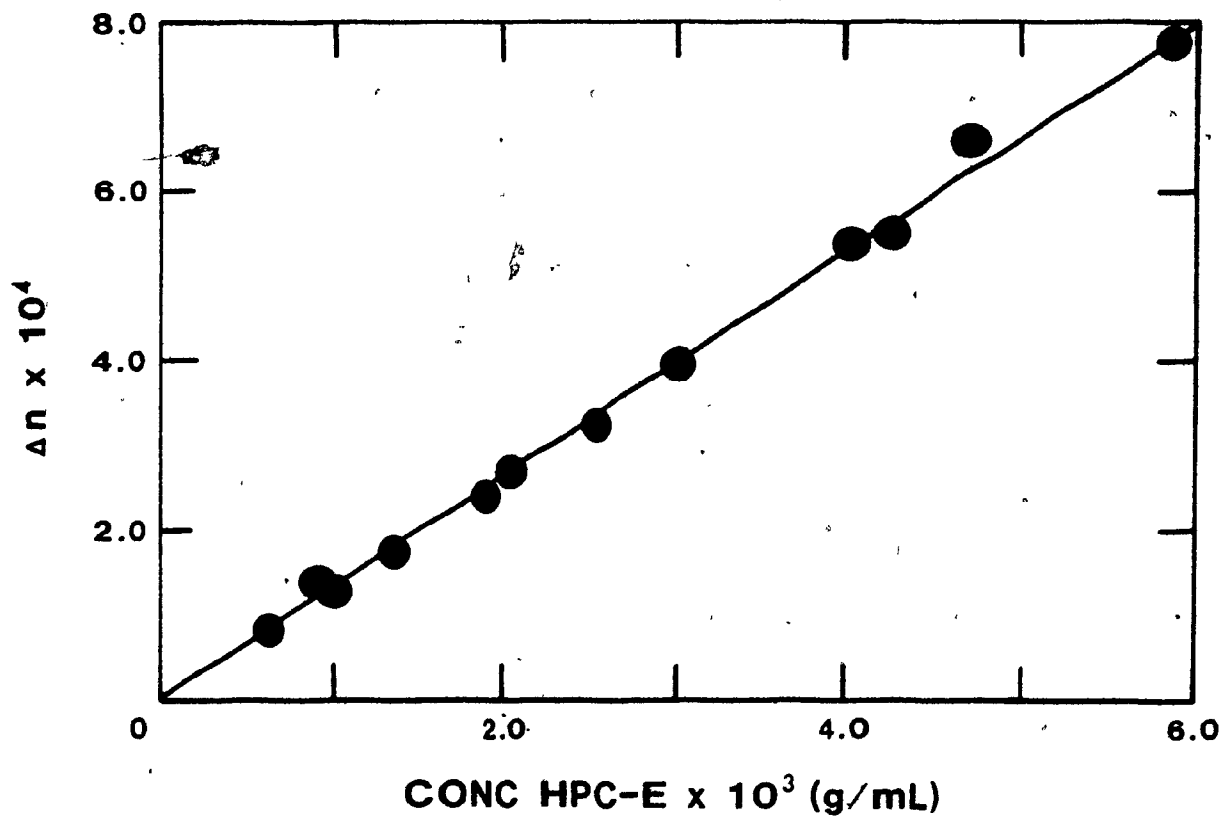


FIGURE II.3 The change in refractive index difference (Δn) with concentration for aqueous HPC-E solutions at 25°C and $\lambda \approx 560$ nm.

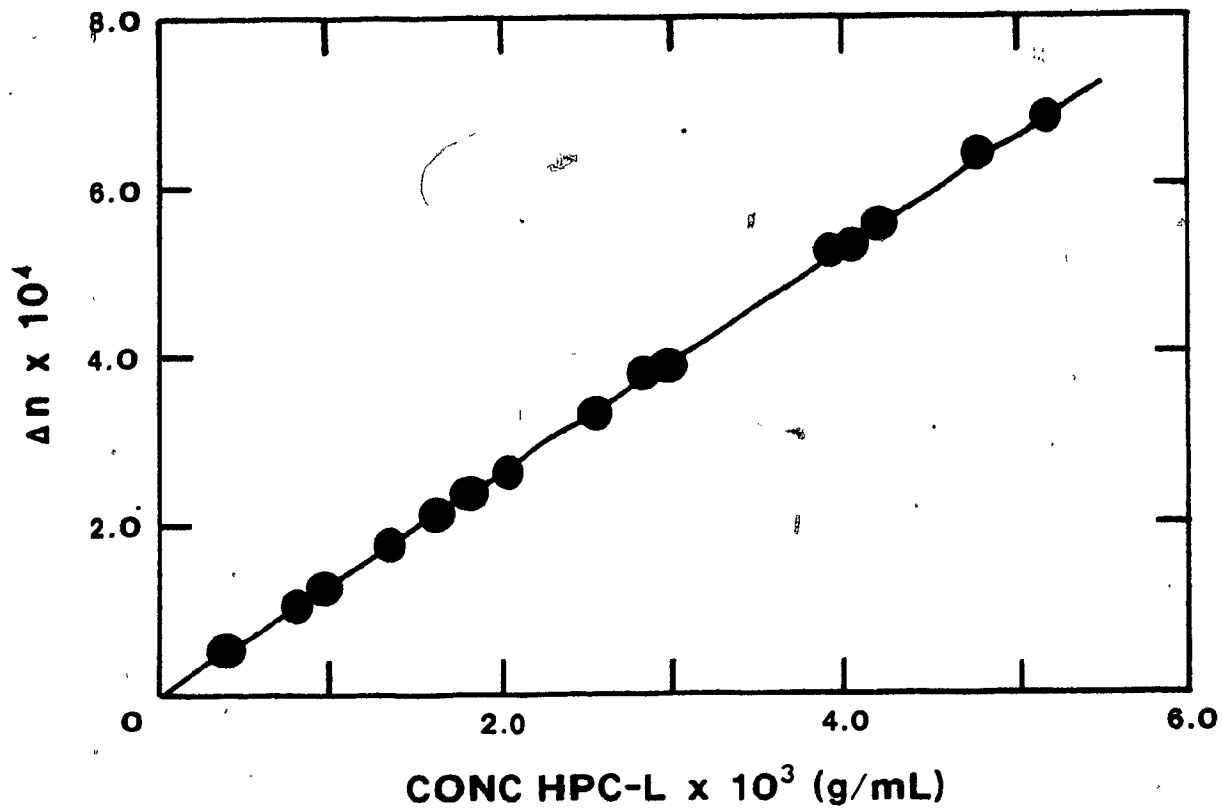


FIGURE II.4 The variation in refractive index difference (Δn) with concentration for aqueous HPC-L solutions at 25°C and $\lambda \approx 560$ nm.

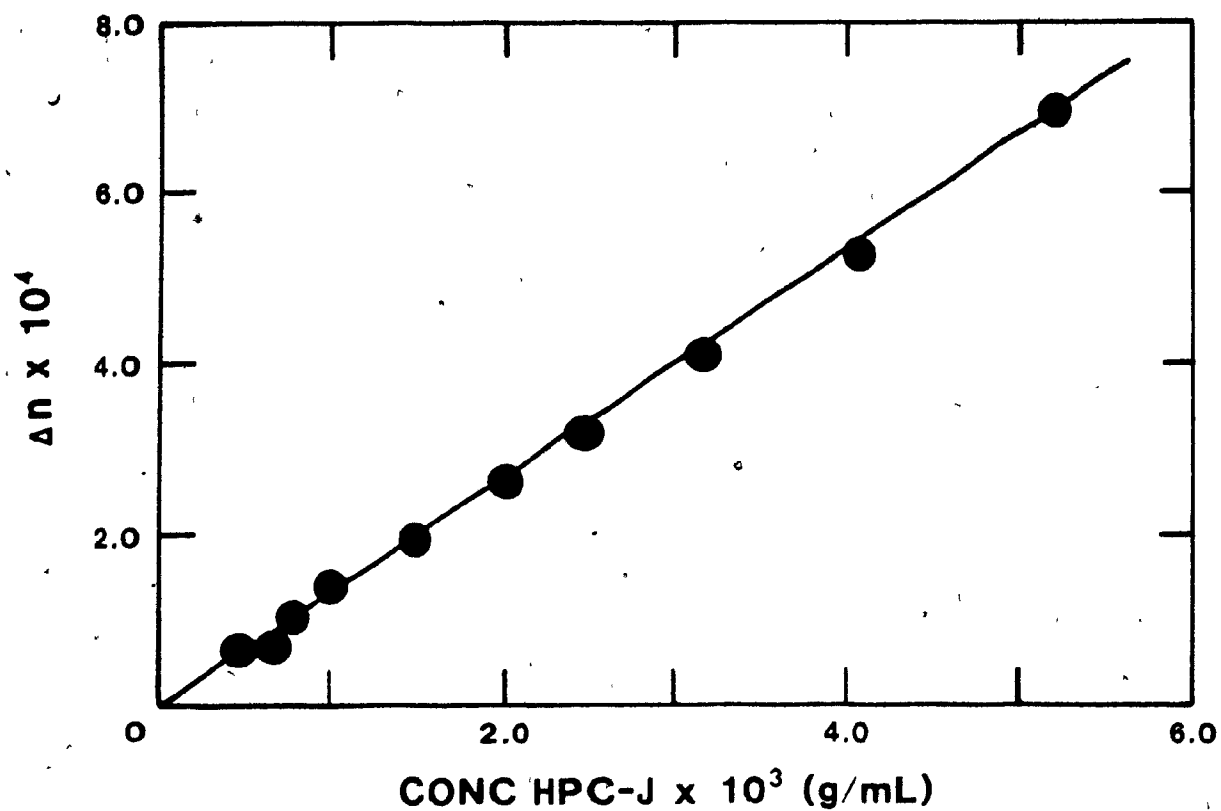


FIGURE II.5 The change in refractive index difference (Δn) with concentration for aqueous HPC-J solutions at 25°C and $\lambda \approx 560 \text{ nm}$.

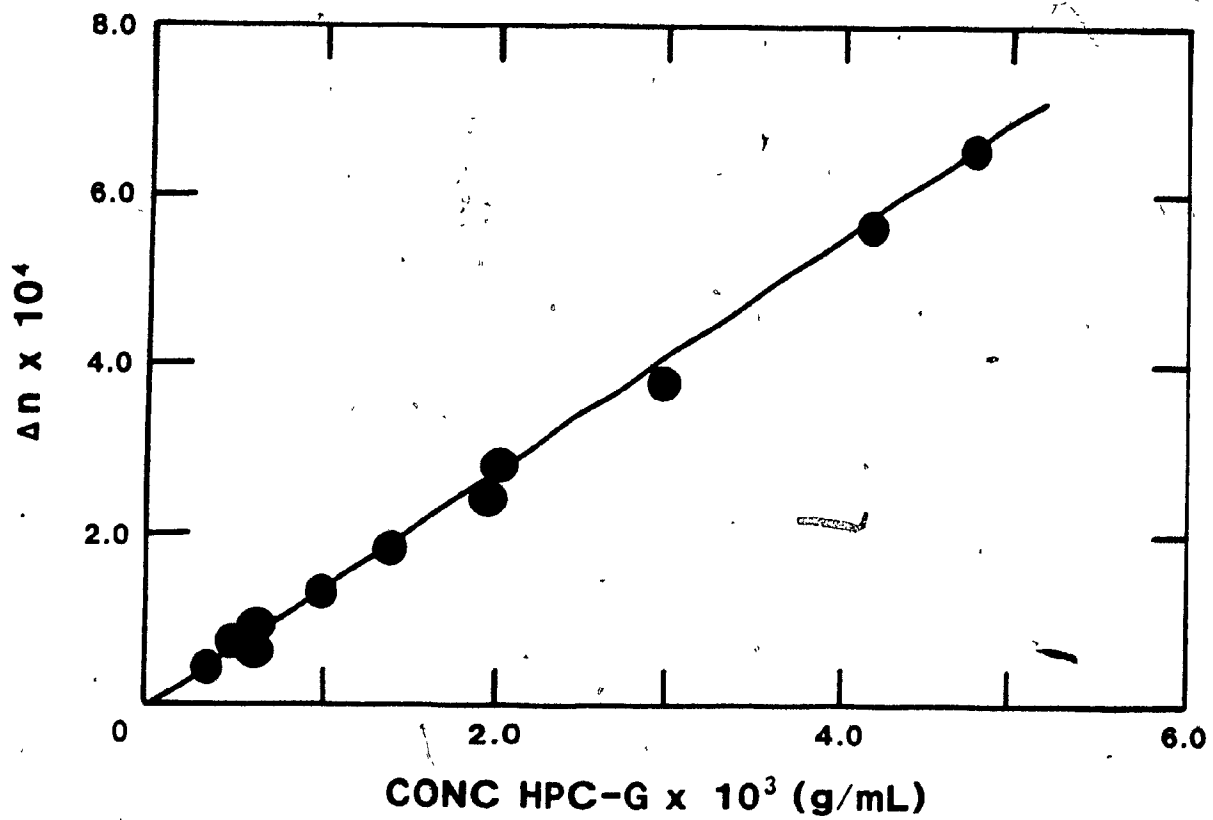


FIGURE II.6 The variation in refractive index difference (Δn) with concentration for aqueous HPC-G solutions at 25°C and $\lambda \approx 560 \text{ nm}$.

concentration for aqueous solutions of HPC-E, L, J, and G respectively. The dn/dc values obtained for the various HPC samples in water and for HPC-L in ethanol and THF are listed in Table II.3. There appears to be no clear trend in the variation of the dn/dc with molar mass for HPC in water. Rather, the dn/dc seems to have an average value of 0.134 ± 0.003 mL/g over the molar mass range investigated (60 000 to 600 000 g/mol). The results for HPC-H have been neglected since they showed a non-linear variation in Δn with concentration.

The differential index of refraction is wavelength dependent and the values listed in Table II.3 were measured at 560 nm the average wavelength for white light interferometry (55). These dn/dc values are believed to vary by 2 or 3% from those required in the calculations of light scattering data at 546 nm and 633 nm. Experimentally, the dn/dc value for HPC-L was 0.117 mL/g at 25°C and 560 nm. The corresponding value reported in the literature (32) in the same solvent, ethanol, is 0.120 mL/g at 25°C and 546 nm. This would seem to confirm the postulated 3% error that is introduced by assuming the dn/dc to be wavelength independent. A similar 3% change in dn/dc with wavelength has been reported for cellulose diacetate solutions (75). Although a 3% error in dn/dc seems somewhat high, it is probably acceptable when it is recalled that the HPC samples being used are highly polydisperse and that the results in Table II.3 show a 2 to 3% variation from the average dn/dc value of 0.134 mL/g with molar mass.

TABLE II.3

Differential Index of Refraction (dn/dc) Values at 25°C
and $\lambda \approx 560 \text{ nm}$ for Several HPC Types in Order
of Increasing Molar Mass

HPC Type	Solvent	dn/dc (mL/g)
E	H_2O	0.133
L	H_2O	0.132
L	$\text{C}_2\text{H}_5\text{OH}$	0.117
L	THF	0.071
J	H_2O	0.134
G	H_2O	0.136
M	H_2O	0.137
H	H_2O	0.118

The weight average molar mass for aqueous HPC-G solutions was calculated from conventional light scattering measurements. The resulting data and Equation II.5 were used in constructing the Zimm plot shown in Figure II.7. The data which showed relatively large deviations from linear behavior were not very good, but this was the best data that could be obtained from the prepared solutions. The scattering at angles over 90° from both the solutions and the pure benzene was very high. This was attributed to back reflection from some part of the system and the data measured above 90° have been neglected. The Zimm plot extrapolation gave a weight average molar mass of approximately 740 000 g/mol for HPC-G. Using Equation II.7 the second virial coefficient (A_2) was determined to be $3.5 \times 10^{-4} \text{ mL mol g}^{-2}$.

$$A_2 = \frac{1000}{2} \text{ slope}_\theta = 0 \quad \text{II.7}$$

The factor of 1000 in Equation II.7 was arbitrarily chosen to produce a good spread of the experimental data on the x-axis of the Zimm plot in Figure II.7. The slope referred to in Equation II.7 is that of the $\theta = 0$ line. The root mean square radius of gyration ($\langle s^2 \rangle^{1/2}$) was calculated using a modified form of Equation II.4

$$\langle s^2 \rangle^{1/2} = \left[\frac{3\lambda^2 M_w}{16\pi^2} \text{ slope}_c = 0 \right]^{1/2} \quad \text{II.8}$$

and its value was found to be 320 nm. This value for the radius of gyration is much larger than expected for a randomly coiled cellulose

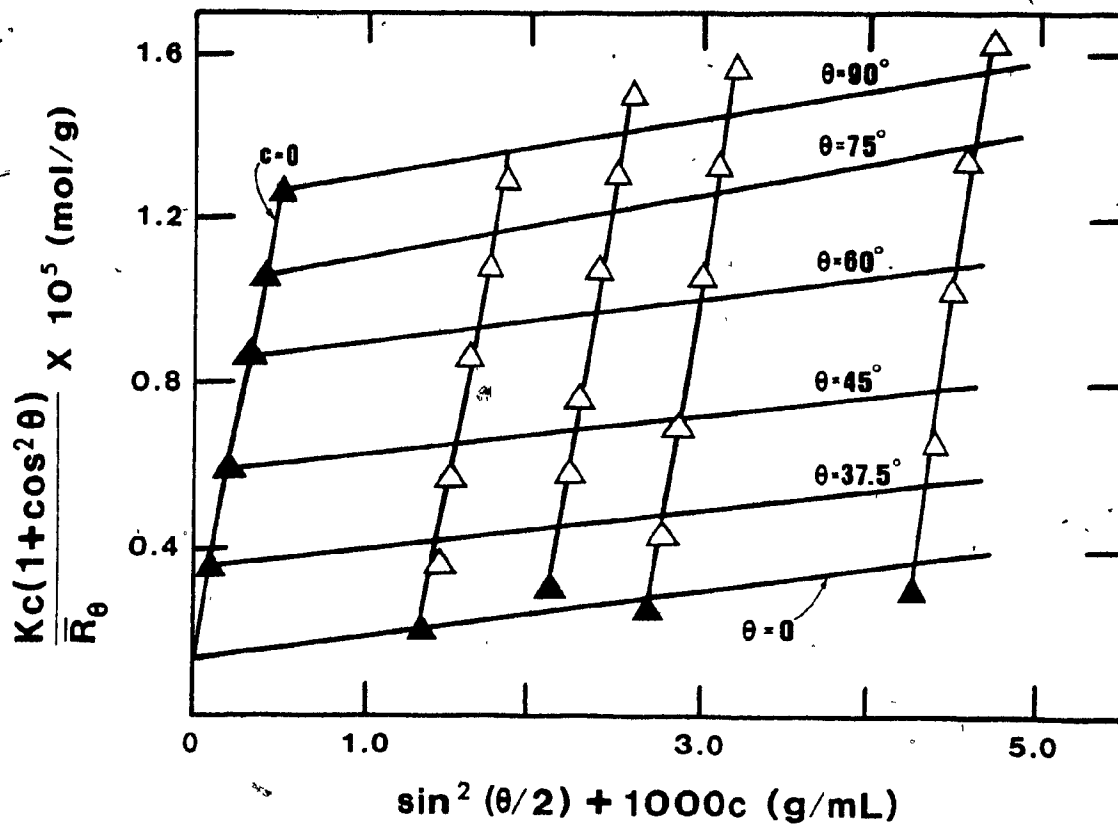


FIGURE II.7 . Typical Zimm plot of light scattering data for HPC-G in aqueous solution: $\bar{M}_w = 7.4 \times 10^5$ g/mol, $A_2 = 3.5 \times 10^{-4}$ mL mol g^{-2} , and $\langle s^2 \rangle^{1/2} = 320$ nm.

chain. Increasing chain stiffness would of course increase the cellulosic radius of gyration but a quantitative interpretation of its significance was not warranted due to the scatter in the experimental data of the Zimm plot. Other HPC samples in aqueous and ethanol solutions showed marked curvature in their respective Zimm plots making it impossible to extrapolate the data for a molar mass value. It would thus appear that conventional light scattering is not the ideal technique to use in evaluating the HPC molar mass.

Low angle laser light scattering measurements were made on several HPC samples. The precision and accuracy of the Chromatix KMX-6 instrument was verified using dextran (T-110, Pharmacia Fine Chemicals, $\bar{M}_w / \bar{M}_n \approx 1.44$) solutions. This polymer is often used as a molar mass standard in aqueous solution. The results obtained are shown in Figure II.8. The molar mass from the graph is 113 000 g/mol; this differs by approximately 3% from the manufacturer's reported value of 110 000 g/mol. The reproducibility in \bar{R}_θ values was excellent. Specifically, \bar{R}_θ was measured five times for each solution concentration and the results averaged. In each case the average \bar{R}_θ differed from the individual \bar{R}_θ values by less than 0.5%. The single closed circles in Figure II.8 represent the average \bar{R}_θ values. To verify that the apparent molar mass of dextran was not changing with time due to aggregation, the light scattering measurements were repeated at two hour, two day, and one week intervals. Every time, \bar{R}_θ was measured five times for each solution concentration and the results averaged. The bars in Figure II.8 indicate the maximum and minimum average \bar{R}_θ values obtained

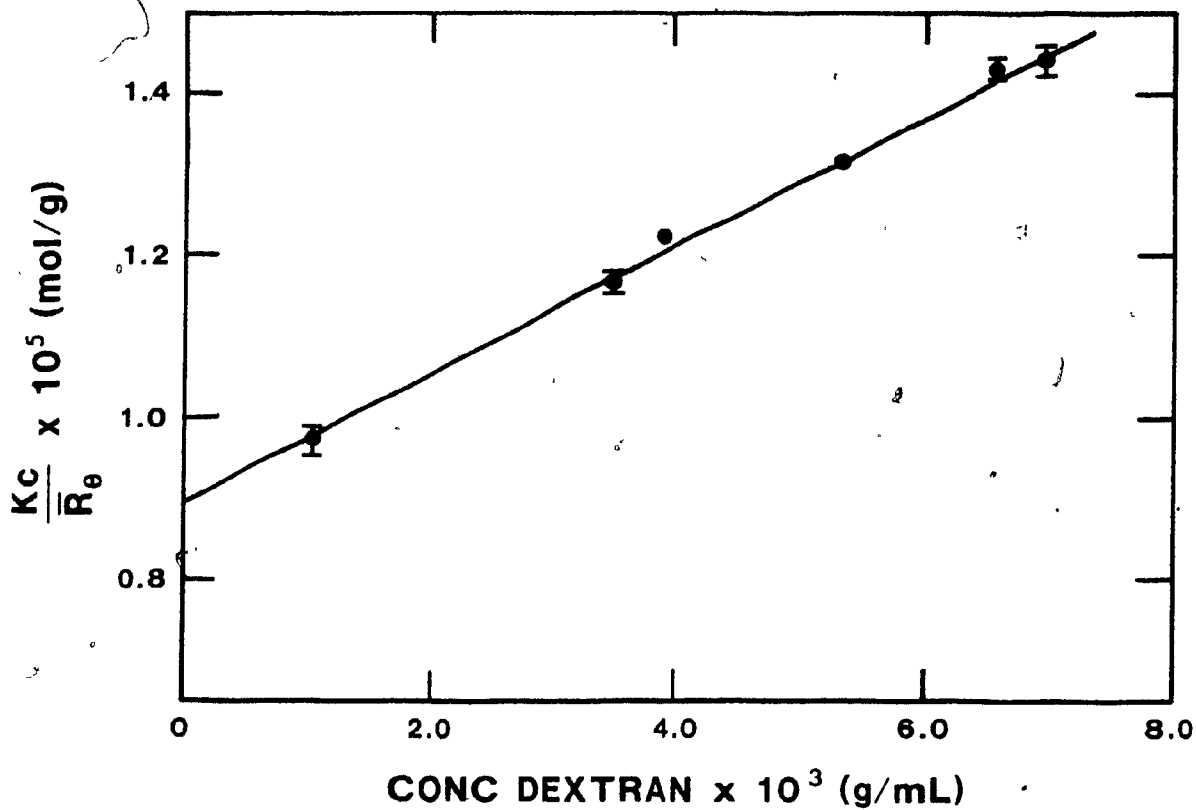


FIGURE II.8, LALLS data for aqueous dextran solutions: $n_{H_2O} = 1.332$, $dn/dc = 0.147 \text{ mL/g}$, $K = 1.565 \times 10^{-7} \text{ mol cm}^2 \text{ g}^{-2}$, $\bar{M}_w = 1.13 \times 10^5 \text{ g/mol}$, and $A_2 = 4.07 \times 10^{-4} \text{ mL mol g}^{-2}$. Closed circles and bars refer to duplicate measurements; see text for details.

from all light scattering measurements on a particular solution concentration. The change in the average \bar{R}_θ with time was less than 4% in every case, indicating that dextran solutions are stable and do not aggregate to any particular extent over the time span investigated. The closed circles superimposed on the bars in Figure II.8 represent an average of the average \bar{R}_θ values used in calculating the reported molar mass. The Chromatix LALLS photometer would thus seem to provide an accurate and precise weight average molar mass value for dextran without the need for many duplicate measurements or a complex Zimm plot.

Low angle laser light scattering measurements were performed on aqueous HPC-G solutions. The data collected and Equation II.5 were used in the construction of Figure II.9. Measurements were repeated at two twenty-four hour intervals and these results are also plotted in Figure II.9. The actual molar masses calculated for HPC-G over the three day time period are listed in Table II.4. The molar mass data clearly show that the HPC-G has undergone a fivefold increase in molar mass over the time span investigated. This result may be explained by postulating that HPC is aggregating and this causes the molar mass to increase. Although the aggregation of HPC in water occurs over a relatively short time span, one week or more is needed before a precipitate becomes visible in the solutions. This molecular aggregation may also partially account for the curvature found in the Zimm plots of conventional light scattering data.

The results of LALLS measurements on HPC-L solutions in water,

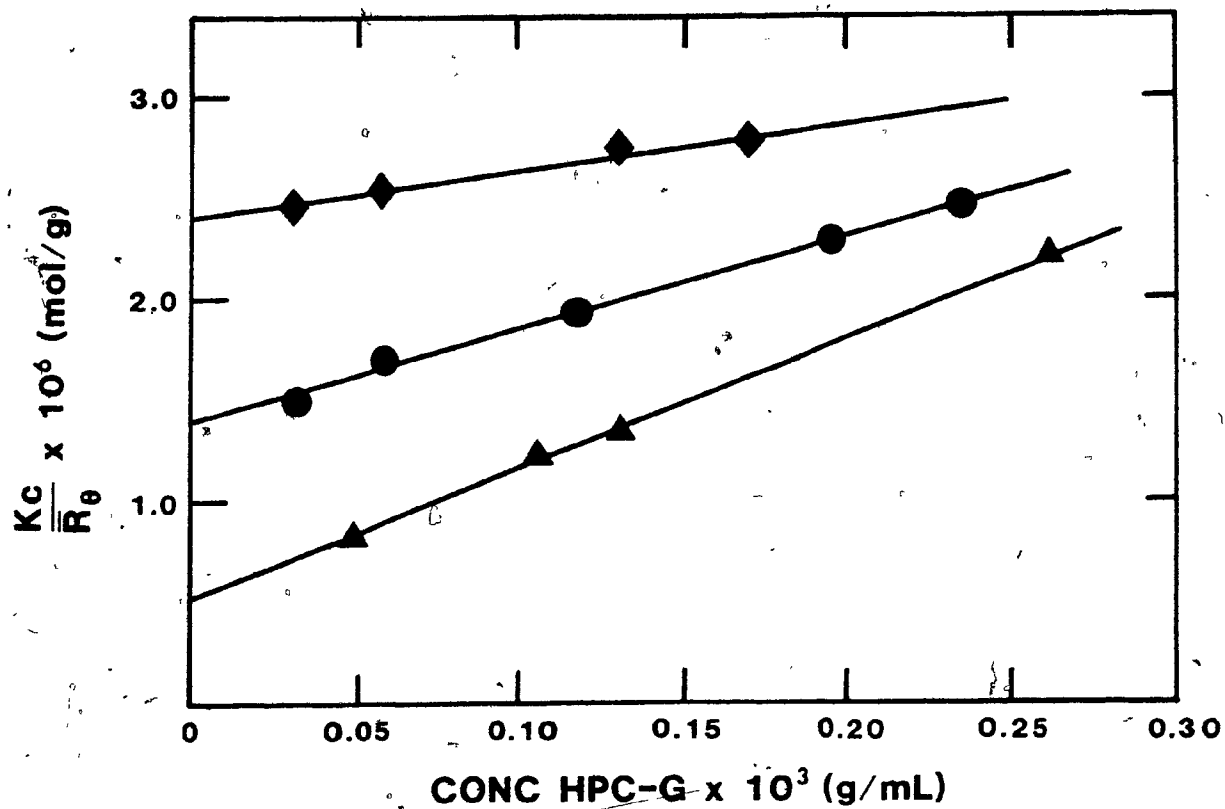


FIGURE II.9 Chromatix LALLS results for several aqueous HPC-G solutions. The data were collected at 24 (◆), 48 (●), and 72 (▲) hour intervals after solution preparation. See Table II.4 for the calculated weight average molar masses.

TABLE II.4

Molar Mass Results for Aqueous HPC-G Solutions from LALLS
Data Collected Over a Three Day Time Period

Day	\bar{M}_w (g/mol)	A_2 (mL mol g ⁻²)
1	420 000	1.11×10^{-3}
2	710 000	2.23×10^{-3}
3	1 900 000	3.22×10^{-3}

THF, and ethanol have been graphed in Figures II.10, II.11, and II.12 respectively. In aqueous solution the LALLS data were not very reproducible and it was extremely difficult to obtain a molar mass value for HPC-L. In Figure II.10, the closed circles represent an average \bar{R}_θ value obtained from between three to ten individual \bar{R}_θ measurements on a particular solution. Unlike dextran solutions, the reproducibility in the individual \bar{R}_θ values for HPC-L was only 3%. Measurements were repeated at two hour and one day intervals for four days. The maximum and minimum average \bar{R}_θ values obtained over the given time period are represented by the bars in Figure II.10. Unlike HPC-G in water, the aggregation of HPC-L does not proceed in a straightforward manner. For instance, the variation in the average \bar{R}_θ for a 1.08 g/L solution changed by 3% whereas for a 0.65 g/L solution the corresponding change was 21% over the same time span. In addition, the change in average \bar{R}_θ values with time was random — increasing for some solutions while decreasing for others. Samples prepared by volumetric dilution frequently gave larger average \bar{R}_θ values than the original, more concentrated, standard solutions. The problems outlined above are reported simply to illustrate that LALLS, although a powerful and useful technique, may not be applicable to all polymeric systems.

The ambiguous LALLS results obtained for aqueous HPC-L solutions may, perhaps, be attributed to both sample polydispersity and aggregation of the HPC on a submicroscopic scale. Published reports (32,38,40) indicate that the sample polydispersity (\bar{M}_w / \bar{M}_n) may vary from 2 to 12 for unfractionated HPC samples. The solution flowing through the LALLS cell

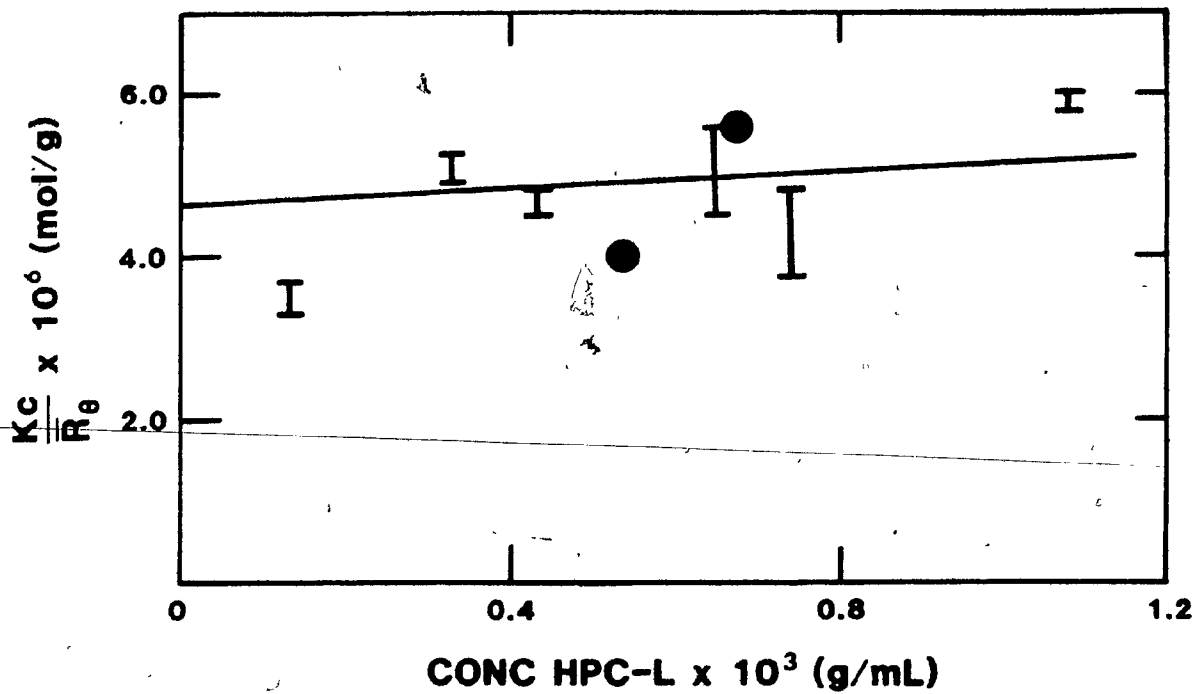


FIGURE II.10 LALLS data for aqueous HPC-L solutions: $n_{\text{H}_2\text{O}} = 1.332$, $dn/dc = 0.132 \text{ mL/g}$, $K = 1.261 \times 10^{-7} \text{ mol cm}^2 \text{ g}^{-2}$, $\bar{M}_w = 2.15 \times 10^5 \text{ g/mol}$, and $A_2 = 2.50 \times 10^{-4} \text{ mL mol g}^{-2}$. See text for explanation of bars and closed circles.

may be subjected to sufficient shear forces to cause shear-induced aggregation. Some evidence to support the aggregation hypothesis was a marked buildup in back pressure at the 0.22- μm filter. The aggregates thus formed are probably large enough to be trapped by the filter. The solution concentration is therefore altered to an extent which could not be estimated. This problem was not encountered with aqueous dextran solutions. The data in Figure II.10 have been extrapolated as well as possible and indicate that HPC-L has a molar mass of 215 000 g/mol while A_2 has a value of 2.50×10^{-4} mL mol g⁻².

Light scattering on HPC-L solutions was performed in THF and ethanol to ascertain if HPC aggregation occurred only in aqueous solutions. Figure II.11 shows the LALLS results obtained for HPC-L in THF. For an explanation of the closed circles, bars, and closed circles superimposed on the bars, see the description given above for dextran solutions. The scatter in the average \bar{R}_θ values is much less than in the aqueous case, but the slightly negative slope of the line is an indication that aggregation of the polymer is occurring. There was also a noticeable buildup of back pressure at the 0.45- μm filter suggesting that some HPC was being trapped. The molar mass for HPC-L in THF was found to be 220 000 g/mol and A_2 was -1.04×10^{-4} mL mol g⁻².

Light scattering results for HPC-L in ethanol were somewhat unusual as is illustrated in Figure II.12. Problems were encountered in obtaining reproducible results on freshly prepared solutions. These

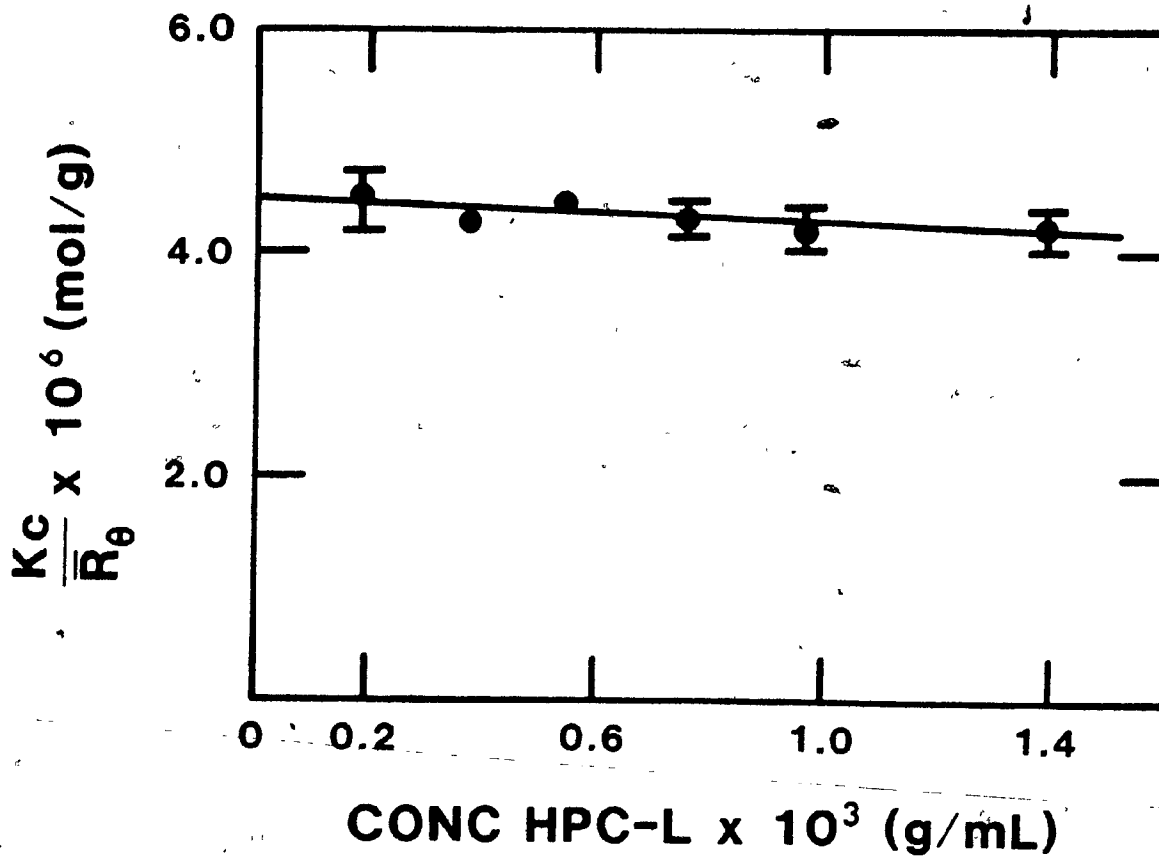


FIGURE II.11 LALLS data for HPC-L solutions in THF: $n_{\text{THF}} = 1.406$, $dn/dc = 0.071 \text{ mL/g}$, $K = 4.065 \times 10^{-8} \text{ mol cm}^2 \text{ g}^{-2}$, $\bar{M}_w = 2.20 \times 10^5 \text{ g/mol}$, and $A_2 = -1.04 \times 10^{-4} \text{ mL mol g}^{-2}$. See text for explanation of closed circles and bars.

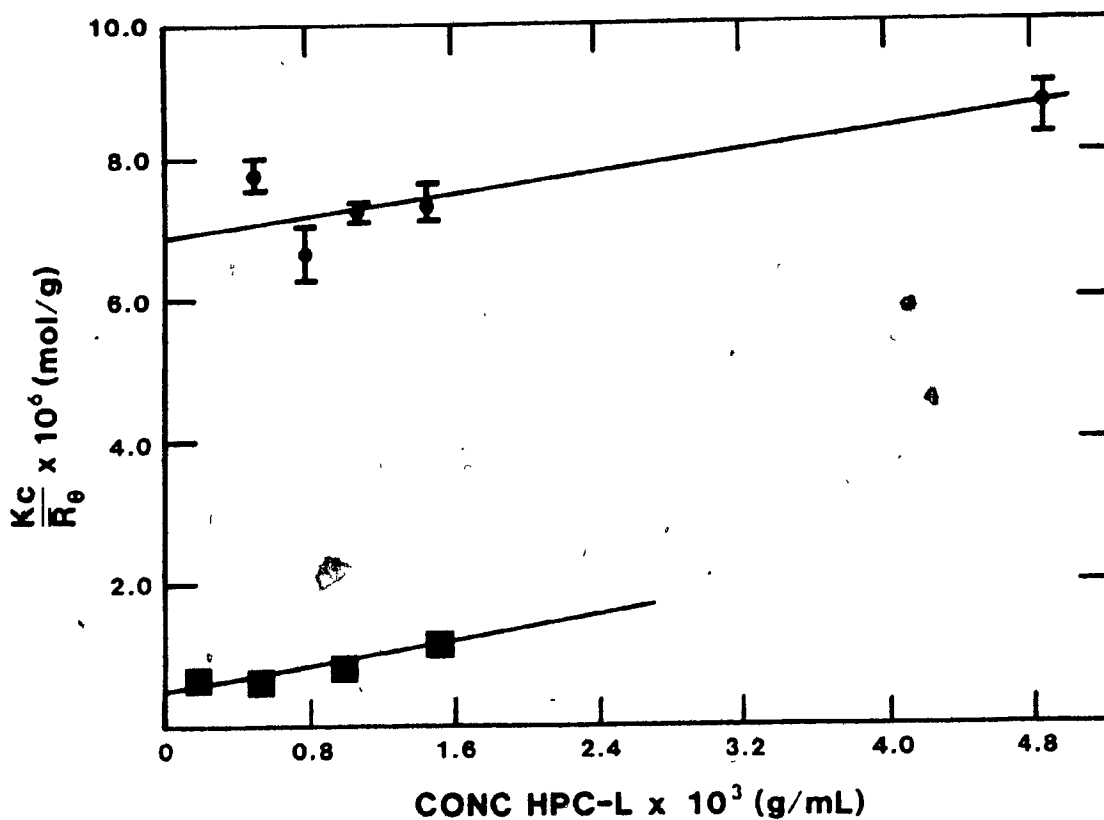


FIGURE II.12 LALLS results for HPC-L solutions in ethanol which were aged for one week (●) and for two months (■): $n_{\text{C}_2\text{H}_5\text{OH}} = 1.359$, $dn/dc = 0.117$, $K = 1.031 \times 10^{-7} \text{ mol cm}^2 \text{ g}^{-2}$, $\bar{M}_w = 1.5 \times 10^4 \text{ g/mol}$ and $A_2 = 1.853 \times 10^{-3} \text{ mL mol g}^{-2}$ (●), $\bar{M}_w = 1.9 \times 10^5 \text{ g/mol}$ and $A_2 = 1.850 \times 10^{-3} \text{ mL mol g}^{-2}$ (■). See text for explanation of closed circles superimposed on bars.

samples were found to contain tiny gel particles large enough to be visible by the naked eye. These particles were probably undissolved HPC. On standing a week, the number of undissolved particles was greatly reduced. Light scattering data on week old samples seems to indicate that initially only the lower molar mass fractions of HPC dissolve since the molar mass was found to be only 15 000 g/mol. Solutions were aged two months and at this time almost no gel particles were visible. The molar mass for HPC-L had increased to 190 000 g/mol. The second virial coefficient in both cases was approximately constant at $1.85 \times 10^{-3} \text{ mL mol g}^{-2}$. The reason why HPC-L behaves so differently in water, THF, and ethanol is not known, but it can be reported that light scattering measurements in organic solvents are more reproducible than in water. In addition, HPC-L seems to aggregate to a lesser extent in THF than in water; whereas, in ethanol the HPC has a hard time dissolving completely, but once it does, it appears to start aggregating. In spite of all the problems encountered, the molar mass for HPC-L appears to be approximately 210 000 g/mol — the average value from light scattering measurements in the three solvents.

Figures II.13 and II.14 illustrate the LALLS results for aqueous HPC-E and J solutions respectively. The data for HPC-E are relatively non-linear. The molar mass was calculated to be 120 000 g/mol and A_2 was $4.09 \times 10^{-4} \text{ mL mol g}^{-2}$. Once again a buildup in back pressure was noted at the filter while measurements were being made. Unexpectedly, the data for HPC-J were very good and it was the only system in which there was no noticeable buildup in back pressure at the filter. In addition, HPC-J

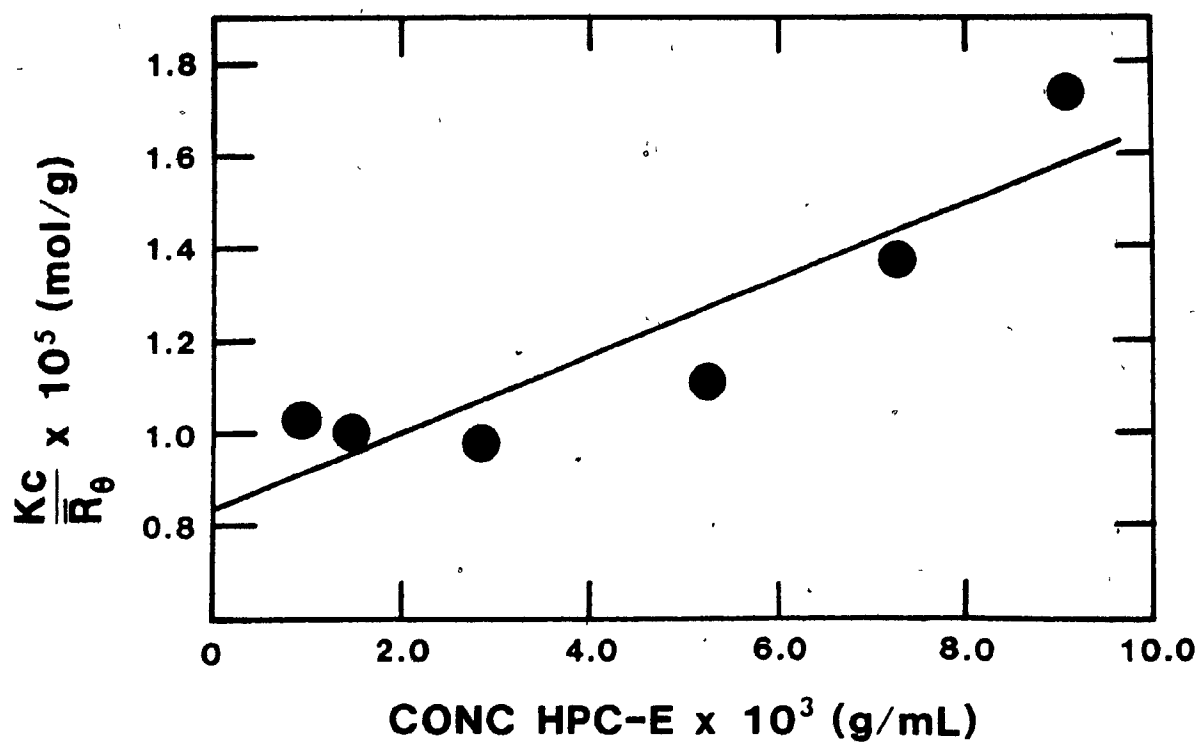


FIGURE II.13 LALLS results for aqueous HPC-E solutions: $n_{\text{H}_2\text{O}} = 1.333$, $dn/dc = 0.133$, $K = 1.282 \times 10^{-7} \text{ mol cm}^2 \text{ g}^{-2}$, $\bar{M}_w = 1.20 \times 10^5 \text{ g/mol}$, and $A_2 = 4.09 \times 10^{-4} \text{ mL mol g}^{-2}$. The closed circles represent the average \bar{R}_θ obtained for five to seven individual measurements.

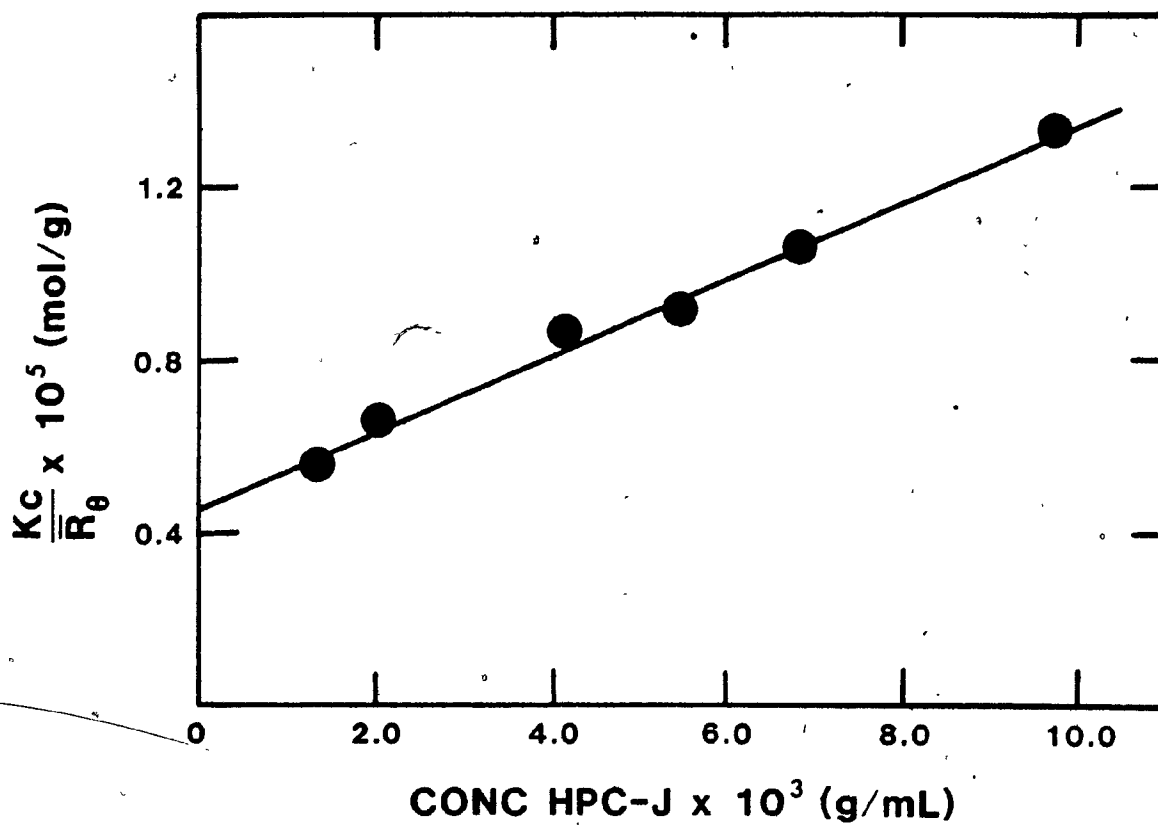


FIGURE II.14 LALLS results for aqueous HPC-J solutions: $n_{H_2O} = 1.333$, $dn/dc = 0.134$ mL/g, $K = 1.301 \times 10^{-7}$ mol cm² g⁻², $\bar{M}_w = 2.12 \times 10^5$ g/mol, and $A_2 = 4.52 \times 10^{-4}$ mL mol g⁻².

would not dissolve in either THF or ethanol. It is believed that the linearity of the data points may result from a more regular or lower substitution pattern which, perhaps, inhibits aggregation or gel formation for HPC-J samples. The molar mass for HPC-J was found to be 212 000 g/mol and A_2 was 4.52×10^{-4} mL mol g⁻². The problems observed for the various HPC solutions were more acute for the higher molar mass samples and no reliable data could be obtained for the HPC-M and HPC-H samples.

II.4.2 SEDIMENTATION EQUILIBRIUM

Introduction

The absolute weight average molar mass for a polymer may be determined by the use of sedimentation velocity or sedimentation equilibrium techniques. Both methods involve the study of molecular motion through a stationary solvent (76-77) and are classified as transport phenomenon. In this work only the latter technique will be described.

When a polymer solution is subjected to a low centrifugal field in an analytical ultracentrifuge, an equilibrium concentration gradient is established. The normal thermodynamic tendency of molecules to diffuse is exactly balanced at every point by the centrifugal field and, consequently, no net flow of molecules across the gradient occurs. Formerly, the long times required for the attainment of equilibrium were a disadvantage of this method; however, by the use of a short column technique developed by Van Holde and Baldwin (78) the time can be reduced to a reasonable level.

Modification of the equation developed by Goldberg (79) for sedimentation equilibrium in a multi-component system permits an apparent molar mass ($\bar{M}_{w,i}$) to be calculated using the equation below

$$\bar{M}_{w,i} = \frac{K_s}{1-v\rho} \cdot \frac{1}{\underline{x}c} \cdot \frac{y_e}{dn/dc} \quad \text{II.9}$$

where ρ = the solution density (g/mL)

v = the specific volume of the solute (mL/g)

c = the solution concentration (g/mL)

\underline{x} = the distance of the gradient midpoint from the center of the rotor

y_e = the height of the gradient mid-point from a reference line on the photographic film

dn/dc = the differential index of refraction (mL/g)

K_s = a constant which is a function of the temperature, rotor speed, and phase plate angle

Sedimentation equilibrium is really only applicable to monodisperse solutions whose behavior may be described as ideal (76). For polydisperse systems the situation is more complex since each molar mass species in the polymer will attain a different equilibrium distribution in the cell. The effects of polydispersity are revealed by an increasing curvature in a logarithmic plot of solution concentration versus \underline{x}^2 . In addition, macromolecular solutions hardly ever exhibit ideal behavior and consequently a correction must be applied for solution non-ideality (43). This is done

by using the relationship below

$$\frac{1}{\bar{M}_w} = \frac{1}{\bar{M}_{w,i}} + B_e c_0 \quad \text{II.10}$$

where \bar{M}_w is the true molar mass, $\bar{M}_{w,i}$ is the molar mass calculated using Equation II.9 assuming ideal behavior ($B_e = 0$), B_e is a non-ideality correction factor, and c_0 is the initial solution concentration. The intercept on plotting $1/\bar{M}_{w,i}$ versus c_0 is the reciprocal of the true molar mass and B_e may be evaluated as the slope of the line.

Experimental

A Beckman Model E Analytical Ultracentrifuge was utilized to determine the molar mass for HPC-E, L, J, G, and M samples in water. The experimental runs were expertly and kindly performed by Mr. W.Q. Yean of the Pulp and Paper Research Institute of Canada. The technique used has been described elsewhere (80-81). Four hours were sufficient for the HPC samples to achieve equilibrium. The time-consuming measurements from the photographic schlieren patterns and subsequent numerical calculations to evaluate the molar mass for each sample were carried out by the author.

Standard double-channel quartz cells were used in the ultracentrifuge. One side of the cell was filled with solution and FC-43 while the other side contained solvent and FC-43. The FC-43 is a very

dense liquid (perfluorotributylamine) which is immiscible with water. Its function is to produce a liquid - liquid boundary at the bottom of the column (82). The cells were centrifuged at various speeds at 25°C. The schlieren patterns were recorded at a phase plate angle of 65° on Kodak Royal Pan film.

Solutions were made up in 15-mL vials on a weight to solvent volume basis. The solvent was added with a 5-mL volumetric pipette. This stock solution was then volumetrically diluted to give more solution concentrations. For some HPC samples all the solutions were prepared directly without subsequent dilutions to check the magnitude of any dilution errors. The solution concentrations prepared for HPC-E, L, J, and G ranged from 1.66 to 10.5 g/L. The HPC-M required the use of more dilute solutions with concentrations between 0.59 and 2.3 g/L.

Several different solution concentrations for each HPC sample were centrifuged at 12 000 rpm. The HPC-L samples were also centrifuged at 8000, 16 000, and 20 000 rpm to verify that there was no speed dependence for the HPC samples. The other HPC samples were only centrifuged at 12 000 rpm. The only exception was HPC-M which was run at 8000 rpm because at the faster speed no solution gradient was visible. No gel particles or precipitate were found at the bottom of the cell on completion of the experiment. A photographic enlarger with a magnification of 8 was used to facilitate the required measurements on the photographic negatives.

The solution density, ρ , was not measured directly but was calculated from the densities of the pure components by use of Equation II.11 which assumes that no volume change occurs on mixing the two components.

$$\rho = \frac{m}{V} = \frac{\rho_1 V_1 + w_2}{V_1 + \frac{w_2}{\rho_2}} \quad \text{II.11}$$

where ρ = the solution density

m = the total mass of both components

V = the total volume of both components

ρ_1 = the solvent density

ρ_2 = the solute density

V_1 = the solvent volume

w_2 = the solute weight

The use of Equation II.11 introduces only a small error in the density for the dilute solutions being investigated. Density measurements at higher dilutions using a Paar Precision Densitometer gave scattered results; measurements at higher HPC concentrations were difficult due to the viscous nature of the solutions.

Results and Discussion

An apparent molar mass ($\bar{M}_{w,i}$) for each HPC concentration can be

calculated by use of Equation II.9 and the sedimentation equilibrium data. Figure II.15 illustrates a typical schlieren pattern obtained for an aqueous HPC solution. The y_a and δ_x marked on the film were measured directly and divided by the magnification factor of 8. Values of δ_x were used to evaluate the \underline{x} needed in Equation II.9 by using the following relationship

$$\underline{x} = 7.3 - \frac{\delta_x}{2.144} \quad \text{II.12}$$

where 2.144 is an internal camera magnification factor and 7.3 is the distance from a reference line to the rotor center. The other variables used in Equation II.9 had the following values: K_s at 25°C and a 65° phase plate angle was 141.8 at 12 000 rpm and 319.1 at 8000 rpm. The dn/dc was taken as 0.134 mL/g and it was assumed to be independent of molar mass. The solute specific volume (v) was calculated as 0.81 mL/g since it is defined as the reciprocal of the solute density ($\rho_{\text{HPC}} = 1.23$ g/mL) (83). The solution density was found to be 0.998 g/mL by using Equation II.11.

A graph of $1/\bar{M}_{w,i}$ versus concentration for each HPC sample (E, L, J, G, and M) was constructed and the data extrapolated to zero concentration to eliminate any effects arising from non-ideal behavior. In each case the intercept gave a true molar mass and these results can be found in Figure II.16. The molar masses reported are believed to be accurate to within $\pm 15\%$ based on probable measurement errors and the use of calculated

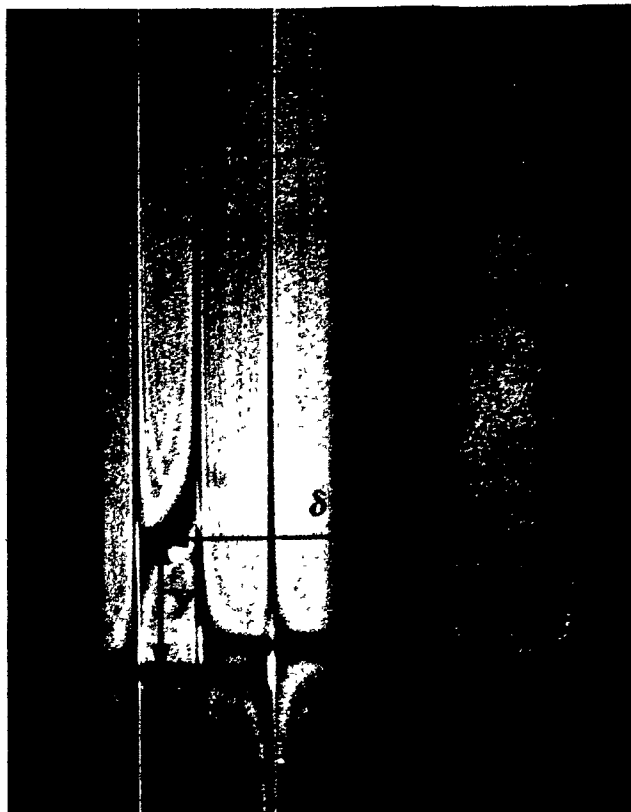


FIGURE II.15 Typical sedimentation equilibrium schlieren pattern obtained for an aqueous HPC-E solution (7.86×10^{-3} g/mL) at 25°C and 12 000 rpm: y_e is the height of the ordinate from the base line to the midpoint of the meniscus as indicated in the above figure and δ_x is the distance from the rotor center reference line to the solution column midpoint as noted in the above figure.

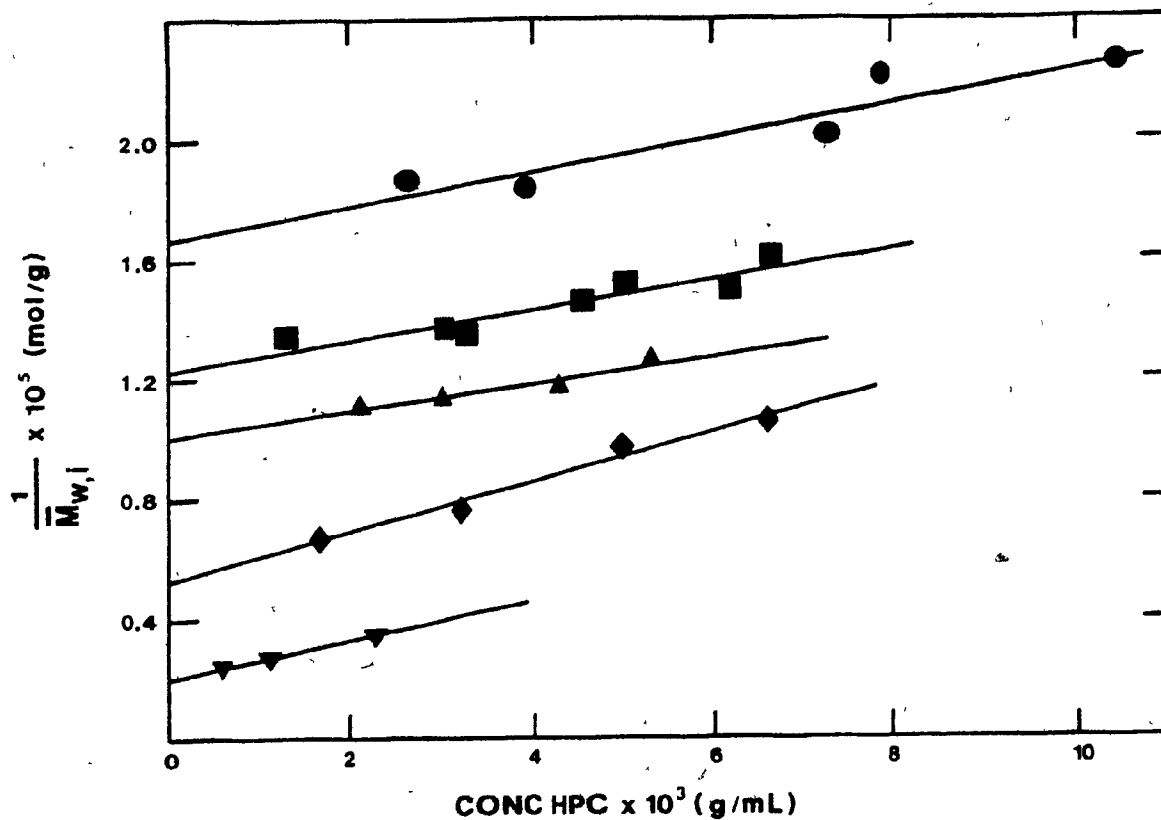


FIGURE II.16 Variation in apparent molar mass with concentration for several HPC samples in aqueous solution: ● HPC-E ($\bar{M}_w = 6.0 \times 10^4$ g/mol, $A_2 = 2.96 \times 10^{-4}$ mL mol g⁻²), ■ HPC-L ($\bar{M}_w = 8.2 \times 10^4$ g/mol, $A_2 = 2.61 \times 10^{-4}$ mL mol g⁻²), ▲ HPC-J ($\bar{M}_w = 1.0 \times 10^5$ g/mol, $A_2 = 2.19 \times 10^{-4}$ mL mol g⁻²), ◆ HPC-G ($\bar{M}_w = 1.9 \times 10^5$ g/mol, $A_2 = 4.11 \times 10^{-4}$ mL mol g⁻²), ▼ HPC-M ($\bar{M}_w = 5.3 \times 10^5$ g/mol, $A_2 = 3.15 \times 10^{-4}$ mL mol g⁻²).

density and specific volume values. The only literature value available for comparison with our experimental results on molar mass was obtained on a dialyzed HPC-L sample by sedimentation velocity (38). The reported \bar{M}_w value of 73 000 g/mol agrees well with our experimental value of 82 000 g/mol and is within the experimental error limits noted above.

II.4.3 COMPARISON OF MOLAR MASS TECHNIQUES

The advantages of LALLS over conventional light scattering are many but only four points will be mentioned. Low angle laser light scattering utilizes the special characteristics of a laser to measure absolute scattered light intensities at low angles eliminating the need for calibrating solutions or solvents and the tiresome calculations necessary in constructing a Zimm plot. The high sensitivity of the LALLS photometer permits the use of very low solution concentrations, thereby making the extrapolation to zero concentration more accurate than conventional Zimm plot results. The difficulties in clarifying the 15 to 25 mL of static solution required in conventional light scattering are greatly reduced when a smaller scattering volume (0.5 μ L) is needed. In addition, the ocular lens on a LALLS photometer allows direct viewing of the scattering solution and foreign particles flowing through the solution are easily recognized and these scattering results neglected. Any or all of the above reasons may account for the difference in molar mass for HPC-G from conventional ($\bar{M}_w = 740\ 000$ g/mol) and LALLS ($\bar{M}_w = 420\ 000$ g/mol) measurements. The only drawback to all light scattering measurements is the well

documented tendency of cellulose derivative dilute solutions to aggregate with time (84,85).

Both light scattering and sedimentation equilibrium techniques provide absolute weight average molar masses which should be almost identical. Manley (43) in work on ethyl hydroxyethylcellulose found that the molar masses calculated from the two techniques differed by a factor of two for the same samples. Manley postulated that on etherification of alkaline cellulose a uniform distribution of substituents is not achieved. The highly crystalline sections of the original cellulose react more slowly than do the amorphous portions of the chains. On dissolving the cellulose derivative, a large portion of the material dissolves totally; however, a small fraction remains insoluble -- crystalline remnants of the original cellulose. The presence of this material does not appear to affect the molar mass calculated from sedimentation equilibrium data. But this insoluble material cannot be filtered out of light scattering solutions and appears to have a profound effect on the molar mass that is calculated from light scattering data.

Table II.5 summarizes the molar mass results for the HPC samples calculated from LALLS and sedimentation equilibrium measurements. The data clearly show that the molar mass obtained from light scattering is approximately twice as large as the corresponding value calculated from sedimentation equilibrium results. The exact reason for the factor of two discrepancy in molar mass between the two methods is unknown. However,

TABLE II.5

Calculated Molar Masses (\bar{M}_w) and Second Virial Coefficients (A_2)
for HPC Samples from Low Angle Laser Light Scattering (LALLS)
and Sedimentation Equilibrium (SE) Measurements

HPC Type	LALLS		SE	
	$\bar{M}_w \times 10^{-3}$ (g/mol)	$A_2 \times 10^4$ (mL mol g ⁻²)	$\bar{M}_w \times 10^{-3}$ (g/mol)	$A_2 \times 10^4$ (mL mol g ⁻²)
E	120	4.09	60	2.96
L	210	2.50	82	2.61
J	212	4.52	100	2.19
G	420	11.1	190	4.11
M	-	-	530	3.15
H	-	-	900*	-

* Value from sedimentation velocity technique (40)

four possible reasons for the difference in molar mass may be proposed. First, the light scattering photometer may exhibit a systematic error in its results. This idea can be immediately discarded because the dextran solutions gave excellent molar mass results and others in this laboratory (86) have obtained excellent molar mass results for National Bureau of Standards polystyrene samples. Second, since the HPC is produced by a heterogeneous reaction between alkaline cellulose and propylene oxide, the HPC is necessarily polydisperse. The high molar mass fractions of HPC may not achieve equilibrium in the centrifugal field and, perhaps, only the low and medium weight fractions determine the average molar mass. This proposal, although possible, is unlikely because there was no precipitate visible in the centrifuge cells. Third, it is possible that the two techniques do not even measure the same weight average molar mass because the effects of sample polydispersity on the average molar mass value are different (45,76). Fourth, the presence of time or shear induced molecular aggregation seems most likely on the basis of some of the light scattering data presented. It is, therefore, the opinion of this author that either molecular aggregation or sample polydispersity are somehow responsible for the higher molar masses calculated for HPC from light scattering data. Aggregates of HPC, if they exist, do not appear to affect sedimentation equilibrium measurements. It is possible that the centrifugal field is strong enough to break up any aggregates and, hence, the molar mass calculated by this technique is the true molar mass.

The characterization of cellulose derivatives is a difficult task.

The effects of polydispersity, non-homogeneous substitution, and molecular aggregation on measured molar masses remain ill-defined. In the preceding sections an attempt has been made to characterize several HPC samples as well as the techniques currently available permitted; the problems encountered show that such measurements are not routine and that several methods should be applied.

II.4.4 VISCOSITY

Introduction

The polydispersity of HPC samples precludes the use of the $P(\theta)$ values from light scattering in evaluating molecular shape. The effects of sample polydispersity and particle shape superimpose to the extent that the interpretation of $P(\theta)$ values is meaningless. In an effort to learn more about the molecular shape of the HPC molecules in solution, viscosity measurements were undertaken. The viscosity of a fluid is a measure of its internal friction or its resistance to flow. Addition of a polymeric solute to a solvent causes an increase in the viscosity of the resulting solution over that of the pure solvent. Under favorable conditions viscosity measurements can be used to evaluate the conformation of the solute molecules. In principle viscosity measurements may also be utilized to derive a molar mass for the solute; however, this molar mass is not absolute and it must be calibrated against another method like light scattering. The use of viscosity measurements in evaluating molar masses is very limited in scope and its principle function is to provide

data on the transport processes occurring in solution (87).

In capillary viscometry a solution is allowed to flow through a capillary of a given length under the influence of gravity. The time required for a given volume of solution to pass through the capillary is compared with the corresponding time for the same volume of pure solvent. Generally, dilute polymer solutions are used and it is assumed that the solvent and solution densities are approximately equal. As a result, the viscosity ratio or relative viscosity (η_r) is simply the flow time of the solution divided by that of the solvent. The viscosity of a solution varies with the solute concentration. To minimize concentration effects the viscosity number or reduced viscosity (η_{red}) has been defined as

$$\eta_{red} = \left(\frac{\eta_{sp}}{c} \right) = \frac{(\eta_r - 1)}{c} \quad \text{II.13}$$

where c is the solution concentration in g/100-ml of solution and η_{sp} is the specific viscosity. The viscosity number is really made up of two parts. First, individual polymer molecules contribute to the solution viscosity. Second, since polymers are relatively large flexible molecules they easily interact with one another and, for this reason, molecular interactions also affect the solution viscosity. To minimize the effects of intermolecular interference, the viscosity number is extrapolated to zero concentration and the intercept gives the limiting viscosity number or intrinsic viscosity ($[\eta]$) defined in Equation II.14 below.

$$[\eta] = \left(\frac{\eta_{sp}}{c} \right)_{c=0} \quad \text{II.14}$$

The limiting viscosity number is a tangible measure of the ability of the polymer to enhance the viscosity of the solvent in the absence of intermolecular effects. Viscosity data may also be expressed as a logarithmic viscosity number or inherent viscosity (η_i) defined in Equation II.15.

$$\eta_i = \left(\frac{\ln \eta_r}{c} \right) \quad \text{II.15}$$

To evaluate $[\eta]$ accurately, the experimental finite concentration viscosity data are usually fitted to a semi-empirical formula developed by Huggins.

$$\left(\frac{\eta_{sp}}{c} \right) = [\eta] + k[\eta]^2 c \quad \text{II.16}$$

Equation II.16 predicts that a plot of (η_{sp}/c) versus concentration will be linear with an intercept of $[\eta]$ and the slope of the line will vary as the square of $[\eta]$ for a particular polymer-solvent pair. For flexibly coiled polymers k is a constant which ranges from 0.3 to 0.5 (87). Alternatively, a $[\eta]$ value can be obtained by the use of inherent viscosity data and Kraemer's equation illustrated below

$$\eta_i = \left(\frac{\ln \eta_r}{c} \right) = [\eta] + k'[\eta]^2 c \quad \text{II.17}$$

where $k' = k - 0.5$ of the Huggins equation. The Kraemer equation yields a line of lower slope than does the Huggins equation and so may be preferred for extrapolation purposes. The best method is to plot the finite concentration data according to both Equations II.16 and II.17 and to take the common intercept as the limiting viscosity number. If the Huggins equation plot shows upward curvature then the Martin equation, illustrated below, finds extensive use.

$$\log \left(\frac{\eta_{sp}}{c} \right) = \log [\eta] + k''[\eta]c \quad \text{II.18}$$

The Mark - Houwink equation, shown below, relates the limiting viscosity number ($[\eta]$) to the polymer molar mass (\bar{M}_w).

$$[\eta] = K \bar{M}_w^\alpha \quad \text{II.19}$$

The values of K and α are determined from a double logarithmic plot of $[\eta]$ versus \bar{M}_w . The intercept of this plot is K and α is the slope. The values of K and α are constant for a particular polymer-solvent pair. The shape of the solute particles in solution may be inferred from the value of α (87). Equation II.19 is strictly only applicable to mono-disperse polymers but it may also be used qualitatively for polydisperse systems.

Experimental

Viscosity measurements were obtained for HPC-E, L, J, and G samples in both acetic acid and 1-pentanol. Twenty solutions, five per HPC type, were prepared using the procedure already outlined. The solvents were used as received from the manufacturer. Solutions were clear and gel-free except for HPC-G/1-pentanol solutions in which gel particles were very evident indicating that the high molar mass HPC-G had only marginal solubility in 1-pentanol. Solution concentrations ranged from 0.04 to 0.46 g/dL in 1-pentanol and from 0.07 to 0.68 g/dL in acetic acid.

Viscosities were measured using Ubbelohde capillary viscometers (Fisher brand, size 100) which were calibrated with distilled water. The viscometers were immersed in a 30-L glass bath (Townson and Mercer Ltd) thermostatted at $25^{\circ} \pm 0.01^{\circ}\text{C}$. Solutions were equilibrated for fifteen minutes in the viscometers which were immersed in the bath. Viscosity measurements were made between five and eight times and the results were averaged. The flow times were recorded using an ordinary stopwatch (Heuer Inc) or an automatic timer (Rinco Instrument Co) and were reproducible to within $\pm 0.3\%$.

Results and Discussion

The solvents chosen for viscosity measurements were those which gave significantly different critical volume fraction values for mesophase

formation (see next chapter). The idea was to see if the effect of solvent on this critical volume fraction was related to the polymer conformations in these solvents as reflected by their dilute solution viscosities. The limiting viscosity number in both acetic acid and 1-pentanol was taken to be the common intercept of the experimental viscosity data when it was plotted according to both the Huggins and Kraemer equations. The viscosity data obtained for HPC-E, L, J, and G in 1-pentanol and acetic acid are plotted in Figures II.17 and II.18 respectively. The data for HPC-G in 1-pentanol have been omitted since the presence of gel particles interfered with viscosity measurements. Wirick and Elliott (88) reported that the viscosity data for HPC in water, ethanol, and a 50:50 water:ethanol mixture fit the Martin equation much better than the Huggins equation. The viscosity data for the HPC solutions in 1-pentanol and acetic acid were plotted according to the Martin equation and the resulting graphs are shown in Figures II.19 and II.20. The viscometric data for HPC in 1-pentanol and acetic acid seem to fit both the Huggins and Martin equations equally well.

The limiting viscosity numbers obtained from the Huggins, Kraemer, and Martin equations should be almost identical for a particular polymer-solvent combination. Examination of the data listed in Table II.6 illustrates that for each HPC type there is good agreement for the limiting viscosity numbers calculated from the three equations. In addition, the data show that as the molar mass of the HPC is increased, there is a corresponding increase in the limiting viscosity number as predicted by the Mark - Houwink equation. The Huggins, Kraemer, and Martin constants, k , k' ,

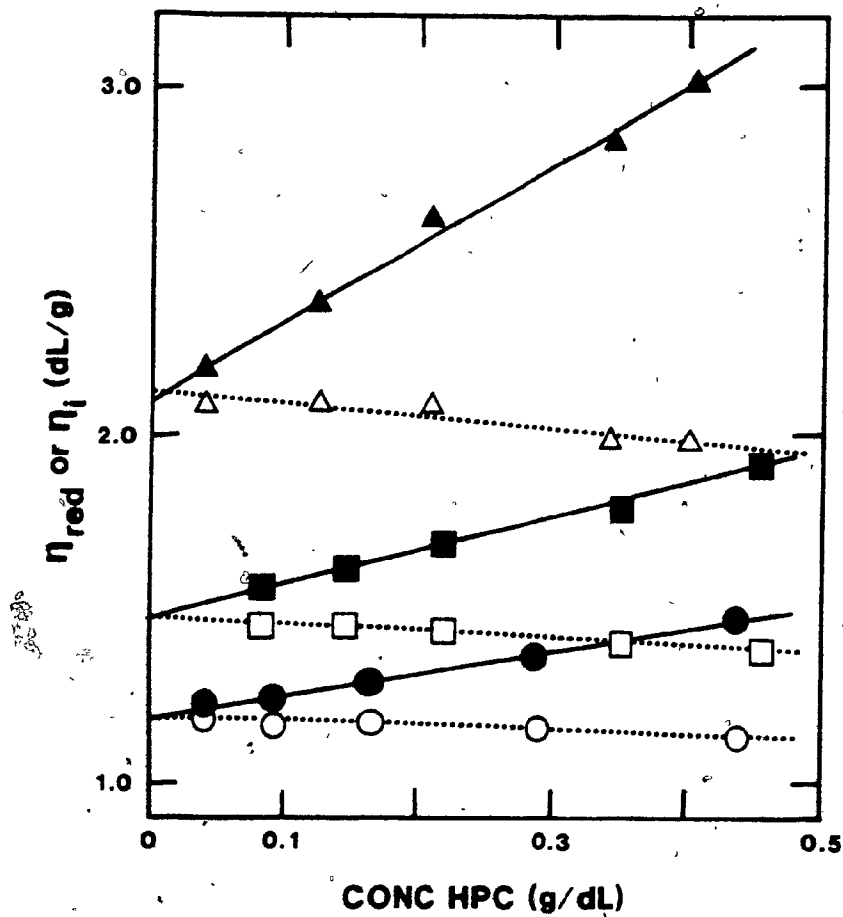


FIGURE II.17 Huggins (closed symbols) and Kraemer (open symbols) equation plots of the viscosity data obtained for HPC-E (●,○), L (■,□), and J (▲,△) in 1-pentanol at 25°C.

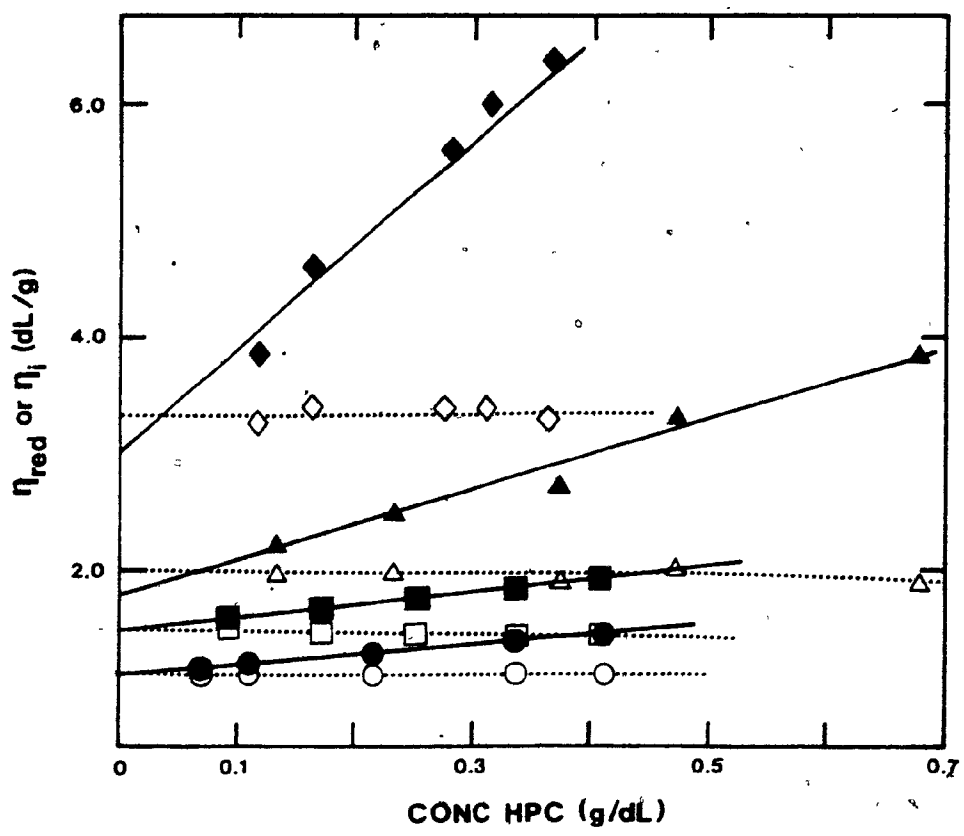


FIGURE II.18 Huggins (closed symbols) and Kraemer (open symbols) equation plots of the viscosity data obtained for HPC-E (●,○), L (■,□), J (▲,△), and G (◆,◇) in acetic acid at 25°C.

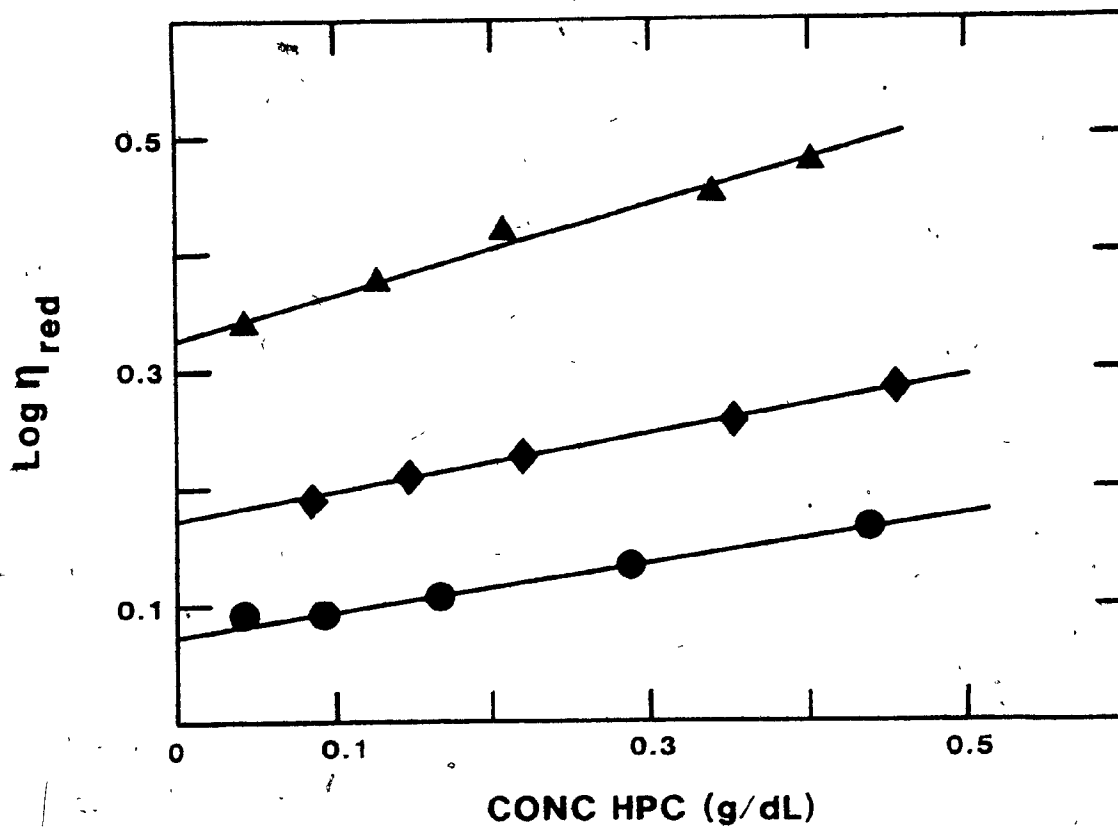


FIGURE II.19 Martin equation plot of the viscosity data obtained for HPC-E (●), L (◆), and J (▲) in 1-pentanol at 25°C.

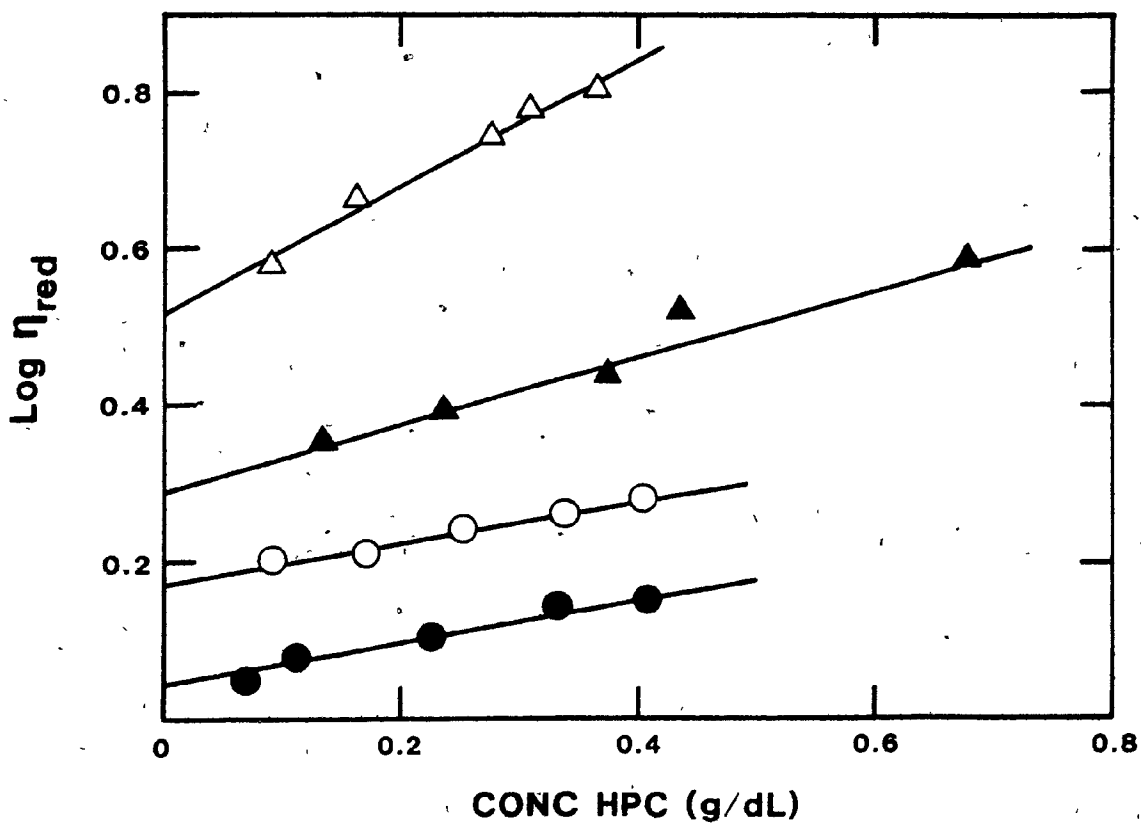


FIGURE II.20 Martin equation plot of the viscosity data obtained for HPC-E (●), L (○), J (▲), and G (△) in acetic acid at 25°C.

TABLE II.6

Summary of Limiting Viscosity Number ($[\eta]$) and k , k' , k'' Constants from the Huggins, Kraemer, and Martin Equations Respectively for HPC Samples at 25°C

HPC Type	Solvent	Huggins		Kraemer		Martin	
		$[\eta]$ (dL/g)	k	$[\eta]$ (dL/g)	k'	$[\eta]$ (dL/g)	k''
E	1-C ₅ H ₁₁ OH	1.18	0.44	1.19	-0.10	1.19	0.17
	CH ₃ COOH	1.10	0.69	1.11	-0.05	1.11	0.26
L	1-C ₅ H ₁₁ OH	1.48	0.45	1.48	-0.11	1.49	0.16
	CH ₃ COOH	1.47	0.51	1.48	-0.07	1.48	0.19
J	1-C ₅ H ₁₁ OH	2.10	0.51	2.13	-0.08	2.13	0.18
	CH ₃ COOH	1.76	0.99	1.97	-0.02	1.94	0.23
G	1-C ₅ H ₁₁ OH	-	-	-	-	-	-
	CH ₃ COOH	2.98	1.1	3.34	0.01	3.29	0.25

and k'' respectively, which should be independent of molar mass for a particular polymer-solvent pair, exhibited some random variation with molar mass for the HPC in both solvents. This behavior is often observed for cellulose derivatives (85,88). The three constants seem to vary more in acetic acid than in 1-pentanol and the Huggins constant has a higher average value in acetic acid ($k = 0.82$) than in 1-pentanol ($k = 0.47$).

The Mark - Houwink K and a parameters for HPC in 1-pentanol and acetic acid were evaluated from a double logarithmic plot of limiting viscosity number versus molar mass. The relevant data have been listed in Table II.7. The molar masses are those determined from sedimentation equilibrium and the listed limiting viscosity numbers are the average values of these quantities reported in Table II.6. The Mark - Houwink equation is only applicable for narrow molar mass polymer fractions. However, in applying this equation to the polydisperse HPC system some information may be extracted. The different a values for HPC in 1-pentanol and acetic acid indicate that the molecules have slightly different conformations in these two solvents. Further, the HPC molecules are intermediate in shape between a random coil ($a = 0.6 - 0.8$) and a rigid rod ($a = 1.8$). The slightly larger a value in 1-pentanol would seem to imply that the HPC molecules are stiffer in this solvent than in acetic acid. Table II.8 lists re-calculated K and a values from the literature, assuming that the molar masses for HPC listed in Table II.7 are used instead of the manufacturer's reported molar masses for corresponding HPC samples. Examination of the data shows some scatter in the Mark - Houwink

TABLE II.7

Data Used to Evaluate the Mark - Houwink K and α Parameters for
HPC in 1-Pentanol and Acetic Acid

HPC Type	\bar{M}_w (g/mol)	1-Pentanol	Acetic Acid
		$[\eta]$ (dL/g)	$[\eta]$ (dL/g)
E	60 000	1.19	1.11
L	82 000	1.48	1.48
J	100 000	2.12	1.89
G	190 000	-	3.20
	K (dL/g)	6.98×10^{-6}	4.54×10^{-5}
	α	1.09	0.92

TABLE II.8

Mark - Houwink Constants for HPC in Various Solvents

Solvent	$K \times 10^{-5}$ (dL/g)	a	Reference
CH_3COOH	4.54	0.92	(89)
CH_3COOH	1.60	1.02	(90)
H_2O	5.32	0.88	(91)*
H_2O	1.36	1.02	(90)
$\text{C}_2\text{H}_5\text{OH}$	2.60	0.915	(32)•
$\text{C}_2\text{H}_5\text{OH}$	6.74	0.88	(25)
$\text{C}_2\text{H}_5\text{OH}$	9.85	0.85	(90)
$\text{CH}_3(\text{CH}_2)_4\text{OH}$	6.98	1.09	(89)

* Temperature 38°C ; all other viscosity data at 25°C

• Reported molar masses from light scattering of fractionated HPC

parameters for a particular polymer-solvent combination. This may reflect the polydispersity of the HPC samples and the uncertainty in the average molar mass of each fraction. For this reason it is believed that these α parameters cannot reliably be used to predict in which solvent HPC has a stiffer conformation.

II.4.5 MOLAR SUBSTITUTION

Introduction

The characterization of HPC would not be complete without some comment on the MS. The exact effect of MS on the behavior of HPC in light scattering, sedimentation equilibrium, and viscosity measurements is unknown. The only available information suggests that the MS of the sample plays a vital role in determining the solubility of the HPC in various solvents (2,8).

Experimental

Nuclear magnetic resonance (NMR) was chosen as the technique by which to try and determine the MS of the HPC-E and L samples. The HPC was dissolved in deuterated chloroform to give solutions of 7.6% HPC-E and 7.0% HPC-L by weight. A Varian T-60 spectrometer was used to record the NMR spectra at 35°C. Standard 0.5-mm outer diameter glass tubes were used to hold the sample which was preheated for ten minutes at 35°C prior to insertion in the spectrometer probe. Tetramethylsilane was added to the

tubes to serve as a reference for chemical shift.

Results and Discussion

The NMR spectra for the HPC were interpreted using the method developed by Ho (13). Figure II.21 illustrates a typical NMR spectrum for HPC which consists of two relatively broad peaks. The low field or so called methyl peaks (A) arise solely from CH₃ hydrogens on the substituents of the cellulose ring. All other hydrogens, whether they be on the cellulose or the substituents, contribute to the higher field peak (B). According to Ho the MS is given by the equation below where A and B refer to the areas under the low and high field peaks respectively.

$$MS = \frac{10 A}{3 (B - A)} \quad \text{II.20}$$

Calculated MS values for HPC-E and L ranged from 5 to 8. The precision of this technique was therefore not very good. In addition, work in progress by Perlin and Lee (92-94) indicates that the NMR spectrum for HPC is more complex than that originally proposed by Ho. This is clearly shown in the presence of a third unexplained low field peak in Figure II.21. For these reasons the manufacturer's reported data for the MS, measured by a modification of the terminal methyl method developed by Lemieux and Purves (12), was assumed to be correct. Very recently, Lee and Perlin have confirmed that for HPC-E the DS is 2.5 and the MS is approximately 4 by

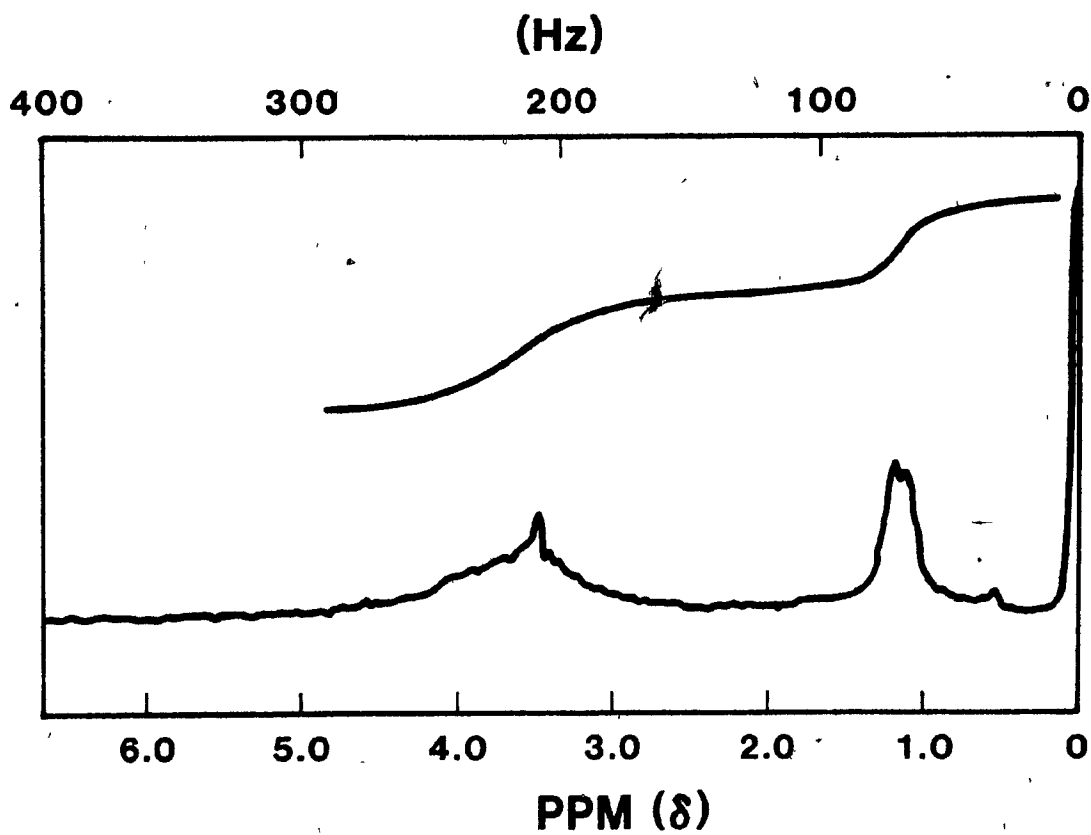


FIGURE II.21 A typical NMR spectrum obtained for HPC-L in CDCl_3 at 38°C .

the use of a high resolution C^{13} NMR technique (10).

II.5 Conclusion

The weight average molar masses calculated from light scattering data are high and approximately twice those calculated from sedimentation equilibrium data for all HPC types investigated. Two possible explanations have been proposed to account for this discrepancy in molar mass calculated by the two techniques. Firstly, the average molar mass measured by each technique may be different because of sample polydispersity. Secondly, time or shear induced aggregation of the HPC appears to have a more pronounced effect on the light scattering results than on the sedimentation equilibrium results. For this latter reason the true molar mass of the HPC is believed to be that determined by the sedimentation equilibrium technique.

The molecular conformation of HPC in dilute 1-pentanol and acetic acid solutions is neither a rigid rod nor a flexible coil as indicated by the viscosity data presented in this chapter. Rather the HPC molecules appear to have some intermediate conformation.

References

1. "KLUCEL Hydroxypropyl Cellulose: Chemical and Physical Properties", Hercules Inc., Wilmington, Delaware, 1976.
2. E.D. Klug, U.S. Patent 3 278 521, 1966.
3. R.G. Bishop, U.S. Patent 3 351 583, 1967.
4. E.D. Klug, U.S. Patent 3 278 520, 1966.
5. E. Gipstein and E. Wellisch, J. Appl. Polym. Sci., 17, 2783-90 (1973).
6. R.T. Morrison and R.N. Boyd, "Organic Chemistry", 2nd ed., Allyn and Bacon Inc., Boston, 1966, pp. 1026-37.
7. A.H. Nissan and G.K. Hunger in "Encyclopedia of Polymer Science and Technology", H.M. Mark, N.G. Gaylord, and N.M. Bikales, Eds., John Wiley & Sons Inc., New York, 1965, Vol. 3, pp. 131-35, 291-92, and 459-71.
8. E.D. Klug, J. Polym. Sci., Polym. Phys. Ed., 36, 491-508 (1971).
9. M.G. Wirick, J. Polym. Sci., Polym. Chem. Ed., 6, 1965-74 (1968).
10. D.S. Lee, McGill University, private communication, 1981.
11. J.D. Angerer, Hercules Inc., private communication, 1978.
12. R.U. Lemieux and C.B. Purves, Can. J. Res., 25 B, 485-89 (1947).
13. F.F.L. Ho, R.R. Kohler, and G.A. Ward, Anal. Chem., 44, 178-81 (1972).
14. A.B. Savage in "Derivatives of Cellulose", N.M. Bikales and L. Segal, Eds., Wiley-Interscience Inc., New York, 1971, Vol. 5, Part 5, Chapter XVII-C.
15. B.V. Vasiliev, G.I. Bleivas, M.V. Prokofieva, and D.G. Tarakanov, Cellulose Chem. Technol., 7, 293-306 (1973).
16. R.S. Werbowyj and D.G. Gray, Mol. Cryst. Liq. Cryst., 34, 97-103 (1976).
17. N. Sarkar, J. Appl. Polym. Sci., 24, 1073-87 (1979).
18. E.D. Klug, U.S. Patent 3 314 809, 1967.
19. S. Yolles, J.F. Morton, and M.F. Sartori, J. Polym. Sci., Polym. Chem. Ed., 17, 4111-13 (1979).

20. E.D. Klug, U.S. Patent 3 357 971, 1967.
21. S.L. Tseng, A. Valenta, and D.G. Gray, Macromolecules, 14, 715-19 (1981).
22. S.L. Tseng and D.G. Gray, presented in part at the 64th CIC Conference, Halifax, May-June 1981.
23. D.G. Gray, PPRIC and McGill University, private communication, 1980.
24. S.L. Tseng, G. Laivins, and D.G. Gray, presented in part at the 21st High Polymer Forum, Kingston, August 1981.
25. S.A. Chang and D.G. Gray, J. Colloid Interface Sci., 67, 255-65 (1978).
26. J.H. Elliott, J. Appl. Polym. Sci., 13, 755-64 (1969).
27. G.A.F. Roberts and I.M. Thomas, Polymer, 19, 459-61 (1978).
28. M.G. Wirick, J. Polym. Sci., Polym. Chem. Ed., 6, 1705-18 (1968).
29. J.R. DeMember, L.D. Taylor, S. Trummer, L.E. Rubin, and C.K. Chiklis, J. Appl. Polym. Sci., 21, 621-27 (1977).
30. A. Parfondry and A.S. Perlin, Carbohydr. Res., 57, 39-49 (1977).
31. S.L. Malhotra, presented in part at the 64th CIC Conference, Halifax, May-June 1981.
32. M.G. Wirick and M.H. Waldman, J. Appl. Polym. Sci., 14, 579-97 (1970).
33. J.S. Aspler, Ph.D. Thesis, McGill University, Montreal, Quebec, 1980.
34. J.S. Aspler and D.G. Gray, Macromolecules, 12, 562-66 (1979).
35. J.S. Aspler and D.G. Gray, Macromolecules, 14, 1546-49 (1981).
36. J.S. Aspler and D.G. Gray, Polymer, 23, 43-46 (1982).
37. L.O. Sundelöf and B. Nyström, J. Polym. Sci., Polym. Lett. Ed., 15, 377-84 (1977).
38. B. Nyström and R. Bergman, Eur. Polym. J., 14, 431-37 (1978).
39. R. Bergman and L.O. Sundelöf, Eur. Polym. J., 13, 881-89 (1977).
40. B. Nyström and J. Roots, Eur. Polym. J., 16, 201-04 (1980).
41. R.J. Samuels, J. Polym. Sci., Polym. Chem. Ed., 7, 1197-258 (1969).

42. F.W. Billmeyer Jr., J. Polym. Sci., Polym. Symp., 55, 1-10 (1976).
43. R.St.J. Manley, Arkiv För Kemi, 9, 521-79 (1956).
44. I. Jullander, Svensk Papperstidn., 55, 197-211 (1952).
45. N.C. Billingham, "Molar Mass Measurements in Polymer Science", Kogan Page Ltd., Great Britain, 1977, Chapter 5.
46. H. Bolker, "Natural and Synthetic Polymers", Marcel Dekker Inc., New York, 1974, pp. 623-49.
47. J.W. Strutt (Lord Rayleigh), Phil. Mag., 41, 107-20, 447-54 (1871).
48. P. Debye, J. Appl. Phys., 15, 338-42 (1946).
49. P. Debye, J. Phys. Colloid Chem., 51, 18-32 (1947).
50. P.J. Flory, "Principles of Polymer Science", Cornell Univ. Press, Ithaca, New York, 1953, Chapter 7.
51. C. Tanford, "Physical Chemistry of Macromolecules", John Wiley & Sons, New York, 1961, Chapter 5.
52. B.H. Zimm, J. Chem. Phys., 16, 1093-99 (1948).
53. "Aldrich Catalog Handbook of Fine Chemicals", Aldrich Chemical Co. Inc., Milwaukee, Wisconsin, 1980, p. 550.
54. R.W. Hall in "Techniques of Polymer Characterization", P.W. Allen, Ed., Butterworths Scientific Publ., London, 1959, Chapter 2.
55. N. Bauer, K. Fajans, and S.Z. Lewin in "Physical Methods of Organic Chemistry", 3rd ed., A. Weissberger, Ed., Interscience Publ. Inc., New York, 1960, Vol. I, Part II, pp. 1139-45, 1232-38, 1249-65.
56. H.H. Willard, L.L. Merritt Jr., and J.A. Dean, "Instrumental Methods of Analysis", 5th ed., D. Van Nostrand Co., New York, 1974, Chapter 14.
57. "Hilger and Watts M154 Interference Refractometer Instruction Manual", Hilger & Watts Ltd., London, 1965.
58. P.H. Norberg and L.O. Sundelöf, Makromol. Chem., 77, 77-89 (1964).
59. A. Krius, Z. Phys. Chem., 34 B, 13-50 (1936).
60. "Chromatix Application Note No. LS-1", Chromatix Inc., Sunnyvale, Calif., 1977.

61. M.B. Huglin in "Light Scattering from Polymer Solutions", M.B. Huglin, Ed., Academic Press, New York, 1972, Chapter 6.
62. B.A. Brice and M. Halwer, J. Opt. Soc. Am., 41, 1033-37 (1951).
63. D. Margerison and G.C. East, "An Introduction to Polymer Chemistry", Pergamon Press, Oxford, 1967, Chapter 2.
64. "SOFICA Light Scattering Manual", Société Française d'Instruments de Contrôle et d'Analyse, France, 1968.
65. M.L. McConnell, Am. Lab., 63-75 (May 1978).
66. A.C. Quano, J. Colloid Interface Sci., 63, 275-81 (1978).
67. A.C. Quano, J. Polym. Sci., Polym. Chem. Ed., 12, 1151-62 (1974).
68. A.C. Quano, J. Chromatogr., 118, 303-12 (1976).
69. D.E. Axelson and W.C. Knapp, J. Appl. Polym. Sci., 25, 119-23 (1980).
70. "LALLS Photometer Manual", Chromatix Inc., Sunnyvale, Calif., 1977, Chapters 1, 3, and 9.
71. W. Kaye, A.J. Havlik, and J.B. McDaniel, J. Polym. Sci., Polym. Lett. Ed., 9, 695-99 (1971).
72. W. Kaye and A.J. Havlik, Appl. Opt., 12, 541-50 (1973).
73. W. Kaye, Anal. Chem., 45, 221A-25A (1973).
74. T.M. MacRury and M.L. McConnell, J. Appl. Polym. Sci., 24, 651-62 (1979).
75. H. Suzuki, Y. Miyazaki, and K. Kamide, Eur. Polym. J., 16, 703-08 (1980).
76. N.C. Billingham, "Molar Mass Measurements in Polymer Science", Kogan Page Ltd., Great Britain, 1977, Chapter 6.
77. H. Morawetz, "Macromolecules in Solution", Interscience Publ., New York, 1965, pp. 181-95.
78. K.E. Van Holde and R.L. Baldwin, J. Phys. Chem., 62, 734-43 (1958).
79. R.J. Goldberg, J. Phys. Chem., 57, 194-202 (1953).
80. W.Q. Yean and D.A.I. Goring, J. Appl. Polym. Sci., 14, 1115-20 (1970).
81. W.Q. Yean, A. Rezanowich, and D.A.I. Goring, Actes du Symp. Int. de Grenoble, July 1964, p. 327.

82. R.G. LeBel, Ph.D. Thesis, McGill University, Montreal, Quebec, 1962, pp. 90-100.
83. E.D. Klug in "Encyclopedia of Polymer Science and Technology", N.M. Mark, N.G. Gaylord, and N.M. Bikales, Eds., Wiley-Interscience Inc., New York, 1971, Vol. 15, pp. 307-14.
84. G.C. Berry and M.A. Leech in "Solution Properties of Polysaccharides", D.A. Brant, Ed., ACS Symposium Series #150, Washington, D.C., 1981, pp. 61-80.
85. K. Kamide, T. Terakawa, and Y. Miyazaki, Polym. J., 11, 285-98 (1979).
86. S.L. Tseng and D.G. Gray, PPRIC and McGill University, private communication, 1980.
87. N.C. Billingham, "Molar Mass Measurements in Polymer Science", Kogan Page Ltd., Great Britain, 1977, Chapter 7.
88. M.G. Wirick and J.H. Elliott, J. Appl. Polym. Sci., 17, 2867-75 (1973).
89. This Thesis, Chapter II.
90. D.G. Gray and R. DeIure, PPRIC and McGill University, private communication, 1978.
91. D.G. Gray, PPRIC and McGill University, private communication, 1977.
92. A.S. Perlin and D.S. Lee, presented in part at the 64th CIC Conference, Halifax, May-June 1981.
93. D.S. Lee and A.S. Perlin, Carbohydr. Res., 91, C5-C8 (1981).
94. D.S. Lee and A.S. Perlin, PPRIC PGRP Reports #58, Montreal, Quebec, December 1980.

CHAPTER III

PHASE SEPARATION OF HYDROXYPROPYLCELLULOSE
SOLUTIONS

III.1 Introduction

Hydroxypropylcellulose is unique among cellulose derivatives because it can exhibit two distinct types of phase separations: one brought about by temperature, the other arising solely from particle asymmetry. Temperature induced phase separation is a common occurrence among non-ionic water soluble cellulose derivatives (1). This process is reversible and its product is a polymer-rich phase which may eventually gel to produce a three-dimensional cross-linked network (2-3). The temperature at which phase separation occurs on cooling is known as the upper consolute temperature (UCT) (4-5); the temperature at phase separation on heating is referred to as the lower consolute temperature (LCT) (6). Detailed thermodynamic information about polymer solubility and phase separation can be found in the classic work of Huggins (7-10), Flory (11-14), and other researchers (15-21). For cellulose derivatives considerable evidence suggests that the existence of the LCT may be attributed to the presence of a highly hydrogen-bonded structure which breaks up on heating (1,22-23).

The idea that particle asymmetry alone may be responsible for a second type of phase separation is a relatively recent concept. This type of transition results in the formation of an ordered anisotropic phase known as a liquid crystal or lyomesophase. The origin of this idea for very dilute solutions can be traced to Onsager (24) and Isihara (25). Onsager proposed that as the solute concentration of rod shaped particles in an isotropic solution is increased an instability develops in the system

resulting in phase separation. One phase consists of isotropic randomly oriented particles while the coexisting phase contains particles possessing orientational order. The driving force for this spontaneous transition from ~~random~~ isotropic solution to ordered anisotropic phase as more solute is added to the system is entropic in nature and is independent of any specific polymer-solvent interactions. According to Onsager a random distribution of rods in solution minimizes the "orientational entropy" of the system, whereas a parallel or ordered array of rods will minimize the "translational entropy" of the system. The competition between these two entropic components determines if the system will phase separate to form a stable mesophase. Samulski (26) has shown that the critical volume fraction of polymer in the anisotropic phase (ϕ_c^0) at phase separation according to Onsager's theory is

$$\phi_c^0 = 4.5(d/L) \quad \text{III.1}$$

where d is the diameter and L is the length of the polymer rods in solution.

In the late fifties Flory developed a theory, based on a statistical thermodynamic approach, to account for the anisotropic phase separation exhibited by both semi-flexible (27) and rigid (28) rod monodisperse polymer chains in binary athermal solutions. The basic premise of his theory is that long chains of consecutively connected segments can be packed most efficiently into a given volume element in an ordered array. A random distribution of such chains must necessarily waste space while from a

thermodynamic viewpoint a mixture of ordered and random chains is unstable (14). Using a lattice model Flory was able to break down the solution free energy into two components: the first, a mixing term depending only on solution concentration and the second, a disorientation term depending on chain flexibility. In placing rigid chain segments on a lattice a collinear sequence of segments is produced because the chains are rigid and cannot bend to fill the lattice in a disordered array. As more segments are added, the system must either develop order by a parallelization of the segments or by sacrificing some chain rigidity. It is the rivalry between these two effects which determines if an anisotropic phase separation will occur. If chain segments are inflexible, Flory has shown that a disordered array of such chains at a high density is both statistically and thermodynamically unfavorable. The competition for space at high density makes an ordered array of parallel rods the most thermodynamically stable state. An anisotropic phase will form when a critical volume fraction of rods given by Equation III.2 has been exceeded.

$$\phi_c^F = (8/x)(1 - 2/x) \quad \text{III.2}$$

where x is the axial ratio of the polymer (rod length divided by rod diameter) and ϕ_c^F is the volume fraction of polymer in the anisotropic phase at the onset of phase separation according to Flory. A consequence of Equation III.2 is that particle asymmetry (x) alone is responsible for the anisotropic phase separation which occurs in rod-like polymer systems. Flory's theory is applicable to both dilute and concentrated solutions and,

as such, has a broader scope than Onsager's theory which is applicable only to dilute solutions.

The phase diagram for a polymeric system exhibiting anisotropic phase separation should consist of three distinct regions according to Flory's theory: an isotropic, a coexistence, and an anisotropic region. Dilute solutions of the polymer should behave isotropically. As more polymer is added to the solution, the critical concentration of rods given by Equation III.2 is exceeded and a phase separation occurs. This concentration is referred to as the A point and it signals the start of a narrow two phase coexistence region which consists of the parent isotropic solution and the new anisotropic lyomesophase. Within this region the concentration of the two phases should remain constant and only their relative proportions should change. Ultimately the solution becomes totally anisotropic and the concentration at which the last trace of isotropic material disappears is referred to as the B point. Poly- γ -benzyl-L-glutamate (PBLG) has been reported to undergo an anisotropic phase separation in several solvents when a critical concentration of polypeptide has been exceeded (29-31). This occurs only in solvents in which the PBLG is known to exist in an α -helical or relatively stiff conformation. Flory (32) has calculated the axial ratios for several different PBLG samples and has found a reasonably good agreement between his theoretical predictions and the experimentally determined A and B concentrations for this polymer. The agreement, however, was not exact and Flory attributed the difference to sample polydispersity. Straley (33) has criticized Flory's theory because it predicts

spontaneous phase separation regardless of the diluteness of the solution. Straley has shown that the PBLG results fit Onsager's theory much better than they do Flory's theory but, again the agreement between the theoretical and experimental results is not exact. Okamoto (34) has for this reason questioned the validity of phase separation theories to do more than merely predict a general behavioral trend. The theoretical predictions and the experimental results for anisotropic phase separation do however agree on one vital point and, that is, that the volume fraction of rods at phase separation is independent of the solvent but varies only as the axial ratio or molar mass of the sample. Therefore, molecular asymmetry and not any specific polymer-solvent interaction is responsible for anisotropic phase separation.

Miller and Wee (35-37) have evaluated the phase diagram for PBLG in dimethylformamide using several different techniques to determine the A and B concentrations for this system. Their phase diagram of temperature versus concentration is very similar to that predicted by Flory's theory and it is characterized by three distinct regions. They conclude that any discrepancy between Flory's predicted phase diagram and the experimental phase diagram can be attributed to the fact that PBLG molecules are neither completely rigid nor impenetrable. They further report that Flory's phase diagram exhibits subtle changes depending upon whether the molecules are assumed to be rigid impenetrable, semi-flexible impenetrable, or rigid penetrable rods (36). They also have found that side chain flexibility appears to play some role in determining the phase diagram for PBLG.

Samulski (38) has suggested that any discrepancy between Flory's theory and the actual phase diagram results for PBLG may perhaps be attributed to a distribution of axial ratios in the polydisperse samples being investigated. It has even been proposed that a random coil to helix transition may occur simultaneously with the formation of the anisotropic phase in polypeptides (39-42) and, if true, then Flory's theory may not be applicable to systems which exhibit spontaneously induced chain rigidity.

Flory has recently undertaken a refinement (43-44) of his original theory to take into account more than just monodisperse athermal polymer solutions. He has extended his theory to take cognizance of sample polydispersity (45-46), varying polymer rod lengths (47), the partitioning of rod-like species between the isotropic and anisotropic phases (48), the replacement of rigid rods by a series of flexibly connected joints (49), flexible systems with regular rod-like sequences (50), and, finally, of ternary polymer systems (51-52). Flory has also reported (53) that the mixing of flexible side chains with the solvent makes a contribution to the entropy of the system and, thus, side chain flexibility may play an unspecified role in anisotropic phase separation.

The discovery that cellulosic mesophases do exist (54) has generated much interest in cellulose and its derivatives. Flory originally believed that the inflexibility of cellulosic chains played a dominant role in their crystallization and precluded the formation of a stable mesophase (27). It has been reported that the critical concentration of cellulose acetate

required to form an anisotropic mesophase is dependent upon the sample degree of polymerization and substitution (55). This is to be expected from Flory's theory since both these factors would alter the axial ratio of the polymer. Aharoni has shown that this critical concentration varies considerably with the solvent in which the cellulose acetate is dissolved (56). This is in contrast to Flory's theory and the experimental results for PBLG in which the A point is found to be independent of any solvent-polymer interaction. Aharoni suggests that for all cellulosic mesophases a direct relationship exists between the polymer-solvent interaction parameter, $\chi_{1,2}$, and the critical concentration for phase separation (57). It has even been proposed that the critical volume fraction of cellulosic material at the A point can be correlated with the solvent acidity (58).

Hydroxypropylcellulose is the only known cellulosic to form a lyomesophase in water and in simple organic solvents like methanol and ethanol. Previously the only aqueous polymeric systems to exhibit anisotropic phase separation were polyelectrolytes; in these compounds it was impossible to determine if electrostatic attraction, molecular asymmetry, or a combination of both factors was responsible for the phase separation (36). The HPC system, being non-ionic, would seem to be an ideal one to test the validity of the hypothesis that geometric factors alone may be responsible for a phase transition at relatively high polymer concentrations. It is also of interest to determine exactly how well the HPC system fits Flory's theory, if the HPC system behaves like other cellulosic mesophases with respect to the A point varying with solvent, and what the

phase diagram for HPC might look like. The following investigation was undertaken to answer these questions.

III.2 Experimental

III.2.1 CLOUD POINT MEASUREMENTS

Aqueous HPC solutions undergo a reversible phase separation on heating above 40°C. This phase separation is accompanied by the transformation of a previously clear solution into one with an opaque white appearance. Several techniques were employed in attempting to quantify the change in solution turbidity with temperature. The cloud point, or start of solution turbidity, was arbitrarily chosen as the temperature at which light scattered at 90° to the incident beam of a SOFICA light scattering photometer went off scale on the least sensitive photometer range. The solution heating rate used was 0.2°C per minute and the solution concentrations investigated ranged from 5×10^{-5} g/mL to 2×10^{-1} g/mL for all six available HPC types (E, L, J, G, M, and H). The solutions were prepared according to the procedure previously outlined (59). A Reichert Zetopan light microscope equipped with a light meter and a Mettler FP52 hot stage were also used to obtain solution cloud points. Solutions were placed in hanging drop microscope slides (Fisher Ltd) and were examined under the light microscope while being heated at a rate of 0.2°C per minute. Light meter readings were taken as a function of temperature

and the cloud point determined as the first significant change in transmitted light intensity.

Turbidity measurements were also made on concentrated aqueous HPC solutions (9 and 41% HPC by weight). In this case the solutions were sealed in parallel-sided 0.4-mm thick microslides (Vitro Dynamics Inc) which were then placed between the heating plates of a Mettler FP52 hot stage. The heating rate of the hot stage was 0.2°C per minute. The sample and hot stage were then placed within the laser beam of the Chromatix KMX-6 photometer and light intensity readings were taken every five minutes.

III.2.2 LYOMESOPHASE PREPARATION

Dried HPC-E, L, J, G, M, and H were weighed into 15-mL vials (Kimble Glass Ltd) to which various amounts of water that had been distilled twice were added. Solutions from 5 to 80% HPC by weight were prepared in approximately 2% increments. These samples were allowed to stand at room temperature ($\sim 21^{\circ}\text{C}$) for one month with daily rotation of the vials to ensure the total dissolution of the HPC. The samples were then gravimetrically analyzed with a Cahn Gram Electrobalance and aluminum differential scanning calorimetry (DSC) pans (Perkin Elmer Co) to verify the solution concentration. The DSC pans were weighed and then approximately 10 to 20-mg of each HPC solution were placed in the pan. The pan was reweighed and then dried at 85°C for thirty minutes using forced air circulation (Mettler FP52 hot stage). The pan was next placed

in an oven (105°C) for two and one-half hours to remove any residual water in the sample. The dried HPC in the pan was weighed, dried for an additional one and one-half hours, and then reweighed. Each analysis was performed in triplicate and, in almost all cases, the concentration of the analyzed sample was within $\pm 1\%$ of the originally prepared solution concentration.

Aqueous solutions were generally very clean, showing only small bits of undissolved cellulose fibers. The solutions were placed on flat microscope slides (Fisher Ltd) and then examined for birefringence under the crossed polars of a light microscope. Dilute solutions (up to about 40% polymer by weight) were clear and exhibited no birefringence. More concentrated solutions appeared cloudy and were found to show varying amounts of birefringence. Two particular solution concentrations were made note of during this investigation for solution birefringence. The A concentration or start of the two phase coexistence region was taken as the point where the first traces of birefringence were observed in a solution. The B concentration or start of the pure mesophase region was chosen as the point at which a solution began to exhibit iridescence. Experimentally it was difficult to determine conclusively at what point all the isotropic material in a sample disappeared; however, it was reasoned that an iridescent mesophase would be unlikely to contain any isotropic material and so this concentration was chosen as the B point or upper limit for the end of the two phase coexistence region.

Hydroxypropylcellulose was found to form a lyomesophase in several polar organic solvents. Approximately 30 to 40 solutions of HPC were prepared in each of the following solvents: methanol, ethanol, cellosolve, dimethylsulphoxide (DMSO), dimethylformamide (DMF), dioxane, tetrahydrofuran (THF), acetic acid, acetic anhydride, formic acid, 2-methyl-2-propanol, morpholine, 1-pentanol, 1-propanol, 2-propanol, and pyridine. The solution concentrations ranged from 5 to 95% HPC by weight in approximately 3% increments. Only DMSO and DMF were dried over molecular sieves prior to use. All other solvents were used as received from the manufacturer and were either spectral or analar grade reagents. Solutions were prepared in 15-ml vials which were rotated daily for one month to ensure solution homogeneity. These solutions were then analyzed gravimetrically as described previously for aqueous solutions. Depending upon the solvent and the amount of HPC in the sample, the solutions varied greatly in appearance being clear, yellow, opaque, or even iridescent. The yellow color of some HPC solutions (notably in acetic acid or anhydride and formic acid) was attributed to the partial degradation of HPC in these solvents. These degraded HPC samples exhibited both mesomorphic phase separation and iridescent colors at higher HPC concentrations. In contrast to the aqueous HPC solutions, some organic HPC solutions (in DMSO, DMF, THF, methanol) were found to be clear and mesomorphic. For this reason all solutions were examined for birefringence under the crossed polars of a light microscope.

III.3 Results and Discussion

III.3.1 PHASE SEPARATION IN AQUEOUS SOLUTION ON HEATING

Dilute aqueous HPC solutions are clear and relatively homogeneous below 40°C. These same solutions if heated above 40°C turn cloudy and HPC precipitates out of solution. Under the light microscope this turbid solution appears as roughly spherical particles of one micron diameter. Further heating results in a marked increase in the number of particles and they appear to coalesce as depicted in Figure III.1. The precipitated HPC coagulates to form a white gel-like substance surrounded by a clear aqueous layer. The opacity of the gel precludes its examination for birefringence or coalescing particles. There does, however, appear to be a critical concentration of 25 weight % HPC-L below which the HPC will not coagulate but remains uniformly dispersed in the solution as colloidal particles. As the molar mass of the HPC is increased this critical concentration for coagulation decreases in an irregular fashion and is ultimately 6% for HPC-H. The transition from clear to turbid solution is relatively sharp and easily detected visually for solution concentrations above the critical coagulation value. Very dilute solutions (< 1% HPC by weight) appear to exhibit several different degrees of cloudiness before turning completely white.

The cloud point or temperature at which the aqueous solutions began to turn white was evaluated as a function of HPC concentration and molar mass. The results obtained have been summarized in Table III.1. The

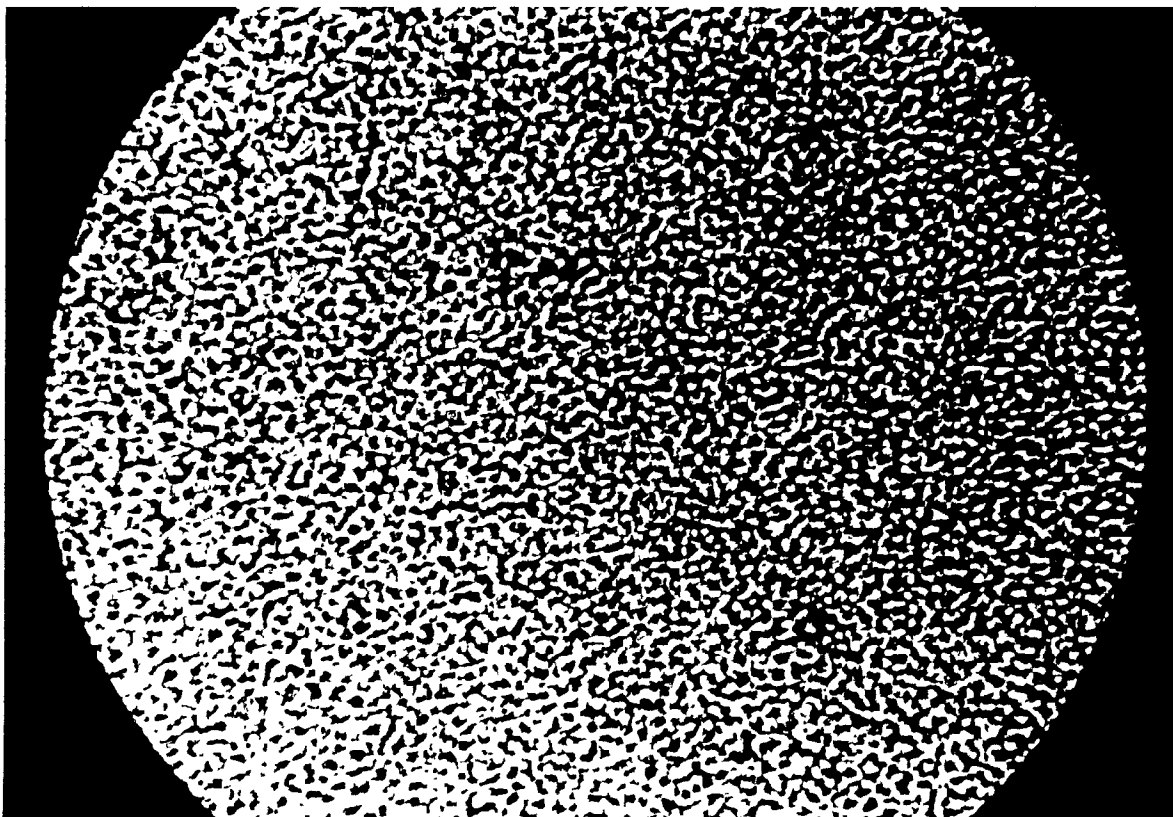


FIGURE III.1 Microscopic view of the particles formed on heating a dilute aqueous HPC solution above 40°C. The diameter of the depicted particles is approximately one micron.

TABLE III.1

Variation of the Cloud Point with Molar Mass and Concentration
for Aqueous HPC Solutions

HPC Type	\bar{M}_w (g/mol)	Concentration Range (g/mL)	Cloud Point ($\pm 1^\circ\text{C}$)	
			Heating	Cooling
E	60 000	0.00005 - 0.09	44	41
L	82 000	0.00049 - 0.30	44	41
J	100 000	0.00049 - 0.05	41	37
G	190 000	0.0005 - 0.05	44	41
M	530 000	0.0063 - 0.05	41	37
H	900 000	0.0054 - 0.05	41	37

reversibility of the solution cloud point was verified by slowly cooling each opaque solution and noting the temperature at which the last trace of spherical particles associated with the turbid phase disappeared. Hydroxypropylcellulose E, L, and G solutions had a cloud point of 44°C on heating and 41°C on cooling. The corresponding temperatures were 41°C and 37°C for HPC-J, M, and H solutions. The hysteresis of the cloud point on heating and cooling is believed to be a kinetic phenomenon and is a common occurrence for aqueous polymer systems (1). There does not appear to be any regular variation in the cloud point with the HPC molar mass. But it is known that the polymer molar substitution (MS) has a marked influence on the cloud point (1). Examination of the MS data for HPC in Table II.1 shows that the cloud point is constant for samples with a MS between 3.50 and 3.84 and that it decreases by 3°C if the MS is between 3.93 and 4.21. The only exception to this behavior is HPC-J and the reason for this is unknown. Since the HPC samples investigated could not be fractionated successfully the effects of sample polydispersity on the cloud point could not be assessed.

The above described phase separation which HPC undergoes is very similar to that observed for other cellulose ethers like hydroxyethylcellulose (HEC) and methylcellulose (MC) (23). Methylcellulose exhibits spherical particle formation at a temperature of 60°C ; this is only marginally lower than its reported cloud point of 62°C (2). The relatively low cloud point (41°C - 44°C) of HPC relative to MC (62°C) or HEC ($> 100^{\circ}\text{C}$) can be attributed to the long and bulky hydroxypropyl side groups which

make HPC, the least hydrophilic cellulosic ether (23). Hydroxypropylcellulose is unusual only in that it does not immediately gel like MC but, rather, that it precipitates out of solution prior to gelation. A possible explanation for this behavior is that MC on heating slowly loses water, allowing the buildup of a three-dimensional network between the polymer molecules before total dehydration occurs. The HPC, being more hydrophobic, on heating rapidly loses water thus precluding the formation of a network.

Two final points should be noted about the behavior of dilute aqueous HPC solutions. Firstly, all dilute solutions exhibit a fibrillar-like precipitate which becomes visible anywhere from one week to three years after solution preparation. Figure III.2 illustrates a typical example of this precipitate viewed in the light microscope. Papkov (60) has suggested that an important characteristic of polymers likely to form lyomesophases is their ability to separate from solution in unusual morphological forms with a fibrillar structure. Secondly, aqueous HPC solutions were found to be very sensitive to the presence of organic solvents. Two drops of acetic acid in 20 mL of a 15% HPC by weight aqueous solution were sufficient to prevent the phase separation of HPC at any temperature.

Concentrated aqueous HPC solutions (>40% HPC by weight) exhibit heat induced phase separation but their behavior is more complex than that of dilute solutions. Figure III.3 depicts the turbidity changes observed on heating a 9% and a 41% by weight HPC aqueous solution. The 9% HPC



FIGURE III.2 Typical fibrillar structure visible in the light microscope on examination of the precipitate found to form with time in dilute aqueous HPC solutions.

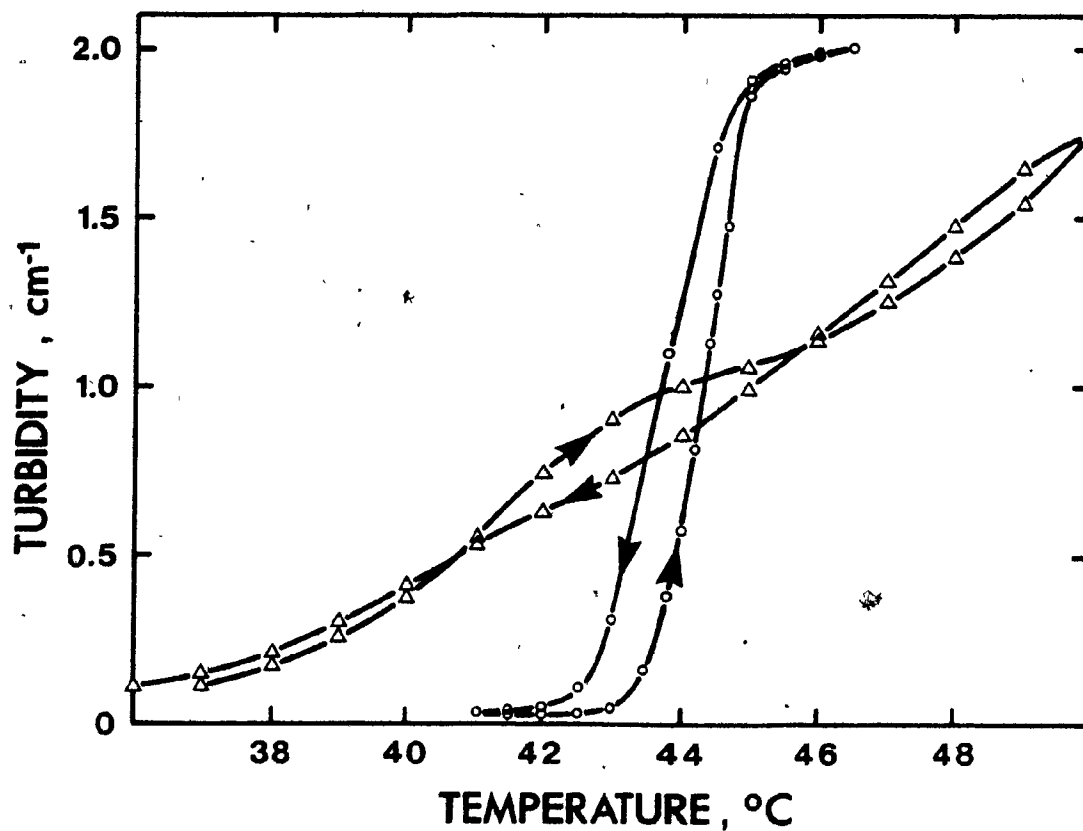


FIGURE III.3 The change in solution turbidity with temperature for two aqueous HPC-L solutions: 9% (○) and 41% (Δ) HPC by weight. The data were obtained with a Chromatix KMX-6 photometer and thin glass microslides. The data are uncorrected for scattering at the cell faces.

solution shows the behavior previously described for dilute solutions — a sharp increase in turbidity over a relatively narrow temperature range with some hysteresis on cooling. The 41% HPC solution shows a two-step increase in turbidity over a much broader temperature range. The concentration of this latter solution is very close to that at which HPC undergoes an anisotropic phase separation (see next section). The complex turbidity data may reflect a non-equilibrium situation involving two concentrated phases. Aqueous solutions containing more than 55% HPC by weight are anisotropic and display cholesteric colors (61). These solutions are also found to turn white and phase separate on heating, yet the cholesteric colors return on cooling. An explanation of the turbidity changes with temperature for anisotropic HPC solutions is beyond the scope of this work.

III.3.2 CONCENTRATED AQUEOUS MESOPHASE FORMATION

At room temperature concentrated aqueous HPC solutions form anisotropic lyomesophases (54). Such solutions are characterized by a cloudy or iridescent appearance and are birefringent when examined under the crossed polars of a light microscope. The critical concentration of HPC necessary for the formation of this liquid crystalline phase does not vary very much with the HPC molar mass. Specifically 42% HPC-L, 41% of both HPC-E and J, and 39% HPC-H by weight were the concentrations in water above which mesomorphic behavior was noted. Hydroxypropylcellulose H solutions containing between 31 and 38% HPC by weight were birefringent, but this birefringence dissipated with time and so was ascribed to shear

orientation effects resulting from sample preparation. The mesophase was found to form at the same critical concentrations, noted above, for each HPC type even when the solutions were heated to 30° and 35°C. However, at 40°C formation of the mesophase appeared to take place at slightly lower HPC concentrations. For example, a 38 weight % HPC-L solution was found to be birefringent at 40°C. This temperature is very close to the cloud point of HPC and its effect on the formation of the mesophase is uncertain.

Aqueous solutions containing between 42 and 55% HPC-L by weight were cloudy and exhibited a mixture of both birefringent and non-birefringent areas when examined under the crossed polars of a light microscope. As the HPC concentration increased within the above limits it was noted that the non-birefringent areas gradually disappeared leaving only anisotropic material at 55% HPC. It was difficult to determine exactly at what point the last trace of isotropic material disappeared and, for this reason, the concentration at which the solutions began to exhibit cholesteric colors (see below) was chosen as the upper limit for the end of the two phase coexistence region. In general there was no tendency for the coexisting isotropic and anisotropic regions to exhibit a sharp phase separation; rather, both phases were found to coexist in a homogeneous mixture. The notable exceptions to this behavior were HPC-E and J solutions. In this case the solutions on standing from one to two years were found to contain two distinct separated phases — a clearer upper layer and a cloudy more dense lower layer. Figure III.4 shows a typical example of such a phase separation for a HPC-E solution. Figure III.5 illustrates schematically



FIGURE III.4 Solutions depicting the three distinct phases which aqueous HPC solutions can exhibit: clear isotropic, coexisting isotropic — anisotropic, and cloudy anisotropic.

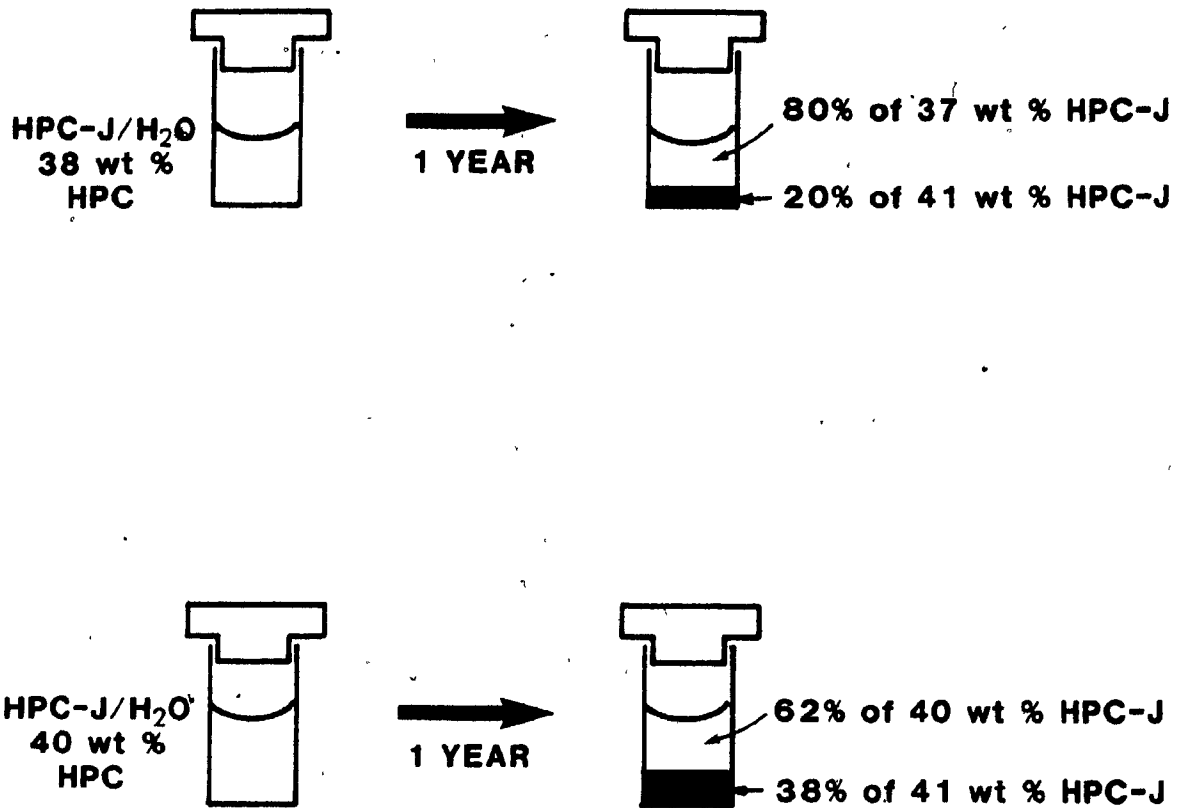


FIGURE III.5 A schematic view of two aqueous HPC-J solutions which on standing for one year phase separated into the two distinct layers that characterize the coexistence region of the liquid crystal. The lower phases are cloudy and anisotropic whereas the upper phases are clear and isotropic. The proportion and composition of each phase have been noted in the diagram.

the layer composition and the proportion of each layer contained within two typical HPC-J samples after standing for one year. According to Flory's theory (28) the composition of each phase should remain constant as their proportions change within the coexistence region. For the HPC-E and J solutions it was found that the compositions of the two layers depended to a certain extent on the volume fraction of the original HPC solution prior to phase separation. This confirms a similar conclusion reported for a different lyotropic polymer system (62). No explanation for this very peculiar behavior has yet appeared in the literature. Once phase separation has occurred, the proportions of the two coexisting phases will not change as long as the evaporation of solvent can be prevented. Solvent evaporation in tightly closed sample vials was not really a problem since it was found that over a four year time span the solution concentrations had changed an average of only 3%. In addition, the coexisting isotropic and anisotropic phases were found to remain stable indefinitely and there appeared to be no driving force for the conversion of one phase into the other.

Aqueous solutions containing more than 55% HPC by weight exhibited lovely iridescent colors in white light. This iridescence ranged from red to violet through the entire visible spectrum as the HPC concentration was increased to an upper limit of 72 weight %. Above this limit solutions no longer appeared fluid but exhibited rubbery gel properties. This gel material was clear and relatively hard but it still exhibited a marked birefringence. For comparison with organic HPC solutions (see next section) it was convenient to convert the HPC weights to weight fractions and then to

volume fractions, assuming that no volume change took place on mixing the HPC with solvent. Equations III.3 and III.4 were used for this purpose.

$$\omega_1 = \frac{w_1}{w_1 + w_2} \quad \text{and} \quad \omega_2 = \frac{w_2}{w_1 + w_2} \quad \text{III.3}$$

$$\phi_1 = \frac{w_1/\rho_1}{w_1/\rho_1 + w_2/\rho_2} \quad \text{and} \quad \phi_2 = \frac{w_2/\rho_2}{w_1/\rho_1 + w_2/\rho_2} \quad \text{III.4}$$

where 1 refers to the solvent and 2 refers to the solute, ω_1 and ω_2 are weight fractions, w_1 and w_2 are the actual weights used to prepare the sample, ρ_1 and ρ_2 are the densities, and ϕ_1 and ϕ_2 are the volume fractions. The density of water was 0.99707 g/mL (63) while that of HPC was 1.23 g/mL (23). The organic solvent densities used were taken from a chemical handbook (63). Table III.2 lists the volume fraction of HPC in water needed to produce a particular iridescent color. These numbers are not absolute but they can serve as a guide since often a mixture of iridescent colors can be observed for a homogeneous sample because of optical effects (61). Figure III.6 illustrates three examples of the iridescent colors exhibited by aqueous HPC solutions. More will be said about the origin and properties of these iridescent colors in the next chapter. It is sufficient for the present merely to state that heating iridescent samples results in a color shift to longer wavelengths, whereas the application of pressure to a sample causes a shift in color to shorter wavelengths. The effects of both processes are completely reversible. The pH of the aqueous solution used

TABLE III.2

Variation in Mesophase Iridescence with HPC Volume
Fraction in Aqueous Solution

Iridescent Color	HPC Volume Fraction (ϕ_2)
Red	0.50 - 0.54
Green	0.55 - 0.58
Blue	0.59 - 0.63
Violet	0.64 - 0.68

COLOURED PICTURES
Images en couleur

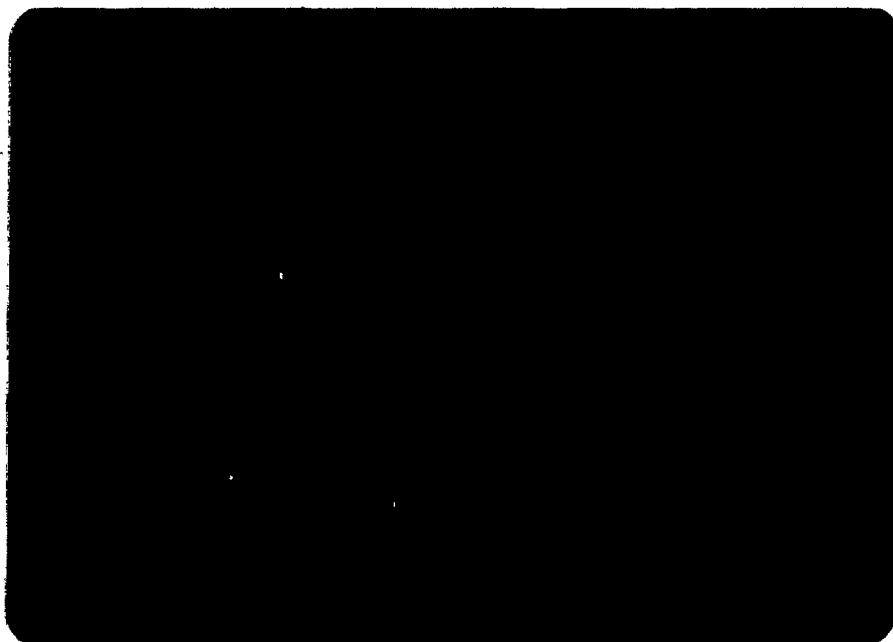


FIGURE III.6 Typical iridescent colors exhibited by different HPC concentrations in water: the red sample is 58%, the green sample is 62%, and the blue sample is 66% HPC by weight.

to prepare the samples does not have any effect on the formation of the mesophase or the appearance of the iridescent colors. The sole disadvantage in using highly acidic or basic media in the preparation of solutions is the gradual degradation of the HPC with time. Lyotropic aqueous HPC solutions when examined under the light microscope appear relatively fluid and are characterized by the textures illustrated in Figures III.7 and III.8. Unlike other lyotropic systems HPC solutions do not exhibit focal conic textures in the light microscope.

Having investigated the behavior of aqueous HPC solutions from the dilute through the rubbery gel states, it was possible to construct a qualitative diagram showing the various "phases" which HPC can adopt in aqueous medium. This "phase" diagram consists of four distinct regions as is illustrated in Figure III.9 for a representative HPC-L sample. Solutions are clear and isotropic below 44°C up to a solution concentration of approximately 40% HPC by weight. The solution behavior at 44°C for solutions containing more than 40% HPC is difficult to evaluate precisely because of the onset of anisotropic phase separation and the relatively slow attainment of equilibrium for very viscous solutions. However it does appear that over the entire HPC concentration range investigated a white precipitate or gel is formed above 44°C . The exact nature of this gel is unknown. Below 44°C between a concentration range of 42 and 55 weight % HPC the solutions consist of a mixture of isotropic and anisotropic phases whose proportions change gradually with concentration as does their composition. Between 56 and 72% HPC by weight only a pure anisotropic iridescent mesophase exists

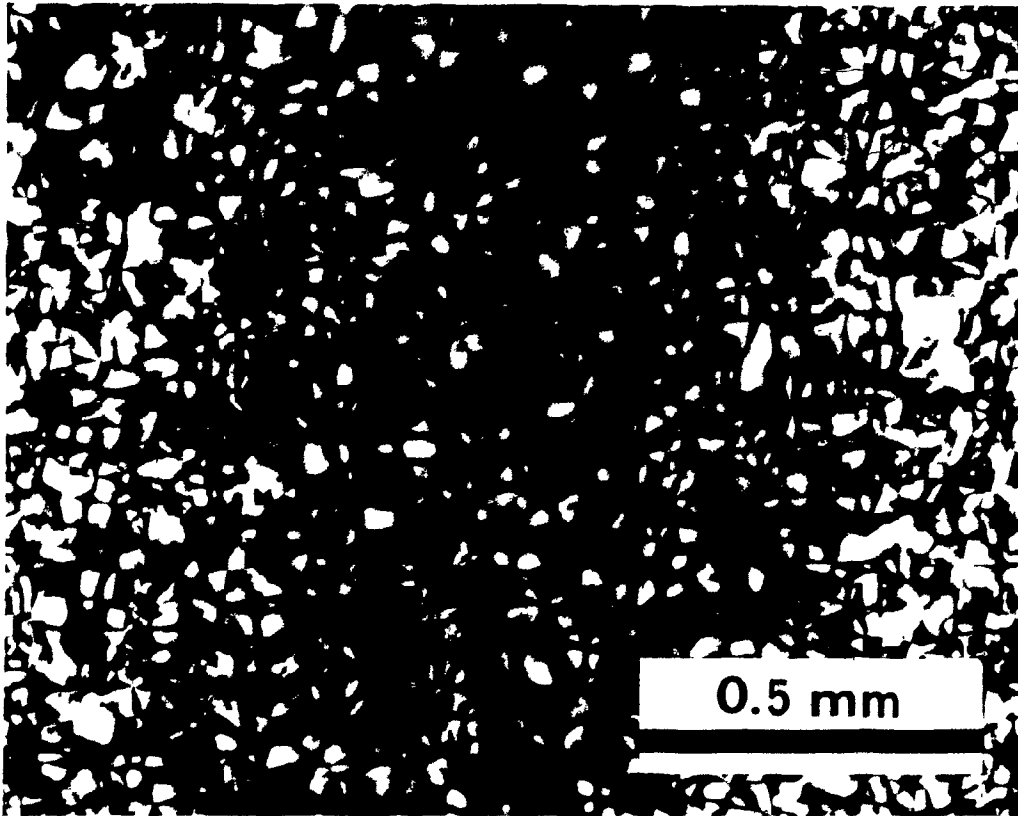


FIGURE III.7 Characteristic texture exhibited by lyotropic aqueous HPC solutions between the crossed polars of a light microscope. The sample is 70% HPC by weight.

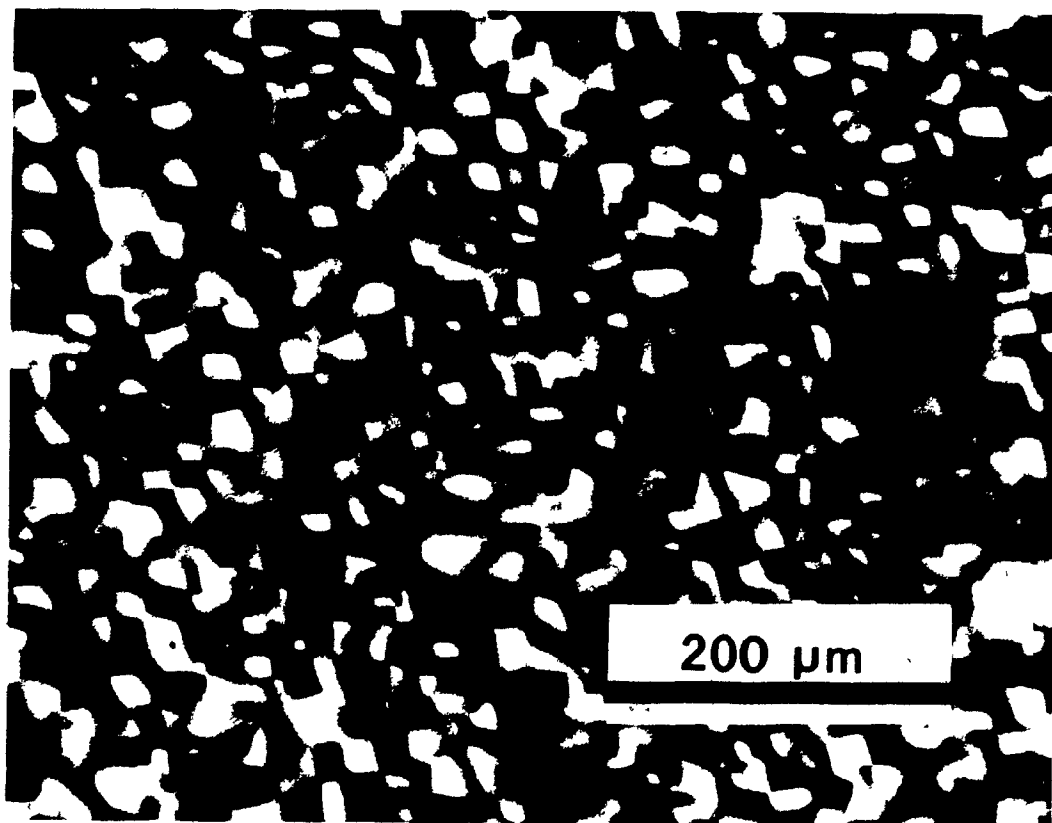


FIGURE III.8 Microscopic texture of an aqueous HPC solution under crossed polars. The sample is 70 weight % HPC but is at a slightly higher magnification than that depicted in Figure III.7.

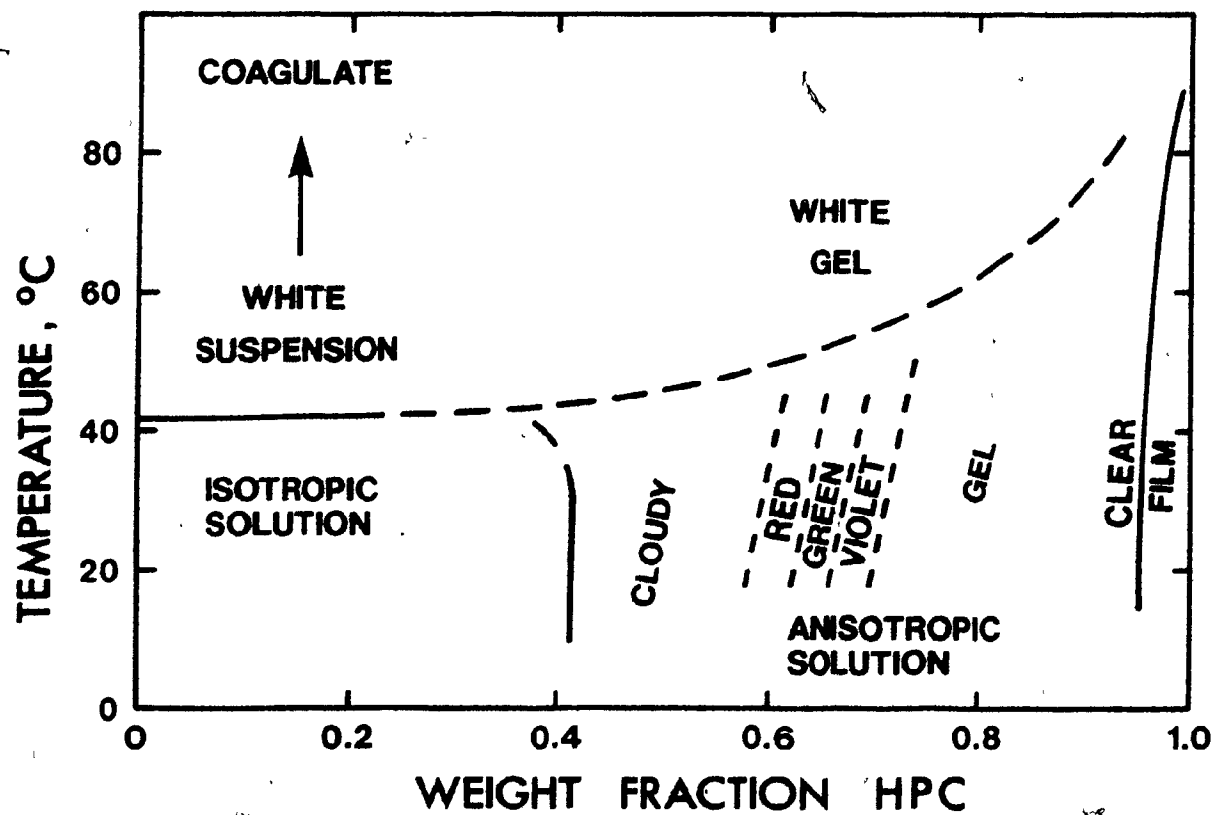


FIGURE III.9 Sketch illustrating the various "phases" which aqueous HPC solutions can exhibit as a function of temperature and concentration.

below 44°C. The final region of the "phase" diagram is that in which the HPC exists in the form of a hard rubbery gel above 72 weight % HPC.

III.3.3 MESOPHASE FORMATION IN ORGANIC SOLVENTS

Hydroxypropylcellulose is soluble in a wide range of organic solvents (23,64) and in several of these solvents HPC has been found to form an ordered mesophase (58,65-66). The critical concentration of HPC-L required for mesophase formation in sixteen different solvents has been listed in Table III.3. Although the values reported in Table III.3 are for HPC-L it has been verified experimentally that all the HPC types (E, J, G, M, and H) will form mesophases in the listed solvents at marginally different volume fractions. It would thus appear that in one particular solvent the molar mass of the HPC plays a negligible role in determining the critical concentration for mesophase formation. However it was noted that longer time periods were required for the higher molar mass HPC samples (G, M, and H) to form a mesophase. It might also be noted that the HPC samples investigated probably had broad molar mass distributions, which may have masked any effect of molar mass on phase separation. The data in Table III.3 show no clear correlation between the critical weight or volume fraction of HPC at anisotropic phase separation and the refractive index, density, molar mass, molar volume, and boiling or melting point of each of the solvents. Aspler and Gray (67) have measured the solute-solvent interaction parameter ($\chi_{1,2}$) for HPC in several of the solvents listed in Table III.3 and, contrary to published reports (57), there appears to be no

TABLE III.3

Weight and Volume Fraction of HPC Required to Form a Mesophase in
Various Organic Solvents

Solvent	HPC Weight Fraction (ω_2)	HPC Volume Fraction (ϕ_2)
Formic Acid	0.28	0.28
Acetic Anhydride	0.29	0.26
Acetic Acid	0.30	0.27
Morpholine	0.33	0.29
Pyridine	0.36	0.31
Dioxane	0.38	0.34
Tetrahydrofuran	0.40	0.42
Dimethylsulphoxide	0.41	0.38
Dimethylformamide	0.42	0.36
Cellosolve	0.43	0.36
Methanol	0.43	0.33
Ethanol	0.46	0.35
1-Pentanol	0.47	0.37
1,1-Dimethyl-1-ethanol	0.48	0.37
1-Propanol	0.49	0.38
2-Propanol	0.49	0.38

relationship between $X_{1,2}$ in a particular solvent and the critical concentration of HPC required to form the mesophase in that solvent. The only conclusion to be reached from the data in Table III.3 is that the mesophase forms at lower critical volume fractions in acids than in alcohols and that within a particular homologous series of solvents there is no regular variation in the mesophase critical volume fraction.

Mesomorphic aqueous and organic HPC solutions exhibited some marked dissimilarities in appearance and behavior. All aqueous HPC mesomorphic solutions were cloudy or iridescent and all flowed easily despite their high viscosity. Organic HPC mesophase solutions ranged from extreme fluidity (in acetic acid) to hard iridescent glasses (THF and dioxane). It was impossible to predict from the character of the solvent the type of mesophase likely to form: fluid, gel, or glass. The two phase coexistence region was found to be much broader in organic solvents than in water. Typical limits for the two phase region in water were between 42 and 55% HPC by weight, while in organic solvents the corresponding values were from 30 to 65% HPC. In addition some organic solutions (in pyridine, morpholine, methanol, cellosolve, formic acid, acetic acid, and acetic anhydride) exhibited distinct periodicity lines (to be elaborated on in the next chapter) within the two phase region when examined in the light microscope. Figures III.10, III.11, and III.12 show typical examples of these periodicity lines which are totally absent in aqueous solutions. Finally, although there exists a larger density difference between HPC in some of the organic solvents and HPC in water, there was no tendency for the organic solutions



FIGURE III.10 Polarizing micrograph of a 40 weight % HPC acetic acid solution exhibiting distinct coexisting isotropic and anisotropic regions.

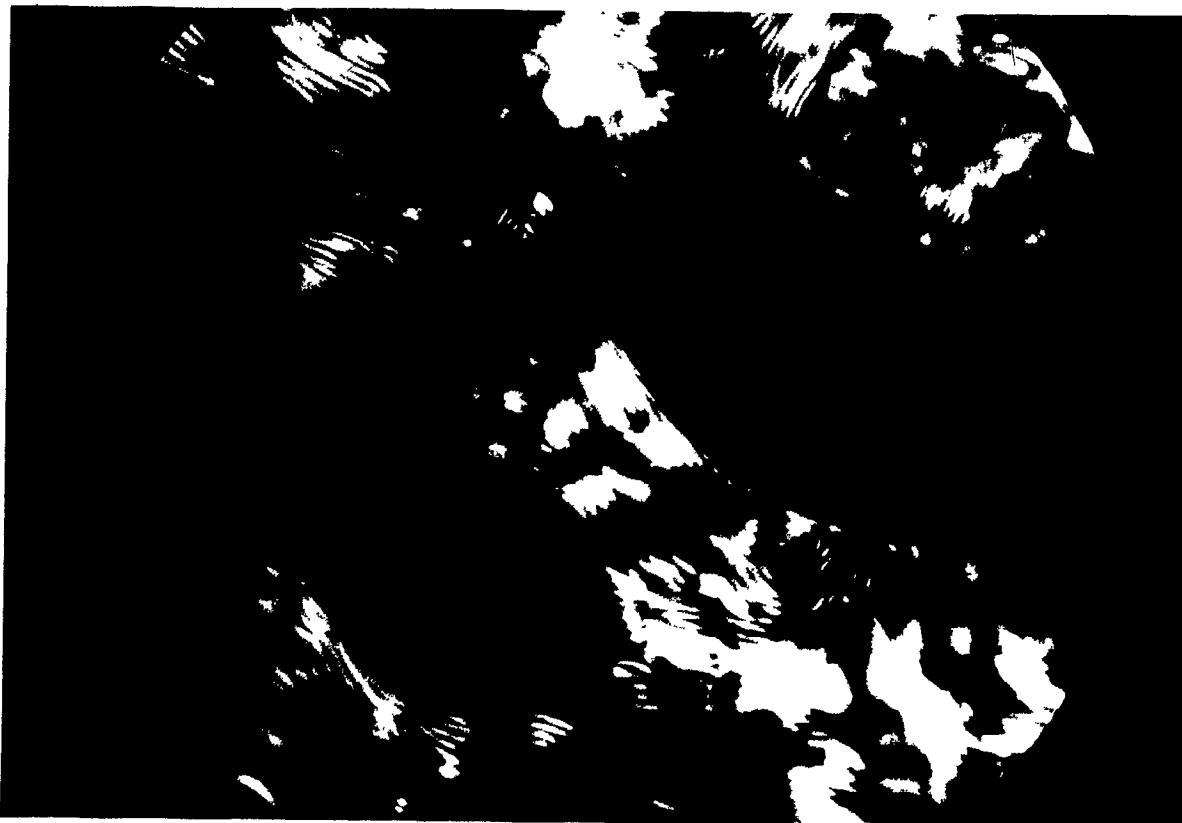


FIGURE III.11 Unusual cell structure found in a 30 weight % HPC acetic acid sample when viewed between the crossed polars of a light microscope. The periodicity between the lines is approximately 3000 nm.



FIGURE III.12 Polarizing micrograph of a 43 weight % HPC methanol solution exhibiting periodicity lines at approximately 1040 nm intervals.

to separate into the two distinguishable phases within the coexistence region.

Hydroxypropylcellulose solutions in acetic acid and acetic anhydride display characteristic periodicity lines in the two phase coexistence region. In contrast to other lyotropic systems, the periodicity between the lines was found to decrease on heating the solutions. At 40°C the lines seem to disappear, although they may simply have moved too close together to be distinguishable in the light microscope. The exact reason for this behavior is unknown. It should also be noted that HPC reacts chemically with both acetic acid and acetic anhydride to produce a partially acetylated HPC sample. This was confirmed by infrared spectra which showed characteristic acetate substituent peaks at 1735 cm^{-1} and 1240 cm^{-1} . The area of these peaks increased with time over a four week period, indicating that the HPC was reacting progressively with the solvent. Acetoxypropylcellulose (APC) is synthesized from HPC and it also forms a lyomesophase at room temperature (68).

III.3.4 FLORY'S THEORY AND HYDROXYPROPYLCELLULOSE

The basic premise of Flory's theory is that molecular asymmetry is responsible for the formation of an anisotropic ordered phase in a solution of rod shaped particles. Specific polymer-solvent interactions are believed to have a negligible effect on the anisotropic phase separation and, consequently, a particular polymer should exhibit phase separation at the same

critical volume fraction of rods in several solvents. The important parameter for mesophase formation is the axial ratio of the polymer and so, indirectly, its molar mass. Polymer chain flexibility (27,49) and sample polydispersity (45) are also believed to influence phase separation behavior.

Hydroxypropylcellulose undergoes an anisotropic phase separation in both aqueous and organic solutions at markedly different critical volume fractions of HPC. This behavior is contrary to theory (28) and to observations (31-32) of rigid rod systems where the axial ratio of the rods is the critical factor governing phase separation. Chain flexibility has been invoked (69) to account for the unexpected behavior exhibited by HPC mesophases. The Mark - Houwink equation α parameter (see Equation II.19) gives a rough estimate of the flexibility or stiffness of a polymer chain (60,70). Poly- γ -benzyl-L-glutamate (PBLG) has an α parameter of 1.7 in solutions exhibiting mesomorphic behavior (71). In these solutions PBLG is in a helical conformation and is thus believed to behave like a rigid rod. The critical volume fraction of HPC for mesophase formation in acetic acid and 1-pentanol is significantly different and, for this reason, these two solvents were chosen for the viscosity measurements described in the preceding chapter. It had been anticipated that the resulting α parameters could be correlated with the HPC chain stiffness to explain the onset of mesomorphic behavior, that is, the stiffer the HPC chains are in a solvent, the lower the critical volume fraction of HPC needed to form the mesophase. Unfortunately this hypothesis could not be verified or disproved because the α parameter for the HPC solutions was not precise enough to allow the

chain flexibility of the polydisperse samples to be evaluated unequivocally. The viscosity measurements did, however, show that the HPC molecules in solution are in an intermediate conformation between that of rigid rods and random coils. The flexibility of a polymer chain may also be quantified by the length, l' , of the Kuhn statistical segment defined in Equation III.5

$$l' = \langle r_0^2 \rangle / nl \quad \text{III.5}$$

where $\langle r_0^2 \rangle$ is the mean square unperturbed end-to-end distance of a chain consisting of n links each of length l . The Kuhn length l' is thus the length of a freely-jointed segment in a hypothetical chain of nl/l' segments with the same end-to-end distance as the real chain. For HPC samples the Kuhn length l' has been shown to vary between 13 and 21 nm depending upon the sample degree of polymerization (69).

According to Flory's theory the volume fraction of rod-like molecules at anisotropic phase separation is given by Equation III.2.

$$\phi_c^F = (8/x)(1 - 2/x) \quad \text{III.2}$$

It is difficult, if not impossible, to measure the axial ratio of HPC in water, let alone in sixteen different solvents, to test the applicability of Flory's equation to the HPC mesophase. The HPC rod length should be the same in all solvents but the rod diameter can vary from solvent to solvent because of side chain-solvent interactions. It is possible to calculate a

theoretical axial ratio for a HPC sample of known molar mass (72). This calculation involves assuming reasonable values for the rod length, diameter, and molar mass of the HPC structural unit. For example, a HPC sample with a molar mass of 82 000 has a theoretical axial ratio of 130. If this value is inserted into Equation III.2 the resulting critical volume fraction for mesophase formation is 0.06. This value is almost one order of magnitude different from the critical volume fractions determined experimentally for HPC mesophase formation. It would thus appear that HPC does not form a mesophase in the manner described by Flory's rigid rod theory. However, if a polymer chain can be replaced by a series of freely-jointed rods, each with an axial ratio of x , then Flory has shown (49) that the axial ratio, and not the number of such segments, governs the phase separation behavior. If the length of the freely-jointed rods postulated to exist in HPC is chosen as being equivalent to the Kuhn segment lengths of between 13 and 21 nm, then the axial ratios for these segment lengths can be evaluated if the rod diameter is known. X-ray diffraction studies on HPC fibers indicate that the molecules have a center-to-center separation of approximately 1.28 nm (69). If this distance is assumed to be equivalent to the HPC rod diameter, then the axial ratios for HPC range from 10 to 16. Inserting these values into Equation III.2 gives critical volume fractions of HPC between 0.44 and 0.64 for mesophase formation. These values are of the correct order of magnitude but they are slightly larger than the values reported in Table III.3. In view of the experimental difficulties associated with the use of the Kuhn segment length and the use of the HPC center-to-center separation as the diameter of the HPC molecules in solution,

the agreement between the estimated segment axial ratio and that required by Equation III.2 ($x \approx 20$) is probably as good as can be expected for HPC in water. Thus an appropriate and realistic choice of values, based on the limited available data, for the length and diameter of the HPC molecules shows that the experimental critical volume fraction results agree reasonably well with those predicted by Flory's theory for a series of freely-jointed rather than rigid rods.

III.4 Conclusion

Aqueous HPC solutions exhibit a LCT on heating. This LCT or cloud point was found to depend more on the MS of the HPC rather than on its molar mass. Some hysteresis was evident in the cloud points obtained on heating and on cooling. Both very dilute and very concentrated aqueous HPC solutions were found to undergo this particular phase separation. A qualitative "phase" diagram was presented for aqueous HPC solutions.

Hydroxypropylcellulose was also found to undergo an anisotropic phase separation at room temperature when a critical volume fraction of HPC had been exceeded in water and in several organic solvents. Contrary to Flory's rigid rod theory the critical volume fraction for phase separation varied from solvent to solvent. In addition, there was no solvent property which could be used to predict at what critical volume fraction the meso-phase would form, or, if it would be fluid, gel-like, or glassy. Flory's

rigid rod model is not applicable to the HPC system. However, if the rigid rods of the theory are replaced by freely-jointed segments equivalent to the Kuhn statistical segment length of the polymer chain, then the agreement between the experimentally determined and the theoretically predicted critical volume fractions for HPC anisotropic phase separation is quite good.

2

References

1. E.D. Klug, J. Polym. Sci., Polym. Phys. Ed., 36, 491-508 (1971).
2. N. Sarkar, J. Appl. Polym. Sci., 24, 1073-87 (1979).
3. H. Morawetz, "Macromolecules in Solution", 2nd ed., Wiley Interscience, New York, 1975, p. 78.
4. H. Tompa, "Polymer Solutions", Butterworths, New York, 1956, Chapters 2, 3, and 4.
5. C. Tanford, "Physical Chemistry of Macromolecules", John Wiley and Sons Inc., New York, 1961, pp. 245-53.
6. P.I. Freeman and J.S. Rowlinson, Polymer, 1, 20-26 (1960).
7. M.L. Huggins, J. Chem. Phys., 9, 440 (1941).
8. M.L. Huggins, Ann. N.Y. Acad. Sci., 43, 1-32 (1942).
9. M.L. Huggins, J. Phys. Chem., 46, 151-58 (1942).
10. M.L. Huggins, J. Am. Chem. Soc., 64, 1712-19 (1942).
11. P.J. Flory, J. Chem. Phys., 9, 660-61 (1941).
12. P.J. Flory, J. Chem. Phys., 10, 51-61 (1942).
13. P.J. Flory, "Principles of Polymer Chemistry", Cornell Univ. Press, Ithaca, New York, 1953.
14. P.J. Flory, Discuss. Faraday Soc., 49, 7-29 (1970).
15. D. Patterson, Rubber Chem. Technol., 40, 1-35 (1967).
16. D. Patterson, Macromolecules, 2, 672-77 (1969).
17. E.F. Casassa, J. Polym. Sci., Polym. Symp., 54, 53-83 (1976).
18. F.W. Billmeyer Jr., "Textbook of Polymer Science", 2nd ed., Wiley Interscience, New York, 1971, pp. 23-61.
19. J.M.G. Cowie, "Polymers: Chemistry and Physics of Modern Materials", Intertext Books, New York, 1973, Chapter 7.
20. H. Morawetz, "Macromolecules in Solution", 2nd ed., Wiley Interscience, New York, 1975, Chapter 2.

21. N.C. Billingham, "Molar Mass Measurements in Polymer Science", Kogan Page Ltd., Great Britain, 1977, Chapter 2.
22. P. Howard and R.S. Parikh, J. Polym. Sci., Polym. Phys. Ed., 30, 17-25 (1970).
23. E.D. Klug in "Encyclopedia of Polymer Science and Technology", H.M. Mark, N.G. Gaylord, and N.M. Bikales, Eds., Wiley-Interscience Inc., New York, 1971, Vol. 15, pp. 307-14.
24. L. Onsager, Ann. N.Y. Acad. Sci., 51, 627-59 (1949).
25. A. Isihara, J. Chem. Phys., 19, 1142-47 (1951).
26. E.T. Samulski in "Liquid Crystalline Order in Polymers", A. Blumstein, Ed., Academic Press, New York, 1978, Chapter 5.
27. P.J. Flory, Proc. R. Soc. London, Ser. A, 234, 60-73 (1956).
28. P.J. Flory, Proc. R. Soc. London, Ser. A, 234, 73-89 (1956).
29. A. Elliott and E.J. Ambrose, Discuss. Faraday Soc., 9, 246-51 (1950).
30. C. Robinson, Trans. Faraday Soc., 52, 571-92 (1956).
31. C. Robinson, Mol. Cryst., 1, 467-94 (1966).
32. P.J. Flory, J. Polym. Sci., Polym. Symp., 49, 105-28 (1961).
33. J.P. Straley, Mol. Cryst. Liq. Cryst., 22, 333-57 (1973).
34. A. Okamoto, K. Kubo, and K. Ogino, Bull. Chem. Soc. Jpn., 47, 1054-57 (1974).
35. E.L. Wee and W.G. Miller, J. Phys. Chem., 75, 1446-52 (1971).
36. W.G. Miller, C.C. Wu, E.L. Wee, G.L. Santee, J.H. Rai, and K.G. Goebel, Pure Appl. Chem., 38, 37-58 (1974).
37. W.G. Miller, V. Voltaggio, S. Chakrabarti, and K. Tohyama, Polym. Prepr., Am. Chem. Soc., Div. Polym. Chem., 20 (1), 62-65 (1979).
38. D.B. DuPré and E.T. Samulski in "Liquid Crystals: The Fourth State of Matter", F.D. Saava, Ed., Marcel Dekker Inc., New York, 1979, Chapter 5.
39. J.H. Schellman, J. Phys. Chem., 62, 1485-94 (1958).
40. P. Pincus and P.G. De Gennes, J. Polym. Sci., Polym. Symp., 65, 85-90 (1978).

41. Y. Kim and P. Pincus in "Mesomorphic Order in Polymers and Polymerization in Liquid Crystalline Media", A. Blumstein, Ed., ACS Symposium Series #74, Washington, D.C., 1978, pp. 127-35.
42. E.T. Samulski and D.B. DuPré in "Advances in Liquid Crystals", Academic Press Inc., New York, 1979, Vol. 4, pp. 121-45.
43. P.J. Flory and G. Ronca, Mol. Cryst. Liq. Cryst., 54, 289-310 (1979).
44. P.J. Flory and G. Ronca, Mol. Cryst. Liq. Cryst., 54, 311-30 (1979).
45. P.J. Flory and A. Abe, Macromolecules, 11, 1119-22 (1978).
46. M. Warner and P.J. Flory, J. Chem. Phys., 73, 6327-32 (1980).
47. R.S. Frost and P.J. Flory, Macromolecules, 11, 1134-38 (1978).
48. P.J. Flory and R.S. Frost, Macromolecules, 11, 1126-33 (1978).
49. P.J. Flory, Macromolecules, 11, 1141-44 (1978).
50. R.R. Matheson and P.J. Flory, Macromolecules, 14, 954-60 (1981).
51. A. Abe and P.J. Flory, Macromolecules, 11, 1122-26 (1978).
52. P.J. Flory, Macromolecules, 11, 1138-41 (1978).
53. P.J. Flory and W.J. Leonard Jr., J. Am. Chem. Soc., 87, 2102-08 (1965).
54. R.S. Werbowyj and D.G. Gray, Mol. Cryst. Liq. Cryst., 34, 97-103 (1976).
55. S. Dayan, P. Maissa, M.J. Vellutini, and P. Sixou, J. Polym. Sci., Polym. Lett. Ed., 20, 33-43 (1982).
56. S.M. Aharoni, Mol. Cryst. Liq. Cryst., 56, 237-41 (1980).
57. S.M. Aharoni, Polym. Prepr., Am. Chem. Soc., Div. Polym. Chem., 22 (1), 116-17 (1981).
58. J. Bheda, J.F. Fellers, and J.L. White, Colloid & Polymer Sci., 258, 1335-42 (1980).
59. This Thesis, Chapter II.
60. S.P. Papkov, Polym. Sci. USSR, 19, 1-19 (1977).
61. This Thesis, Chapter IV.
62. G. Conio, E. Bianchi, A. Ciferri, and A. Tealdi, Macromolecules, 14, 1084-87 (1981).

63. "Handbook of Chemistry and Physics", 56th ed., Robert Weast, Ed., CRC Press Inc., Ohio, 1975-76.
64. "KLUCEL Hydroxypropyl Cellulose: Chemical and Physical Properties", Hercules Inc., Wilmington, Delaware, 1976.
65. R.S. Werbowyj and D.G. Gray, presented in part at the 179th ACS National Meeting, Houston, March 1980.
66. T. Tsutsui and R. Tanaka, Polym. J., 12, 473-74 (1980).
67. J.S. Aspler and D.G. Gray, Polymer, 23, 43-46 (1982).
68. S.L. Tseng, A. Valente, and D.G. Gray, Macromolecules, 14, 715-19 (1981).
69. R.S. Werbowyj and D.G. Gray, Macromolecules, 13, 69-73 (1980).
70. N.C. Billingham, "Molar Mass Measurements in Polymer Science", Kogan Page Ltd., Great Britain, 1977, Chapter 7.
71. W.G. Miller, Ann. Rev. Phys. Chem., 29, 519-35 (1978).
72. Y. Onogi, J.L. White, and J.F. Fellers, J. Polym. Sci., Polym. Phys. Ed., 18, 663-82 (1980).

CHAPTER IV

OPTICAL PROPERTIES OF HYDROXYPROPYLCELLULOSE

LYOMESOPHASES

IV.1 Introduction

Cholesteric lyomesophases are ordered fluids which are characterized by a very high optical activity and a brilliant iridescence. Both these properties are a consequence of the unique molecular architecture to be found in cholesterics. The constituent molecules of a cholesteric must be optically active, strongly elongated, and relatively stiff. Such molecules are believed to align with their long axes nearly parallel to form a continuous layer. Successive layers pack to produce the stratified structure illustrated in Figure IV.1. Each layer of this structure is slightly twisted so that its molecules point in a different direction from that of the molecules in the layer below. The distance over which the molecules undergo a 360 degree change in orientation is referred to as the helicoidal pitch of the cholesteric lyomesophase.

In 1951 De Vries proposed a theory to account for the unusual optical properties exhibited by cholesterics (1). This theory assumed that a cholesteric material is adequately described as a series of birefringent layers in a helicoidal arrangement. The optical properties for such a molecular model could be calculated according to the theory if only the helicoidal pitch, refractive index, and layer birefringence for the material were known. De Vries showed that the helicoidal pitch and the mesophase refractive index are directly related to the wavelength of light normally reflected by the cholesteric planar structure (see Figure IV.2.A) according to Equation IV.1.

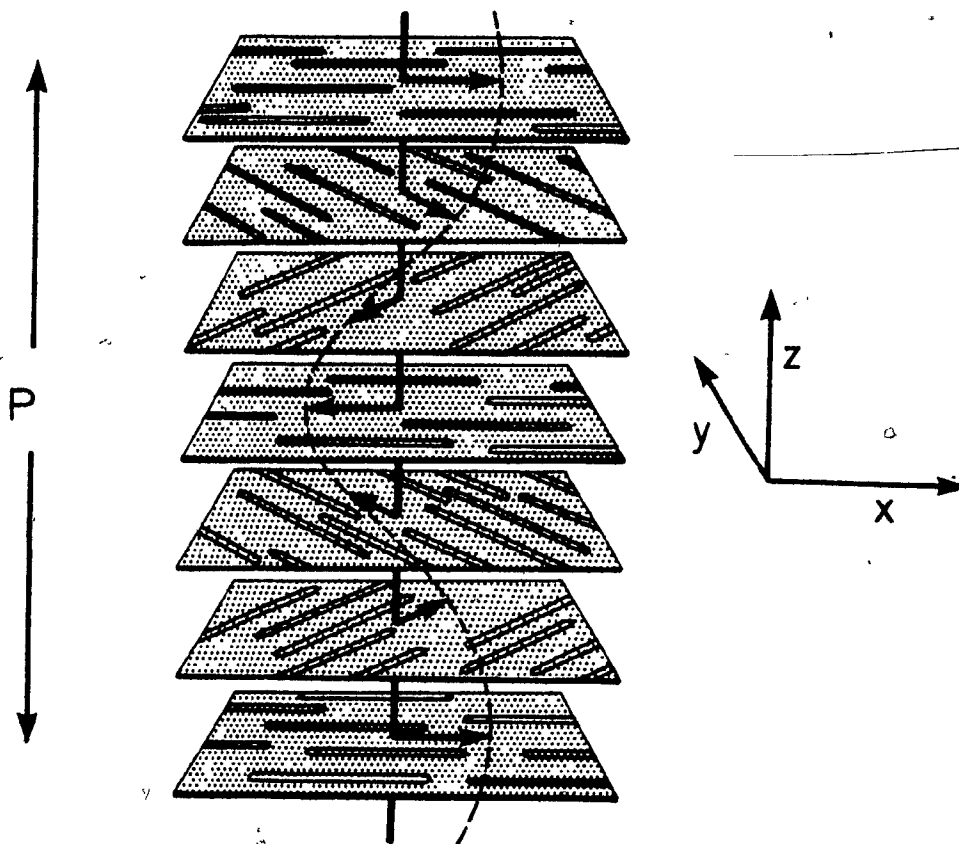


FIGURE IV.1 Idealized molecular arrangement found in a cholesteric lyomesophase. . . Successive layers illustrated are not physically distinct but are simply an aid in visualizing the helicoidal structure of pitch, P , in the cholesteric mesophase.

$$\lambda_0 = nP$$

IV.1

where λ_0 is the reflection wavelength, n is the average refractive index of the mesophase, and P is the helicoidal pitch. When a cholesteric is illuminated with white light it reflects one circularly polarized component of the light (2) in a narrow wavelength band around λ_0 . This reflection band, if within the visible region (300 to 700 nm) of the electromagnetic spectrum, is responsible for the iridescent colors exhibited by most cholesteric mesophases.

De Vries, in his optical theory for cholesterics, developed an equation which allows the variation in optical activity or rotatory power with wavelength to be calculated. This equation is shown below for systems where the helicoidal pitch is approximately equal to the incident light wavelength

$$\theta = - \frac{\pi \Delta n^2 P}{4 \lambda^2 [1 - (\lambda/\lambda_0)^2]} \quad \text{IV.2}$$

where θ is the rotatory power (rad/nm) at a wavelength λ , Δn is the layer birefringence, λ_0 is the reflection wavelength, and P is the helicoidal pitch. Equation IV.2, although predicting a change in sign for the rotatory power on passing through the reflection wavelength, is only applicable outside the reflection region. A simpler form of Equation IV.2, shown below, can be used for cholesteric systems in which the helicoidal

pitch is larger than the incident light wavelength ($P > \lambda$)

$$\theta = - \frac{\pi \Delta n^2 P}{4 \lambda^2}$$

IV.3

where the variables are the same as those defined in Equation IV.2. De Vries' theory has been applied to a solid cholesteric analogue (scarabaeid beetle exocuticle) and the predicted rotatory power is in qualitative agreement with the experimental results obtained for this system of multiple reflecting layers in a helicoidal arrangement (3). Robinson (4-6) has applied De Vries' simplified rotatory power equation to cholesteric poly- γ -benzyl-L-glutamate systems and both the calculated and experimental optical activities are reported to be in good agreement. But DuPré and Patel (7-8) have questioned the validity of De Vries' simplified equation when the pitch values are much greater (a 100 or 1000 times) than the incident light wavelength. In this case, they report that the rotatory power varies inversely as the pitch ($\theta \propto P^{-1}$) and this confirms an earlier report by Goossens (9).

More recently Chandrasekhar and co-workers (10-13) have tried to extend De Vries' theory so as to determine the rotatory power within the reflection region. According to these authors Equation IV.4 should be used to calculate the optical activity for a cholesteric within the reflection region

$$\theta = -\frac{\pi\Delta n^2 p}{4\lambda^2} + \frac{\pi(\lambda - \lambda_0)}{p\lambda} \quad \text{IV.4}$$

whereas Equation IV.5 should be used outside the reflection region.

$$\theta = -\frac{\pi\Delta n^2 p}{4\lambda^2} + \frac{\pi(\lambda - \lambda_0)}{p\lambda} \left[1 - \left(1 - \frac{(p\Delta n/\lambda_0)^2}{(-2\pi(\lambda - \lambda_0)^2/\lambda)} \right) \right]^{1/2} \quad \text{IV.5}$$

The variables are the same as those defined previously in Equation IV.2. Rotatory power values calculated using Equations IV.3 and IV.5 are reported to differ by one order of magnitude (3). More work is required in this area if the discrepancy between the two equations is to be satisfactorily explained.

A series of birefringent layers stacked one atop another can take up several different orientations when confined between two flat surfaces. Two idealized possible arrangements are depicted schematically in Figure IV.2. Following the convention of Chandrasekhar (14) the layered arrangement illustrated in Figure IV.2.A is referred to as a planar texture. Texture, in this work, is taken to mean the macroscopic arrangement visible under the light microscope. The planar texture exhibits large optical rotation, birefringence, and selective reflection of incident light according to Bragg's law. At normal incidence the light reflected from the planar texture is strongly circularly polarized (14). The cholesteric arrangement depicted in Figure IV.2.B is birefringent and exhibits little

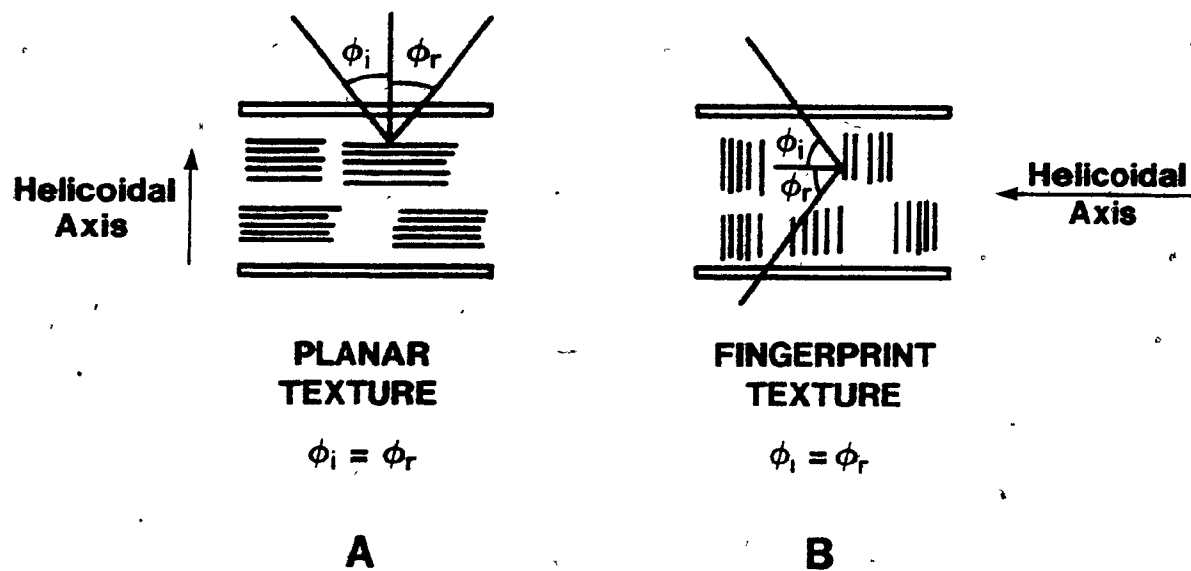


FIGURE IV.2 Idealized helicoidal arrangements possible when a cholesteric structure is constrained between two flat surfaces: ϕ_i and ϕ_r are angles of incidence and reflection respectively. See text for the different properties exhibited by the planar and fingerprint textures depicted.

or no optical activity (15). Such samples of sufficiently long pitch, when viewed in the light microscope, are characterized by a series of equally spaced lines whose periodicity varies from 1 to 50 μm depending on the solution concentration. These periodicity lines are found to equal one-half of the helicoidal pitch (6). The periodicity lines in these samples are very reminiscent of a human fingerprint and hence their fingerprint texture name is derived. Samples possessing this texture exhibit a shimmering iridescence that is distinctly different in appearance from the cholesteric iridescence displayed by short pitch samples with planar texture. The long pitch shimmering iridescence may be attributed to the scattering of light from a structure resembling a liquid diffraction grating. Figures IV.3 and IV.4 respectively illustrate the distinctly different types of iridescence exhibited by the cholesteric planar and fingerprint textures. The iridescent scattering behavior of a cholesteric mesophase is thus determined by the macroscopic helicoidal arrangement found within the sample.

De Vries' equation relating the helicoidal pitch and the reflection wavelength (Equation IV.1) was developed for use with normal incident light. Two general theories (16-17) have been developed to explain how the use of arbitrary angles of incidence might alter the normal reflection wavelength of a cholesteric mesophase. Since both theories are very similar, only the one developed by Ferguson (17) will be presented. Ferguson has shown that the reflection wavelength, $\lambda_{o,i}$, at an arbitrary incident light angle of ϕ is given by Equation IV.6

COLOURED PICTURES
Images en couleur

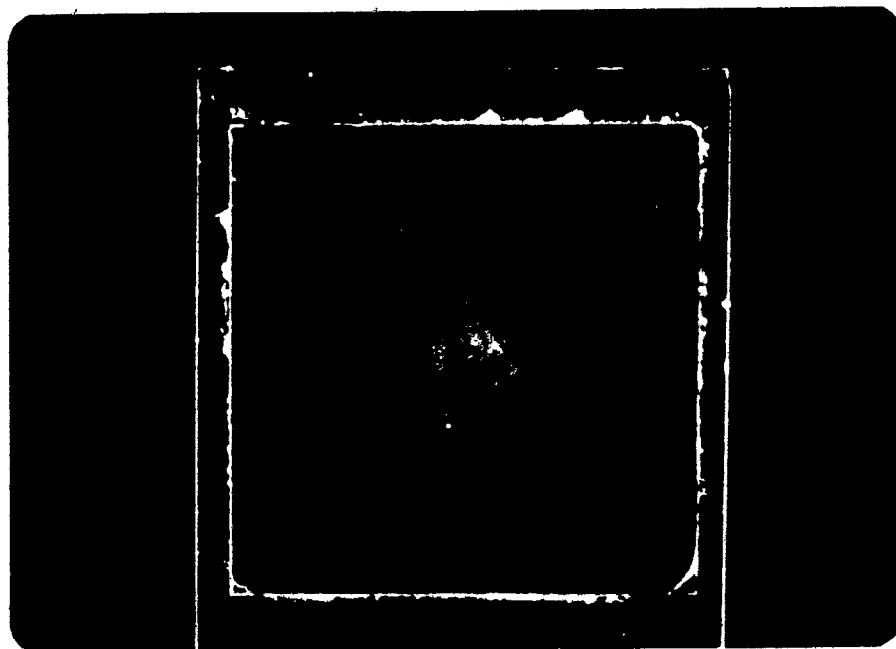


FIGURE IV.3 Cholesteric iridescent color of a typical concentrated aqueous HPC-L sample which exhibits a planar texture on examination in the light microscope. The two color appearance of the sample is due to faster solvent evaporation from the sample edges.

COLOURED PICTURES
Images en couleur

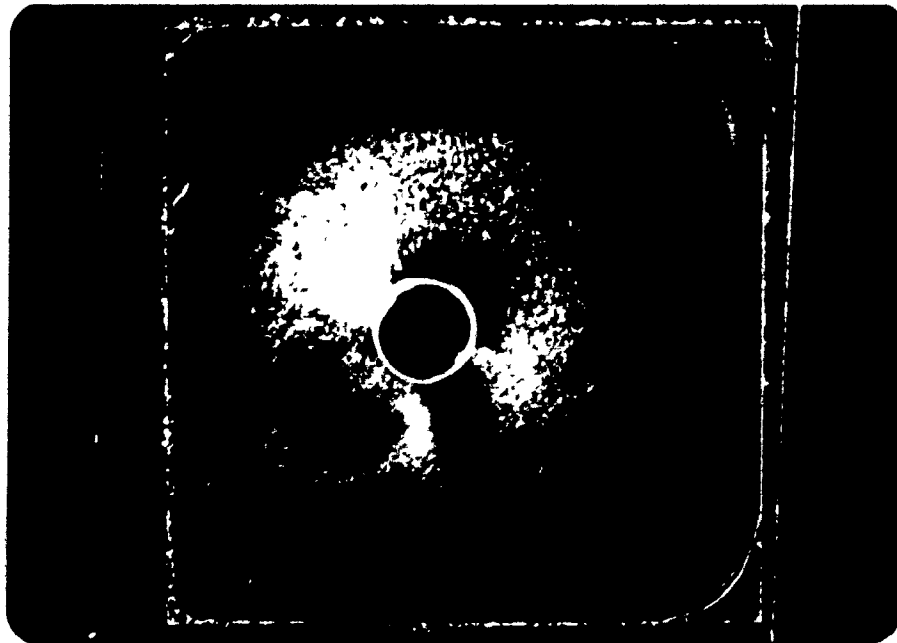


FIGURE IV.4 Shimmering iridescent color of a typical concentrated HPC-1 acetic acid sample which exhibits a fingerprint texture on examination in the light microscope.

$$\lambda_{o,i} = \frac{nP}{m} \cos \left[\frac{1}{2} \sin^{-1} \left(\frac{\sin \phi_i}{n} \right) + \frac{1}{2} \sin^{-1} \left(\frac{\sin \phi_r}{n} \right) \right] \quad \text{IV.6}$$

where m is the reflection order, n is the refractive index of the mesophase, P is the helicoidal pitch, and ϕ_i and ϕ_r are the incident and reflection angles respectively in air. This equation clearly shows that the incident and reflecting or viewing angles have a marked effect on the wavelength of the light reflected by the cholesteric structure. For systems where the pitch is large and the cholesteric structure behaves as a liquid diffraction grating, a corresponding equation for the dependence of the shimmering color on incident and reflection light angles can be devised by using Snell's law, interference theory (18), and De Vries' Equation IV.1. The resulting equation is shown below

$$\lambda_{o,i} = \frac{nP}{m} \sin \left[\frac{1}{2} \sin^{-1} \left(\frac{\sin \phi_i}{n} \right) + \frac{1}{2} \sin^{-1} \left(\frac{\sin \phi_r}{n} \right) \right] \quad \text{IV.7}$$

where the variables are the same as those defined in Equation IV.6.

The iridescence of cholesteric mesophases is not affected solely by incident and reflection angles. De Vries' Equation IV.1 clearly shows that the sample iridescence or the reflection wavelength varies as the helicoidal pitch; any factor, therefore, that alters the helicoidal pitch must necessarily alter the sample iridescence. For lyomesophases the helicoidal pitch varies with solution concentration and solvent. Temperature changes

alter the pitch in thermomesophases. Much work has been done on the latter types of systems (19-22) whereas only a few investigations (5,23) have been carried out on the former systems. The work on HPC mesophases will revolve around discovering the functional dependence of pitch on solution concentration.

IV.2 Experimental

IV.2.1 LYOMESOPHASE PREPARATION

Hydroxypropylcellulose lyomesophases were prepared following the two gravimetric methods outlined below. Dried HPC was weighed into 15-ml glass vials (Kimble Glass Ltd) to which an appropriate amount of solvent was added. The solutions were permitted to stand at room temperature for one month with daily rotation of the vials to ensure homogeneity. These solutions were then analyzed by using the procedure outlined earlier (24) and the concentrations agreed to within $\pm 1\%$ of the originally prepared solutions.

The second method of lyomesophase preparation involved the concentration of a dilute solution. A stock solution of about 30% HPC by weight was made up. After seventy-two hours of gentle agitation the clear yellowish solution appeared quite uniform and gel-free. Solutions were viscous yet they still poured easily. Stock solutions of higher molar mass

samples (G, M, and H) were prepared containing only 8 to 10% HPC by weight. These stock solutions exhibited viscosities comparable to those of the more concentrated lower molar mass HPC solutions. The stock solutions were divided into approximately 10-ml portions which were transferred into 15-ml vials. These samples were then suspended in boiling water for ten minutes. At this temperature the solutions phase separated and the HPC precipitated out of solution as a highly swollen coagulated floc. The solvent-rich phase was decanted off and the remaining solution, on cooling, was cloudy in appearance. This boiling, decanting, and cooling procedure was repeated several times for each solution. Eventually after successive coolings the samples exhibited a marked iridescence. Unless otherwise stated iridescent colors in this work refer to reflected colors at approximately normal incident and viewing angles. The iridescent solutions were then analyzed using the procedure outlined (24) to determine their concentration.

IV.2.2 OPTICAL ACTIVITY AND REFLECTION

The optical activity for HPC solutions was determined by optical rotatory dispersion (ORD) measurements. An ORD spectrum records the change in rotatory power with wavelength from 300 to 700 nm and therefore provides more complete information than corresponding polarimetry measurements which can only be made at five or six discrete wavelengths. A Jasco ORD/UV5 spectrometer was used to obtain the ORD spectra for both dilute and concentrated HPC solutions. In this work dilute solution refers to HPC concentrations up to approximately 20%. The term concentrated solution

will generally mean solutions containing from 25 to 80% HPC by weight or volume. Aqueous D-glucose solutions were used to calibrate the ORD spectrometer.

Dilute HPC solutions were poured into the 10-ml ORD sample cell. The cell was mounted in the ORD holder and the spectra were recorded from 700 to 300 nm at a scan rate of 20 $\mu\text{m}/\text{sec}$. The temperature was 21°C. Iridescent HPC samples were too viscous to pour and it was necessary to devise a modified ORD cell. A small amount of the iridescent sample was placed between two cover glasses (Corning, 18-mm sq) which were then sealed together with epoxy (Conap) around their edges to reduce the evaporation of solvent from the sample. This cell was permitted to stand for twenty-four hours to remove any strain in the sample. A precision micrometer was then used to determine the sample thickness. This technique was adequate although some uncertainty existed as to the uniform thickness of the sample. To avoid this problem a pair of quartz cells (Hellma Canada) with a 0.01-mm spacing were used as the spectrometer ORD cell. This quartz cell was sealed with molten wax to reduce evaporation of the solvent during the twenty-four hour period prior to running the sample. The modified cell was mounted on the ORD holder and the spectra were recorded at the same temperature, scan speed, and over the same wavelength range as the dilute solutions. The base line for the ORD spectra was obtained with distilled water in the quartz cell. The HPC lyomesophase has a very large optical rotation and, since the maximum rotation measured by the spectrometer is $\pm 2^\circ$, it was necessary to use a very small amount of sample in the range of 20 to

40-mg.

In addition to the optical activity, the ORD spectrum of a HPC lyomesophase also provides a wavelength value for the light normally reflected by the cholesteric structure. This reflection wavelength corresponds to the inflection wavelength of the ORD spectrum. Circular dichroism measurements on the Jasco spectrometer confirmed that the light normally reflected by the HPC lyomesophase was circularly dichroic. The reflection wavelength can also be measured spectrophotometrically (15,25) since at this wavelength only 50% of normal unpolarized light is transmitted. The reflection wavelengths (λ_0) obtained from the ORD spectra were compared with reflection wavelengths acquired by using a Carey Model 17 automatic recording spectrophotometer. The reflection wavelength range on the Carey extends up to 1500 nm and is thus much greater than the 700 nm limit imposed by ORD measurements. A Pye Unicam SP8-150 UV-VIS spectrophotometer equipped with a variable angle specular reflectance accessory (26) was used to measure the change in reflection wavelength for several HPC samples when the incident light angle was varied from 10° to 75° .

IV.2.3 LASER LIGHT DIFFRACTION

Cloudy organic HPC solutions were placed in hanging drop slides (Fisher Ltd, 0.8-mm deep) and allowed to equilibrate for twenty-four hours. These samples were then examined under a polarizing microscope (Reichert Zetopan). In several of the solvents the samples exhibited distinct

fingerprint periodicity lines. A Nikon F camera equipped with Kodak Plus-X 35-mm black and white Pan film (ASA 125) was mounted on the light microscope to take photos of these fingerprint textured samples. The resulting negatives were enlarged and the spacing between the periodicity lines was measured. A standard slide with etched spacings of 0.1-mm and 0.01-mm was used as a magnification reference.

The samples examined above were also found to produce light diffraction patterns analogous to those obtained from x-ray diffraction studies. The hanging drop slides were mounted on a movable stand permitting the sample-to-film distance to be varied. The light source used was either a Kodak slide projector or a He-Ne laser (Spectra Physics Model 145) of wavelength 633 nm. The entire system was placed in a dark room. The diffraction pattern was recorded on Polaroid 4x5 Land film which was inserted into a polaroid film holder. The film was exposed from one to three seconds and provided both a positive print and a negative. It was possible to evaluate the periodicity giving rise to the laser diffraction pattern by measuring both the sample-to-film distance and the radius of the diffraction ring recorded on the polaroid film and then making use of Equation IV.8 for a diffraction grating (27).

$$\lambda = d \sin \theta \quad \text{IV.8}$$

where λ = wavelength of laser

d = periodicity spacing

θ = angle of scattered light, where $\tan\theta$ is defined by the radius of the diffraction ring divided by the sample-to-film distance

IV.2.4 REFRACTIVE INDEX AND BIREFRINGENCE

The refractive index (n) for HPC solutions in water, methanol, and acetic acid was measured with a Carl Zeiss Model 44159 Abbé refractometer. Although this instrument employs a white light source, the refractive index measured is that of the sodium D line (589 nm); two identical Amici prisms within the viewing telescope disperse all other wavelengths except that of the sodium D line (28-29). Measurements in all solvents were made at 21°C and all samples were prepared in an identical manner. Solutions were made up by weight in 15-mL glass vials (Kimble Glass Ltd). The solution concentrations ranged from 5 to 70% HPC by weight in approximately 5% increments. The solutions were allowed to stand for at least three weeks and for up to two months at room temperature with daily rotation of the vials to ensure homogeneity of the solutions, especially those at the higher concentrations.

Dilute isotropic solutions gave only one refractive index value that increased linearly with the HPC volume fraction. As the solutions entered the two phase region consisting of isotropic and anisotropic mesomorphic material, two distinct lines were observed in the viewing telescope of the refractometer as indicated in Figure IV.5. According to Schael (30) by inserting a polarizer at the eyepiece of the refractometer

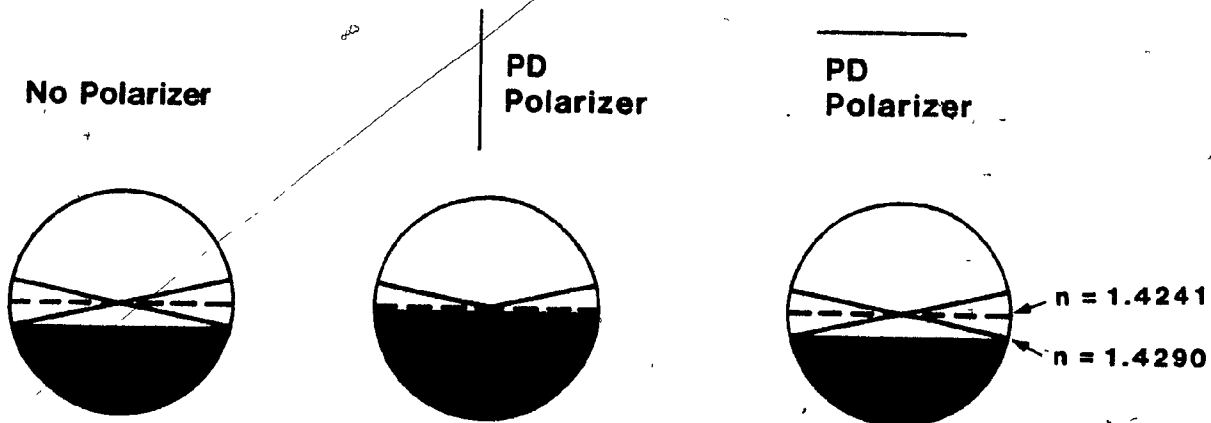


FIGURE IV.5. The schematic view of an anisotropic aqueous HPC solution through an Abbé refractometer telescope with no polarizer at the eyepiece (left), with the privileged direction (PD) of the polarizer perpendicular to the refractometer field line (center), and with the PD of the polarizer parallel to the refractometer field line (right). In each case the refractometer cross-hairs are centered on the upper of the two refractive index lines visible in the refractometer eyepiece.

it is possible to enhance one line at the expense of the other. Specifically when the privileged direction (PD) of the polarizer is perpendicular to the line separating the fields of the refractometer only the upper line is visible. Rotation by 90° results in the PD of the polarizer lying parallel to the field line and now the lower line is again distinctly visible whereas the upper line appears very faint. The difference in refractive index in two directions gives a value for the solution birefringence.

Solutions were equilibrated in the refractometer for two minutes before measurements were made. Five measurements were taken for each solution and the results were averaged. Data were reproducible to within $\pm 2.0 \times 10^{-4}$, the rated accuracy of the Abbé refractometer. It was necessary to complete all measurements within five minutes or reproducible results could not be obtained. In dilute solutions this was due to solvent evaporation, whereas in more concentrated solutions it is believed that the pressure exerted by the prism surfaces on the mesophase causes a molecular re-orientation that is responsible for the change in relative separation between the two refractive index lines with time.

IV.3 Results and Discussion

IV.3.1 OPTICAL ROTATORY DISPERSION

Above a critical concentration both aqueous and organic HPC solutions

were found to be iridescent and to exhibit birefringence when examined under crossed polars (24). Since both these properties are characteristic of liquid crystals it was hoped that optical activity measurements would confirm the cholesteric nature of the HPC solutions. The optical activity of dilute HPC solutions arises from the additive chirality of individual HPC molecules. Concentrated HPC solutions, if indeed they are cholesteric lyomesophases, should exhibit optical activities one or two orders of magnitude higher than those exhibited by dilute solutions. The very high optical activity of cholesterics is attributed to the presence of the helicoidal structure illustrated in Figure IV.1.

Dilute HPC solutions in both aqueous and organic media exhibit similar plain negative ORD curves. Figure IV.6 illustrates the ORD spectra obtained for HPC in water and three organic solvents. Such curves are classified as plain (31) because they show no inflection point (where the optical rotation is zero). These curves are also referred to as negative (32) because the rotatory power falls off with decreasing wavelength. Aqueous HPC solutions exhibited slightly larger optical activities than corresponding acetic acid, methanol, and cellosolve HPC solutions. The plain negative ORD curves that result would seem to imply that the HPC molecules are in a random rather than in a helical molecular conformation in solution. This is further confirmed in that the experimental ORD data can be fitted to a one term Drude equation (33). This equation predicts that the specific rotation, $[\alpha]$, should vary linearly with $1/\lambda^2$. The ORD data for aqueous HPC solutions show this linear dependence of $[\alpha]$ on $1/\lambda^2$ as illustrated in

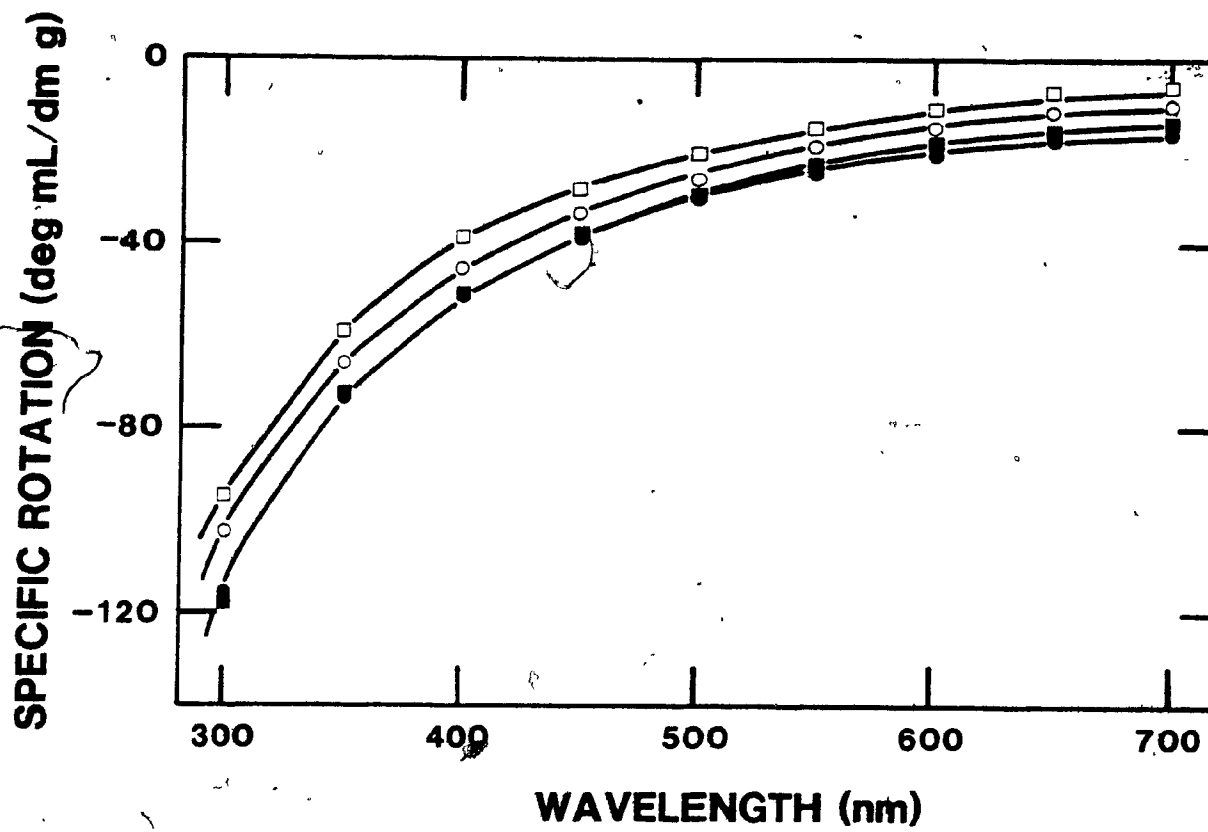


FIGURE IV.6 Typical plain negative ORD spectra for HPC in water (●), methanol (■), acetic acid (○), and cellosolve (□) at 21°C.

Figure IV.7. The specific rotation for dilute aqueous HPC solutions ranges from approximately -15 to -125 deg mL/dm g from 700 to 300 nm respectively.

Concentrated aqueous and organic HPC solutions exhibit anomalous negative ORD curves. Anomalous ORD curves are characterized by an inflection point where the optical rotation drops to zero and then changes sign (32). In the case of cholesteric mesophases the regions of opposite rotatory power are separated by a region of reflection of circularly polarized light (32). This reflection region arises from a Bragg type scattering of the incident light from the ordered arrangement of layers in the helicoidal cholesteric structure. Figure IV.8 illustrates two anomalous negative ORD curves for HPC. The curves are described as negative because the trough of the reflection region occurs at a longer wavelength than does the peak. The specific rotations of concentrated HPC solutions in both water and methanol are much greater than the specific rotations of dilute HPC solutions in the same solvents at corresponding wavelengths. Typically the specific rotation for a concentrated aqueous HPC solution ranges from about -2000 to $+12\ 000$ deg mL/dm g from 700 to 300 nm respectively. This higher optical activity for concentrated HPC solutions can only be accounted for if HPC does indeed form a cholesteric lyomesophase.

To confirm conclusively the cholesteric character of concentrated HPC solutions, the experimental ORD results were fitted to De Vries' rotatory power equation which by substituting Equation IV.1 into Equation

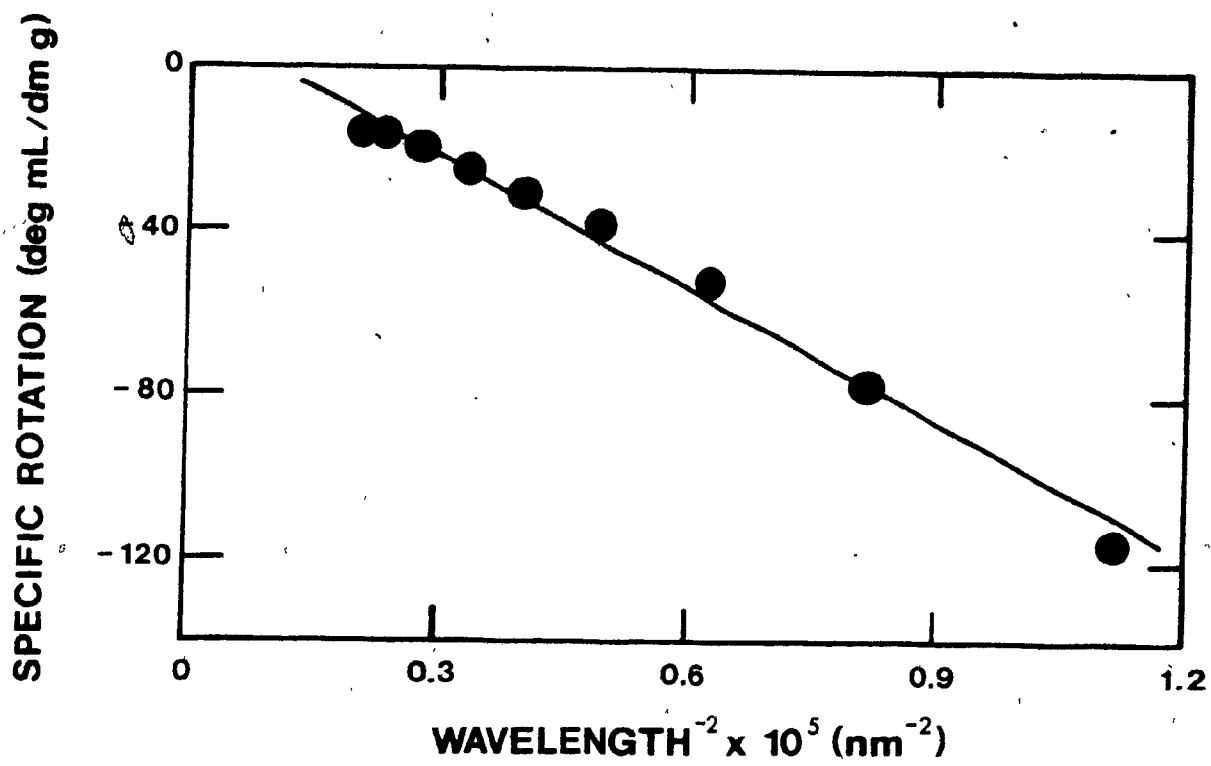


FIGURE IV.7 Dependence of the solution optical activity on wavelength for a typical dilute aqueous HPC solution.

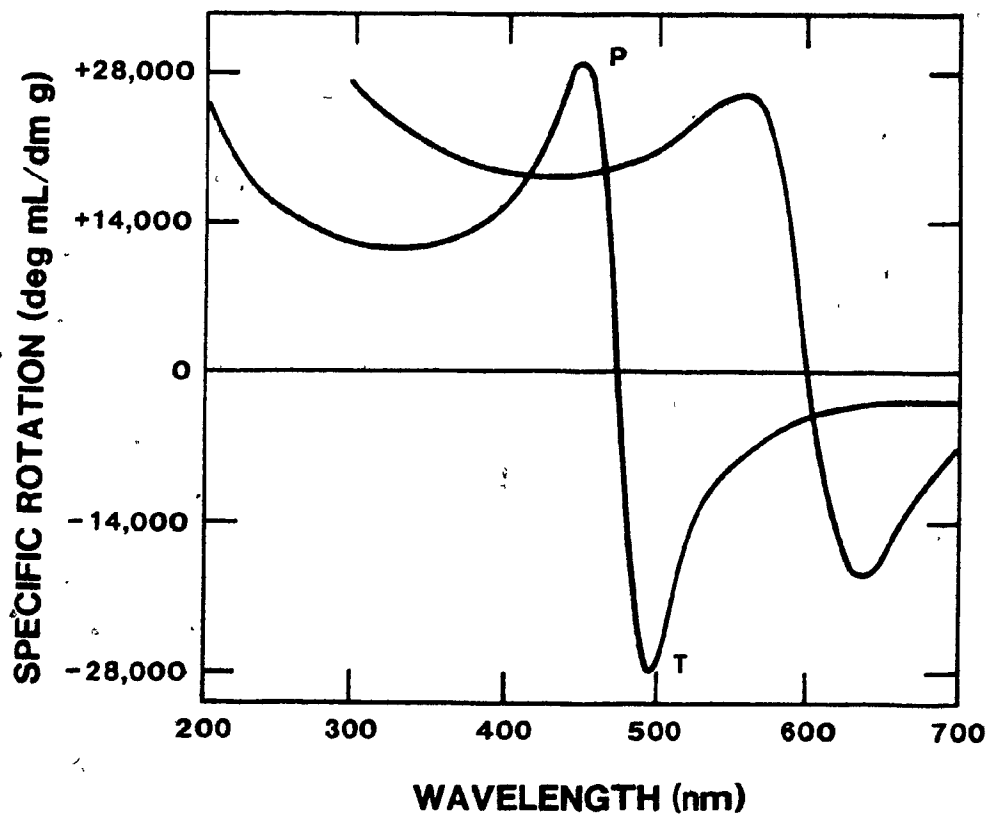


FIGURE IV.8 Typical anomalous negative ORD curves for HPC-L in methanol ($\lambda_0 = 600$ nm) and in water ($\lambda_0 = 475$ nm): P = peak and T = trough. Both samples were 0.01 mm thick.

IV.2 then becomes

$$\theta = - \frac{\pi \Delta n^2 \lambda_0}{4 \lambda^2 n [1 - (\lambda/\lambda_0)^2]} \quad \text{IV.9}$$

The experimental ORD curve provides values for λ_0 , λ , and θ ; the only unknowns in Equation IV.9 are the refractive index and the layer birefringence. The solution refractive index was easily measured using an Abbé refractometer and the results have been plotted in Figures IV.9, IV.10, IV.11, and IV.12. In aqueous HPC solutions the refractive index was found to vary linearly with the HPC volume fraction. There was apparently no variation in refractive index with the HPC molar mass as can be seen when the data for HPC-L (Figure IV.9) and HPC-J (Figure IV.10) are compared. The refractive index for HPC-L was also measured in methanol and acetic acid, and the results can be found in Figures IV.11 and IV.12 respectively. The methanol data show the same linear dependence of refractive index on volume fraction as do the aqueous solutions; however, in acetic acid the refractive index varies linearly with the weight fraction rather than with the volume fraction of polymer. Hydroxypropylcellulose is believed to react slowly with acetic acid to produce a partially acetylated HPC or acetoxypopylcellulose (APC). The resulting mixture of HPC and APC in acetic acid probably affects the volume fraction (since HPC and APC have different densities) more than the weight fraction value and this may, perhaps, account for the non-linear variation in refractive index with volume fraction

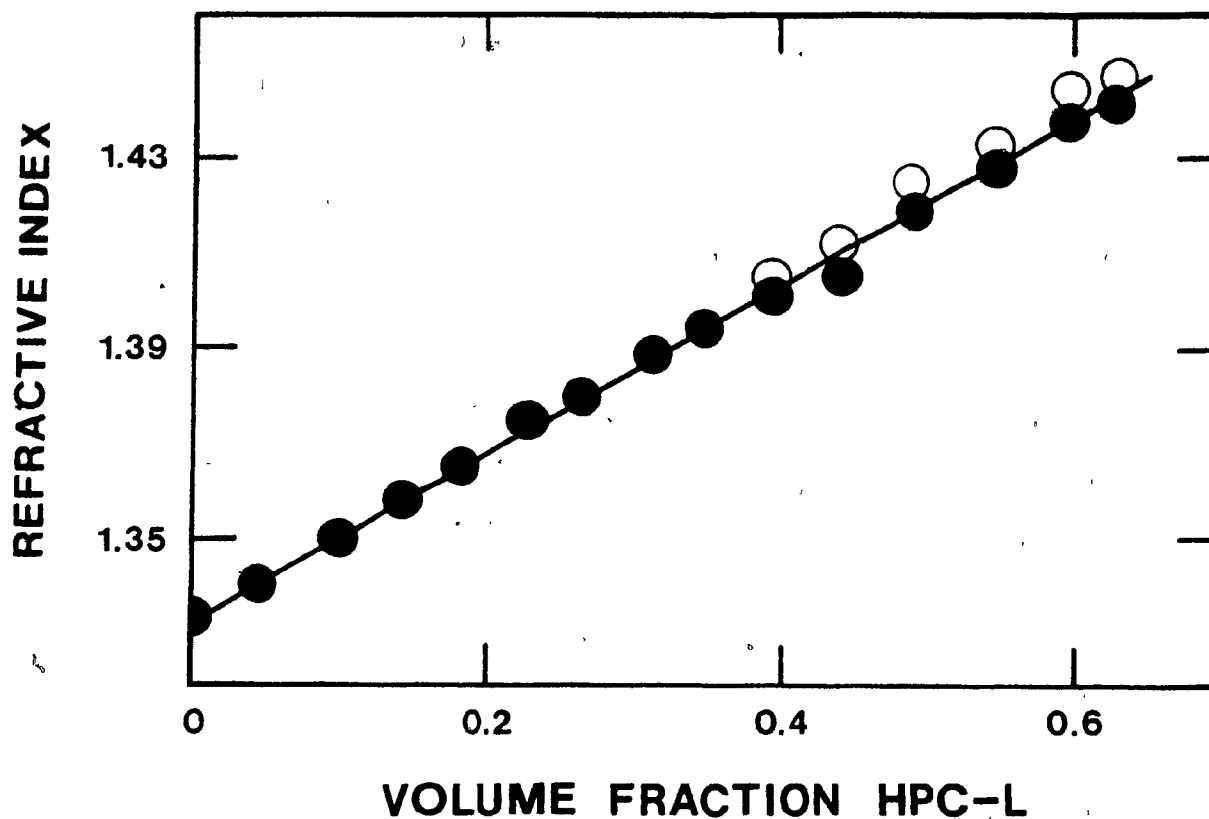


FIGURE IV.9 Refractive index data for aqueous HPC-L solutions as a function of the HPC volume fraction at room temperature ($\sim 21^{\circ}\text{C}$). The open circles represent the second refractive indices measured in the Abbé refractometer for the HPC lyomesophase.

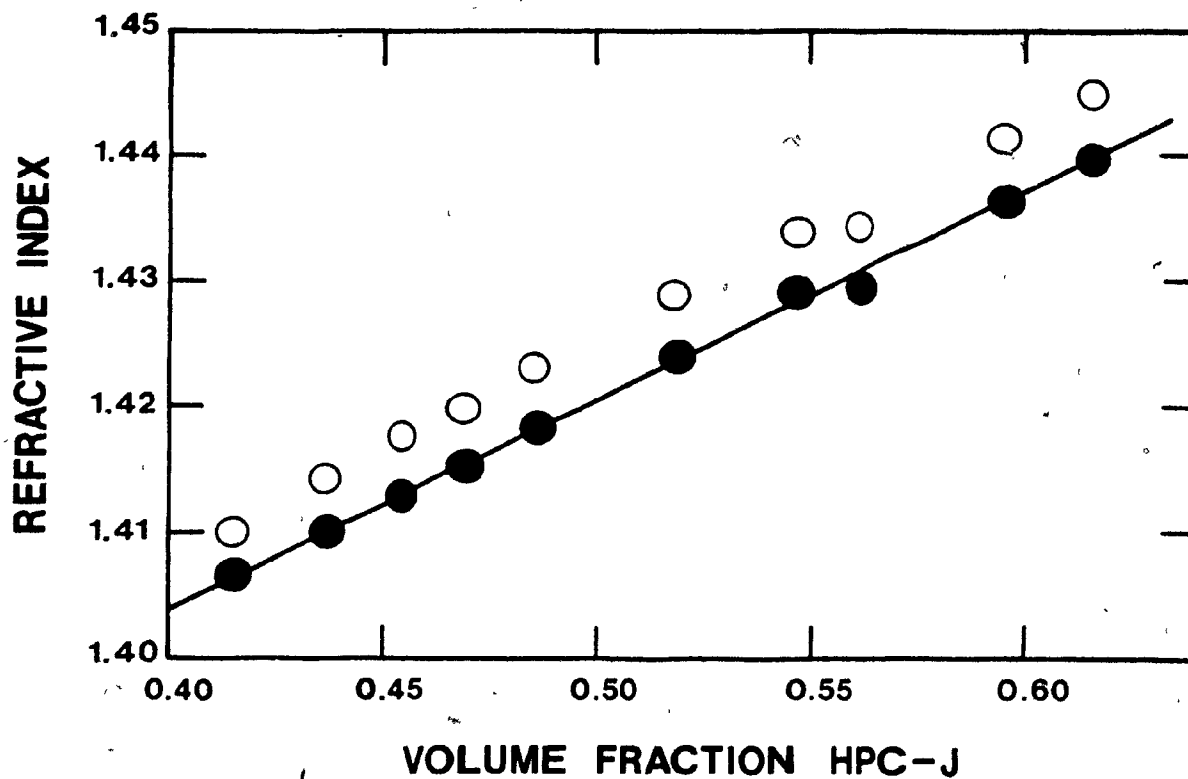


FIGURE IV.10 The variation in refractive index with HPC-J volume fraction in aqueous solution at 21°C. The open circles are the second refractive index values measured in the Abbé refractometer for the anisotropic HPC mesophase.

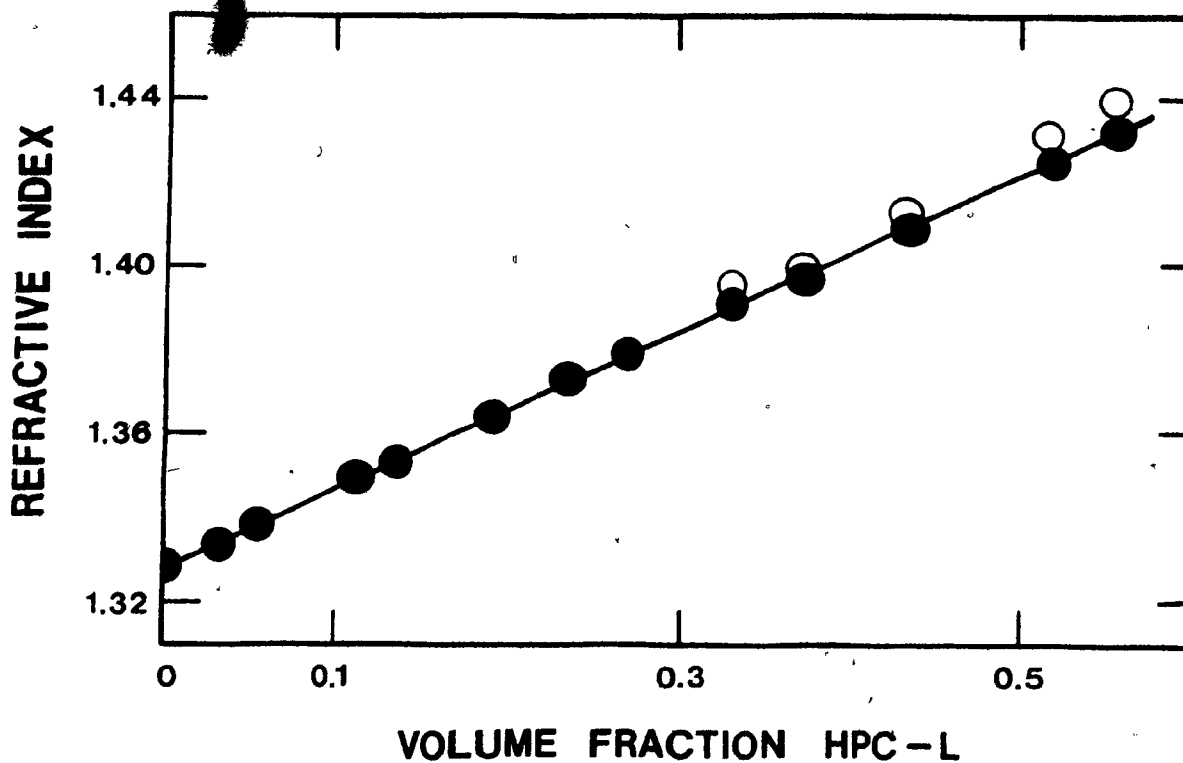


FIGURE IV.11 Refractive index data for HPC-L methanol solutions as a function of the HPC volume fraction at 21°C. The open circles represent the second refractive indices measured in the Abbé refractometer for anisotropic HPC solutions.

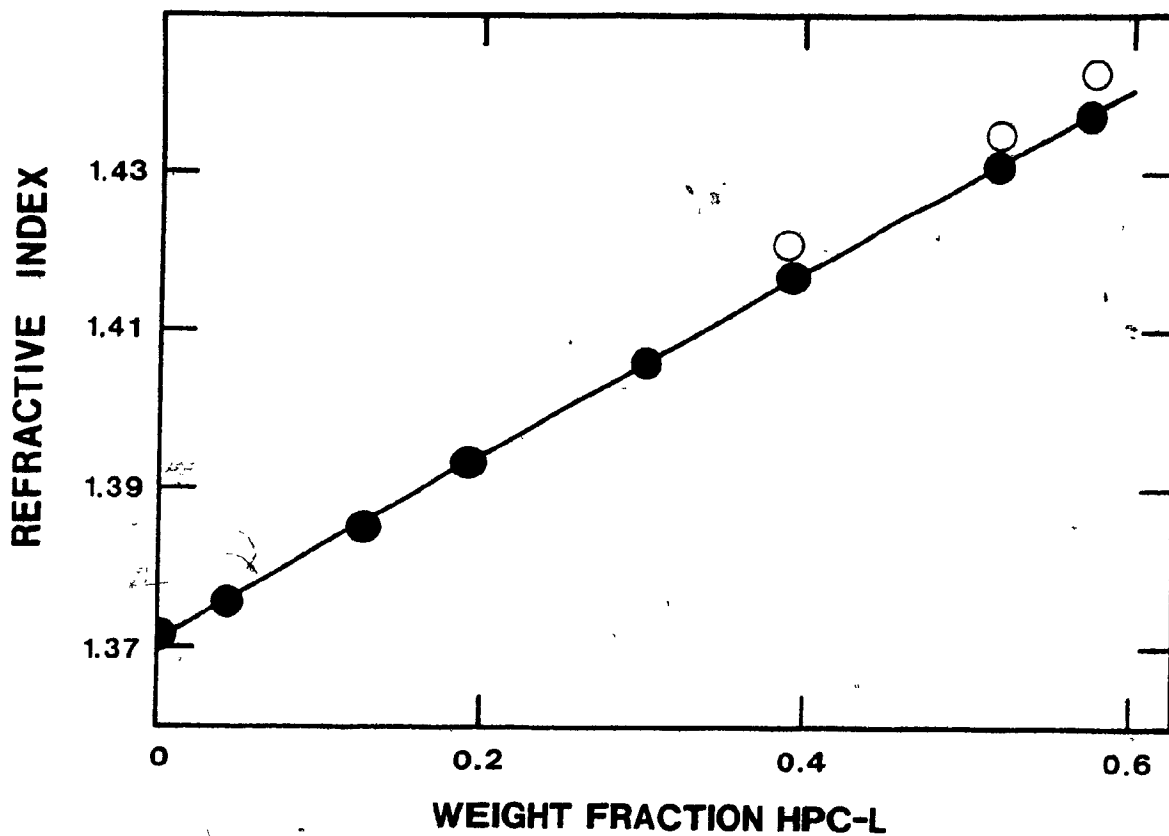


FIGURE IV.12 The variation in refractive index with HPC-L weight fraction in acetic acid solution at 21°C. The open circles are the second refractive indices measured in the Abbé refractometer for the HPC mesophase.

for HPC acetic acid solutions. The open circles in Figures IV.9 through IV.12 represent a second refractive index which was measured in the Abbé refractometer for all anisotropic HPC solutions. The difference between these two refractive indices provides a measured birefringence value for the samples. However, as will be explained in the next section, this value is not the birefringence required in Equation IV.9. For the present, the layer birefringence may be taken as a fitting parameter between Equation IV.9 and the experimental ORD results. The exact details of the fitting procedure will be elaborated on in the next section. Figure IV.13 shows a typical example of the rotatory power agreement between the experimental results and those predicted by De Vries' Equation IV.9 by the use of only one fitting parameter, the layer birefringence. Recall that De Vries' theory is applicable only outside the reflection region bounded by the peak and the trough of the ORD curve. Concentrated HPC solutions behave optically like cholesteric mesophases in that they exhibit optical rotations hundreds or thousands of degrees larger than their dilute solutions. This same rotatory power data for concentrated solutions agrees very well with the predictions of De Vries' theory for cholesterics using only one fitting parameter, the layer birefringence.

IV.3.2 BIREFRINGENCE

The birefringence as defined in De Vries' theory is the birefringence of an individual layer in the untwisted cholesteric structure.

Cholesteric lyomesophases based on polypeptide systems exhibit different

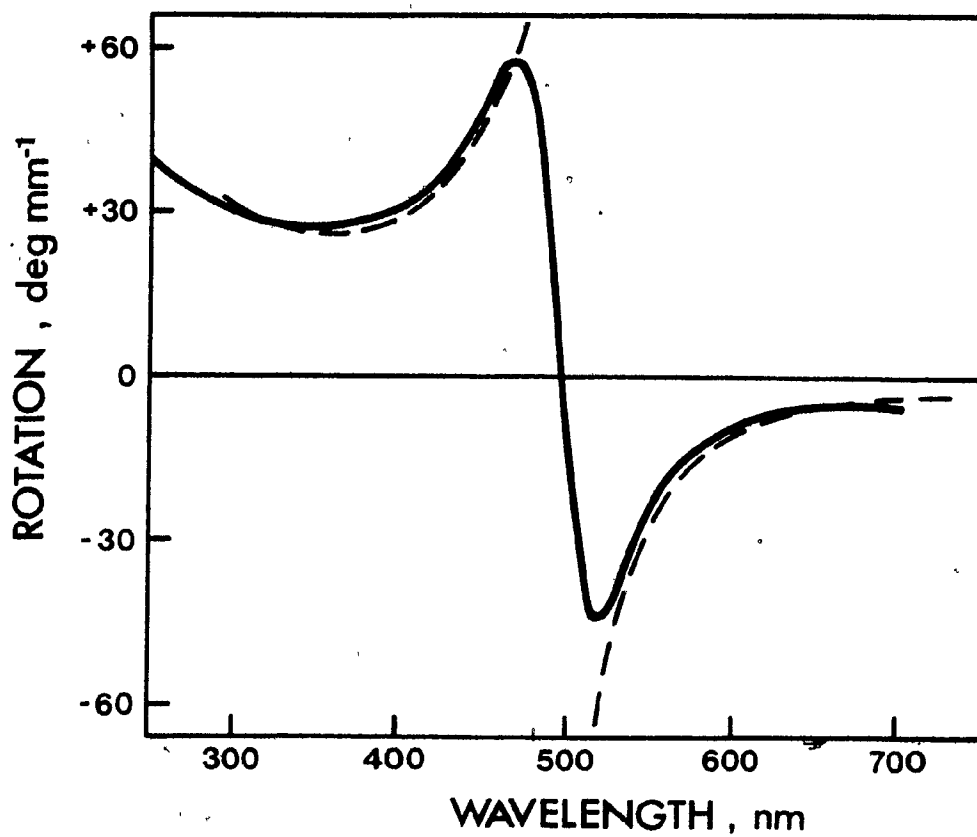


FIGURE IV.13 - The variation in rotatory power with wavelength for an aqueous solution of 0.57 volume fraction HPC-E. The solid curve is the experimental ORD spectrum and the broken curve is the rotatory power calculated using Equation IV.9 where Δn was 0.01, n was 1.433, and λ_0 was 496 nm.

helicoidal handedness in different solvents (6,34). By choosing a suitable combination of two solvents it is possible to obtain an untwisted cholesteric whose layer birefringence can be measured. Alternatively, an electric or magnetic field can be applied to untwist the cholesteric structure (35). Unfortunately HPC exhibited the same helicoidal handedness in all the solvents investigated. Hydroxypropylcellulose is believed to have a right-handed helicoidal structure following the accepted convention (34) that if the rotatory power is positive for $\lambda < P$ then the cholesteric is right-handed. The application of an electric or a magnetic field seemed to have either no effect or a very transitory effect on the HPC cholesteric structure. It was thus impossible to measure the layer birefringence of the untwisted cholesteric HPC mesophase directly; rather, De Vries' rotatory power equation, shown below, was fitted to the experimental ORD data and then solved for the layer birefringence.

$$\theta = - \frac{\pi \Delta n^2 \lambda_0}{4 \lambda^2 n [1 - (\lambda/\lambda_0)^2]} \quad \text{IV.9}$$

Specifically, n was known from Abbé refractometer measurements and θ , λ , and λ_0 were obtained from the experimental ORD curves. Clearly, if a least squares plot of θ versus $[\lambda^2(1 - [\lambda/\lambda_0]^2)]^{-1}$ is constructed, the slope of the resulting straight line is given by $\pi \Delta n^2 \lambda_0 / 4n$ which can be solved for the layer birefringence. A typical example of this plot is illustrated in Figure IV.14. The layer birefringence thus determined was found to vary from 0.007 to 0.016 over the HPC volume fraction range of 0.50 to 0.63

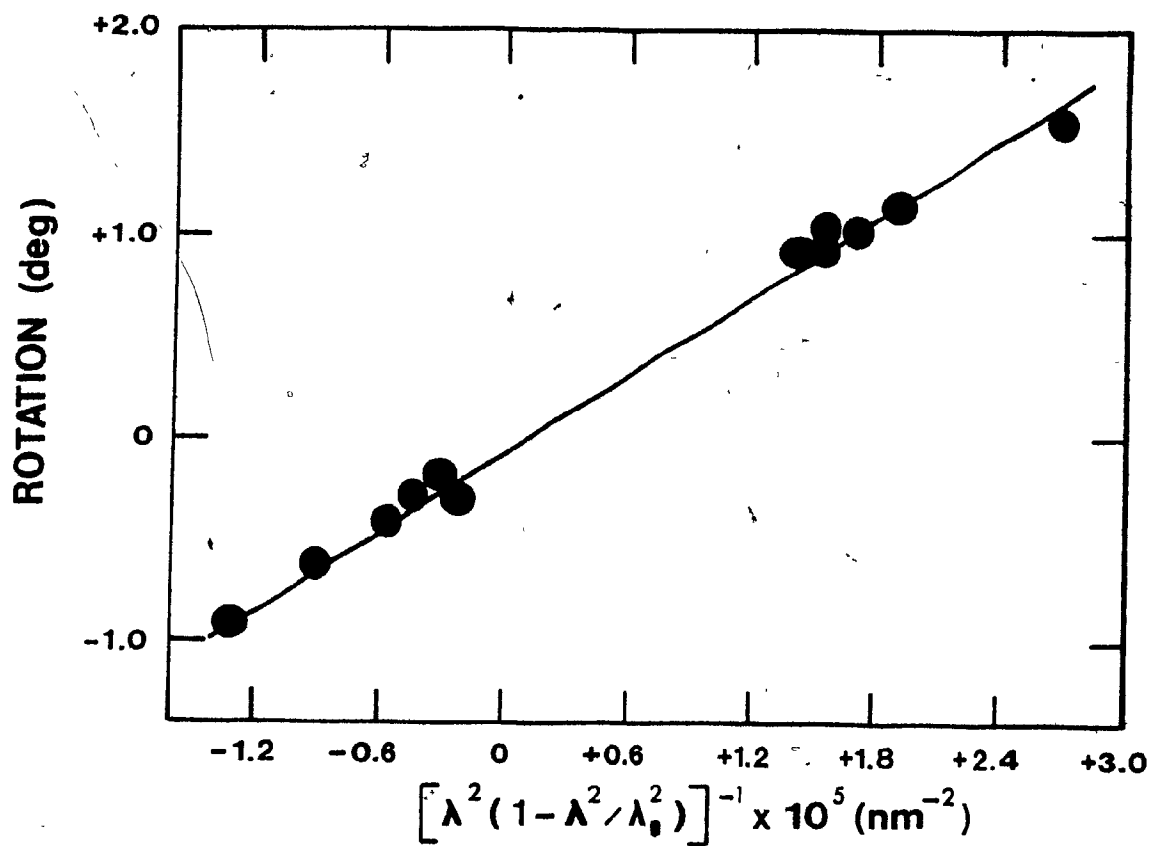


FIGURE IV.14 The change in optical activity as a function of wavelength for an aqueous HPC-J solution: Δn was 0.0075, n was 1.431, λ_0 was 524 nm, and the sample thickness was 69 μm .

respectively. The layer birefringence data have been listed in Table IV.1. De Vries' theory requires the layer birefringence to be constant for a particular solution concentration and to be independent of wavelength. Equation IV.9 was rearranged in the following form

$$\Delta n^2 = - \frac{4\lambda^2 n \theta [1 - (\lambda/\lambda_0)^2]}{\pi \lambda_0} \quad \text{IV.9}$$

and solved for a layer birefringence value at each individual wavelength. Figure IV.15 shows the variation in layer birefringence with wavelength for a typical aqueous HPC solution. Although there is some scatter in the data, it would appear that the layer birefringence slowly increases as the wavelength is decreased. This trend follows that reported for liquid crystalline films of methoxybenzylidene butylaniline (36). The variation in layer birefringence with wavelength may partially account for the irregularities reported in Table IV.1 where the layer birefringence should increase with increasing HPC volume fraction.

As mentioned previously, lyotropic HPC solutions exhibited two refractive indices both of which could be measured if a polarizer was inserted at the eyepiece of the Abbé refractometer. The difference in refractive indices or measured birefringence values have been listed in Table IV.2. Examination of this data shows that the measured birefringence increases with increasing volume fraction of HPC in methanol and acetic acid. This same trend is also evident in aqueous HPC solutions but there

TABLE IV.1

Layer Birefringence Values Calculated by Fitting De Vries'
Rotatory Power Equation to the Experimental ORD
Results for Aqueous HPC Solutions

HPC Volume Fraction (ϕ_2)	Layer Birefringence (Δn)
0.495	0.0074
0.498	0.0075
0.508	0.0076
0.520	0.0057
0.538	0.0088
0.549	0.0099
0.562	0.0099
0.573	0.0108
0.580	0.0115
0.589	0.0098
0.601	0.0188
0.611	0.0159
0.622	0.0122
0.633	0.0160

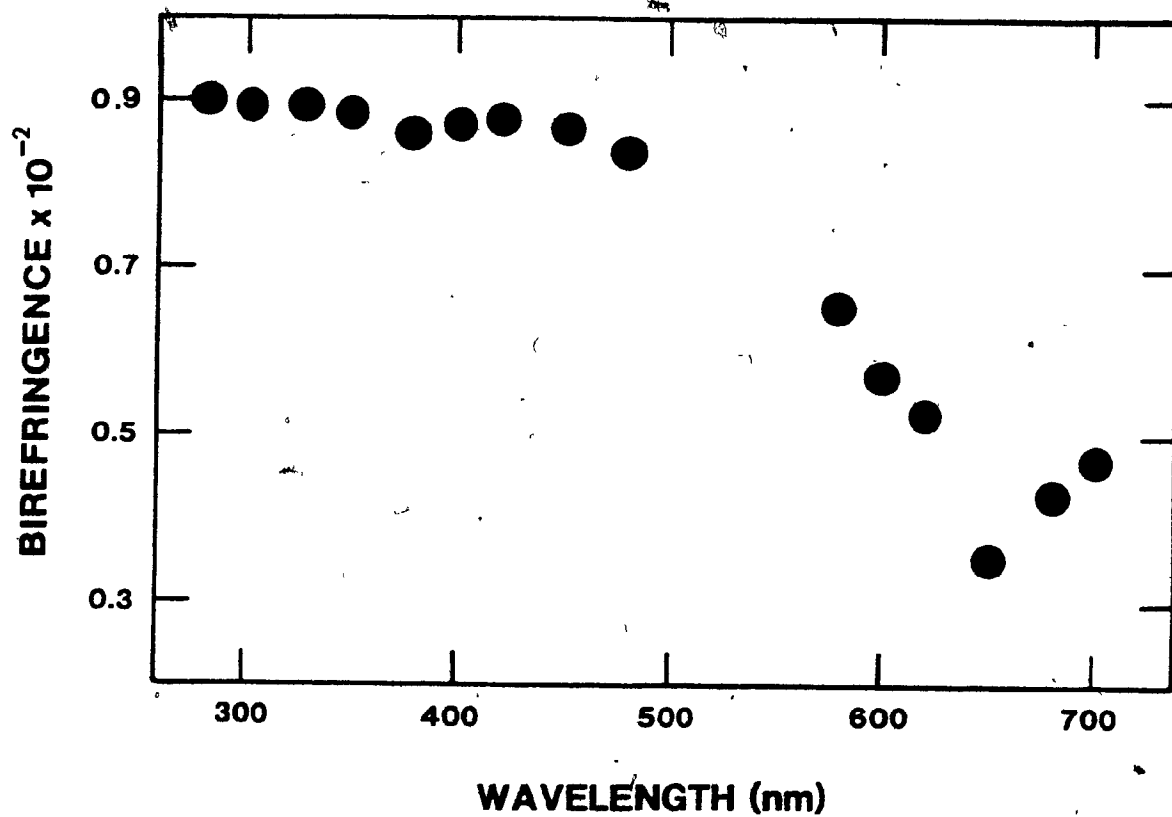


FIGURE IV.15 The variation in birefringence with wavelength for an aqueous HPC-L solution. Birefringence values at each wavelength were obtained by fitting the experimental ORD data to Equation IV.9 which was then solved for the birefringence.

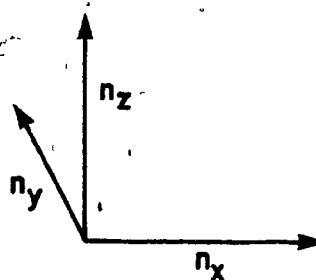
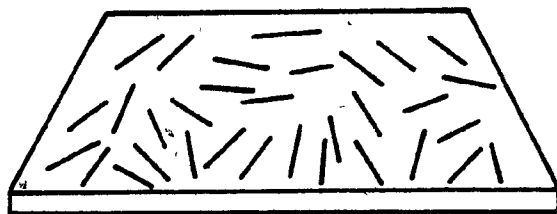
TABLE IV.2

Birefringence Values Measured for HPC Solutions
with the Abbé Refractometer

HPC Volume Fraction (ϕ_2)	Solvent	Birefringence (Δn)
0.330	CH ₃ OH	0.0022
0.370		0.0026
0.433		0.0042
0.516		0.0048
0.554	CH ₃ COOH	0.0065
0.353		0.0040
0.480		0.0043
0.538		0.0063
0.393	H ₂ O	0.0020
0.415		0.0035
0.437		0.0046
0.439		0.0058
0.455		0.0044
0.469		0.0045
0.486		0.0046
0.490		0.0037
0.518		0.0049
0.544		0.0038
0.546		0.0048
0.562	0.0041	
0.595	0.0049	
0.598	0.0078	
0.616	0.0056	
0.632	0.0055	

is considerably more scatter in the birefringence data than in organic solvents. Birefringences measured for elongated water-cast HPC films are reported to vary from 0.002 to 0.009 depending upon the elongation of the HPC films (37). These birefringence values are the same order of magnitude as the birefringences measured for aqueous HPC solutions. In water the measured birefringences ranged from 0.002 to 0.006 over the HPC volume fraction range of 0.40 to 0.63 respectively. These measured birefringence values are approximately half of those calculated from the ORD data and Equation IV.9. Figure IV.16 illustrates schematically one way in which the discrepancy in measured and calculated birefringence can be accounted for. The cholesteric planar structure illustrated in the upper half of Figure IV.16 can be visualized as being viewed along the z-axis of the Abbé refractometer. The molecules depicted in Figure IV.16 are those within the plane of the Abbé refractometer plate (xy plane). When viewing a sample of the helicoidal cholesteric material along the z-axis, the molecules in the xy plane have an equal probability of being aligned in all directions and thus the molecules appear to have a random distribution. Assume that the polymer molecules can be represented as cylinders. In this case, the molecules have only two different refractive indices — one in the axial (n_a) and one in the radial (n_r) direction. The birefringence measured with the Abbé refractometer is given as $n_x - n_z$ or the difference in refractive indices across and perpendicular to the prism surfaces of the Abbé refractometer. Using the polymer molecule axis system defined above, the refractive indices depicted in the upper half of Figure IV.16 have the following values: $n_x = n_y = \frac{n_a + n_r}{2}$ and $n_z = n_r$. Substituting these

MEASURED BIREFRINGENCE : $n_x - n_z$



CHOLESTERIC "LAYER" BIREFRINGENCE : $n_x - n_y$

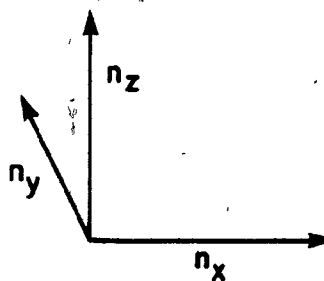
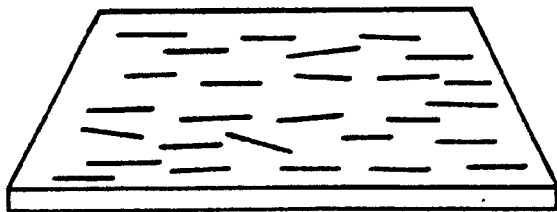


FIGURE IV.16 Schematic view of the model invoked to account for the difference in birefringence measured with the Abbé refractometer (upper) and the layer birefringence as required by De Vries' rotatory power theory (lower). See text for a more detailed explanation of the model.

results into the above expression for measured birefringence it can be seen that

$$\begin{aligned} n_x - n_z &= \frac{n_a + n_r}{2} - n_r \\ &= \frac{n_a - n_r}{2} \quad \times \end{aligned} \quad \text{IV.10}$$

is the birefringence measured with the Abbé refractometer.

The lower half of Figure IV.16 illustrates the layer birefringence as defined by De Vries in his theory for cholesteric materials. Clearly the helicoidal structure has been untwisted and now all the molecules within the xy plane point in the same direction. As illustrated the layer birefringence is again the difference in refractive indices across and perpendicular to the Abbé prism surfaces or $n_x - n_z$. Employing the polymer molecule axes defined in the previous paragraph, it can be shown that the second molecular arrangement in figure IV.16, when viewed in the Abbé refractometer, should give a birefringence of

$$n_x - n_z = n_a - n_r \quad \text{IV.11}$$

According to this simple model, the birefringence for the untwisted cholesteric layers should be double that for the twisted cholesteric

structure as determined in Equation IV.10. This explains the difference in birefringence values reported for the HPC solutions in Tables IV.1 and IV.2. Specifically, the birefringences measured in the Abbé refractometer were on the natural helicoidal cholesteric material. The layer birefringences calculated by fitting Equation IV.9 to the ORD data were birefringences for the untwisted cholesteric material as defined by De Vries. Comparison of the data in Tables IV.1 and IV.2 shows that for a particular HPC volume fraction the measured birefringence (Table IV.2) is half the calculated layer birefringence (Table IV.1). These results would seem to confirm the correctness of the models proposed to account for the birefringence of the twisted and untwisted cholesteric structures and also provide an independent method for evaluating the layer birefringence.

IV.3.3 CHOLESTERIC COLORS AND SHORT PITCH SAMPLES

Both spectrophotometric and ORD data prove that the reflection wavelength at normal incidence changes with concentration for lyotropic HPC solutions. This is illustrated for several aqueous HPC samples in Figures IV.17 and IV.18. This effect was also confirmed visually in that the cholesteric iridescent color of the samples varied with the HPC concentration as is depicted in Figure IV.19 and as is summarized in Table IV.3. These same samples in the light microscope exhibited a birefringent planar texture as shown in Figure IV.20. The helicoidal pitch, as defined in Figure IV.1, is a fundamental parameter of the cholesteric mesophase. For this reason, the variation in pitch with solution concentration is of more

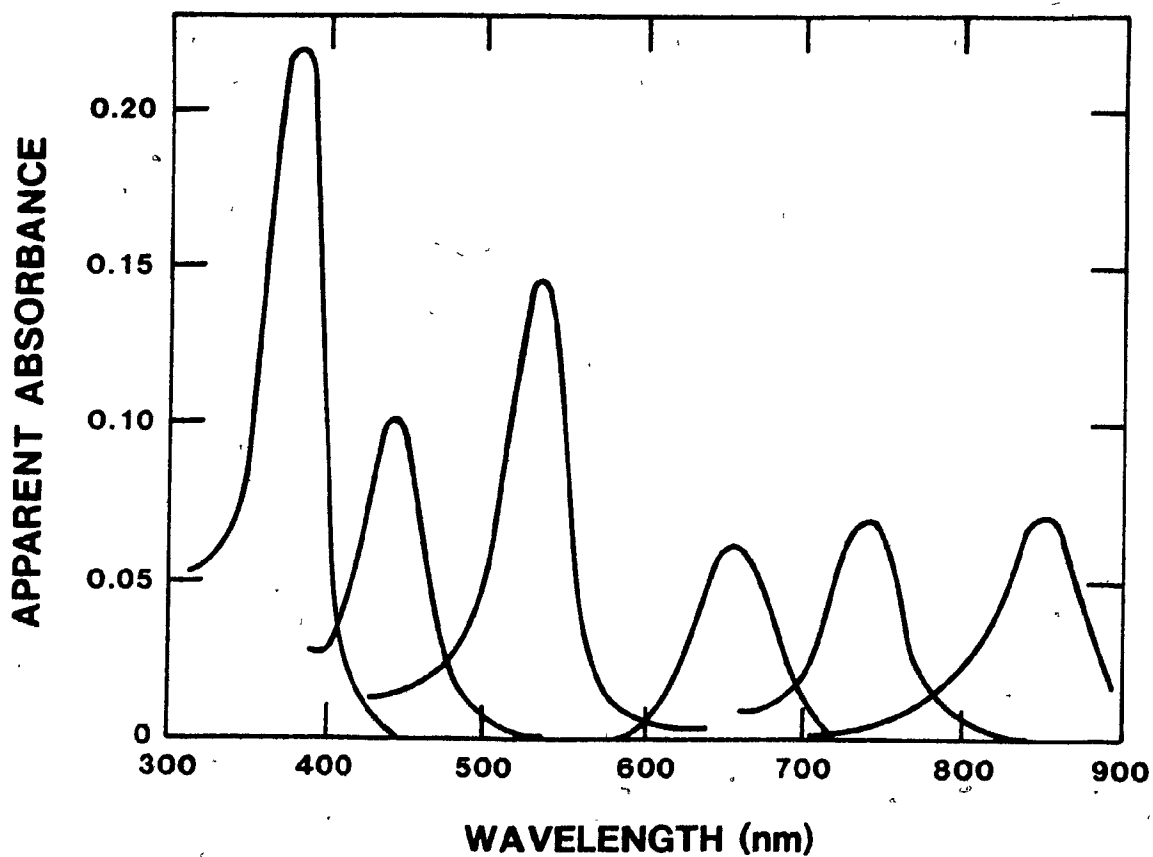


FIGURE IV.17 Spectrophotometric data illustrating the change in reflection wavelength maxima with the HPC-E and L concentration in water. From right to left — $\phi_2 = 0.488$, $\phi_2 = 0.494$, $\phi_2 = 0.517$, $\phi_2 = 0.545$, $\phi_2 = 0.584$, and $\phi_2 = 0.611$.

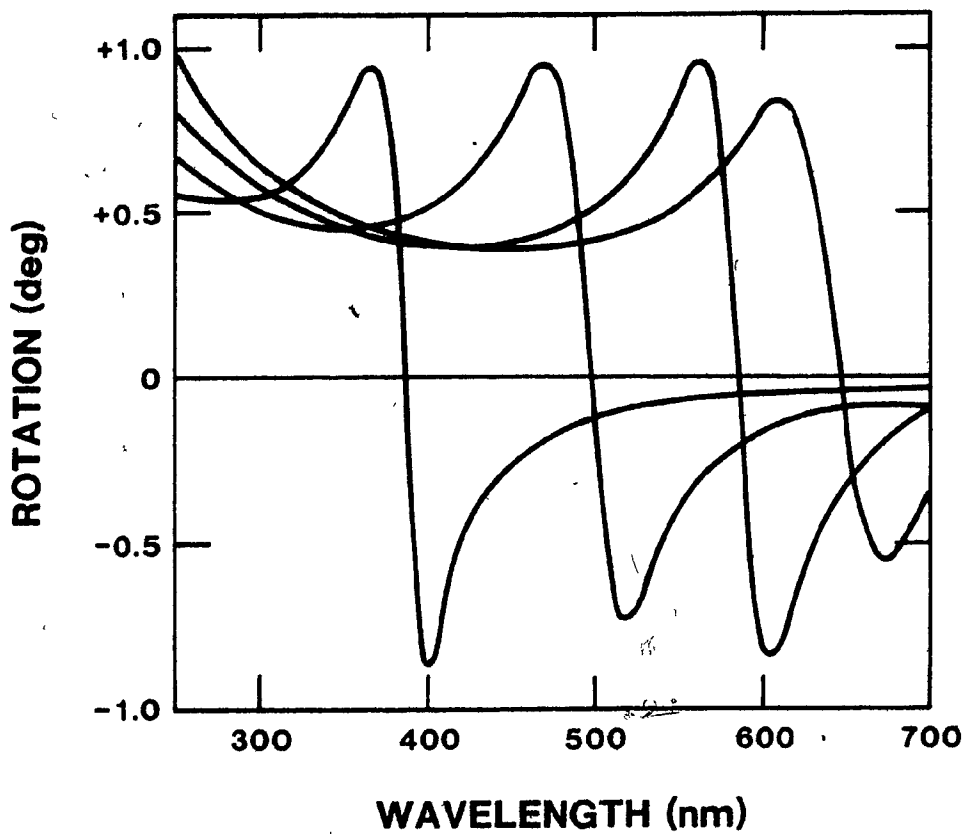


FIGURE IV.18 Variation in reflection wavelength from ORD spectra with HPC-E and L concentration in aqueous solution. From right to left — $\phi_2 = 0.540$, $\phi_2 = 0.562$, $\phi_2 = 0.573$, and $\phi_2 = 0.630$.

COLOURED PICTURES
Images en couleur



FIGURE IV.19 Three typical examples of the lovely cholesteric iridescent color exhibited by short pitch (375 - 700 nm) aqueous HPC solutions.

TABLE IV.3

Hydroxypropylcellulose Weight Fraction in Water Needed to
Produce a Particular Cholesteric Iridescence

Iridescent Color	HPC Weight Fraction (ω_2)
Red	0.55 - 0.59
Green	0.60 - 0.63
Blue	0.64 - 0.68
Violet	0.69 - 0.72

COLOURED PICTURES
Images en couleur



FIGURE IV.20 Planar texture exhibited by a 0.50 weight fraction HPC-L aqueous solution when examined in the light microscope without crossed polars.

interest than the variation in reflection wavelength with concentration. Using the refractive index data of Figures IV.9 and IV.10, the helicoidal pitch for the HPC solutions was determined from Equation IV.1.

$$P = \lambda_0/n \quad \text{IV.1}$$

The helicoidal pitches, thus calculated, were found to vary inversely with the third power of the polymer weight or volume fraction. This same relationship between pitch and volume fraction has previously been reported for aqueous (25,38) and organic (38) HPC solutions. However in both published reports only one technique, either spectrophotometric (25) or ORD (38), was used in the evaluation of the pitch values. In this work both of the aforementioned techniques were used to calculate the helicoidal pitch for three different types of HPC samples in aqueous solution and these results are illustrated in Figure IV.21. Although there is considerable scatter in the experimental points when both ORD and spectrophotometric data for the three HPC types are plotted on the same graph, the reported relationship between pitch and the HPC weight or volume fraction is found to be valid as is shown more clearly in Figures IV.22 through IV.25. Figures IV.22 and IV.23 show the variation in pitch values determined from ORD and spectrophotometric data respectively with HPC-L volume fraction. Identical plots have been made for aqueous HPC-E solutions and these are presented in Figures IV.24 and IV.25. Comparison of Figures IV.22, IV.23, IV.24, and IV.25 illustrates four interesting points. Firstly, there is more scatter in the pitch values calculated from the ORD data than from the

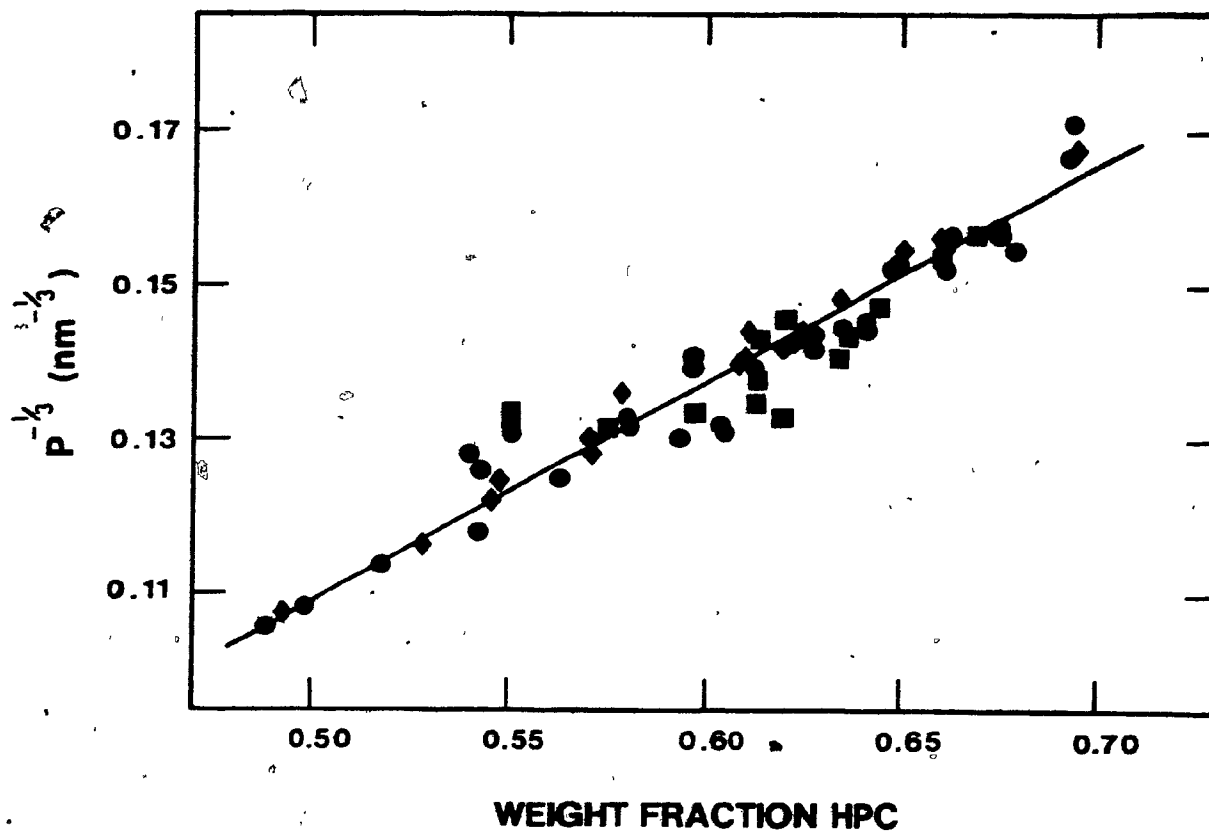


FIGURE IV.21 The variation in helicoidal pitch (P) with HPC-E (◆), L (●), and J (■) weight fraction in aqueous solution. The pitch values were obtained from both ORD and spectrophotometric data.

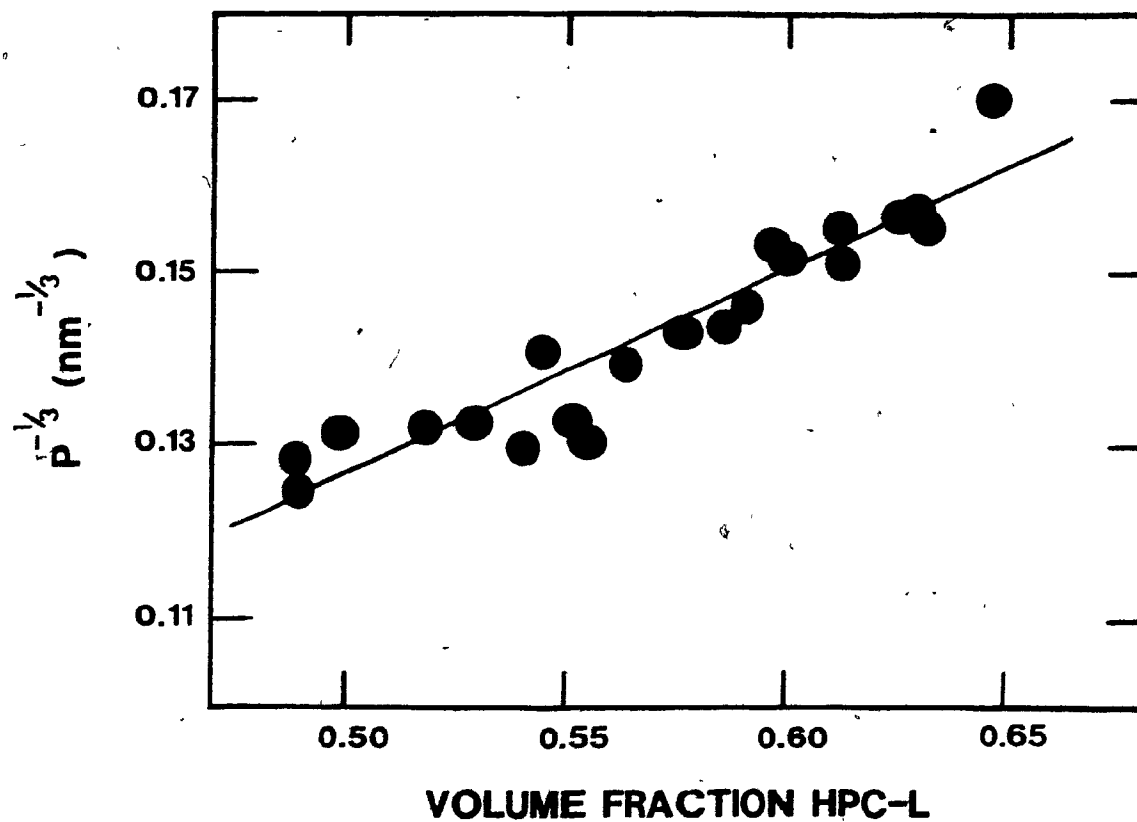


FIGURE IV.22 Variation in helicoidal pitch (P) with HPC-L volume fraction in aqueous solution. The pitch values were obtained only from ORD data.

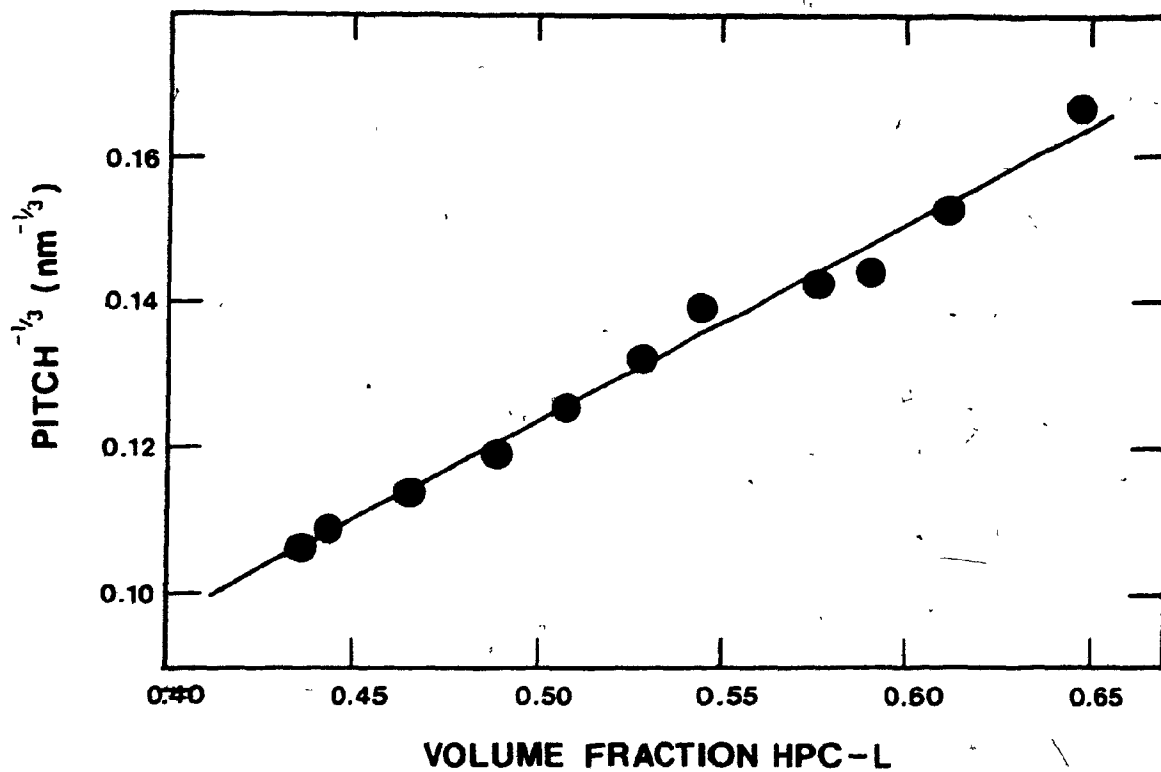


FIGURE IV.23 Variation in helicoidal pitch (P) with HPC-L volume fraction in aqueous solution. Only spectrophotometric data was used in evaluating the helicoidal pitch.

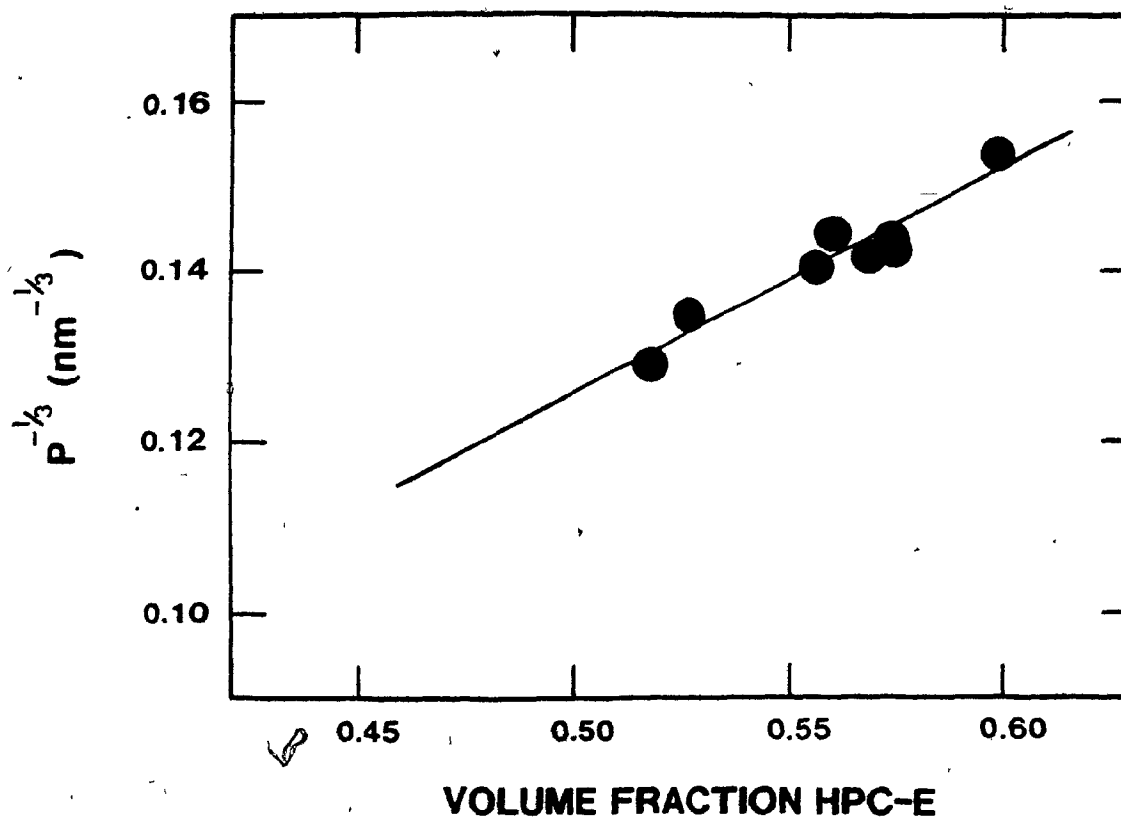


FIGURE IV.24 Variation in the helicoidal pitch (P) calculated from ORD data with the HPC-E volume fraction in aqueous solution.

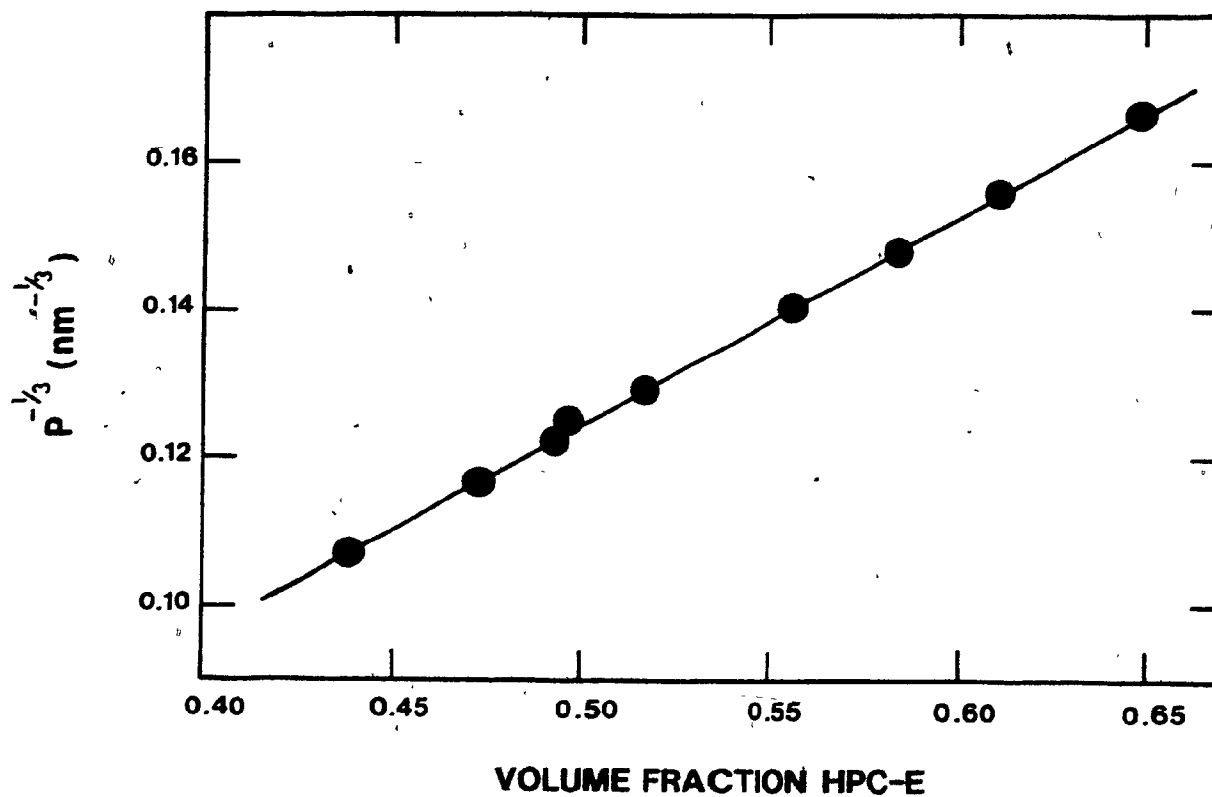


FIGURE IV.25 Variation in the helicoidal pitch (P) calculated from spectrophotometric data with the HPC-E volume fraction in aqueous solution.

spectrophotometric data. A possible reason for this behavior will be elaborated on in the next paragraph. Secondly, the slopes of Figures IV.22 and IV.23 and Figures IV.24 and IV.25 are very similar in spite of the scatter in the ORD calculated values. This was taken as confirmation that both the ORD inflection wavelength and the spectrophotometric reflection maximum are measuring the same phenomenon — the selective reflection of light from a series of equally spaced birefringent layers stacked one atop another. Thirdly, the slopes of Figures IV.23 and IV.25 are very similar but not exactly identical indicating, perhaps, that molar mass has a very slight effect on the helicoidal pitch. Empirically for aqueous HPC-L solutions the relationship between helicoidal pitch (P) and the HPC volume fraction (ϕ_2) can be expressed as

$$P^{-1/3} = 0.271\phi_2 - 0.0123 \quad \text{IV.12}$$

while for aqueous HPC-E solutions the corresponding expression is

$$P^{-1/3} = 0.282\phi_2 - 0.0163 \quad \text{IV.13}$$

Fourthly, the excellent correlation coefficients of 0.993 and 0.999 for Figures IV.23 and IV.25 respectively would seem to confirm the validity of the postulated relationship between helicoidal pitch and HPC volume fraction. The above result is in contrast to polypeptide lyomesophases where the helicoidal pitch has been found to vary inversely as the square of the polymer concentration in g/100 mL (5-6). It may be argued that over

the rather narrow volume fraction and pitch ranges investigated any functional relationship ($P^{-1/2}$ vs ϕ_2 , $P^{1/2}$ vs ϕ_2 , $P^{1/3}$ vs ϕ_2 , P^{-2} vs ϕ_2 , etc) between P and ϕ_2 will be approximately linear. This is in fact true as is shown in Figure IV.26 where the data of Figure IV.25 have been replotted in the form of $P^{-1/2}$ versus ϕ_2 and the correlation coefficient for this plot is 0.998. Based solely on correlation coefficient values, the best data fit is obtained with the inverse third power relationship between P and ϕ_2 . Data to be presented in the next section covers a much broader pitch and concentration range in a different solvent and it strongly supports the chosen inverse third power relationship between the helicoidal pitch and the HPC volume fraction.

As previously mentioned the wavelength of light normally reflected by a cholesteric structure is given by Equation IV.1. However if the incident light strikes the helicoidal structure at an angle other than 90° then the wavelength of light reflected by the cholesteric depends upon the angle of incidence as indicated by Equation IV.6. By equipping a Pye Unicam spectrophotometer with a variable angle specular reflectance accessory it was possible to measure a reflectance wavelength at several different angles of incidence for the HPC samples. These results are depicted as closed circles in Figures IV.27 and IV.28 for two typical HPC solutions. The solid lines in these Figures represent the theoretical change in reflection wavelength with angle of incidence as calculated using Equation IV.6. The excellent agreement between the experimental and theoretical values for the reflection wavelength, once again, confirms the

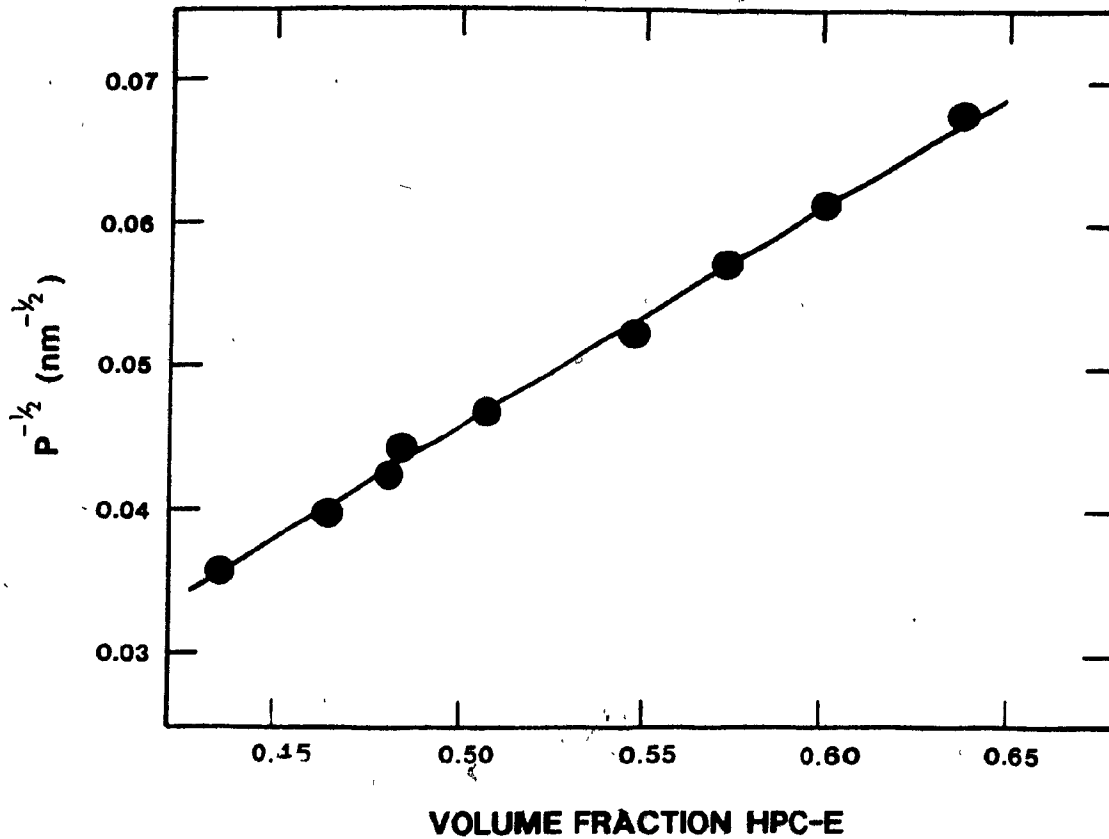


FIGURE IV.26 The variation in helicoidal pitch (P) with HPC-E volume fraction in aqueous solution. The above data are the same as those in Figure IV.25 but a different functional relationship between P and the HPC volume fraction has been plotted. See text for more details.

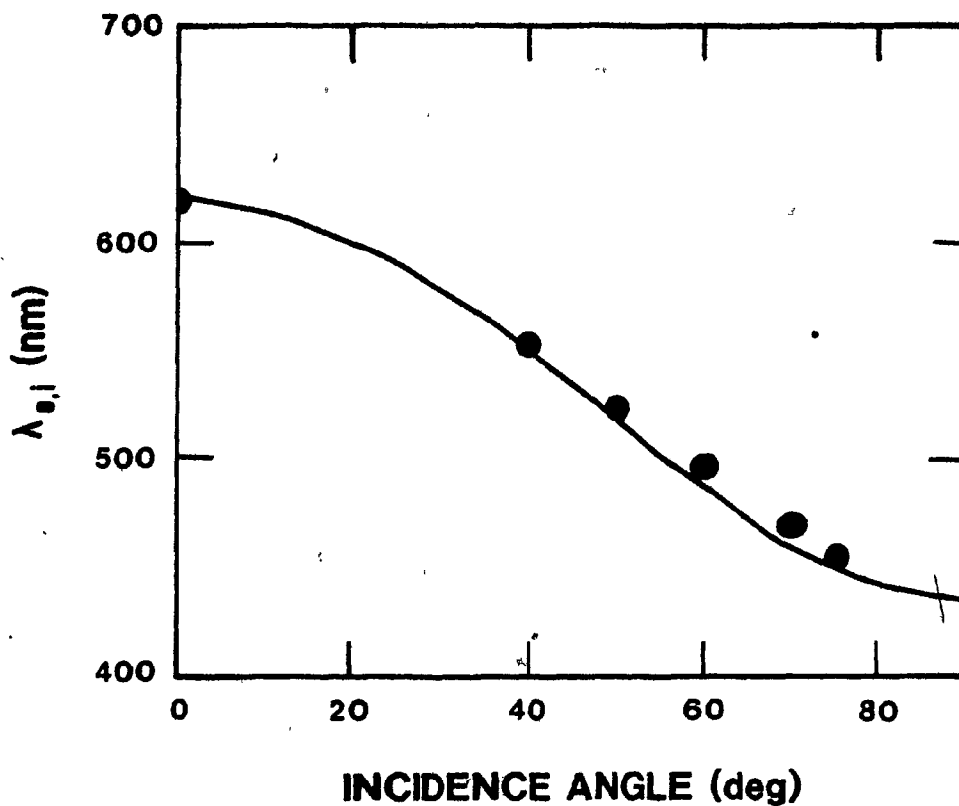


FIGURE IV.27 The variation in reflection wavelength ($\lambda_{o,i}$) with incident light angle (ϕ_i). The solid line is the theoretically predicted variation in $\lambda_{o,i}$ with ϕ_i calculated using Equation IV.6 and the following data: $n = 1.425$, $p = 434$ nm, and $\phi_i = \phi_r$. The closed circles represent experimental reflection wavelengths obtained for a 0.58 HPC-L weight fraction aqueous solution at various incident light angles.

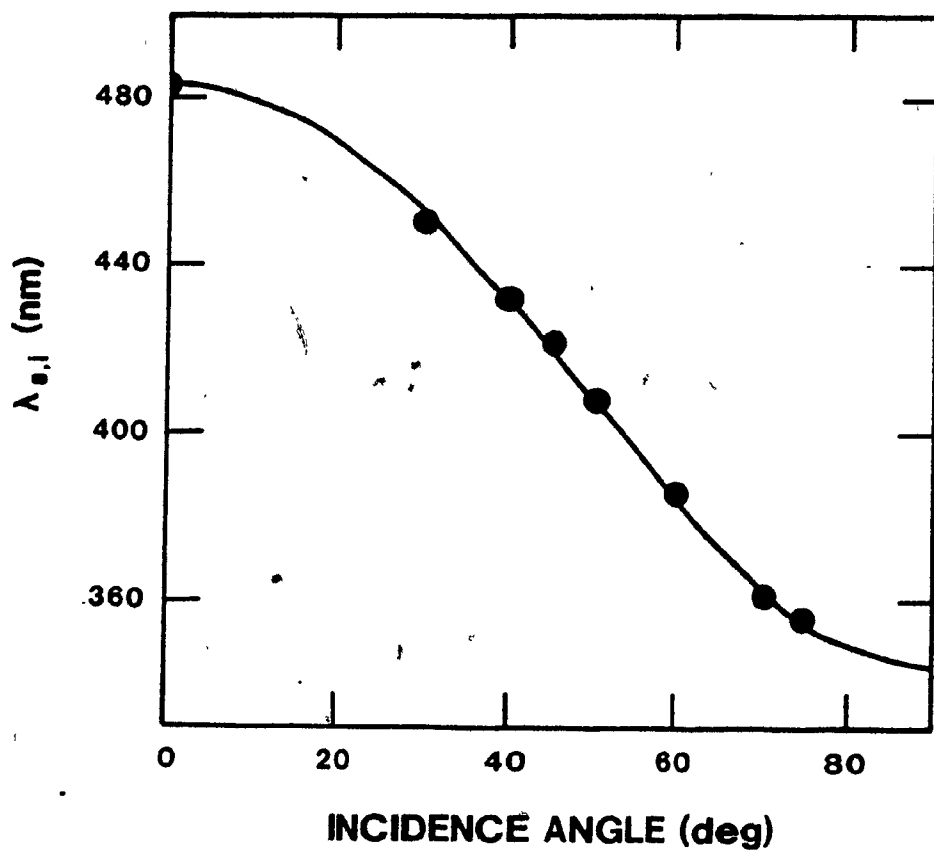


FIGURE IV.28 The variation in reflection wavelength ($\lambda_{o,i}$) with incident light angle (ϕ_i) for a 0.64 weight fraction HPC-L solution in water. The closed circles are experimentally determined reflection wavelengths at various incident light angles. The solid line is the theoretically predicted variation in $\lambda_{o,i}$ with ϕ_i calculated using Equation IV.6 and the following data: $n = 1.436$, $P = 336$, and $\phi_i = \phi_r$.

cholesteric character of the HPC solutions. The thin Hellma cell was difficult to position exactly perpendicular to the ORD incident light beam. Any misalignment of the cell would result in a shift of λ_0 for the sample to lower wavelengths as predicted by Equation IV.6. This may explain the slightly higher and more scattered values calculated for the helicoidal pitch from ORD data than from spectrophotometric data.

IV.3.4 SHIMMERING COLORS AND LONG PITCH SAMPLES

Hydroxypropylcellulose solutions in organic media, notably acetic acid, exhibited distinct periodicity lines when examined in the light microscope. An example of these lines is shown in Figure IV.29 for a typical fingerprint textured sample of HPC. The observed periodicity lines correspond to one-half of the helicoidal pitch and are a reflection of a layer-like structure which repeats itself every one to three microns depending on the solution concentration. As reported by Uematsu and Uematsu (39) for polypeptides it was found that a thick sample of polymer in a dished microscope slide (0.8-mm deep) was required to produce distinct and highly visible periodicity lines. A thin sample of the same HPC solution on a flat microscope slide exhibited no periodicity lines. Figure IV.30 illustrates one way in which this "now you see them now you don't" effect of the periodicity lines can be explained. The depth of a dished microscope slide can easily accommodate the depicted orientations in which some layers have their helicoidal axes parallel to the cover glass surface and the helicoidal layers appear as discrete equally spaced lines

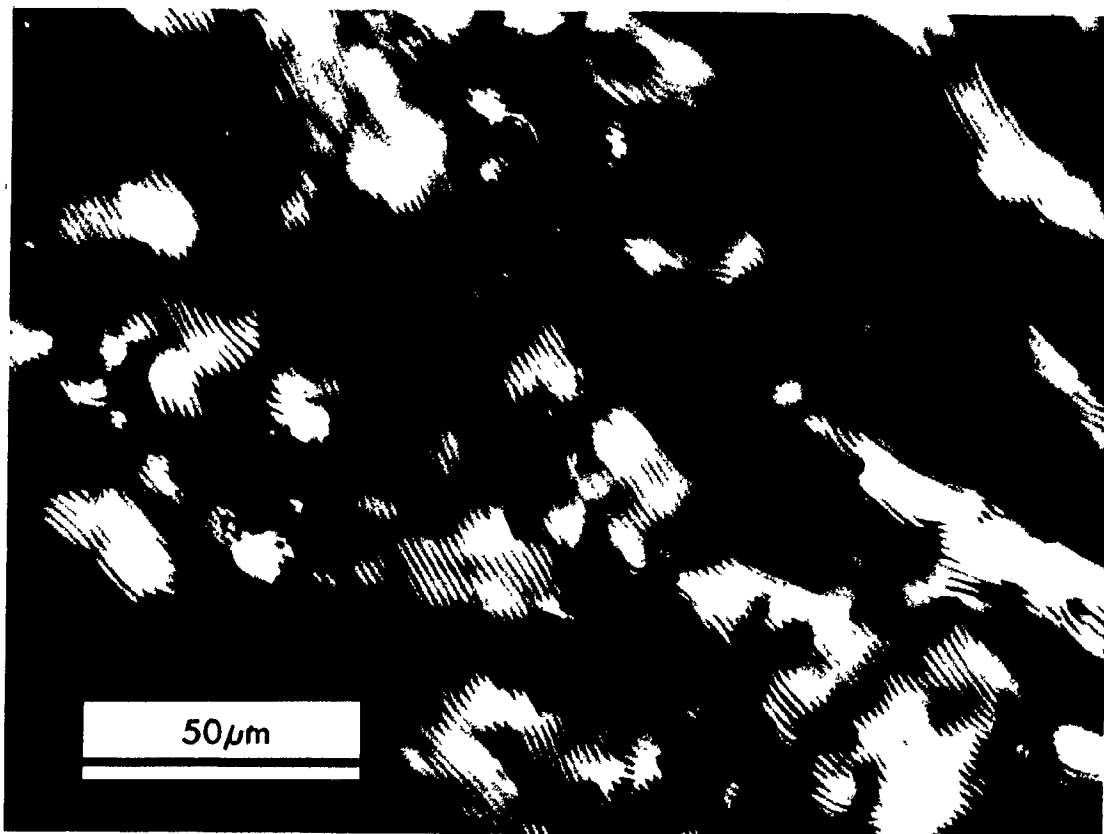


FIGURE IV.29 Typical periodicity or fingerprint lines visible in the light microscope on examination of an organic HPC solution with large pitch. The sample was 42.9% HPC-L by weight in acetic acid. The periodicity spacing is 1310 nm and therefore the sample pitch is 2620 nm.



Dished Slide



Flat Slide

FIGURE IV.30 A schematic view of the probable helicoidal orientation of HPO in a dished and a flat microscope slide.

when viewed from above. On a flat microscope slide the helicoidal axis is essentially always perpendicular to the cover glass surface and no lines are visible.

As noted earlier the fingerprint spacing was found to vary with the HPC concentration. Specifically as the HPC concentration increased, the spacing between the periodicity lines decreased, until ultimately they could no longer be distinguished in the light microscope. The open circles in Figure IV.31 show how the helicoidal pitch (or double the periodicity spacing) varied with the solution concentration as measured in the light microscope. The resulting straight line has an empirical equation given by

$$p^{-1/3} = 0.119\phi_2 + 0.0239 \quad \text{IV.14}$$

This inverse third power relationship between pitch and HPC volume fraction is identical to that found for short pitch HPC samples. The helicoidal pitch for fingerprint textured samples was also measured using a laser light diffraction technique. Normal illumination of a long pitch HPC sample with a He-Ne laser produced one relatively sharp diffraction ring as illustrated in Figure IV.32. Illumination of this same sample with white light produced a series of concentric colored rings as depicted in Figure IV.33. By the use of Equation IV.8 for the scattering of light from a diffraction grating, it was possible to calculate the periodic spacing responsible for the diffraction ring illustrated in Figure IV.32. This was done for several

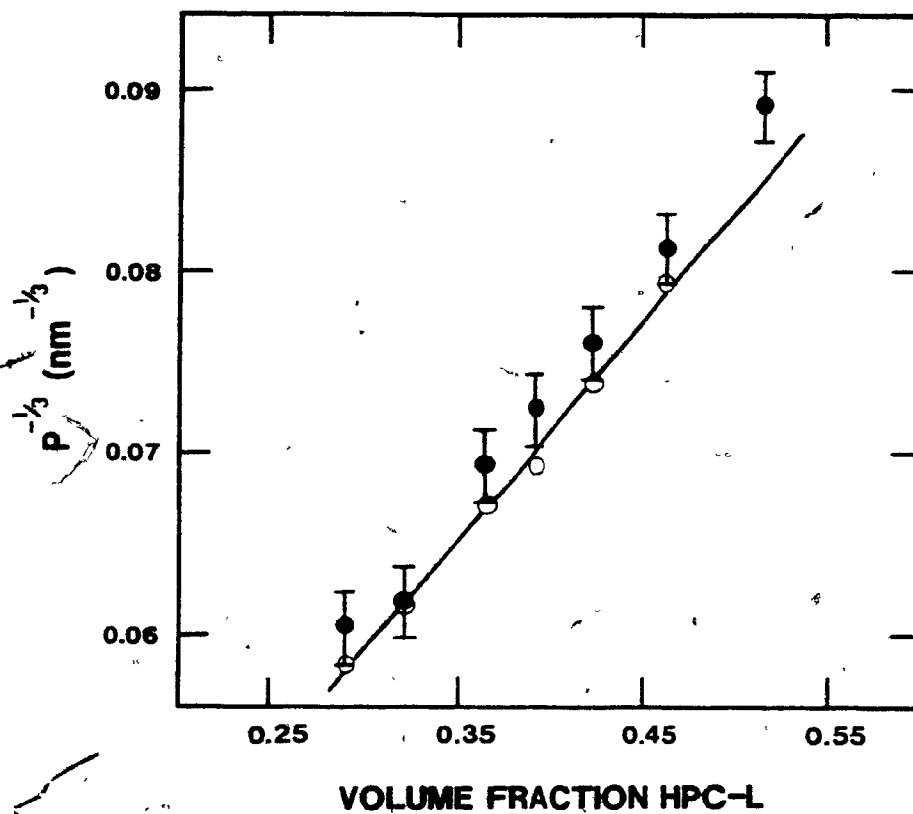


FIGURE IV.31 Variation in helicoidal pitch (P) with HPC-L volume fraction in acetic acid solutions exhibiting fingerprint textures under the crossed polars of a light microscope. The open circles represent the pitch values obtained by direct measurement of the sample periodicity lines visible in the light microscope. The closed circles superimposed on bars represent the sample pitch values calculated from laser diffraction patterns. See text for more details.

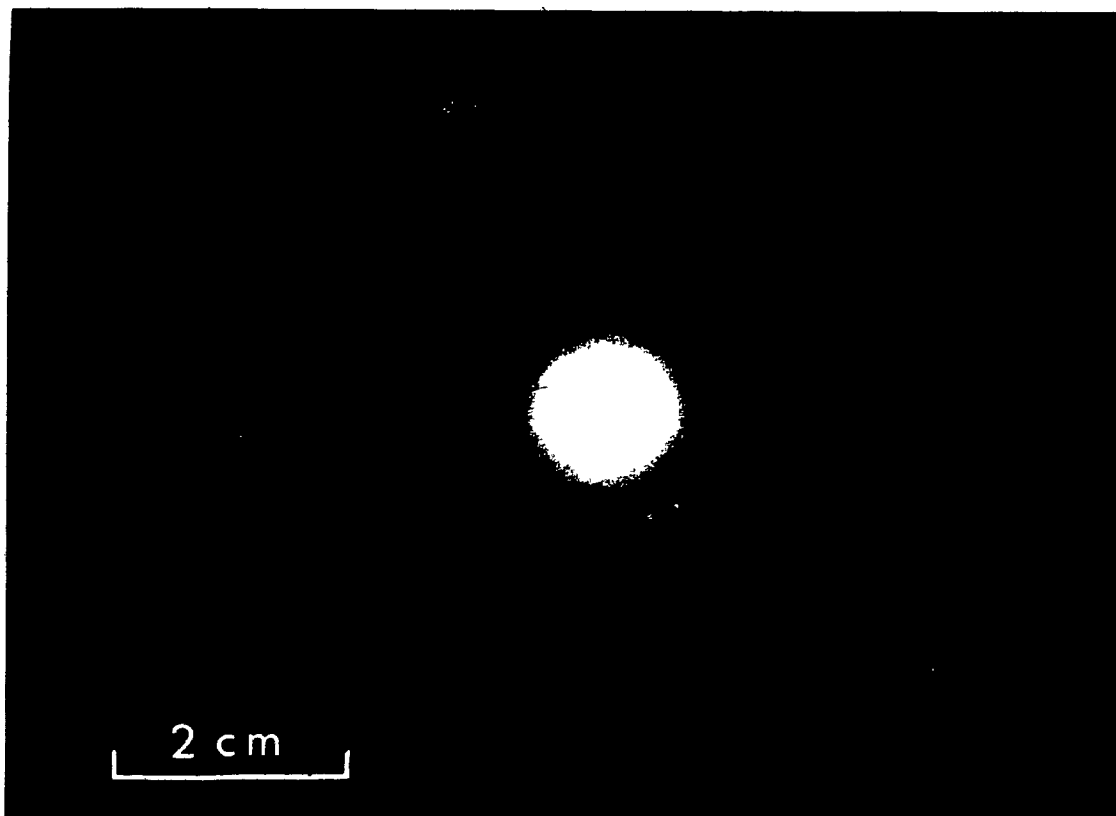


FIGURE IV.32 Print illustrating the light diffraction pattern obtained for a 0.39 weight fraction HPC-acetic acid solution by using a He-Ne laser as the light source. The sample-to-film distance was 6.6 cm.

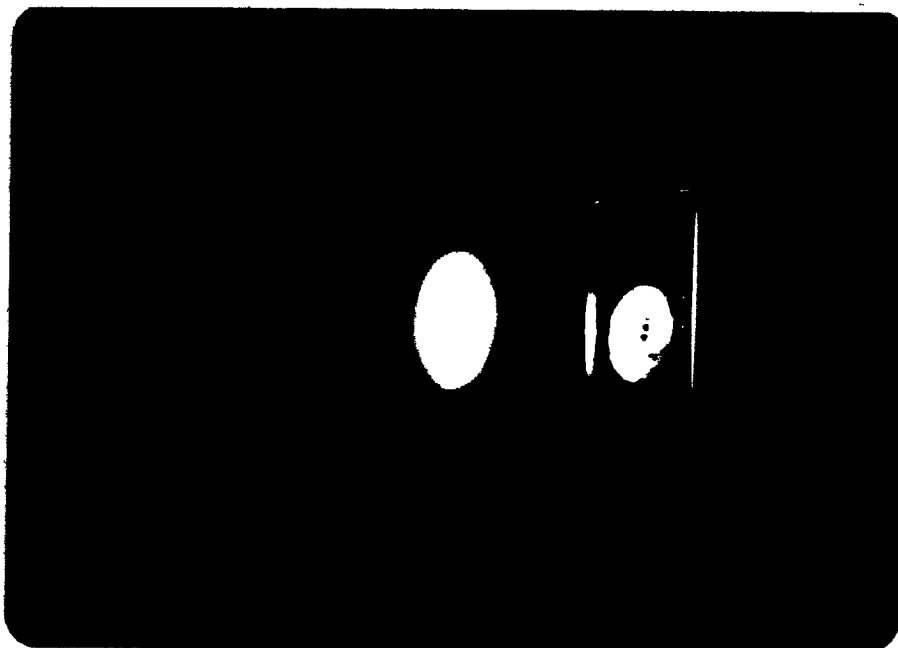


FIGURE IV.33 Illustration of the rainbow-like diffraction pattern obtained for a HPC-L acetic acid solution which is illuminated by white light.

different HPC solution concentrations and the pitch values obtained are plotted as closed circles with error bars in Figure IV.31. The closed circles represent pitch values calculated assuming the diffraction ring midpoint defines the radius of the ring. The error bar limits represent pitch values calculated from the corresponding inner and outer radii of the diffraction ring. Intuitively one would expect the diffraction ring midpoints to give pitch values identical to those measured in the light microscope. This, however, was not the case since the data in Figure IV.31 clearly show that the pitch values calculated from the optical diffraction rings appear larger than those measured by optical microscopy. The reason for this systematic result is not known but its origin cannot be solely attributed to measurement errors. Identical pitch values for optical diffraction and microscope measurements on polypeptide solutions have recently been reported (40), but the authors included a refractive index term in their calculations that is inappropriate for this diffraction situation (27).

Fingerprint textured samples although having pitch values between 1000 and 6000 nm — well outside the visible region of the spectrum (300 to 700 nm) — nevertheless, exhibited lovely shimmering colors that have been attributed to the scattering of light from a structure resembling a liquid diffraction grating. These shimmering samples were found to change color dramatically as the sample viewing angle was varied. This is illustrated in Figure IV.34 where the same sample is viewed at three slightly different incident light angles. Unfortunately, unlike the smaller pitch samples, it

COLOURED PICTURES
Images en couleur

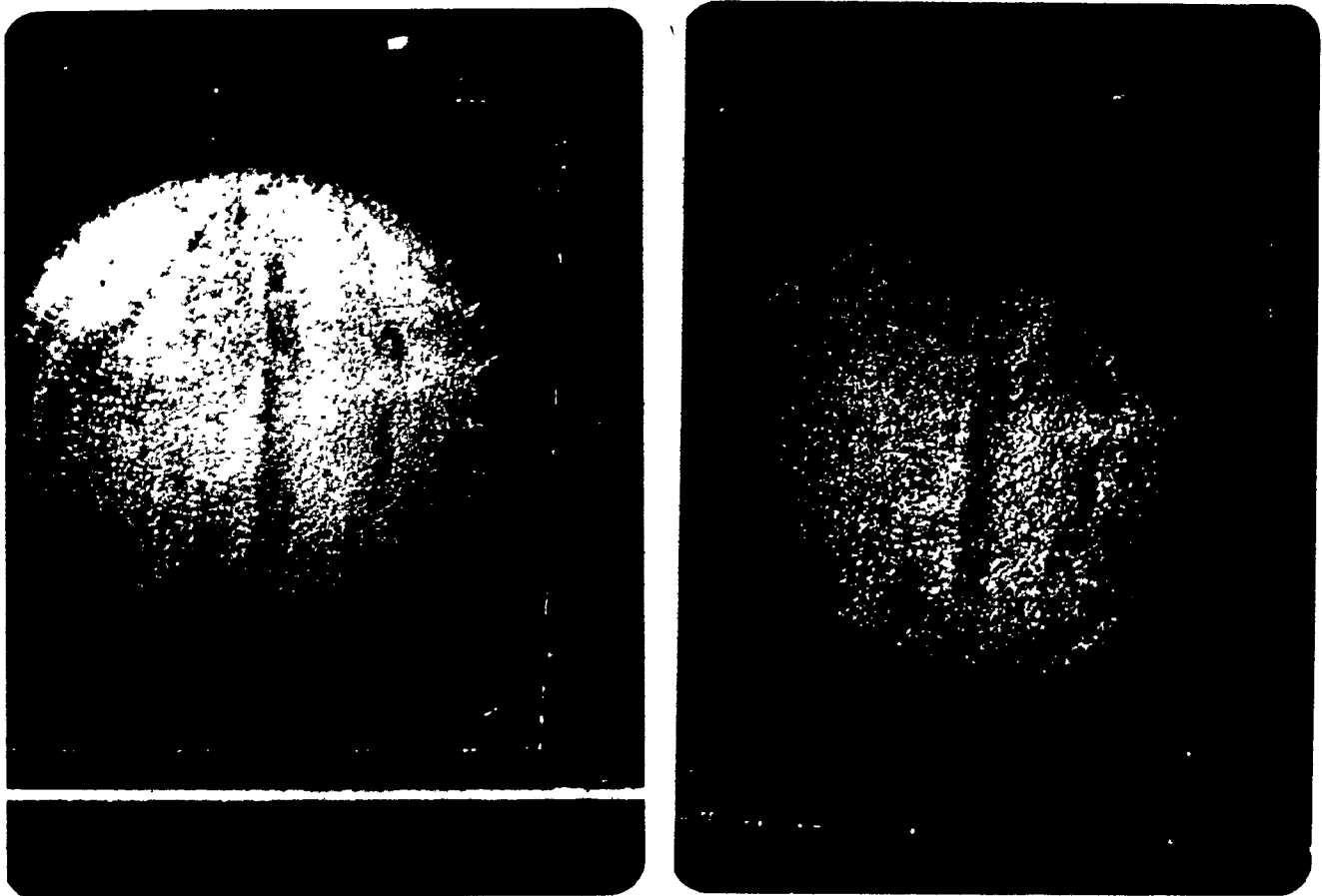


FIGURE IV.34 Shimmering iridescent colors exhibited by a HPC-L acetic acid solution viewed at three slightly different incident light angles (third photo on next page) to illustrate the dramatic effect of viewing angle on the reflection wavelength of the sample.

COLOURED PICTURES
Images en couleur



FIGURE IV.34 Third photo.

was not possible to obtain transmitted light intensities for these shimmering samples on the Pye Unicam spectrophotometer. It was thus impossible to test the validity of Equation IV.7 quantitatively on these samples. Qualitatively, however, the reflected wavelength for the long pitch fingerprint samples varied much more with the incidence angle than it did for the short pitch cholesteric samples.

IV.3.5 SHORT AND LONG PITCH SAMPLES IN METHANOL

Aqueous HPC solutions exhibited neither long pitch periodicity lines nor shimmering colors. Acetic acid HPC solutions exhibited short pitch cholesteric colors at a HPC volume fraction of approximately 0.65 to 0.79. However these solutions could not be used in the ORD spectrometer because they were very inhomogeneous and virtually glassy gels. Some effort was, therefore, expended in searching for a single solvent in which both long and short pitch liquid crystalline solutions of HPC might be obtained. Only in such a solvent could it be stated with confidence that the helicoidal pitch varied with the solution concentration in the same manner regardless of the system pitch range (long or short).

Hydroxypropylcellulose methanol solutions were found to exhibit short pitch cholesteric colors and planar textures over the HPC volume fraction of 0.45 to 0.66. Over the volume fraction range of 0.33 to 0.37 the samples exhibited long pitch shimmering colors and fingerprint textures. This system of HPC and methanol, therefore, seemed to be an ideal one in

which to verify the proposed inverse third power variation in helicoidal pitch with HPC volume fraction. The wide range of pitch values accessible in this system should eliminate any questions concerning the uniqueness of the relationship between P and ϕ_2 for HPC solutions. The pitch results for the HPC methanol solutions are presented in Figure IV.35. The large pitch values were obtained from both laser diffraction patterns and microscopic measurements, while the short pitch values were determined from both spectrophotometric and ORD data. Empirically it was found that in methanol

$$p^{-1/3} = 0.206\phi_2 + 0.00965 \quad \text{IV.15}$$

The exact physical significance of the different slope and intercept values for the pitch and volume fraction relationships in the three solvents investigated is unknown at present, but on comparison of Equations IV.12, IV.14, and IV.15 the interesting point arises that the lower the critical volume fraction for mesophase formation, the higher the slope and intercept values for the P versus ϕ_2 equation in that solvent. These results are summarized in Table IV.4.

IV.4 Conclusion

Dilute HPC solutions exhibited plain negative ORD spectra indicating that the individual HPC molecules are optically active. The good fit of this same data to a one term Drude equation indicates that

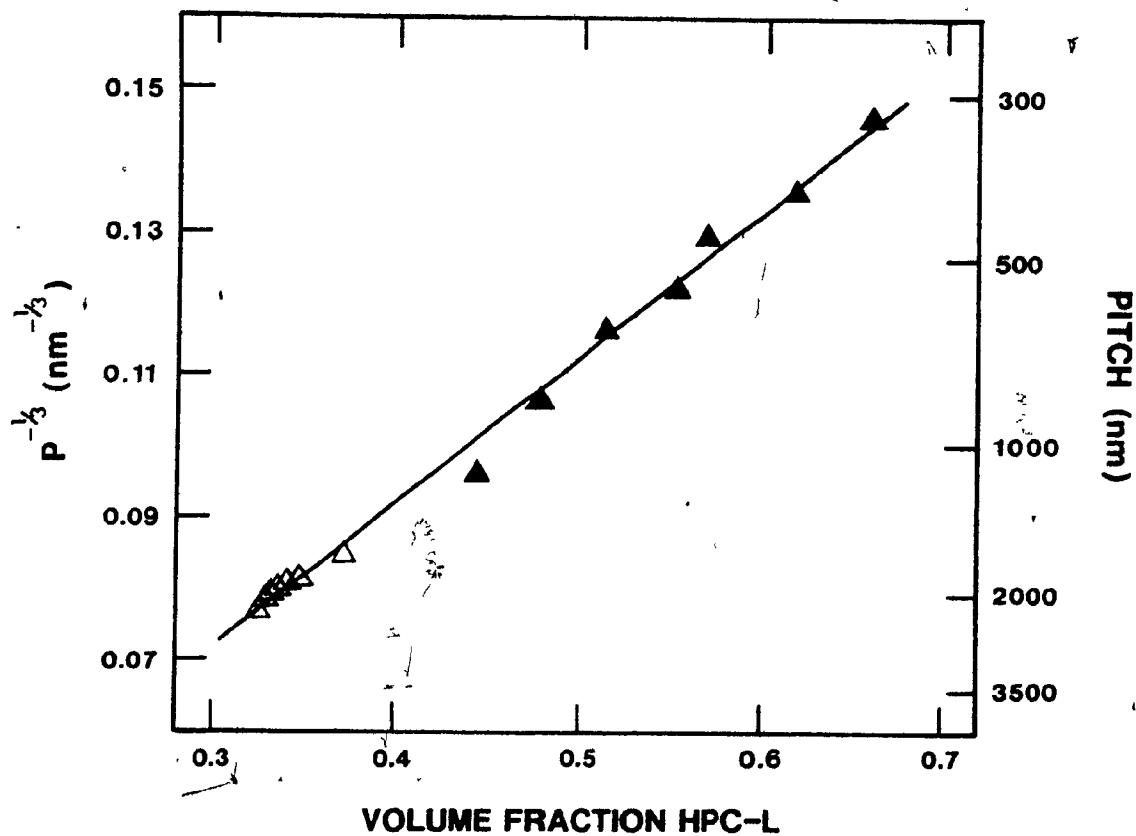


FIGURE IV.35 Variation in helicoidal pitch (P) with HPC-L volume fraction in methanol solution. The open triangles represent both laser diffraction and microscope results obtained for large pitch samples. The closed triangles represent ORD and spectrophotometric results obtained for short pitch samples.

TABLE IV.4

Slope and Intercept Values from Plots of Pitch Versus Volume
Fraction for HPC in Several Solvents

HPC Mesophase Volume Fraction (ϕ_c)	Solvent	Slope	Intercept
0.27	CH ₃ COOH	0.119	0.0239
0.33	CH ₃ OH	0.206	0.00965
0.37	H ₂ O	0.271	-0.0123

the HPC molecules are in a random rather than helical conformation in solution. Concentrated HPC solutions exhibited anomalous negative ORD spectra in which the optical activity of the samples was hundreds or thousands of degrees larger than that obtained for the dilute solutions. The only explanation for this behavior was that HPC forms a cholesteric lyomesophase in concentrated solutions. This was confirmed in that the optical data for HPC could be fitted very well to De Vries' theory of cholesterics by using only one fitting parameter — the layer birefringence.

The birefringence for anisotropic HPC solutions was measured with an Abbé refractometer. This measured birefringence was half of the calculated fitting layer birefringence obtained above. A model was proposed to explain the discrepancy between the measured and the calculated birefringence. In addition, the angular dependence of the reflection wavelength was investigated and it was found to agree with the theoretical predictions of Ferguson's equation for cholesteric systems (Equation IV.6).

An inverse third power relationship between the helicoidal pitch and the HPC volume fraction was found to exist in several solvents over a relatively large range of pitch values. Hydroxypropylcellulose was also found to display both cholesteric short pitch and shimmering long pitch iridescent colors in the same (methanol) and in different (water, acetic acid) solvents.

References

1. Hl. De Vries, Acta. Cryst., 4, 219-26 (1951).
2. W.A. Shurcliff and S.S. Ballard, "Polarized Light", Van Nostrand, Princeton, New Jersey, 1964, pp. 7-12.
3. A.C. Neville and S. Caveney, Biol. Rev., 44, 531-62 (1969).
4. C. Robinson, J.C. Ward, and R.B. Beevers, Discuss. Faraday Soc., 25, 29-42 (1958).
5. C. Robinson, Tetrahedron, 13, 219-34 (1961).
6. C. Robinson, Mol. Cryst., 1, 467-94 (1966).
7. D.B. DuPré and D.L. Patel, Polym. Prepr., Am. Chem. Soc., Div. Polym. Chem., 21 (2), 69 (1980).
8. D.L. Patel and D.B. DuPré, J. Chem. Phys., 72, 2515-24 (1980).
9. W.J.A. Goossens, Mol. Cryst. Liq. Cryst., 12, 237-44 (1971).
10. S. Chandrasekhar and J.S. Prasad, Mol. Cryst. Liq. Cryst., 14, 115-28 (1971).
11. S. Chandrasekhar and G.S. Ranganath, Mol. Cryst. Liq. Cryst., 25, 195-97 (1974).
12. J.S. Prasad and M.S. Madhava, Mol. Cryst. Liq. Cryst., 22, 165-74 (1973).
13. S. Chandrasekhar, G.S. Ranganath, U.D. Kini, and K.A. Suresh, Mol. Cryst. Liq. Cryst., 24, 201-11 (1973).
14. S. Chandrasekhar, "Liquid Crystals", Cambridge Univ. Press, Cambridge, 1977, pp. 187-211.
15. H.W. Gibson in "Liquid Crystals: The Fourth State of Matter", F.D. Saeva, Ed., Marcel Dekker Inc., New York, 1979, Chapter 3.
16. R. Dreher, G. Meier, and A. Saupe, Mol. Cryst. Liq. Cryst., 13, 17-26 (1971).
17. J.L. Ferguson, Mol. Cryst., 1, 293-307 (1966).
18. R. Stevenson and R.B. Moore, "Theory of Physics", W.B. Saunders Co., Philadelphia, 1967, pp. 435-41.

19. J. Voss and E. Sackmann, Z. Naturforsch. A, 28, 1496-99 (1973).
20. S. Masubuchi, T. Akahane, K. Nakao, and T. Tako, Mol. Cryst. Liq. Cryst., 35, 135-42 (1976).
21. W.J.A. Goossens, J. de Physique, 40, C3-158 - C3-163 (1979).
22. H. Kimura, M. Hosino, and H. Nakano, J. de Physique, 40, C3-174 - C3-177 (1979).
23. J. Adams and W. Haas, Mol. Cryst. Liq. Cryst., 30, 1-9 (1975).
24. This Thesis, Chapter III.
25. Y. Onogi, J.L. White, and J.F. Fellers, J. Polym. Sci., Polym. Phys. Ed., 18, 663-82 (1980).
26. "Pye Unicam SP8-100 Series Users Manual", Pye Unicam Inc., Cambridge, England, 1979, Publication No. 4013 229 98561, pp. 1-7.
27. "Encyclopedia of Physics", S. Flügge, Ed., Springer-Verlag, Berlin, 1967, Vol. 29, pp. 456-59.
28. H.H. Willard, L.L. Merritt, and J.A. Dean, "Instrumental Methods of Analysis", 5th ed., D. Van Nostrand Co., New York, 1974, pp. 422-24.
29. D.J. Pasto and C.R. Johnson, "Organic Structure Determination", Prentice-Hall Inc., New Jersey, 1969, pp. 68-71.
30. G.W. Schael, J. Appl. Polym. Sci., 8, 2717-22 (1964).
31. P. Crabbé, "ORD and CD in Chemistry and Biochemistry", Academic Press, New York, 1972, Chapters I, II, and V.
32. C. Djerassi, "Optical Rotatory Dispersion", McGraw Hill, New York, 1960, Chapters 1, 2, and 12.
33. "Newer Methods of Polymer Characterization" B. Ke, Ed., Interscience Publ., New York, 1964, Chapter 3.
34. N.H. Hartshorne in "Liquid Crystals & Plastic Crystals", G.W. Gray and P.A. Winsor, Eds., Ellis Horwood Ltd., England, 1974, Vol. 2, pp. 24-51.
35. D.L. Patel and D.B. DuPré, J. Polym. Sci., Polym. Lett. Ed., 17, 299-303 (1979).
36. R. Chang, Mol. Cryst. Liq. Cryst., 28, 1-8 (1973).

37. R.J. Samuels, J. Polym. Sci., Polym. Chem. Ed., 7, 1197-258 (1967).
38. R.S. Werbowyj and D.G. Gray, presented in part at the 179th ACS National Meeting, Houston, March 1980.
39. Y. Uematsu and I. Uematsu, Polym. Prepr., Am. Chem. Soc., Div. Polym. Chem., 20 (1), 66-69 (1979).
40. H. Toriumi, Y. Kusumi, I. Uematsu, and Y. Uematsu, Polym. J., 11, 863-69 (1979).

CHAPTER V

X-RAY DIFFRACTION OF CELLULOSIC LYOMESOPHASES

V.1 Introduction

X-ray diffraction can be a very powerful technique for determining the structure of materials. At one extreme, where perfect single crystals of pure components are available, detailed diffraction patterns can provide exact information on the geometrical distribution of the scattering elements. At the other extreme, scattering from liquids or amorphous solids gives a broad continuum of diffraction intensities from which the distribution function of electron densities can be determined. Wide-angle x-ray scattering provides information about the arrangement of atoms in space because the x-ray wavelengths are comparable to the interatomic distances in crystals (1). Larger periodicities arising from lamellar structures are generally investigated by the low-angle x-ray scattering method (1).

Liquid crystalline systems, being by definition ordered fluids, exhibit intermediate diffraction patterns. Specifically, nematic liquid crystals are characterized by only one relatively broad halo in the wide-angle x-ray region which is attributed to the short-range positional order associated with nematics (2). Smectic mesophases are characterized by several sharp reflections in the low-angle x-ray region and one broad halo in the wide-angle region. In general, the sharp reflections are attributed to the regular packing of the smectic layers and the broad halo reflects the positional order of the side groups within the layers (2-3). Cholesteric mesophases, possessing no distinct molecular layers, do not exhibit any reflections in the low-angle x-ray region. Since a cholesteric is sometimes

regarded as a twisted nematic (4) it is not surprising to discover that cholesterics usually exhibit only a diffuse halo in the wide-angle x-ray region unless they have been subjected to a shear gradient, in which case the molecules become preferentially aligned in the shear direction and distinct arcs are visible at the halo equator. X-ray diffraction patterns have been used to study the polymeric liquid crystalline phases of poly- γ -benzyl-L-glutamate (5-6) and polymeric nematics and smectics (7). An x-ray diffraction investigation of the cholesteric HPC mesophase was undertaken in the hope that this would yield some information about the chiral forces existing between the HPC chain segments.

V.2 Experimental

X-ray scattering experiments were performed with a Philips PW 1730 nickel-filtered Cu K α ($\lambda = 0.154$ nm) x-ray generator and a Warhus flat film camera. The outer and inner pinhole (or collimeter) diameters were 0.015 and 0.025 in respectively. The x-ray scattering was recorded photographically on Kodak "No Screen" film with exposure times varying from three to eight hours depending on the solvent and HPC solution concentration. The experiments were performed under vacuum to minimize the effects of background scattering. The mesophases studied included HPC in water, HPC in methanol, HPC in acetic acid, and acetoxypopylcellulose (APC) in acetone. Gentle water suction was used to fill 0.5-mm diameter thin wall quartz capillaries (Charles Supper Co) with the mesophase. The filling process required from

one to forty-five minutes depending on the viscosity of the solution being used. Capillaries were filled three-quarters full and then flame sealed. The ends were dipped in molten wax to ensure a firm seal. Samples were allowed to stand overnight to remove any orientational effects introduced by the suction filling process. It was hoped that the effects of any solvent evaporation occurring at the suction end of the capillary might be rendered negligible by positioning only the lower half of the filled capillary over the collimeter during irradiation. The mesophase solutions were prepared following the procedure already described in Chapter III and they ranged in concentration from 35 to 70% HPC by weight in water, methanol, acetic acid, dioxane, and morpholine and from 55 to 100% APC by weight in acetone.

Calibration of the sample-to-film distance on the x-ray instrument was achieved by obtaining a diffraction pattern for cholesterol. Eight of the strongest diffraction rings were then matched with literature ring spacings (8-9) and the calculated sample-to-film distance was 17.4 cm. Both the HPC and APC solutions gave x-ray diffraction halos rather than sharp rings. The distance from the diffraction pattern center to the halo midpoint was taken as the x-ray ring radius. The radius was measured at twelve different points around the diffraction ring and at any point on the ring the radius did not vary by more than 0.05 cm. In addition if two different capillaries were filled with the same solution, the resulting diffraction halos gave x-ray spacings which were reproducible to within 0.04 nm.

V.3 Results

Hydroxypropylcellulose lyomesophase solutions exhibited wide-angle x-ray diffraction patterns consisting of only one broad diffuse halo, an example of which is illustrated in Figure V.1. The halo diameter decreased steadily as the HPC concentration of the solution was increased. The x-ray d spacings were calculated by using Bragg's scattering equation which is shown below

$$\lambda = 2d \sin\theta \quad \text{V.1}$$

where λ = the x-ray beam wavelength

d = the distance between the scattering elements

θ = the angle of diffraction defined by $\tan 2\theta =$

r/l where r is the diffraction ring radius

and l is the sample-to-film distance

The resulting x-ray d spacings for several aqueous HPC solutions have been listed in Table V.1. The diffuseness of the x-ray halo in aqueous media made it very difficult to determine an unequivocal relationship between d and the HPC volume or weight fraction. For this reason, x-ray diffraction studies were also undertaken on some other mesophase systems, namely, HPC in methanol, acetic acid, dioxane, and morpholine and on APC (10-11) in acetone. Figure V.2 shows the slightly sharper x-ray diffraction halos obtained for some typical HPC methanol and APC acetone solutions. The

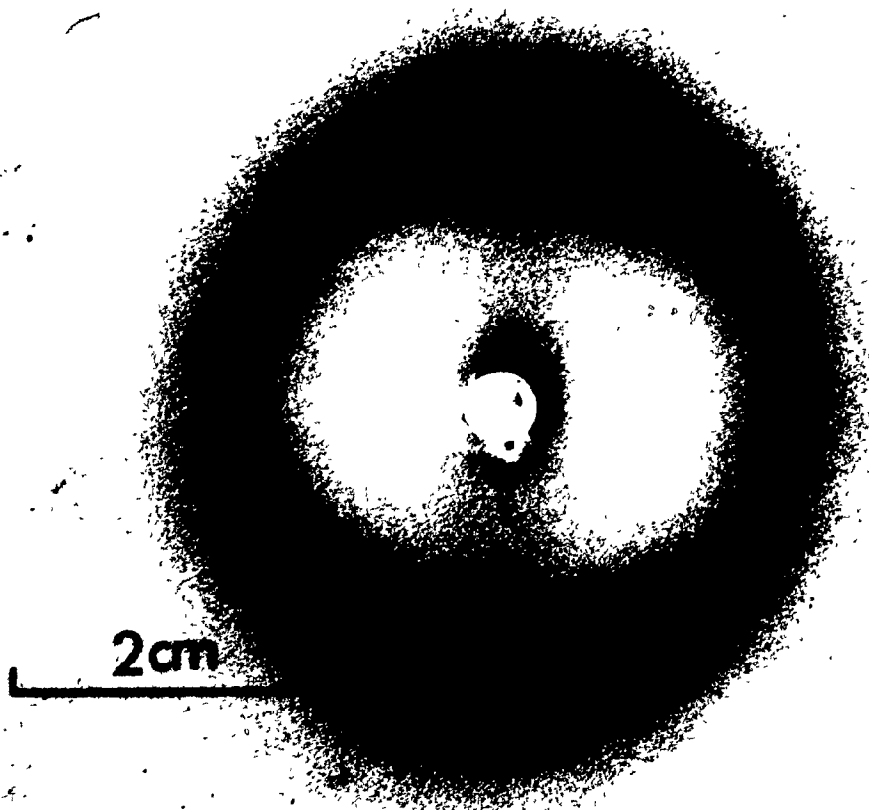


FIGURE V.1 X-ray diffraction pattern generated by a 0.489 volume fraction HPC-L aqueous solution. The sample-to-film distance was 17.4 cm and the calculated d spacing was 1.35 nm.

TABLE V.1

Variation in X-ray d Spacing with HPC-L Concentration in Aqueous
and Organic Solutions

Solvent	HPC Weight Fraction (ω_2)	HPC Volume Fraction (ϕ_2)	d (nm)
H ₂ O	0.5173	0.465 ^a	1.35
	0.5416	0.489	1.35
	0.5796	0.528	1.34
	0.5960	0.545	1.33
	0.6121	0.561	1.32
	0.6600	0.611	1.29
	0.6771	0.629	1.28
CH ₃ COOH	0.3576	0.322	1.58
	0.6508	0.614	1.31
C ₄ H ₈ O ₂	0.3836	0.343	1.54
	0.5066	0.463	1.35
	0.6037	0.561	1.28
C ₄ H ₉ OH	0.6056	0.555	1.42

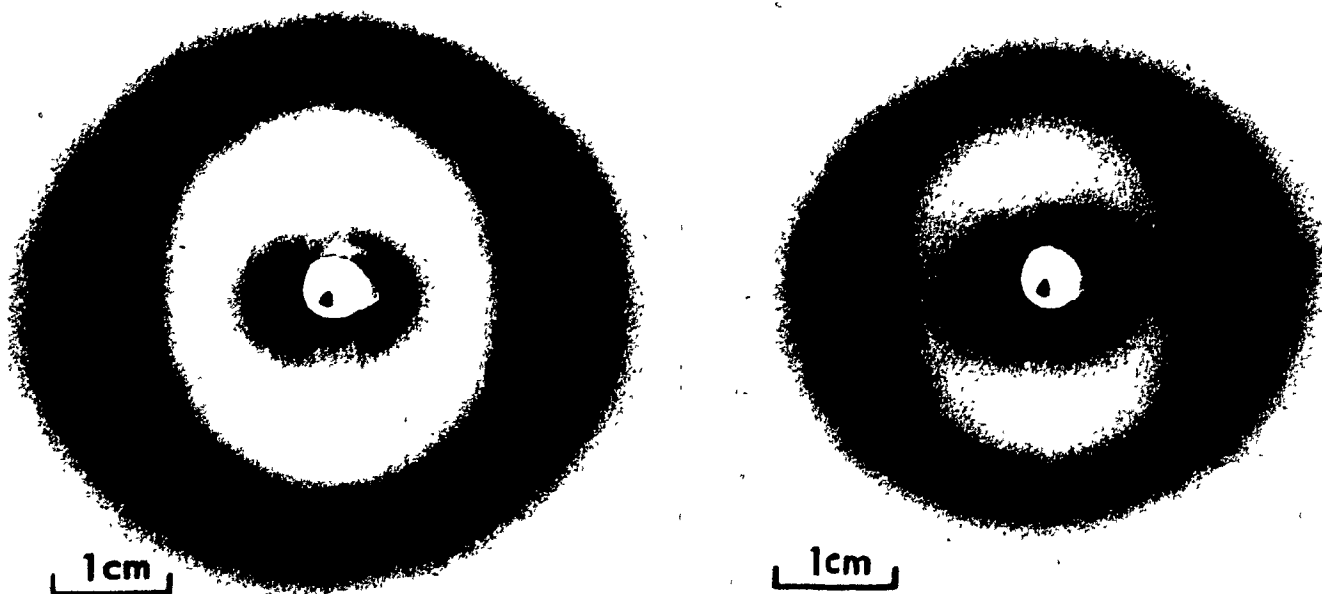


FIGURE V.2 The x-ray diffraction pattern on the left was obtained for a HPC methanol solution in which $\phi_2 = 0.608$ and d was calculated to be 1.35 nm. The x-ray diffraction pattern on the right was obtained for an APC acetone solution in which $\phi_2 = 0.601$ and d was calculated to be 1.54 nm.

variation in calculated x-ray d spacing with polymer volume fraction for HPC in methanol and for APC in acetone is depicted in Figures V.3 and V.4 respectively. The x-ray d spacing for HPC in other organic solvents was also found to decrease as the polymer concentration was increased as is shown by the data listed in Table V.1. Practical difficulties, arising from the extremely viscous nature of the HPC solutions, made it impossible to fill the x-ray capillaries with solutions whose volume fraction exceeded 0.76 HPC. The APC solutions exhibited much more fluidity and, as a result, the highest usable volume fraction for these solutions was 0.90 APC.

The x-ray d spacing results of Figures V.3 and V.4 can be qualitatively explained in the following way. Region A is the two phase region where both isotropic and anisotropic material coexist; within this region the concentration of each phase should remain constant, only their proportions should change. Thus it is not surprising to find that within this region the x-ray d spacing is essentially constant. Region B consists solely of anisotropic material and the x-ray d spacing decreases gradually as the concentration of polymer in the solution is increased. This result was expected as will be elaborated on in the next section. The relatively narrow range of d spacing values from 1.2 to 1.7 nm. is really too small for an absolute relationship between d and the polymer volume fraction (ϕ_2) to be established. However, from the available data the best correlation coefficients are obtained when d is allowed to vary linearly with ϕ_2 . The lyomesophase volume fraction at which the d spacing begins to decrease may perhaps be used to detect the end of the two phase coexistence region. It

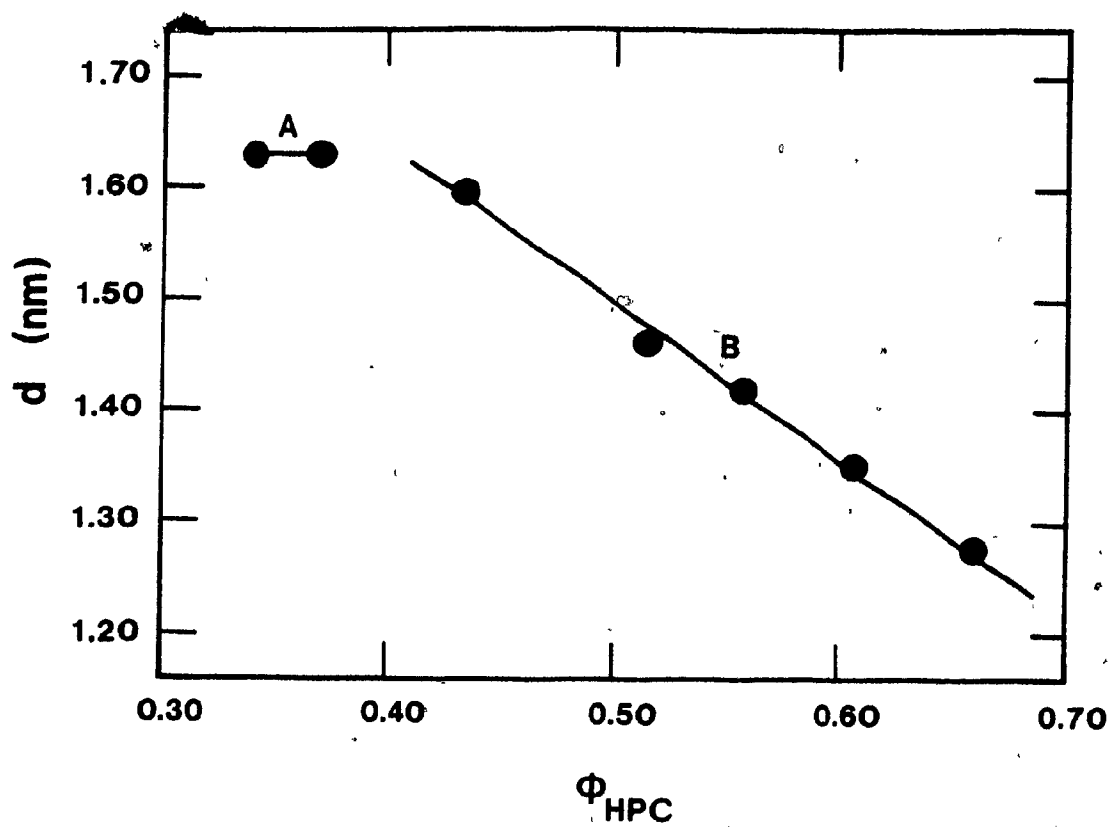


FIGURE V.3 The variation in x-ray d spacing with HPC volume fraction (ϕ_{HPC}) in methanol solutions. For an explanation of the A and B regions see text.

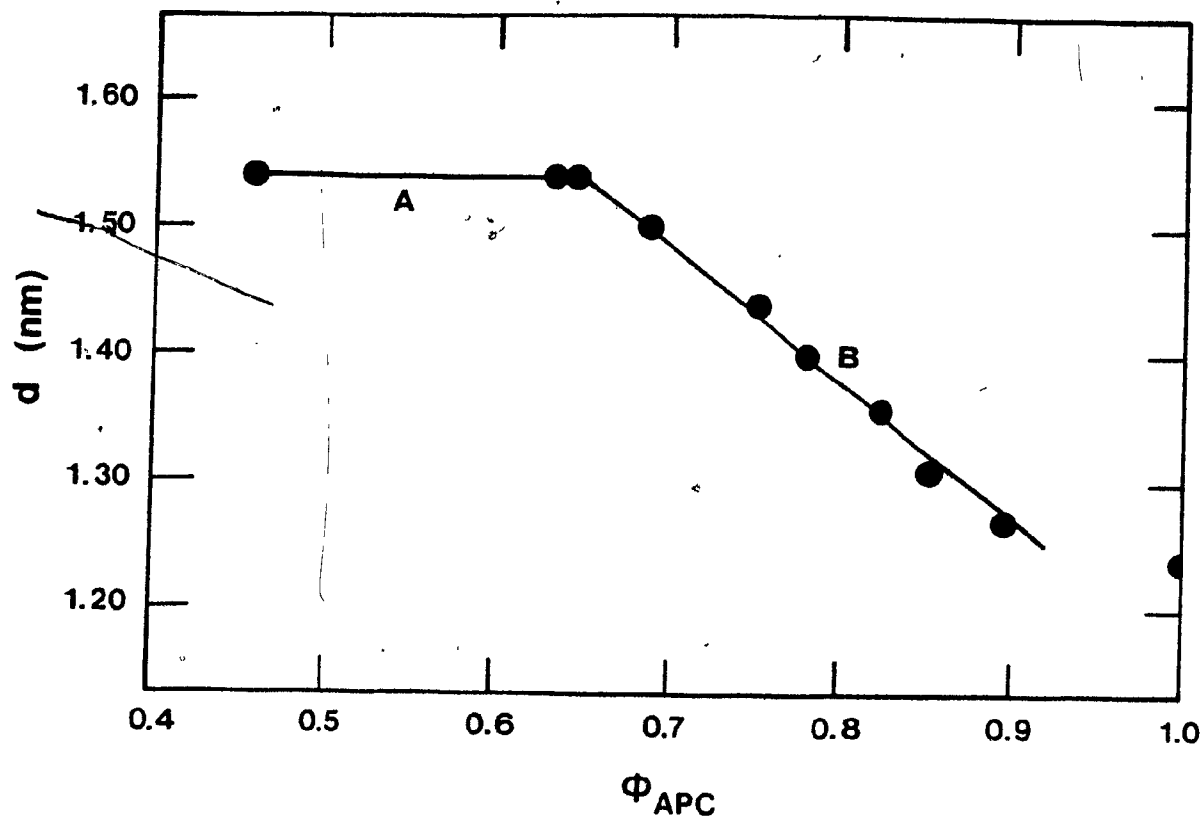


FIGURE V.4 The variation in x-ray d spacing with APC volume fraction (ϕ_{APC}) in acetone solutions. See text for an explanation of the A and B regions.

is interesting to note that for APC from x-ray data the end of the two phase region occurs at an APC volume fraction of 0.65. This value agrees very well with the APC volume fraction of 0.64 previously reported as corresponding to the start of the purely anisotropic mesophase (10). For aqueous HPC solutions the end of the two phase region is reported to occur at a 0.51 HPC volume fraction (12). This value agrees relatively well with the 0.49 HPC volume fraction deduced as the start of the purely anisotropic mesophase from the x-ray data contained in Table V.1.

V.4 Discussion

The physical significance of the experimentally determined x-ray d spacing and its variation with the mesophase volume fraction for both the HPC and APC cholesteric systems will now be considered in greater detail. Firstly, the fact that the diffraction pattern produced by the mesophase is a halo suggests that there is little macroscopic orientation of the sample within the x-ray capillary. The faint arcs which appear in the x-ray patterns illustrated in Figures V.1 and V.2 may perhaps be due to a slight orientation of the mesophase along the capillary walls. However, since these arcs are relatively indistinct, it would seem that no extensive preferential orientation of the mesophase has occurred in the bulk sample. Secondly, the diffuse nature of the diffraction halo indicates that the separation between the scattering elements of the mesophase is not exactly uniform but that it varies about some mean spacing.

This is a reasonable assumption to make because of the fluid character of the liquid crystal. The scattering elements within the cholesteric material must be the constituent rod-like molecules. The x-ray beam passing through a small volume element of the mesophase would see the rod-like molecules as being essentially parallel and thus the x-ray d spacings calculated are most likely to represent the mean spacing between the rod-like molecules in the cholesteric.

The mean spacing between the constituent rods of the cholesteric should vary with the polymer volume fraction; if the number of rod-like molecules in a given volume element is increased then the spacing between the rods should decrease. Lacking any specific information about the packing arrangement of rods in the HPC or APC mesophase, the following general model is proposed to provide a theoretical prediction of how the mean spacing between rods should vary with the polymer volume fraction. The mesophase is to be divided into long volume elements of cross-section A . Each cross-sectional area A should contain part or parts of one rod-like chain molecule whose cross-section is a . This model is depicted schematically in Figure V.5. The volume fraction of chains (ϕ_2) contained within a cross-sectional area A is given by Equation V.2

$$\phi_2 = a/A \quad \text{V.2}$$

and the mean center-to-center distance between neighboring chains (\bar{d}) is given by Equation V.3.

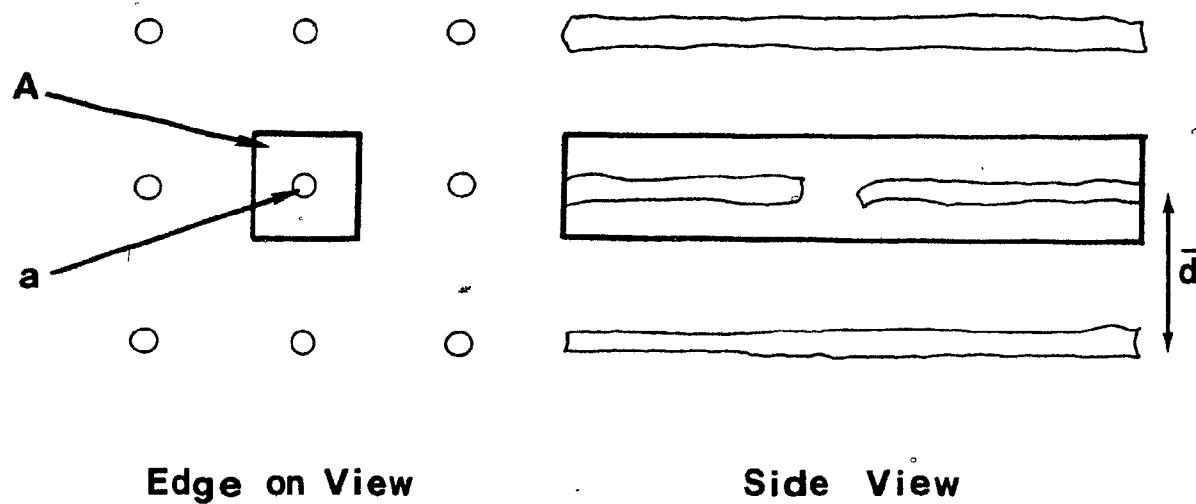


FIGURE V.5 A schematic view of the model proposed to represent the arrangement of rod-like cholesteric molecules within a small arbitrary cross-sectional area A . The molecular cross-sectional area is a and the mean center-to-center distance between the rods is \bar{d} .

$$\bar{d} = \sqrt{A} = \sqrt{a/\phi_2}$$

V.3

Note should be made that chain end effects have been neglected in the above model because if the distance between chain ends is assumed to be of the same order as the mean spacing, \bar{d} , then the probability of finding a chain end gap within a cross-sectional area A is \bar{d}/L , where L is the polymer chain contour length. Since L is very much greater than \bar{d} , chain end effects on the model are negligible. The beauty of Equation V.3 lies in the fact that no particular packing arrangement for the rods has to be assumed and that the slope of a plot of \bar{d} versus $\phi_2^{-1/2}$ gives an estimate of the chain cross-sectional area. In addition at $\phi_2 = 1$ the chain molecule and volume element cross-sections ($a = A$) should be identical — a totally realistic physical picture for the mesophase. The experimentally determined x-ray d spacing data for both HPC and APC have been replotted in the form of d versus the inverse square root of ϕ_2 as required by the above model. These plots are depicted in Figures V.6 and V.7. The correlation coefficients for Figures V.3 and V.6 are 0.9986 and 0.9944 respectively while the corresponding values for Figures V.4 and V.7 are -0.9982 and 0.9928. Clearly, both plots of d versus ϕ_2 and d versus $\phi_2^{-1/2}$ give excellent straight lines. This result might have been anticipated considering the narrow range of experimental d and ϕ_2 values available for both the HPC and APC mesophases. Although the correlation coefficients are marginally better for plots of d versus ϕ_2 , there currently exists no physical explanation for the linear variation of d with ϕ_2 . But the model proposed in this chapter for the mesophase does provide a physically reasonable justification for an inverse

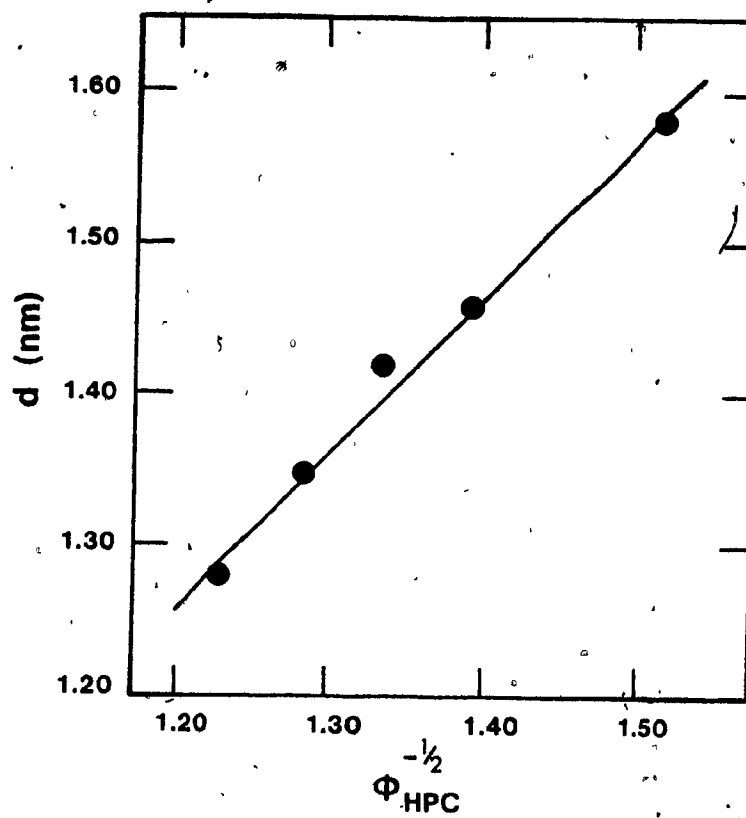


FIGURE V.6 The variation in x-ray d spacing with the inverse square root of the HPC volume fraction (ϕ_{HPC}) in methanol solutions.

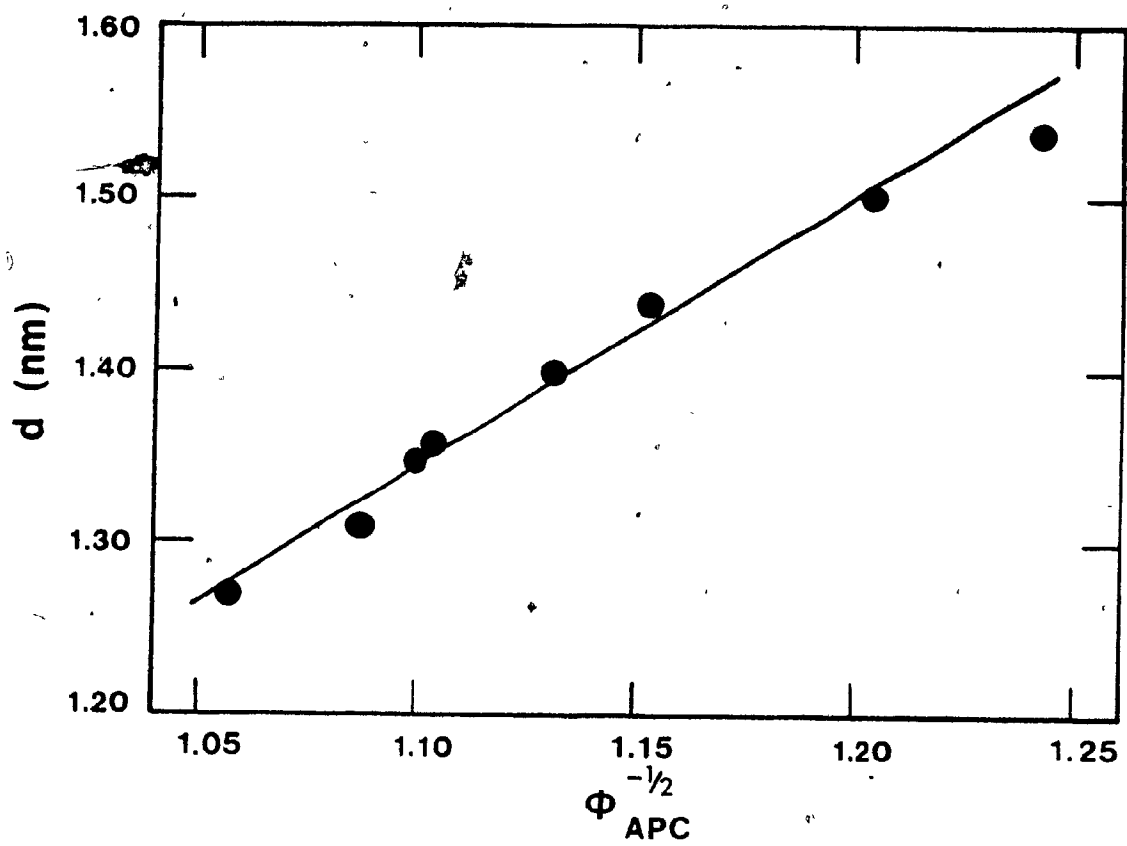


FIGURE V.7 The change in the x-ray d spacing with the inverse square root of the APC volume fraction (ϕ_{APC}) in acetone solutions.

square root dependence of d on ϕ_2 . In addition the slope of the d versus $\phi_2^{-1/2}$ plot for HPC is 1.02 while the intercept at $\phi_2 = 1$ on the d -axis is 1.06. These two values are almost identical and they are plausible values, as predicted by the model, for the HPC molecular cross-sectional area. The corresponding slope and intercept values for APC are 1.46 and 1.20 respectively. The reason for the relatively large difference in these two values for the APC molecular cross-sectional area is unknown but the 1.20 seems a more reasonable value for the APC cross-sectional area because the x-ray d spacing for an APC fiber is 1.24 nm. Acetylated propylene oxide side chains are bulkier than hydroxypropyl side chains; therefore, a cellulose backbone with bulkier side chains should have a greater cross-sectional area than a similar cellulosic with smaller side chains. This is confirmed by examination of the HPC (1.02) and APC (1.20) cross-sectional areas. It thus seems that both the HPC and APC experimental data fit the model behavior outlined reasonably well and, consequently, the x-ray d spacing has been assumed to vary in an inverse square root manner with ϕ_2 for both systems.

As mentioned earlier both HPC and APC possess identical backbones which differ only in their attached side groups. It was anticipated that if side chain effects for both polymers could be eliminated, then the x-ray d spacing should be identical in each system at a given volume fraction of cellulose (ϕ_{cel}). In addition it was hoped that the x-ray d spacing data would show a better inverse square root correlation with the cellulose volume fraction than did the HPC or APC volume fractions. The HPC and APC volume fractions were broken down into individual cellulose volume fractions

by using the following sequence of equations.

$$\frac{w_{\text{cel}}}{w_{\text{der}}} = \frac{M_{\text{cel}}}{M_{\text{der}}} \quad \text{V.4}$$

$$w_{\text{cel}} = \frac{w_{\text{cel}}}{w_{\text{der}} + w_{\text{s}}} \quad \text{V.5}$$

$$v_{\text{cel}} = w_{\text{cel}}/\rho_{\text{cel}}; v_{\text{der}} = w_{\text{der}}/\rho_{\text{der}}; v_{\text{s}} = w_{\text{s}}/\rho_{\text{s}} \quad \text{V.6}$$

$$\phi_{\text{cel}} = \frac{v_{\text{cel}}}{v_{\text{der}} + v_{\text{s}}} \quad \text{V.7}$$

Equation V.7 can be rewritten in the following form by substituting into it Equations V.4, V.5, and V.6.

$$\phi_{\text{cel}} = \frac{M_{\text{cel}}}{\rho_{\text{cel}} M_{\text{der}}} \left(\frac{1}{\rho_{\text{der}}} + \frac{1}{\rho_{\text{s}}} \left[\frac{1}{\omega_{\text{der}}} - 1 \right] \right)^{-1} \quad \text{V.7}$$

where w_{cel} = weight of cellulose in derivative

w_{der} = weight of derivative in solution

w_{s} = weight of solvent in solution

M_{cel} = molar mass of cellulose repeat unit (162 g)

M_{der} = molar mass of derivative repeat unit (HPC 394 g
and APC 515 g)

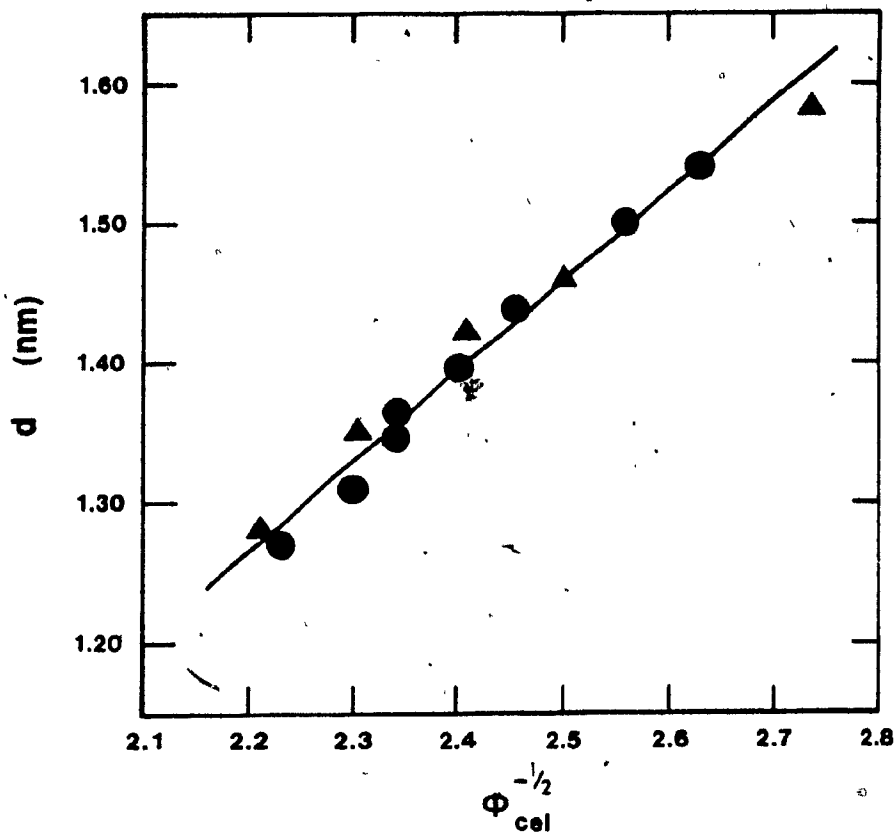


FIGURE V.8 The variation in the x-ray d spacing with the cellulose volume fraction (ϕ_{cel}) of HPC in methanol (▲) and APC in acetone (●) solutions. The cellulose volume fractions were evaluated by making use of Equation V.7.

thermal fluctuations, imperfect rod orientation, or the natural twist of the cholesteric material. Figure V.9 schematically depicts the molecular orientation within two successive layers of the cholesteric material. The spacing between the molecules or layers has been depicted as being approximately equal to the x-ray d spacing, while the angular twist between the cholesteric layers is θ . The origin of the angular twist is uncertain but several theories (5,16-17) have been proposed to account for its existence. The most likely explanation for the helicoidal twist is the existence of asymmetric forces between the chain segments of the cholesteric. These forces in HPC are postulated to arise from the inherent chirality of the individual anhydroglucose units. For cholesteric systems, the helicoidal pitch, P, is related to both d and θ (degrees) by the following geometric relationship

$$P = \frac{360 d}{\theta} \quad \text{V.8}$$

Optical data presented in the previous chapter showed that the helicoidal pitch varies inversely as the third power of the HPC volume fraction ($P \propto \phi_2^{-3}$). Tseng and Gray (10-11) have found this same relationship is valid for the APC acetone lyomesophase. It has been shown in this chapter that the x-ray d spacing varies as the inverse square root of the polymer volume fraction. If P and d are known for a particular sample then Equation V.8 can be used in evaluating θ or the average angular twist for the sample. The data needed to calculate θ for both the HPC and APC

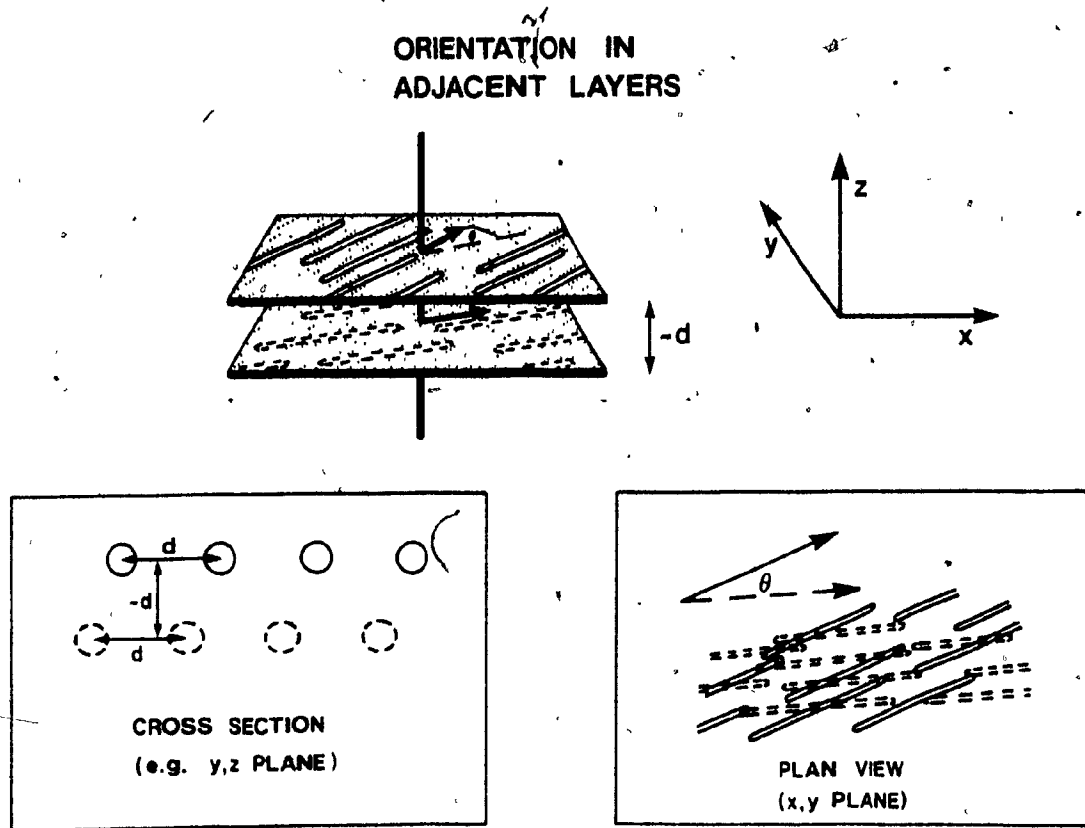


FIGURE V.9 An expanded view of two successive layers in the model proposed to represent a cholesteric lyomesophase. The average distance between the molecules and the molecular layers is $\sim d$ and θ is the average angular twist between molecules in successive layers of the structure.

systems have been listed in Tables V.2 and V.3 respectively. In both systems θ is small and varies from 0.30 to 1.8 degrees over the entire mesophase concentration range. The variation in θ with ϕ_2 can be determined by making use of Equation V.8 and the known variation of P and d with the polymer volume-fraction. Ideally since $P \propto \phi_2^{-3}$ and $d \propto \phi_2^{-1/2}$ then θ should be proportional to $\phi_2^{5/2}$ according to the substitution of the P and d values into Equation V.8. Figure V.10 shows a plot of this predicted variation of θ with ϕ_2 for the APC acetone lyomesophase. Although the data points are not exactly linear they do seem to fit the postulated θ versus $\phi_2^{5/2}$ relationship reasonably well. Currently there exists no real theory to explain why or how θ should vary with the polymer volume fraction.

Hydroxypropylcellulose and APC mesophases differ considerably in their behavior from other polymeric lyomesophases. Consider the case of poly- γ -benzyl-L-glutamate (PBLG) in dioxane where P is reported to vary as c^{-2} where c is the mesophase solution concentration in g/100 mL of solution. The x-ray d spacing varies as $c^{-1/2}$ and consequently θ varies as $c^{3/2}$ (5). As noted previously for both HPC and APC P varies as ϕ_2^{-3} , d varies as $\phi_2^{-1/2}$, and θ varies as $\phi_2^{5/2}$. The reason why PBLG and the HPC/APC lyomesophases differ in their behavior is unknown but a possible explanation may lie in the polymer packing arrangements and their pitch ranges. Low molar mass mixtures of nematic and cholesteric mesophases exhibit an inverse linear relation between P and the cholesteric solution concentration ($P \propto c^{-1}$) (18). The large pitch (> 2000 nm) PBLG system exhibits an inverse

TABLE V.2

Calculated Angular Twist (θ) Between Successive
Layers of the Cholesteric Structure
for HPC Methanol Lyomesophases

ϕ_{HPC}	ω_{HPC}	P (nm)	d (nm)	θ (deg)
0.340	0.4447	1926	1.63	0.305
0.370	0.4773	1640	1.63	0.358
0.433	0.5426	1040*	1.58	0.547
0.516	0.6236	632	1.46	0.832
0.559	0.6589	553	1.42	0.924
0.608	0.7064	405	1.35	1.20
0.660	0.7514	320	1.28	1.44

* Pitch value interpolated using Equation IV.15

TABLE V.3

Calculated Angular Twist (θ) Between Successive
Layers of the Cholesteric Structure
for APC Lyomesophases in Acetone

ϕ_{APC}	ω_{APC}	P^* (nm)	d (nm)	θ (deg)
0.455	0.5482	1756	1.54	0.316
0.563	0.6520	770	1.54	0.720
0.648	0.7280	623	1.54	0.890
0.689	0.7632	525	1.50	1.029
0.752	0.8150	413	1.44	1.255
0.781	0.8283	373	1.40	1.351
0.821	0.8699	325	1.36	1.507
0.826	0.8734	321	1.35	1.514
0.854	0.8951	293	1.31	1.610
0.895	0.9254	260	1.27	1.759
1.000	1.0000	196	1.24	2.278

* Pitch values quoted taken from reference (10)

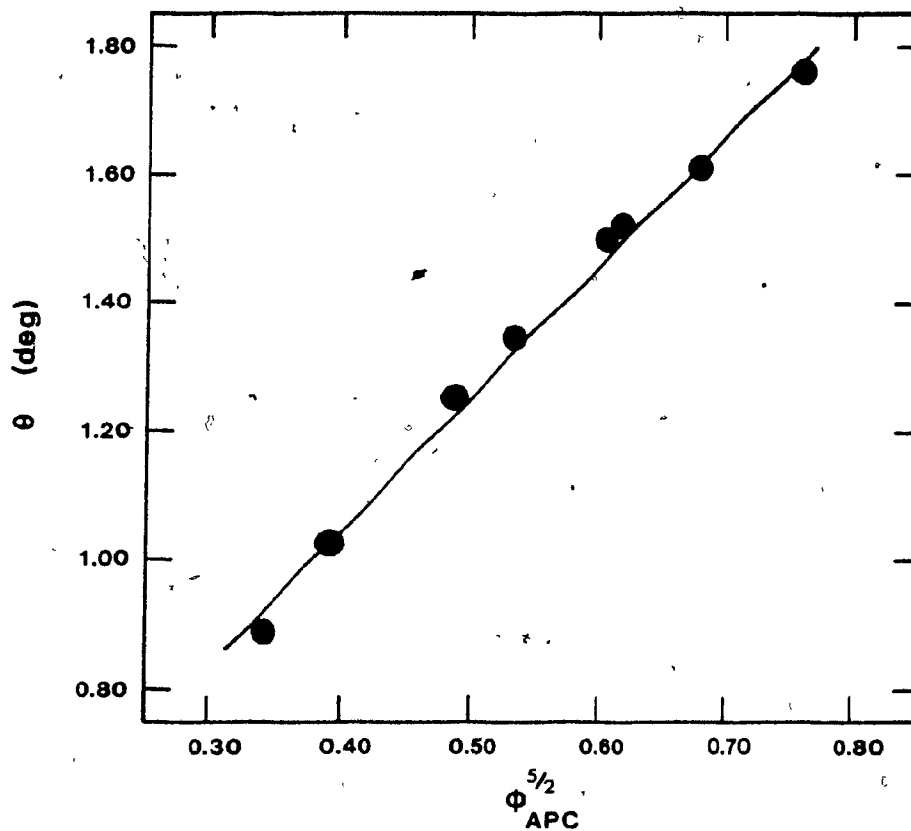


FIGURE V.10 The variation in the angular twist (θ) of the cholesteric structure with the APC volume fraction (ϕ_{APC}) in acetone solutions. The angular twist for each solution was calculated using Equation V.8 and the data contained in Table V.3.

square root dependence of P on concentration ($P \propto c^{-2}$). The HPC and APC mesophases exhibit both long (900 - 5000 nm) and short (300 - 700 nm) pitches which vary in an inverse third power relationship with the polymer volume fraction ($P \propto \phi_2^{-3}$). There thus seems to be a natural progression in the power dependence of the concentration on pitch for cholesteric systems. The reason for this, if true, is unknown. However, it is possible that depending on the helicoidal pitch range in the system the molecules may have different packing arrangements which do not alter the variation in d spacing with concentration very much, but rather profoundly affect the angular twist between the layers.

V.5 Conclusion

The mean spacing between the molecules of both the HPC and APC lyomesophases as determined by x-ray diffraction studies was found to vary with the polymer concentration. However, neither the d spacing nor the ϕ_2 values were broad enough in range to allow an unequivocal relationship between d and ϕ_2 to be established. A general model was presented in which d should vary as $\phi_2^{-1/2}$. The experimental data fit this relationship reasonably well and physically plausible values were obtained for the HPC and APC cross-sectional areas. The polymer volume fractions were also broken down into cellulose volume fractions and this data also fit the d versus $\phi_2^{-1/2}$ relationship quite well. The x-ray d spacing data gave good values for the end of the two phase coexistence region in both polymeric

systems. The angular twist between successive layers of the cholesteric structure was calculated and was found to vary from 0.30 to 1.8 degrees with the solution concentration. The exact relationship between θ and ϕ_2 is unknown but the experimentally calculated data fit a θ versus $\phi_2^{5/2}$ relationship quite well. Finally, a possible explanation was proposed to account for the difference in behavior of the PBLG lyomesophase and the HPC/APC lyomesophases.

References

1. F.W. Billmeyer Jr., "Textbook of Polymer Science", 2nd ed., Wiley Interscience, New York, 1971, pp. 111-14, 146-59.
2. J.H. Wendorff, H. Finkelmann, and H. Ringsdorf, J. Polym. Sci., Polym. Symp., 63, 245-61 (1978).
3. K. Fontell in "Liquid Crystals & Plastic Crystals", G.W. Gray and P.A. Winsor, Eds., Ellis Horwood Ltd., England, 1974, Vol. 2, Chapter 4.
4. This Thesis, Chapter I.
5. C. Robinson, J.C. Ward, and R.B. Beevers, Discuss. Faraday Soc., 25, 29-42 (1958).
6. C. Robinson, Tetrahedron, 13, 219-34 (1961).
7. S.B. Clough, A. Blumstein, and A. deVries in "Mesomorphic Order in Polymers and Polymerization in Liquid Crystalline Media", A. Blumstein, Ed., ACS Symposium Series #74, Washington, D.C., 1978, pp. 1-11.
8. H.L. Spier and K.G. van Senden, Steroids, 6, 871-73 (1965).
9. J. Parsons, W.T. Beher, and G.D. Baker, Henry Ford Hosp. Med. Bull., 6, 365-421 (1958).
10. S.L. Tseng, A. Valente, and D.G. Gray, Macromolecules, 14, 715-19 (1981).
11. S.L. Tseng and D.G. Gray, presented in part at the 64th CIC Conference, Halifax, May-June 1981.
12. J. Bheda, J.F. Fellers, and J.L. White, Colloid & Polymer Sci., 258, 1335-42 (1980).
13. T. Lukanoff and B. Philipp in "Polymer Handbook", J. Brandrup and E.H. Immergut, Eds., Interscience Publ., New York, 1966, Chapter VI.
14. E.D. Klug in "Encyclopedia of Polymer Science and Technology", H.M. Mark, N.G. Gaylord, and N.M. Bikales, Eds., Wiley-Interscience Inc., New York, 1971, Vol. 15, pp. 307-14.
15. "Handbook of Chemistry and Physics", 56th ed., Robert Weast, Ed., CRC Press Inc., Ohio, 1975-76.
16. W.J.A. Goossens, Mol. Cryst. Liq. Cryst., 12, 237-44 (1971).

17. T.V. Samulski and E.T. Samulski, J. Chem. Phys., 67, 824-30 (1977).
18. J. Adams and W. Haas, Mol. Cryst. Liq. Cryst., 30, 1-9 (1975).

APPENDIX

CONCLUDING REMARKS AND SUGGESTIONS FOR FUTURE WORK

The present investigation has encountered the often-reported difficulties in characterizing a highly polydisperse cellulose derivative. The effects of sample polydispersity and polymer aggregation on the characterization techniques employed in this study are not well resolved. Ideally, narrow molar mass fractions of hydroxypropylcellulose are required for both conventional or low angle laser light scattering and sedimentation equilibrium experiments. If both techniques give essentially identical molar masses for each fraction, then sample polydispersity should account for the diverse hydroxypropylcellulose molar mass results reported in this work. Alternatively, if fractionated hydroxypropylcellulose samples give significantly different molar masses from the above two techniques then the role of polymer aggregation (induced either by time or shear) on the characterization process must be re-evaluated. Therefore the primary objective of any further research in the successful characterization of this polymer should be directed towards the development of an effective fractionation method.

Chain stiffness is a necessary but insufficient requisite for anisotropic phase separation in cellulosics. Flexible side groups while increasing polymer solubility may also permit the cellulose chains to slip past one another, thus endowing the system with enough fluidity to

become mesomorphic at high polymer volume fractions. The absence of flexible side groups is believed to result in crystallization or formation of an unoriented gel as is the case for hydroxyethylcellulose. In some solvents strong solvation of the polymer main chain may usurp the role of flexible side groups. The role of side group flexibility on anisotropic phase separation might, perhaps, be best investigated by replacing the hydroxyl groups of hydroxypropylcellulose by a series of more flexible (C_nH_{2n+1}) or stiffer (C_6H_5 or CN) side groups. Viscosity measurements on molar mass fractions of hydroxypropylcellulose might be undertaken to ascertain and assess the role of sample polydispersity on the Mark-Houwink parameter and, thus indirectly, on chain stiffness in various solvents. The effects of non-mesomorphic and ionic groups on the hydroxypropylcellulose mesophase formation could be examined by studying copolymer blends of hydroxypropylcellulose/hydroxyethylcellulose and hydroxypropylcellulose/sodium(carboxymethylcellulose) in aqueous media. The proportions of both components needed to form and/or destroy or inhibit mesophase formation might provide some useful information about the mechanism of anisotropic phase separation.

Hydroxypropylcellulose does not exhibit a lower consolute temperature in polar organic solvents. It should, therefore, be easier to obtain and interpret a qualitative phase diagram for hydroxypropylcellulose in organic rather than in aqueous media. In addition, if narrow molar mass fractions of hydroxypropylcellulose were available, the exact roles of

molar substitution and sample polydispersity on the aqueous cloud point could be assessed and resolved. A more detailed investigation of the coexisting isotropic and anisotropic phases might be worthwhile to determine if anisotropic phase separation selectively fractionates the polymer between the two phases. This type of investigation may perhaps provide a clue to the unusual concentration dependence of both phases across the coexistence region on the originally prepared volume fraction of polymer. It would also be of interest to redissolve a highly concentrated mesophase (~ 70 weight % hydroxypropylcellulose) from which all solvent had been evaporated to determine if, indeed, any fractionation of the polymer had occurred.

The excellent fit of the hydroxypropylcellulose optical rotatory power data to De Vries' optical equations for cholesteric lyomesophases using only the layer birefringence as a fitting parameter confirms conclusively that hydroxypropylcellulose does indeed form a cholesteric lyomesophase in several solvents. The resulting fitted layer birefringence values agree quite well with measured birefringences according to the model presented. A direct measurement of the layer birefringence would be desirable and this might be accomplished by searching for a solvent in which hydroxypropylcellulose exhibits an anomalous positive optical rotatory dispersion curve or by investigating the effects of strong electric or magnetic fields on hydroxypropylcellulose.

The helicoidal pitch of the hydroxypropylcellulose samples was found to decrease continuously with time. It was not possible to determine if this behavior was a kinetic phenomenon resulting from the slow perfection of molecular order in the mesophase or, simply, a result of solvent evaporation. The latter explanation seems to be the more likely, but the relatively regular decrease in pitch with time would seem to support the former explanation. Dissolving the lyotropic polymer in an inert plasticizer rather than in a volatile solvent and studying the change in pitch with time would enable this question to be resolved. An investigation into the effects of pressure and temperature on the helicoidal pitch might provide some additional information about the molecular structure of the mesophase. Theoretical research on the hydroxypropylcellulose mesophase might well be undertaken to ascertain the physical significance of the inverse third power dependence of pitch on the polymer volume fraction. It might also be worthwhile to examine in more detail the relation between the critical volume fraction of polymer for anisotropic phase separation and the slope and intercept of $P^{-1/3}$ versus ϕ_2 plots.

Lyotropic mesophases will on heating always exhibit thermotropic behavior and hydroxypropylcellulose is no exception. Although the present investigation was confined to the lyotropic behavior of hydroxypropylcellulose, it would surely be profitable to examine in greater detail the thermotropic properties of hydroxypropylcellulose itself, as well as its thermotropic behavior in solution. Moreover, a complete spectroscopic

investigation of this polymer by Fourier Transform Infrared (FTIR) and Raman, although very complex, would provide some pertinent information about the possible structural differences existing in dilute and concentrated hydroxypropylcellulose solutions. Preliminary FTIR results show significant differences exist in the 800 to 1500 wavenumber region of the infrared spectrum. Specifically, dilute solutions show no peaks in the noted region, red samples exhibit eleven distinct peaks within the same region, and a whole series of multiplets exist in this region for purple samples. These peaks must certainly be a reflection of the structural changes occurring in the system as the mesophase is formed. The FTIR technique might also provide an alternative method for evaluating the beginning and the end of the biphasic region for the mesophase.

Finally, a more detailed x-ray diffraction investigation of the hydroxypropylcellulose system should be undertaken to determine the molecular packing arrangement existing in the mesophase. Studies of mesophases prepared from other cellulose derivatives and solvents over the broadest possible composition ranges should allow an unequivocal relationship between the x-ray d spacing and the cellulosic volume fraction to be established.

The mesomorphicity of hydroxypropylcellulose may offer a new route to the formation of improved cellulosic fibers possessing higher orientation and, perhaps, more strength. The ready availability of

hydroxypropylcellulose, its resistance to degradation, its reasonable price, and its novel optical properties would seem to predict a very useful future for this polymer.

CLAIMS TO ORIGINAL RESEARCH

The claimed contributions of this work to original research are outlined below.

1. Hydroxypropylcellulose was the first cellulose derivative found to form liquid crystalline solutions in water and in polar organic solvents.
2. Microscopic and optical data were used to prove that hydroxypropylcellulose forms a cholesteric lyomesophase in all the solvents investigated.
3. An in-depth study of this cholesteric lyomesophase in aqueous and in organic media showed that optically this polymer obeys De Vries' optical theory with only one fitting parameter — the layer birefringence.
4. A model has been proposed to account for the discrepancy between measured birefringences in the Abbé refractometer and calculated layer birefringences according to De Vries' theory.
5. The refractive index and the birefringence for hydroxypropylcellulose

in water, acetic acid, and methanol have been measured as a function of polymer concentration.

6. The helicoidal pitch was for the first time evaluated from optical rotatory dispersion spectra and compared with corresponding pitch values obtained spectrophotometrically in both aqueous and organic solutions.
7. Hydroxypropylcellulose was the first known polymeric liquid crystal to exhibit both short pitch cholesteric and long pitch shimmering iridescence in the same solvent.
8. Over the entire pitch range studied it was found that the helicoidal pitch varies inversely as the third power of the hydroxypropylcellulose volume fraction.
9. The characterization of this cellulosic was undertaken to compare, for the first time, the results from conventional light scattering, low angle laser light scattering, and sedimentation equilibrium. Each method gives a different molar mass for the polymer and some reasons for this have been proposed.
10. The differential index of refraction for this polymer was measured in water and was found to be virtually independent of the polymer molar mass.

11. A qualitative phase diagram for hydroxypropylcellulose in water has been presented. It does not agree very well with Flory's theory for mesomorphic phase separation of rod-like molecules and sample polydispersity is an insufficient factor to account for the discrepancy. It has been shown that if the Kuhn statistical segment length rather than the molecule chain length is used in Flory's theory a much better agreement is obtained between the predicted and experimental critical volume fraction of polymer at anisotropic phase separation.
12. It is impossible, at present, to predict at what critical volume fraction of polymer the mesophase will form in any solvent; it does, however, appear that the critical volume fraction of polymer is lower in acids than in alcohols.
13. X-ray diffraction measurements provided a method by which the end of the two phase coexistence region of the mesophase could be evaluated.
14. The x-ray d spacing or average separation between the molecules of the cholesteric lyomesophase varied in an inverse square root manner with the polymer and cellulose volume fractions. A model for the cholesteric was presented to account for this inverse square root dependence of d on volume fraction.
15. The helicoidal or angular twist between the molecules of the

cholesteric was calculated to vary as the $5/2$ power of the hydroxypropylcellulose volume fraction.